Université de Montréal

Analyse des protéines du tégument par virométrie en flux et protéomique des capsides nucléaires du Virus Herpès Simplex de type 1 (VHS-1)

Par

Nabil El Bilali

Département de microbiologie, infectiologie et immunologie

Faculté de Médecine

Thèse présentée à la faculté de médecine
en vue de l'obtention du grade de Philosophiæ Doctor (Ph.D)
en Microbiologie/ immunologie

Avril 2018

Résumé

Le virus herpès simplex de type 1 (VHS-1) est un agent infectieux hautement contagieux qui constitue un véritable problème de santé mondiale causant de nombreuses pathologies allant de l'herpès labial jusqu'aux plus graves comme l'encéphalite et les complications chez les nouveau-nés. Le virus comporte 4 composants structurels distincts : un génome viral d'ADN double brin linéaire englobé dans une capside icosaèdrale de 125 nm, une couche de protéine appelée tégument, et une enveloppe lipidique dérivée de l'hôte dans laquelle les glycoprotéines virales sont ancrées. Le tégument est un réseau très dense et très complexe comprenant des milliers de copies de protéines de différentes tailles qui relient structurellement l'enveloppe virale à la capside. Ces protéines multifonctionnelles remplissent plusieurs fonctions importantes tout au long du cycle viral. Elles sont impliquées dans le transport des capsides entrantes jusqu'aux pores nucléaires, la maturation et la sortie des particules virales nouvellement formées ainsi que l'acquisition de l'enveloppe finale. Les protéines du tégument ont été largement étudiées dans le but de déterminer leurs rôles dans l'infection et la virulence. Cependant, étant limitées par les techniques conventionnelles, toutes ces études considèrent que l'ensemble de la population virale est responsable du phénotype de l'infection sans tenir compte de l'hétérogénéité possible des protéines tégumentaires entre les particules virales et son impact sur l'infectiosité.

Après la fusion de l'enveloppe virale avec la membrane plasmique conduisant à l'entrée du virus, le génome viral est livré au noyau, où il se réplique afin d'amorcer l'assemblage des nouvelles capsides. À ce stade, quatre espèces distinctes de capsides non eveloppées sont présentes. Les procapsides thermodynamiquement instables, les capsides A et B qui ne parviennent pas à incorporer correctement le génome viral, et les capsides C qui incorporent le génome viral et formeront finalement des virions enveloppés matures. Ces capsides peuvent être distinguées les

unes des autres sur la base de leurs composition (ADN et protéines) ainsi que de leur apparence en microscopie électronique. Les capsides A et B sont considérées comme abortives et seuls les C-capsides matures peuvent traverser les deux membranes nucléaires par un mécanisme d'enveloppement / dé-enveloppement et sont finalement réenveloppées dans le TGN. L'acquisition de la couche de tégument est supposée se faire de façon séquentielle du noyau au TGN en passant par le cytoplasme. Cette acquisition est favorisée par un réseau très complexe d'interactions protéiques impliquant la capside et les protéines du tégument. Cependant, la séquence exacte d'addition de ces protéines est encore mal définie.

Dans le premier article présenté dans cette thèse et qui a été publié dans *Journal of Virology*, nous avons analysé la teneur en protéines tégumentaires des particules individuelles du virus de l'herpès simplex 1 en utilisant une approche innovatrice de cytométrie en flux que nous avons développée en laboratoire. Nos données confirment que si certaines protéines virales sont incorporées en quantités contrôlées, d'autres varient considérablement. Ces résultats nous ont également permis de mettre en évidence l'existence d'une corrélation entre l'abondance de protéines tégumentaires spécifiques et l'infectiosité du virus.

Dans le deuxième article, l'emploi de la virométrie en flux nous a également permis non seulement d'analyser les capsides nucléaires, mais aussi d'enrichir la pureté des capsides C. Et pour la première fois, on a été capable d'analyser trois types de capsides nucléaires (A, B et C) par spectrométrie de masse et de déterminer leur composition protéique globale. Ceci appuie fortement la doctrine selon laquelle l'acquisition du tégument démarre hâtivement au niveau du noyau et soutient l'implication probable de ces protéines dans l'enveloppement primaire des capsides. Nous avons également découvert la présence de protéines de l'hôte associées aux capsides.

Mots-clés : VHS-1, capsides nucléaires, tégument, cytométrie de flux, virométrie de flux, spectrométrie de masse, protéomique, infectiosité.

Abstract

Herpes simplex virus type 1 (HSV-1) is a highly contagious infectious agent that constitutes a real global health problem and can cause many pathologies ranging from cold sores to encephalitis and systemic disease in newborns. The virus is composed of 4 distinct structural components: a linear double-stranded DNA viral genome encompassed within a 125 nm icosahedral capsid, a layer of protein called the tegument, and a host-derived lipid envelope in which the viral glycoproteins are anchored. The tegument is a very dense and very complex network comprising thousands of proteins of different sizes that structurally bridge the viral envelope to the capsid. These multifunctional proteins perform several important functions throughout the viral cycle. They are involved in transport and targeting of incoming capsids to nuclear pores, maturation and egress of newly made viral particles, and the acquisition of the final envelope. Tegument proteins have been extensively studied to determine their roles in infection and virulence. However, being limited by conventional techniques, all these studies consider the entire viral population to be responsible for the infectious phenotype without considering the possible heterogeneity of specific tegument proteins among viral particles and its effect on infectivity.

Following fusion of the viral envelope with the plasma membrane leading to entry of the virus, the viral genome is delivered to the nucleus, where it replicates and leads to the assembly of new capsids. Here, four distinct nonenveloped capsid species are present. The thermodynamically unstable procapsids, the A-capsids that fail to properly incorporate the viral genome, the B-capsids that also lack viral DNA and the C-capsids that incorporate the viral genome and ultimately form mature enveloped virions. Those capsids can be distinguished from each other based on their composition (DNA and proteins) contents and their appearance in electron microscopy. A- and B-

capsids are considered to be abortive and only mature C-capsids can travel across the two nuclear membranes by an envelopment/de-envelopment mechanism and are ultimately re-enveloped in the TGN. The acquisition of the tegument layer is believed to be sequential from the nucleus to the TGN via the cytoplasm. This acquisition is favored by a very complex network of protein interactions involving the capsid and the proteins of the tegument. However, the exact sequence of addition of these proteins is still poorly defined.

The first paper presented in this thesis has been published in Journal of Virology. Here, we analyzed the protein content of individual herpes simplex virus 1 particles using an innovative flow cytometry approach we developed in the laboratory. Our data confirm that while some viral proteins are incorporated in controlled amounts, others vary substantially. We also highlighted the correlation between the abundance of specific tegument proteins and the infectivity of the virions.

In the second paper, the use of flow virometry enabled us not only to analyze the nuclear capsids, but also to increase the purity of C-capsids. And for the first time, we were able to analyze three types of nuclear capsids (A, B and C) by mass spectrometry and determine their overall protein composition. These observations strongly support the hypothesis that acquisition of the tegument proteins starts early at the nucleus and support the likely involvement of these proteins in the primary envelopment of the capsids. We also noted the presence of host proteins associated with capsids.

Keywords : HSV-1, nuclear capsids, tegument, flow cytometry, flow virometry, mass spectrometry, proteomics, infectivity.

Table des matières

Liste des tableaux

Tableaux pour Article 1

Tableaux pour Article 2

Liste des figures

Figures pour Article 1

Figures pour Article 2

Liste des abréviations

Abréviation	Appellation en français	Appellation en anglais
3-OS HS	3-O-sulfate d'héparane sulfaté	3-O sulfated heparan sulfate
ADN	Acide désoxyribonucléique	Deoxyribonucleic acid (DNA)
ADNase	Désoxyribonucléase	Deoxyribonuclease (DNase)
AIHV-1	Herpèsvirus alcélaphin 1	Alcelaphine herpesvirus 1
ARN	Acide ribonucléique	Ribonucleic acid (RNA)
ARNase	Ribonucléase	Ribonuclease (RNase)
ARNm	ARN messager	Messenger RNA (mRNA)
av. J.-C.	Avant Jésus-Christ	Before Christ
CVSC	Composant spécifique du vertex de la capside	Capsid vertex specific component
Da/kDa	Dalton/ Kilodalton	Dalton/ Kilodalton
DTT	Dithiothréitol	Dithiothreitol
dUTPase	Désoxyuridine triphosphatase	Deoxyuridine triphosphatase
EBV	Virus d'Epstein-Barr	Epstein-Barr virus
EM	Microscopie électronique	Electron microscopy
EMA	Agence européenne des médicaments	European Medicine Agency
ESCRT	Complexe de tri endosomal requis pour le transport	Endosomal sorting complex required for transport
ESI	Ionisation par électrospray	Electrospray ionization
FACS	Tri par cytométrie en flux	Fluorescence activated cell sorter
FBS	Sérum fœtal bovin	Fetal bovine serum
FDA	Agence de certification des aliments et des médicaments	Food and Drug Administration
FSC	Lumière diffractée mesurée en face	Forward scatter
GAPDH	Glycéraldéhyde-3-phosphate déshydrogénase	Glyceraldehyde 3-phosphate dehydrogenase
gB/gC/gD	Glycoprotéine B (ou C, D, etc.)	Glycoprotein B (or C, D, etc.)
Gène E	Gène précoce ou gène β	Early gene
Gène IE	Gène très précoce ou gène α	Immediate early gene
Gène L	Gène tardif ou gène ϒ	Late gene
GFP	Protéine fluorescente verte	Green fluorescent protein
GM-CSF	Facteur stimulant les colonies de granulocytes et de macrophages	Granulocyte-macrophage colony-stimulating factor
HCMV	Cytomégalovirus humain	Human cytomegalovirus
HHV-6A	Virus herpès humain de type 6A	Human herpesvirus 6A
HHV-6B	Virus herpès humain de type 6B	Human herpesvirus 6B
HHV-7	Virus herpès humain de type 7	Human herpesvirus 7

Abréviation	Appellation en français	Appellation en anglais
hpi	Heures post-infection	Hours post-infection
HVEM	Médiateur de l'entrée du virus herpès simplex	Herpes virus entry mediator
ICP	Protéine de cellule infectée	Infected cell protein
ICTV	Comité international de taxonomie des virus	International Committee on Taxonomy of Viruses
IR_L	Séquence répétée interne de la séquence unique longue	Internal repeat long
IR_S	Séquence répétée interne de la séquence unique courte	Internal repeat short
KSHV	Virus herpès associé au sarcome de Kaposi	Kaposi's sarcoma-associated herpesvirus
LAT	Transcrit associé à la latence	Latency associated transcript
m/z	Rapport masse/charge	Mass-to-charge ratio
MALDI	Désorption-ionisation laser assistée par matrice	Matrix-assisted laser desorption/ionization
MCMV	Cytomégalovirus murin	Murine cytomegalovirus
MDa	Mégadalton (10^6 daltons)	Megadaltons (10^6 daltons)
MES	Acide morpholino-4-éthane sulfonique	4-Morpholineethanesulfonic acid
MHV68	Virus herpès gamma murin 68	Murine gammaherpesvirus 68
miARN	MicroARN	MicroRNA(miRNA)
MNE	Membrane nucléaire externe	Outer nuclear membrane (ONM)
MNI	Membrane nucléaire interne	Inner nuclear membrane (INM)
MNT	Tampon MES, NaCl et Tris	Buffer MES, NaCl and Tris
MOI	Multiplicité d'infection	Multiplicity of infection
MP	Membrane plasmique	Plasma membrane
MS/MS	Spectrométrie de masse en tandem	Tandem mass spectrometry
MVB	Corp multivésiculaire	Multivesicular body
ND10	Domaine nucléaire 10	Nuclear domain 10
NEC	Complexe de sortie nucléaire	Nuclear egress complex
NEM	N-Éthylmaléimide	N-Ethylmaleimide
NPC	Complexes de pores nucléaires	Nuclear pore complexes
nt	Nucléotide	Nucleotide
ORF	Cadre de lecture ouvert	Open reading frame
ori	Origine de réplication	Origin of replication

Abréviation	Appellation en français	Appellation en anglais
ori_L	Origine de réplication de la séquence unique longue	Origin of replication of the unique long region
ori_S	Origine de réplication de la séquence unique courte	Origin of replication of the unique short region
pb / kpb	Paire de bases / kilopaire de bases	Base pair / Kilo base pair
PBS	Tampon phosphate salin	Phosphate-buffered saline
PCR	Réaction de polymérase en chaîne	Polymerase chain reaction
PILRα	Récepteur α couplé à l'immunoglobuline de type 2	Paired immunoglobulin-like type 2 receptor-α
PKC	Protéine Kinase C	Protein Kinase C
PM	Poids moléculaire	Molecular weight (MW)
PML	Protéines de la leucémie pro-myélocytaire	Promyelocytic leukemia protein
pré-miARN	MicroARN précurseur	Precursor microRNA (pre-miRNA)
pri-miARN	MicroARN primaire	Primary microRNA (pri-miRNA)
PRV	Virus de la pseudorage	Pseudorabies virus
pU_LX ou pU_SX	Protéine codée par le gène U_LX ou U_SX	Protein encoded by U_LX or U_SX gene
qPCR	Réaction de polymérase en chaîne quantitative	Quantitative polymerase chain reaction
RE	Réticulum endoplasmique	Endoplasmic reticulum (ER)
RRV	Rhadinovirus de singe Rhésus	Rhesus Monkey Rhadinovirus
SD	Écart-type	Standard Deviation
SIDA	Syndrome d'immunodéficience acquise	Acquired immunodeficiency syndrome
siRNA	Petits ARN interférents	Small interfering RNA
SNC	Système nerveux central	Central nervous system
SSC	Lumière diffractée mesurée sur le côté	Side scatter
TGN	Réseau *trans*-golgien	Trans-Golgi network
TK	Thymidine kinase	Thymidine kinase
TNF-α	Facteur de nécrose tumorale alpha	Tumor necrosis factor alpha
TR_L	Séquence répétée terminale de la séquence unique longue	Terminal repeat long
TR_S	Séquence répétée terminale de la séquence unique courte	Terminal repeat short
U_L	Séquence unique longue	Unique long region
U_S	Séquence unique courte	Unique short region
VHS-1	Virus Herpès simplex de type 1	Herpes simplex virus 1
VHS-2	Virus Herpès simplex de type 2	Herpes simplex virus 2
vhs	Virion host shutoff	Virion host shutoff
VIH	Virus de l'immunodéficience humaine	Human immunodeficiency virus (HIV)
VZV	Virus varicelle-zona	Varicella-zoster virus

À ma très chère maman, ce travail te doit beaucoup… Qu'il soit pour toi le témoignage de mon infinie reconnaissance pour ces années de compréhension, de privations et d'efforts communs.

À mon frère et à mes sœurs, tout étonnés que leur petit frère ait enfin terminé « son Doctorat ».

À mon regretté père qui serait content d'apprendre que son fils a enfin terminé le travail qu'il avait commencé.

À mes regrettés grands-parents et ma regrettée tante Mina qui nous ont quittés pendant que je préparais cette thèse.

Remerciements

En tout premier lieu, je remercie le Bon Dieu, tout puissant, de m'avoir donné le courage pour mener ce projet de thèse à terme, ainsi que la force pour dépasser tous les moments difficiles.

Tout au long de ces années de thèse, j'ai eu le grand privilège de rencontrer de nombreuses personnes. Je ne saurais pas les citer toutes sans dépasser le nombre de pages raisonnablement admis. Je reconnais que chacune a, à des degrés divers, mais avec une égale bienveillance, apporté une contribution positive à la finalisation de ce travail. Mes dettes de reconnaissance sont, à ce point de vue, énormes à leur égard.

Je pense particulièrement à mon directeur de recherche **Dr. Roger Lippé** qui m'a agréablement accueilli dans son laboratoire, m'a encadré, et offert la chance d'évoluer au sein de son laboratoire. Ses remarques successives m'ont permis d'améliorer les différentes versions de ce travail, d'une part, et de sculpter l'esprit critique indispensable dans le monde de la recherche scientifique, d'autre part. Il a toujours trouvé le juste équilibre entre la liberté qu'il m'a laissé dans le choix des grandes orientations et dans la détermination des pistes à suivre. Son perfectionnisme et son abnégation sont un modèle à suivre.

Mes remerciements vont aussi au **Dr. Guy Lemay**, à la **Dre. Carolina Alfieri** et au **Dr. Patrick Labonté** d'avoir bien voulu accepter de juger ce travail sans oublier **Dr. Pierre-Yves Lozach** et **Dr. Dorin-Lucian Ghitescu** pour m'avoir fait l'honneur de participer en tant que membres de mon comité de parrainage. Qu'ils veuillent bien accepter ma sincère considération.

Mes remerciements aussi à tous les membres du laboratoire, passés et présents. Merci à **Johanne**, pour son aide précieuse. Merci à **Daniel**, **Sandra**, et **Kerstin**, d'avoir participé à l'optimisation de

plusieurs techniques indispensables à ce travail. Et merci à **Diane Gingras** pour sa précieuse collaboration en microscopie électronique.

Je remercie particulièrement **Imane**, **Mohamed**, **Ahmed**, et **Younes**, pour leur engagement, leur patience ainsi que leur disponibilité à mon égard.

Je tiens également à remercier et exprimer toute ma reconnaissance à la **Dre. Oudghiri Mounia**, et au **Dr. Abdellah Naya**, pour m'avoir initié à la recherche durant ma Maîtrise à la faculté de sciences de Casablanca au Maroc.

Je remercie du fond de mon cœur mon oncle **Khalid**, et sa femme **Aicha**, pour tout ce qu'ils ont fait pour moi depuis que j'ai décidé de m'installer au CANADA. Que le Bon Dieu protège mes adorables cousines, **Salma**, **Aya** et **Yasmine**.

Je ne saurai terminer sans exprimer ma reconnaissance envers ma femme et mon âme sœur **Madiha**, pour l'amour et la tendresse qu'elle m'offre. Je la remercie de faire partie de ma vie ainsi que de l'embellir.

Un grand merci à mon grand frère **Rachid**, pour tous les sacrifices à l'égard de mes sœurs et moi-même. Merci à ma sœur **Khadija**, pour ses encouragements et ses prières. Merci à ma sœur **Karima**, également pour ses encouragements et ses prières. Que le Bon Dieu protège mes adorables neveux, **Achraf**, et **Hib**.

Mes derniers et énormes remerciements sont dédiés à ma très chère **maman**, tu es mon étoile, ma vie. Tu es ma force, mon courage celle qui fait de moi une bonne personne dans ce monde. Je ne saurai te remercier pour tout ce que tu as fait pour moi. Merci pour tes encouragements, tes prières et l'immense amour que tu me procures. Je t'aime **maman**

Chapitre I - Introduction

Bien que l'existence des virus n'ait été montrée qu'à la fin du 19ème siècle, la virologie possède une histoire remarquable. Avant que le terme « virus » ne soit adopté, ces organismes étaient d'abord reconnus comme étant des « agents filtrables » submicroscopiques, différents de la bactérie et pouvant être la cause de la maladie de la mosaïque du tabac (1). Les maladies virales ont façonné l'histoire et l'évolution de la vie sur terre et au cours des dernières décennies, nos connaissances se sont accrues de façon exponentielle grâce à la culture cellulaire et virale. Ainsi, de nombreux concepts et outils de la biologie moléculaire et de la biologie cellulaire ont été dérivés de l'étude des virus et de leurs cellules hôtes.

Le virus Herpès simplex de type 1 (VHS-1) est l'agent responsable de plusieurs pathologies allant des moins graves - dont les lésions orolabiales, plus connues sous le nom des feux sauvages – aux plus sérieuses telles que les encéphalites, les kératites ou même encore la paralysie de Bell. Ainsi, pour être capable de dominer ces maladies, il faut être en mesure de bien maîtriser le cycle de réplication viral. Cependant, bien que plusieurs recherches aient apporté considérablement de la lumière quant au cycle viral, beaucoup de questions se posent encore concernant la sortie des capsides du noyau ainsi que le processus d'acquisition des protéines du tégument qui relient la capside à l'enveloppe virale. *Ipso facto*, la caractérisation de la composition précise des capsides nucléaires peut ainsi être informative à cet égard afin de déterminer où et quand est-ce que chaque composant du tégument est recruté sur les capsides virales. Aussi, l'étude de l'importance de la quantité relative des protéines tégumentaires et son impact sur l'infectiosité permet d'évaluer directement la pertinence biologique de la variabilité des protéines entre les virions individuels. Les travaux de recherche présentés dans cette thèse de doctorat contribuent significativement à la résolution de ces problèmes.

I.1 Le virus herpès simplex de type 1 (VHS-1)

I.1.1 Historique

Le virus herpès simplex a une histoire remarquablement digne d'intérêt. Bien qu'il ne soit pas exactement connu par qui et quand il a été découvert jusqu'aujourd'hui, le virus herpès simplex est l'un des pathogènes les plus anciens connues de l'homme et avec lequel il a co-évolué pendant des milliers d'années. Il semblerait que tout a commencé il y a 2500 à 3000 ans avant Jésus-Christ (av. J.-C) lorsque des lésions ressemblant à celles causées par le VHS-1 auraient été décrites sur une tablette sumérienne (2, 3) puis sur le papyrus d'Ebers (vers 1500 avant J.-C.)(4). En Grèce antique durant le siècle de Périclès (5ème siècle avant Jésus-Christ) lorsque le père de la médecine Hippocrate utilisa le mot grec *herpes* qui signifie ramper pour la description des lésions et des plaies cutanées qui semblent diffuser le long de la surface de la peau (2, 3, 5-8). Quelques siècles plus tard, l'empereur romain Tibère interdit les échanges de baisers pendant toutes les cérémonies, les évènements publics et les rituels afin de freiner la propagation de l'épidémie de l'herpès de la bouche (9) et un médecin de la même époque nommé *Celsus* (Celse en français) suggéra de cautériser les plaies causées par l'herpès avec du fer chauffé au rouge (10-12).

L'histoire de l'herpès reprend de l'ampleur durant les derniers siècles avec l'émergence de nouvelles définitions tantôt confuses tantôt claires, mais reconnaissant toutes différents types d'herpès (5). Ainsi, à la fin du 17ème siècle, le médecin anglais Richard Morton décrit les boutons de fièvre (*herpes fibrilis*) comme étant de l'herpès (2, 5, 13) puis un autre médecin anglais du 18ème siècle nommé Daniel Turner écrivit le premier livre en langue anglaise entièrement consacré à la dermatologie (14) et dans lequel il qualifie l'herpès de « pustule cholérique qui éclate de la peau » et distingue par conséquent plusieurs types d'herpès (2, 5, 15). Quelques années plus tard, John Astruc étant le médecin du roi Louis XV s'intéressa dans une étude à

examiner des prostituées sous surveillance médicale et publia son traité sur les maladies vénériennes (*De Morbis Veneris*) dans lequel il mit en évidence la relation directe entre l'herpès et les organes génitaux devenant ainsi le premier à décrire l'herpès génital (2, 3, 16). Au 19ème siècle Thomas Bateman reconnait quelques types de lésions à herpès et les décrit comme étant « des lésions récurrentes caractérisées toutes par une ou plusieurs petites vésicules superficielles localisées sur la peau qui guérissent spontanément dans les dix ou douze jours » (2, 6, 17-20) et Paul Gerson Unna quelques années plus tard donna une description plus claire sur l'aspect récurrent de l'herpès génital spécifiquement sur les femmes (21). Presque dans la même période, le dermatologue français Jean-Baptiste Émile Vidal démontra que l'infection pourrait être transmissible d'une personne à une autre (2). Puis les premiers livres sur le diagnostic et le traitement de l'herpès génital voient le jour par Diday en premier puis Fournier par la suite (2, 22, 23).

Le 20ème siècle se démarque par le début de l'expérimentation sur l'herpès spécifiquement en Allemagne avec l'émergence de nouvelles techniques d'isolation et d'analyse et l'utilisation de modèles animaux. Ainsi, l'ophtalmologue allemand Wilhelm Grüter a démontré que l'agent causant les infections herpétiques pourrait être cultivé dans les embryons de lapin et de poulet en mettant le point sur la possibilité de transmettre le virus d'une personne infectée à la cornée d'un lapin développant ainsi le premier test pour le diagnostic de l'herpès « le test de Grater » (2, 24, 25). Dans les années 1930, Andrews et Carmichael ont constaté la présence d'anticorps spécifiques au virus de l'herpès dans le sérum de patients adultes ayant déjà contracté le virus et que seuls ces patients pouvaient avoir des récidives d'infections (2, 3, 26, 27). Cette notion de récurrence chez les patients possédant des anticorps poussa Robert Doerr à admettre que l'infection chez ces patients était due à des agents infectieux endogènes produits sous l'effet de certains stimuli (2, 3, 28). Ainsi, les premières hypothèses sur la latence du virus de l'herpès a vu le jour en 1939 par le virologiste australien

Burnet, Frank Macfarlane et son collègue pédiatre Williams Stanley qui ont confirmé la persistance de l'herpès chez les personnes infectées et sa capacité à se réactiver symptomatiquement (2, 29). Et ce n'est qu'en 1971 que l'hypothèse de la latence sera prouvée par les deux scientifiques Jack Stevens et Marjorie Cook dans leur étude publiée dans Science (30). D'autres membres de la famille des Herpesviridae - pouvant causer d'autres types de maladies avec des complications distinctes - ont pu être isolés grâce au développement et la maîtrise de la culture cellulaire notamment l'isolation du virus Epstein-Barr (EBV) à partir de culture de cellules lymphomateuses d'un lymphome de Burkitt et celle des herpèsvirus humain 6A (HHV-6A), 6B (HHV-6B), 7 (HHV-7) et 8 (HHV-8) à partir de culture de lymphocytes T (2, 31-37). La plupart des médecins croyaient que toutes les infections herpétiques étaient causées par un seul virus, mais le médecin allemand Bernard Lipschutz avait une autre vision et suggéra en 1921 que l'herpès oral et l'herpès génital étaient causés par des virus différents (27). Cependant, il fallait attendre près de deux décennies pour que l'allemand Karl Schneweis et son collègue André Nahmias découvrent qu'il existait deux virus de l'herpès simplex distincts : l'herpès simplex de type I (VHS-1), responsable des lésions dans la région labiale et le virus herpès de type II (VHS-2) responsable des lésions dans les organes génitaux (2, 27, 38). Les recherches sur l'herpès s'accentuent donnant ainsi plus d'informations quant à la structure, l'architecture et la composition en protéines des particules virales (39-50). En même temps, la recherche sur des agents antiviraux commença à voir le jour par le développement du vidarabine qui était capable de réduire la mortalité chez les personnes atteintes d'encéphalites, mais en même temps difficile à administrer et accompagné de toxicité (2, 51). En 1977, la biochimiste Gertrude Elion développa l'Aciclovir : un nouveau médicament antiviral efficace et non toxique cette fois-ci (2, 52-54). La compréhension du cycle viral du VHS-1 et le développement des techniques de biologie moléculaire poussent les chercheurs à exploiter l'aspect infectieux du virus ainsi que les avantages que procure la manipulation de son génome pour le considérer

comme un nouvel agent thérapeutique susceptible de cibler spécifiquement des types cellulaires démontrant ainsi un grand potentiel quant à son utilisation comme agent immuno-prophylactique ou vecteur pour la thérapie génique (2, 55-58). La recherche sur le virus herpès simplex se poursuit toujours afin de mieux comprendre le cycle viral et de développer un vaccin capable de nous protéger des infections, mais aussi pour l'utiliser de façon plus large tel un virus oncolytique dans le traitement de différents types de cancers. Récemment, l'agence Américaine de certification des aliments et des médicaments « *Food and Drug Administration* » (FDA) ainsi que l'Agence européenne des médicaments « *European Medicine Agency* » (EMA) ont officiellement approuvé l'utilisation du Talimogène laherparépvec (T-VEC, aussi connu sous le nom OncoVEXGM-CSF) chez les patients atteints de mélanome (59). Le virus OncoVEXGM-CSF est une souche génétiquement modifiée de VHS-1 obtenu en supprimant de manière fonctionnelle 2 gènes codent pour 2 facteurs de neurovirulence (ICP34.5 et ICP47) et en insérant une cassette codant pour le facteur stimulant les colonies de granulocytes et de macrophages humains « *Granulocyte-macrophage colony-stimulating factor* » (GM-CSF) (59-61). Ces modifications génétiques permettent au virus d'établir une infection productive dans les cellules malignes (mais pas dans les cellules normales) et de favoriser le recrutement et l'activation des cellules présentatrices d'antigènes, permettant ainsi au virus de favoriser l'initiation d'une réponse immunitaire ciblant la tumeur (59-61).

I.1.2 Classification et famille des Herpesviridae

La taxonomie des herpèsvirus a été réalisée pour la première fois par le Comité international sur la taxonomie des virus (ICTV) lors de son premier rapport en 1971 (62). Cette taxonomie reposait principalement sur les caractères morphologiques distinctifs des herpèsvirus à savoir un cœur d'une seule copie d'ADN linéaire double brin de 125-295 kilopaires de bases (kpb) empaqueté à une haute densité dans une capside icosaèdrale de 100-130 nm, une couche

de protéines appelée tégument entourant la capside et une enveloppe lipidique dans laquelle des glycoprotéines virales sont ancrées (63-67).

Tous les herpèsvirus étaient groupés au départ dans une seule et même famille des *Herpesviridae.* Cependant, au fur et à mesure que la classification s'est développée avec l'exploitation des résultats de séquençage de l'ADN viral, il était clair que les herpèsvirus de poissons sont marginalement liés à ceux des mammifères, des oiseaux et des reptiles (65, 67, 68). Ces nouvelles données ont conduit à la révision de cette classification par le Comité international sur la taxonomie des virus et l'adoption de l'ordre *Herpesvirales* (64, 67). Cet ordre est divisé en trois familles liées phylogénétiquement infectant un large éventail d'hôtes. La famille des *Alloherpesviridae* comprend des virus infectant les poissons et les amphibiens (69). La famille des *Herpesviridae* comprend des virus infectant les mammifères, les oiseaux ou les reptiles (70). Enfin, La famille *Malacoherpesviridae* comprend des virus infectant les mollusques bivalves (71) (Figure 1).

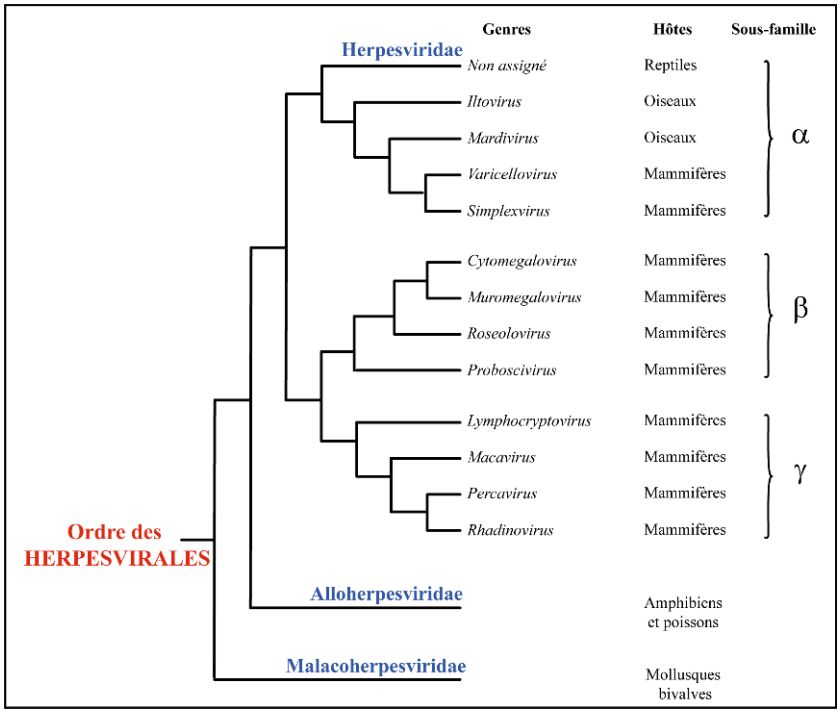

Figure 1: Principales relations phylogénétiques et sous-unités taxonomiques au sein de l'ordre Herpesvirales.

Adapté de Fields Virology **(66).**

La famille des Herpesviridae est de loin la plus importante des herpèsvirus, tant par la grande diversité de ses membres que par le nombre d'études qui leur a été consacré. Ainsi, cette famille regroupe trois sous-familles : *Alphaherpesvirinae*, *Betaherpesvirinae* et *Gammaherpesvirinae*.

La sous-famille des *Alphaherpesvirinae* regroupe des virus ayant un large spectre d'infection avec un cycle viral relativement court. Ils sont capables d'infecter plusieurs lignées cellulaires *in vitro* et de se propager rapidement en culture cellulaire induisant une lyse très efficace des cellules infectées et sont aussi capables d'induire une infection latente principalement et non exclusivement au niveau des ganglions sensoriels (66). Cette sous-famille comprend quatre genres à savoir *Simplexvirus*, *Varicellovirus*, *Mardivirus*, *Iltovirus* et quelques autres virus infectants des reptiles n'appartenant à aucun de ces genres (64, 66, 70).

La sous-famille des *Betaherpesvirinae* regroupe des virus caractérisés principalement par le nombre restreint de cellules qu'ils peuvent infecter et un cycle réplicatif plus lent (plus que 7 jours) et une progression lente en culture cellulaire, mais surtout leur pouvoir à entraîner un élargissement de la taille des cellules infectées (cytomégalie) (66). Ils sont aussi capables d'induire une infection latente dans les glandes sécrétoires, les cellules lymphoréticulaires, les cellules rénales et d'autres tissus. Cette sous-famille comprend quatre genres à savoir *Cytomegalovirus*, *Muromegalovirus*, *Proboscivirus* et *Roseolovirus* (64, 66, 70).

La sous-famille des *Gammaherpesvirinae* regroupe des virus caractérisés aussi par un nombre restreint d'hôtes qu'ils peuvent infecter. Ils sont tous capables de se répliquer dans les cellules lymphoblastiques *in vitro* tandis que quelques-uns seulement peuvent induire une infection lytique dans des lignées cellulaires fibroblastiques ou épithéliales et selon le genre, ils peuvent infecter les lymphocytes T et B et induire des infections latentes dans les tissus

lymphoïdes (66). Cette sous-famille comprend quatre genres à savoir *Lymphocryptovirus*, *Macavirus*, *Percavirus* et *Rhadinavirus*. Certains virus de cette sous-famille se distinguent par leur pouvoir oncogène (KSHV) (64, 66, 70).

La famille des *Herpesviridae* regroupe aujourd'hui plus de 200 virus différents dont seulement neuf sont connus pour causer des maladies chez les humains, c'est pourquoi on les qualifie de virus herpétiques humains (HHV) (72). Dans la sous-famille des *Alphaherpesvirinae,* on retrouve les deux virus herpétiques humains 1 et 2 (HHV-1 et HHV-2) plus connus sous les noms de virus herpès simplex de type 1 et 2 (VHS-1 et VHS-2) causant l'herpès buccal et l'herpès génital respectivement. On retrouve aussi le virus herpétique humain 3 (HHV-3) plus connu sous le nom de virus varicelle-zona (VZV) causant la varicelle et le zona (66, 72). Dans la sous-famille des *Betaherpesvirinae* on retrouve les virus herpétiques humains 5, 6A, 6B et 7 (HHV-5, HHV-6A, HHV-6B, et HHV-7). Le HHV-5 est plus connue sous le nom de cytomégalovirus (CMV) causant plusieurs infections opportunistes chez les personnes immunodéprimées. Les HHV-6A, HHV-6B et HHV-7 sont phylogénétiquement plus proches et causent la roséole (66, 72). Dans la sous-famille des *Gammaherpesvirinae*, on retrouve les virus herpétiques humains 4 et 8 (HHV-4 et HHV-8) plus connus sous les noms de virus d'Epstein-Barr (EBV) et herpèsvirus associé au sarcome de Kaposi (KSHV) respectivement. Le virus d'Epstein-Barr (EBV) cause la mononucléose infectieuse hétérophile-positive alors que l'herpèsvirus associé au sarcome de Kaposi (KSHV) cause le sarcome de Kaposi et d'autres lymphomes des cavités corporelles (66, 72) (Tableau 1).

Sous-famille Genre	Nom Commun	Nom alternatif	Manifestations cliniques
Alphaherpesvirinae			
Simplexvirus	Virus Herpès Simplex de type 1 (VHS-1)	HHV-1	Infections orolabiales, infection oculaire et encéphalites
	Virus Herpès Simplex de type 2 (VHS-2)	HHV-2	Lésions génitales et anales et infections néonatales
Varicelovirus	Virus Varicelle-zona (VZV)	HHV-3	Varicelle et zona
Betaherpesvirinae			
Cytomegalovirus	Cytomégalovirus (HCMV)	HHV-5	Mononucléose, rejet de greffe et rétinite
Roseolovirus	Herpesvirus humain 6 A/B (HHV-6A, HHV-6B)	-	Roséole, encéphalite, mononucléose, pneumonie, néoplasie et sclérose
	Herpesvirus humain 7 (HHV-7)	-	Roséole, encéphalite, mononucléose et syndrome de fatigue chronique
Gammaherpesvirinae			
Lymphocryptovirus	Virus d'Epstein-Barr (EBV)	HHV-4	Mononucléose, lymphome de Burkitt
Rhadinovirus	Virus Herpès associé au Sarcome de Kaposi (KSHV)	HHV-8	Sarcome de Kaposi, Hyperplasie géante

Tableau 1: Principales manifestations cliniques associées aux virus de la famille des Herpesviridae.

Adapté de Fields Virology (66).

I.1.3 Épidémiologie et pathologies associées au virus herpès simplex de type 1

I.1.3.1 Épidémiologie

Le VHS-1 est un agent infectieux hautement contagieux et endémique constituant un véritable problème de santé mondiale. On compte actuellement plus de 3,7 milliards de personnes de moins de 50 ans, soit 67% de la population mondiale qui sont infectées par le VHS-1 avec une haute prévalence en Afrique et au sud-est de l'Asie (72, 73). La transmission se fait principalement par le contact direct avec les surfaces muqueuses d'une personne portant le virus à une personne saine (73). Les personnes portant le virus sont souvent asymptomatiques lors de la période de la latence, mais peuvent cependant présenter des périodes de réactivation accompagnées par des manifestations de sévérité variable (74). Toutefois, dans certains cas les infections au VHS-1 conduisent à des pathologies pouvant avoir une atteinte à la vie de la personne.

I.1.3.2 Pathologies associées au virus herpès simplex de type 1

I.1.3.2.1 Herpès néonatal

L'herpès néonatal est la conséquence clinique directe la plus grave de l'infection par le VHS-1. Il résulte habituellement d'une exposition au VHS-1 ou VHS-2 dans le tractus génital pendant l'accouchement, bien que des infections *in utero* et postnatales puissent survenir. L'herpès néonatal a une mortalité élevée, avec un taux de létalité estimé à 60% sans traitement. La morbidité est également élevée, souvent sous la forme d'incapacités neurologiques à long terme, quel que soit le traitement (75, 76). À l'échelle mondiale, environ 14 000 cas d'herpès néonatal ont été signalés chaque année entre 2010 et 2015 (75, 76). Les estimations globales pourraient sous-estimer le nombre de cas dans les milieux à faibles ressources, où les taux de césariennes peuvent être plus faibles et où la prévalence du VIH est plus élevée (76).

I.1.3.2.2 Herpès oculaire

Les infections de l'œil par le VHS-1 sont la principale cause de cécité cornéenne infectieuse dans les pays développés (77). Environ 500 000 personnes aux États-Unis sont actuellement infectées par le VHS oculaire (77-79). Les infections peuvent survenir dans les segments antérieurs et postérieurs de l'œil (blépharite, conjonctivite), mais le plus souvent l'épithélium cornéen (Kératite) ou même l'iris (iridocyclite) (77, 78). Alors que la plupart des infections sont unilatérales, environ 1,3% à 12% des personnes touchées ont des infections oculaires bilatérales. Les infections bilatérales sont surtout observées chez les patients immunocompromis (77-79). Dans certains cas de réactivation, les lésions sont tellement importantes qu'elles provoquent une détérioration de la cornée nécessitant l'intervention chirurgicale ou même la greffe d'une nouvelle cornée (77-79).

I.1.3.2.3 Herpès mucocutané

Les boutons de fièvre également connus sous le nom de feu sauvage sont les manifestations cliniques les plus marquantes des infections par le VHS-1. Le contact intime entre une personne qui excrète activement le virus et un individu qui est susceptible est nécessaire pour que l'infection se produise. Le contact doit impliquer une peau abrasée ou des muqueuses. Le virus envahit les cellules épidermiques et dermiques et se déplace vers les neurones sensoriels (ganglion de la racine dorsale) où la latence est établie. Le virus se réactive dans le ganglion trigéminal et se déplace le long des axones pour rejoindre ainsi le site épithélial de l'infection où la réplication virale a lieu. Ce processus entraînant des poussées récurrentes. Les éclosions sont souvent induites par l'exposition à la lumière ultraviolette (lumière du soleil et/ou lits de bronzage), au stress, au rhume, à la fatigue, à la fièvre (d'où le terme "bouton de fièvre"), ou trauma de lèvre. La réactivation se manifeste par un groupe de vésicules sur une base érythémateuse douloureuse autour des lèvres ou même dans d'autres emplacements dans le corps (3, 80).

I.1.3.2.4 Encéphalite herpétique

Le VHS est la cause la plus fréquemment identifiée d'encéphalite aiguë et focale sporadique (81, 82). Sans traitement, la mortalité peut atteindre 70% contre 30% avec un traitement adéquat et des séquelles neurologiques fréquentes, même dans les cas traités (81, 82). On estime qu'environ les deux tiers des cas d'encéphalites à VHS surviennent à la suite d'une réactivation plutôt que d'une infection primaire (81, 82). D'autres manifestations cliniques associées aux encéphalites sont nombreuses et incluent la fièvre, une altération de la conscience, un comportement anormal de même que des désordres neurologiques localisés (81, 82). La prise en charge initiale est difficile, car la thérapie précoce est essentielle dans un contexte où les

infections intracrâniennes graves sont causées presque exclusivement par des espèces bactériennes iatrogènes (81, 82).

I.1.3.2.5 Paralysie de Bell

On pense que la paralysie de Bell est causée par une inflammation du nerf facial au niveau du ganglion géniculé, ce qui entraîne une compression et une ischémie et une démyélinisation possible (83-85). Ce ganglion se trouve dans le canal facial à la jonction des segments labyrinthique et tympanique, où le nerf se courbe brusquement vers le foramen stylomastoïdien. Classiquement, la paralysie de Bell a été définie comme idiopathique, et la cause du processus inflammatoire dans le nerf facial reste incertaine. Récemment, l'attention s'est portée sur l'infection par le VHS-1 comme une cause possible, car la recherche a trouvé des titres élevés du virus ainsi que son ADN dans le liquide endoneurial du nerf facial et du muscle auriculaire postérieur chez des patients atteints de paralysie de Bell pendant la chirurgie décompressive (83-85).

I.1.3.2.6 Maladie d'Alzheimer

La maladie d'Alzheimer est la forme la plus fréquente de trouble neurocognitif majeur sans traitement efficace disponible (86, 87). Les signes pathologiques de l'Alzheimer sont des plaques séniles composées de dépôts de peptides bêta-amyloïdes (Aβ) et d'enchevêtrements neurofibrillaires composés de protéine tau hyperphosphorylée (pTau) dans le cerveau, ainsi que la dégénérescence et la perte de neurones caractérisées par une perte progressive et irréversible de la mémoire et des difficultés d'apprentissage (86, 88-93). C'est la sixième cause de décès aux États-Unis, qui touche principalement les personnes âgées de 65 ans et plus (94). Le nombre de patients est estimé à plus de 46 millions dans le monde et il est prévu que ce nombre atteindra 131,5 millions d'ici 2050 (94). Au Canada, on compte plus de 560 000 personnes atteintes de démence avec près de 25 000 nouveaux cas chaque année (95). Plusieurs recherches récentes

soulèvent un rôle majeur d'infections du système nerveux central dans la maladie d'Alzheimer notamment les infections par le VHS-1(96-101). Des recherches indiquent que le virus est présent sous une forme latente chez une proportion élevée de patients atteints d'Alzheimer et que de l'ADN viral est associé aux plaques amyloïdes (Aβ)(102). La réactivation conduisant à une infection productive caractérisée par une action virale directe et/ou une réponse inflammatoire (103). L'aspect récurrent de la réactivation pourrait avoir un effet cumulatif, menant éventuellement à la maladie d'Alzheimer. Une étude en 2011 a démontré une interaction dynamique entre ces capsides nouvellement formées et la protéine précurseur de l'amyloïde « *Amyloid Precursor Protein* » APP (104). D'autres études ont révélé que le VHS-1 causait le dépôt de β-amyloïde (Aβ) (105-108). La protéine tau serait aussi phosphorylée sous l'effet de VHS-1 pour donner la forme hyperphosphorylée de tau (pTau) dans les neurones de souris infectées ou même des cellules en culture (109-112).

I.1.3.2.7 Herpès et patients immunodéficients ou immunodéprimés

Les infections opportunistes sont plus fréquentes dans les pays en cours de développement, mais surtout chez les personnes souffrant du syndrome d'immunodéficience acquise (SIDA) ou ceux immunodéprimés ayant subi des interventions chirurgicales de greffe d'organes. Parmi ces infections opportunistes, on retrouve celles associées à VHS-1 ou VHS-2 et les interactions entre le VIH et le VHS sont de plus en plus détectables (113, 114). Des manifestations plus graves et systémiques de l'infection à VHS comme l'œsophagite, la méningoencéphalite, l'hépatite, la pneumonie et la nécrose rétinienne, sont toutes capables de se manifester chez les personnes à un stade avancé du SIDA (115, 116). Des études ont montré que la réactivation du VHS-1 active les lymphocytes CD4+ qui deviennent des nouvelles cibles pour le VIH (115, 117). L'infection par le VHS-1 favorise également l'excrétion génitale du VHS-2, qui, à son tour, génère un afflux de cellules T activées qui servent de nouvelles cibles

cellulaires pour la réplication du VIH (115, 118). Chez les receveurs de greffe d'organe, l'acquisition d'une infection au VHS à partir d'un organe transplanté a été rapportée. Ces patients peuvent développer une maladie progressive impliquant les voies respiratoires, l'œsophage ou même le tractus gastro-intestinal. Dans certains cas, l'infection au VHS-1 causait le rejet de greffe de foie (119, 120).

I.1.4 Traitement et prévention

Les infections dues au VHS-1 constituent un problème de santé majeur et ont suscité beaucoup d'intérêt pour le développement de plusieurs thérapies, notamment la chimiothérapie antivirale qui a commencé il y a plus de 40 ans avec le développement du premier agent antiviral démontrant beaucoup de succès chez les personnes souffrant d'encéphalite herpétique. Sauf que l'agent en question (la vidarabin) était à la fois difficile à administrer et accompagné de toxicité (2, 51). Puis un nouvel agent ciblant juste les cellules infectées présentant donc moins de toxicité fut développé en 1977 par la biochimiste Gertrude Elion (52-54). D'autres agents antiviraux plus sélectifs avec un succès incontestable ont vu le jour par la suite. De nos jours, les agents antiviraux utilisés dans la lutte contre le VHS-1 se répartissent en trois catégories : Les analogues nucléosidiques (acyclovir, valacyclovir, penciclovir, famciclovir), les analogues nucléotidiques (cidofovir, adéfovir) et les analogues des pyrophosphates (foscarnet). Toutefois, aucun des agents ne permet l'élimination complète du virus qui ne cesse de développer des mécanismes de résistance lui permettant de les contourner (121, 122).

L'acyclovir (ACV) et ses dérivés d'analogues nucléosidiques sont devenus les médicaments de première ligne pour le traitement des infections à VHS (121, 123, 124). L'ACV est un analogue de la guanosine qui doit être triphosphorylé pour être actif (124). Lors de son entrée dans les cellules infectées, la première étape de phosphorylation est réalisée principalement par la thymidine kinase (TK) codée par le virus ce qui cible spécifiquement les

cellules infectées. Cette étape est suivie par deux phosphorylations supplémentaires réalisées successivement par la GMP kinase et la nucléoside diphosphate kinase cellulaires de l'hôte (125, 126). L'ACV-triphosphate (ACV-TP) agit comme substrat à la réaction de l'ADN polymérase virale (ADN pol) et s'incorpore dans l'ADN à son extrémité 3' empêchant ainsi l'allongement de la chaîne (127-129). *In vitro*, l'ACV est le plus puissant contre le VHS-1 (124). Or, sa limitation majeure réside dans sa biodisponibilité orale relativement faible ce qui a conduit au développement du valacyclovir (VACV) qui est une forme L-valyl-ester d'acyclovir (130). Après administration orale, le VACV est rapidement converti en ACV par hydrolyse de l'ester dans l'intestin grêle augmentant ainsi la biodisponibilité de l'ACV (124, 131). Du fait que l'ACV dépend de la TK virale pour l'activation, on retrouve le développement d'une résistance par l'introduction de mutations dans la TK virale, et dans quelques cas, des mutations dans l'ADN polymérase virale aussi (132, 133).

Contrairement à l'acyclovir, le cidofovir qui est un analogue acyclique de la cytidine 5' monophosphate ne nécessite pas de conversion par la TK pour être transformé en une forme active ciblant ainsi même les souches TK-négatives ou ayant muté la TK pour développer une résistance (121, 124). Il est phosphorylé par les kinases cellulaires pour adopter la forme active en CDV-diphosphate (124). Les formes actives sont des inhibiteurs compétitifs de l'ADN polymérase virale bloquant ainsi la synthèse de l'ADN (124, 134). Le traitement par le cidofovir pourrait engendrer de la toxicité rénale parfois irréversible entraînant une insuffisance rénale nécessitant une dialyse pour éviter la mort (135).

Le foscarnet (FOS) est un analogue pyrophosphate qui inhibe l'ADN viral en imitant la structure du pyrophosphate produit au cours de l'allongement de l'ADN (124, 136). FOS ne nécessite pas de phosphorylation par des kinases virales et cellulaires et agit comme un inhibiteur non compétitif de l'activité de l'ADN polymérase virale en se liant au site de liaison

pyrophosphate sur l'ADN polymérase et bloquant la libération de pyrophosphate du nucléoside triphosphate terminal ajouté sur la chaîne d'ADN en croissance (124). Le traitement par le foscarnet peut être associée à une toxicité rénale, un déséquilibre ionique et un risque d'anémie (137).

Les traitements disponibles jusqu'à ce jour ciblent principalement la réplication du virus mais ne permettent pas de l'éliminer complètement. A cela, s'ajoute le problème de la résistance dû aux mutations dans les gènes de la TK et/ou de l'ADN polymérase (121, 124). Il est très important que la recherche scientifique sur le VHS-1 converge vers le développement de nouvelles sortes de médications ciblant d'autres étapes du cycle viral et permettant une élimination du virus. Mais le plus important serait le développement de vaccins prophylactiques ou thérapeutiques. Le développement de tels vaccins permettrait de renforcer la réponse immunitaire et cibler le virus soit au début de son entrée pour les primo-infections ou bien lors de la latence pour empêcher sa réactivation (138). Les principales recherches pour des vaccins impliquent l'utilisation de virus inactivés, de vecteurs viraux recombinants ou encore des *virus like particules* (VLPs) (139). Les vaccins thérapeutiques les plus promoteurs actuellement en développement préclinique ou clinique prenant en charge les infections au VHS-1 sont basés sur la glycoprotéine gD adjuvantée avec des sous unités ou des fragments de certaines protéines virales permettant une réponse immunitaire cellulaire de type T (76, 140-142).

I.2 Architecture structurale et composition du virus herpès simplex de type 1

A l'instar des autres virus herpétiques, le VHS-1 partage les mêmes caractéristiques morphologiques distinctives des herpèsvirus à savoir un core d'une seule copie d'ADN linéaire double brin de 125-295 kilopaires de bases (kpb) empaqueté à une haute densité dans une capside icosaèdrale de 100-130 nm, une couche de protéines appelée tégument entourant la capside et une enveloppe lipidique riche en glycoprotéines virales (63-67). (Figure 2).

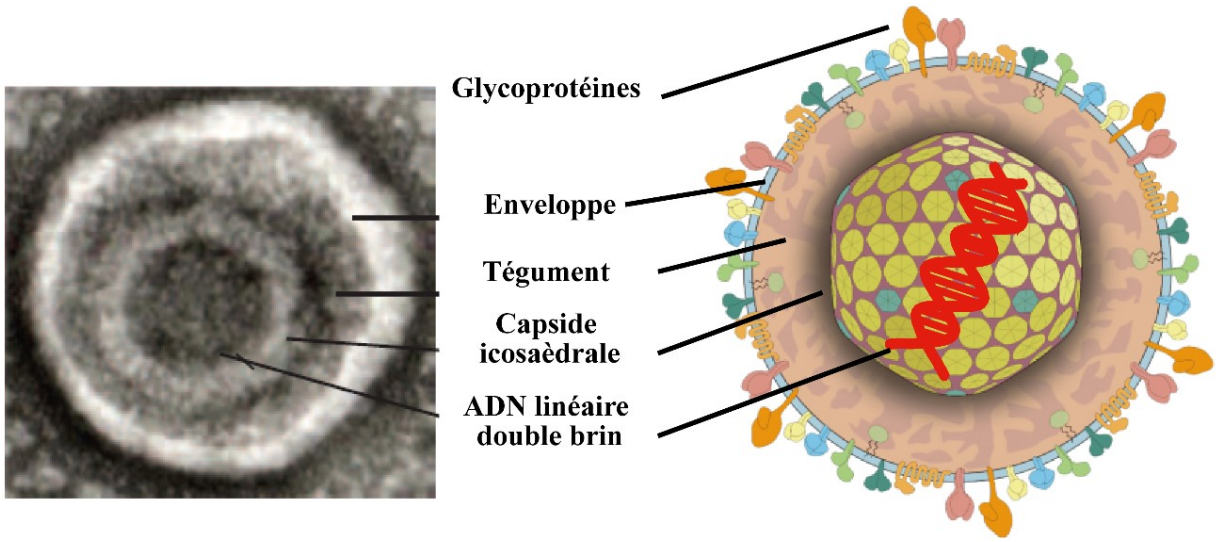

Figure 2 : Structure et composition du VHS-1.

Le VHS-1 est composé d'un core d'ADN linéaire double brin empaqueté à une haute densité dans une capside icosaèdrale de 100-130 nm d'où la couleur noire dans l'image de microscopie électronique, une couche de protéines appelée tégument entourant la capside et une enveloppe lipidique cloutée par des glycoprotéines virales. Adapté de Fields Virology (66) et *de Ke Lan et al (143)*.

I.2.1 Le génome viral

Le génome du VHS-1 est un ADN double brin linéaire fermement empaqueté dans un état liquide-cristallin sous la forme d'une hélice torsadée dont les brins sont espacés d'environ 2.6 nm (144-146). Le séquençage du génome viral complet indique une taille totale de 152 261 paires de bases (pb) avec un C+G de 68.3% (147-157). Il contient 90 cadres de lecture ouverts (*open reading frame*; ORF) codant pour au moins 84 protéines différentes (3). Le génome viral s'organise en deux segments nommés selon leurs longueurs et liés de façon covalente. Ces

segments sont appelés unique long (U_L ; *unique long*) faisant 108 kpb et unique court (U_S ; *unique short*) faisant 13 kpb et sont flanquées par des séquences répétées *a, b, c* désignées TR (*terminal repeats*) ou répétitions terminales et IR (*inverted repeats*) ou répétitions inversées (3, 145, 158, 159). Le segment unique long (U_L) est flanqué par les répétitions *ab* et *b'a'* alors que le segment unique court (U_S) est flanqué par les répétitions *a'c'* et *ca* (3, 145, 158, 159). Chaque segment contient des gènes qui portent le nom du segment en plus d'un chiffre désignant la position du gène dans le génome. Ainsi, le segment U_L contient 56 gènes nommés U_L1 à U_L56, le segment U_S contient 12 gènes nommés U_S1 à U_S12, les séquences longues répétées R_L contiennent 2 gènes nommés R_L1 et R_L2 et les séquences courtes répétées R_S contiennent un seul gène nommé R_S1 (3, 145, 158, 159). Ces gènes codent pour des protéines qui sont classées en trois groupes selon la chronologie de la transcription de leurs gènes : (α) pour les gènes immédiats précoces (2 à 4 h post-infection), (β) pour les gènes précoces (4 à 8 h post-infection) et (γ) pour les gènes tardifs (> 8 h post-infection)(160). Les séquences répétées *a* sont situées aux extrémités des segments U_L et U_S ainsi qu'à la jonction entre les deux segments, et varient en orientation et en nombre de copies en fonction de leur position dans le génome, mais aussi d'une souche virale à une autre (3, 161). Les séquences répétées *a* sont hautement conservées et interviennent dans le clivage et l'encapsidation de l'ADN viral (3, 145, 162, 163). On trouve trois origines de réplication de l'ADN dans le génome du VHS-1 nommées Ori_L et Ori_S selon la région dans laquelle elles sont localisées U_L et U_S respectivement. Ainsi on retrouve une seule copie de Ori_L au milieu du segment U_L et 2 copies de Ori_S dans les répétitions *c* flanquant le segment U_S (3, 159, 164). Le génome du VHS-1 subit des inversions génomiques durant la réplication dans lesquelles les segments uniques longs (UL) et uniques courts (US) sont inversés les uns par rapport aux autres pour donner quatre isomères dans des concentrations équimolaires (165-169) (Figure 3).

Les origines de réplication de l'ADN Ori_L et Ori_S contiennent toutes les deux une région riche en adénine et thymine (A/T) flanquée par des sites (BOX) de fixation de la protéine U_L9 qui se lie à l'origine de réplication de l'ADN (OBP « *origin-binding protein* ») (164). Ori_S contient une séquence palindromique imparfaite de 45 pb dans laquelle la région riche en A/T est flanquée de deux sites de fixation de U_L9 (BOX I et BOX II) (164). Il existe aussi un troisième site de fixation ayant une affinité plus faible (BOX III) adjacent à BOX I (164). Ori_L contient une séquence palindromique parfaite de 144 pb qui comprend quatre sites de reconnaissance pour U_L9. Il semble aussi que Ori_L et Ori_S, codent pour des micro ARN (miARN) (164, 170).

Une liste complète des gènes et des protéines virales codées par le génome du VHS-1 est présentée en annexe (Annexe 1).

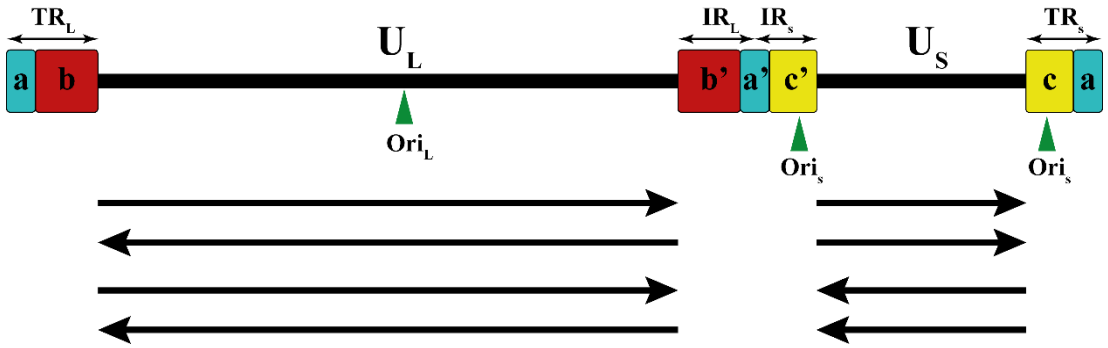

Figure 3: Organisation du génome du VHS-1.

TR_L, régions terminales répétées longues ; U_L, région unique longue ; IR_L, régions internes répétées longues ; IR_S, régions internes répétées courtes ; US, région unique courte ; TR_S, régions terminales répétées courtes, Ori ; origine de réplication. Pendant l'infection, les deux régions uniques s'inversent l'une par rapport à l'autre. Les flèches reflètent les orientations possibles des segments UL et US à la suite de l'inversion génomique. Adapté de Fields Virology (3), *Kennedy et al (159) et de Weir (171).*

I.2.2 La capside

La capside a une forme icosaèdrale (T = 16) avec une taille d'environ 125 nm de diamètre (145, 172-174). Elle est formée de 161 capsomères divisés en 150 hexamères (hexons) et 11 pentamères (pentons) (145, 172-176). Les pentons et les hexons sont composés respectivement de cinq et six copies de la protéine majeure de la capside VP5 (U_L19) (3, 145, 158, 175). A la pointe de chaque protéine VP5 de chaque hexon on retrouve une copie de la protéine VP26 (U_L35) (il y a environ 900 copies par capside) (145, 175-177). Les capsomères sont reliés entre eux par des triplex dont chacun est composé d'une copie de la protéine VP19C (U_L38) et de deux sous-unités de VP23 (U_L18) et dans chaque capside on trouve 320 triplex (3, 145, 175). En plus des pentons et des hexons, la protéine pU_L6 forme un complexe dodécamérique (12 copies) sous forme de cylindre nommé *portal* permettant l'internalisation ou la libération de l'ADN viral (176, 178-181). La partie externe du *portal* est couronnée par la protéine U_L25 formant un bouchon (182). Toutefois, la fixation de cette protéine nécessite la présence de la protéine pU_L17 avec laquelle elles forment un hétérodimère impliqué dans l'encapsidation de l'ADN viral nommé le composant spécifique du vertex de la capside (CVSC) (145, 178, 182-187) (Figure 4).

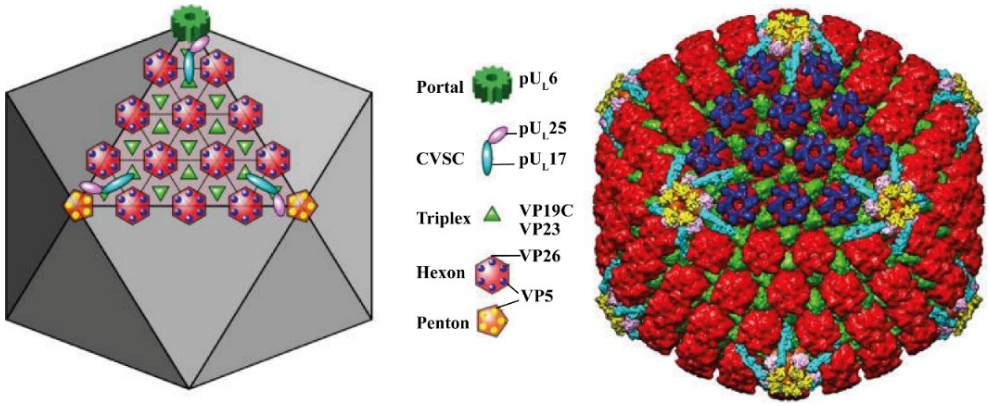

Figure 4: Structure et organisation de la capside du VHS-1

La capside virale est composée majoritairement par quatre protéines virales VP5(U_L19), VP26 (U_L35), VP23 (U_L18) et VP19C (U_L38) avec quelques copies de pU_L6, pU_L17 et pU_L25. Le complexe portal occupe un sommet unique de penton et sert pour l'assemblage de la capside et pour permettre l'entrée et la sortie du génome viral. Les hexons sont coiffés par VP26, tandis que les pentons se lient à la protéine du tégument pU_L36, qui interagit avec pU_L25 pour former ensemble, avec pU_L17, le CVSC. Les complexes triplex relient les capsomères entre eux. Adapté de *Heming et al (145).*

I.2.3 Le tégument

Le tégument est un réseau très dense et très complexe comprenant des milliers de copies de protéines de différentes tailles reliant la capside à l'enveloppe virale. L'analyse protéomique des virions extracellulaires par spectrométrie de masse a identifié 23 protéines virales constituant le tégument, mais en trouve aussi quelques 49 protéines cellulaires incluant des protéines impliquées dans le trafic cellulaire et l'exocytose, en particulier des membres des familles Annexin et Rab GTPase dont la déplétion par des ARN interférents (siRNA) réduit significativement l'entrée et la réplication (188, 189). Les protéines du tégument varient en taille et en abondance, la plus petite protéine pU_L11 est estimée à environ 10,5 kDa et la plus grande pU_L36 (VP1/2) à environ 330 kDa (190). Les protéines du tégument les plus abondantes sont pU_L47 (VP13/14), pU_L48 (VP16) et pU_L49 (VP22). Ces deux dernières sont présentes en grand nombre de copies par particules virales et leur stœchiométrie est très variable d'une particule à une autre (190, 191).

Les protéines du tégument se répartissent en deux classes selon la difficulté à les extraire des virions matures avec le détergent Triton X-100 ou en utilisant des concentrations variées de sels (NaCl). Ainsi, celles qui sont relativement faciles à extraire sont considérées des protéines du "tégument externe" et les plus résistantes à extraire sont considérées des protéines du "tégument interne". Les protéines du tégument interne sont étroitement associées ou interagissent directement avec la capside tandis que les protéines du tégument externe sont étroitement associées ou interagissent directement avec l'enveloppe virale (190, 192-196). Ces protéines assurent plusieurs fonctions très importantes durant le cycle viral. Elles entrent dans la cellule hôte dès la fusion de l'enveloppe virale avec la membrane cytoplasmique et assurent un certain nombre de fonctions structurales et non structurales commençant par le transport des capsides vers le noyau, le recrutement de moteurs moléculaires cellulaires, la régulation de l'expression des gènes viraux et cellulaires, et l'assemblage des virions durant la sortie (190,

194, 197, 198). Alors que la plupart des protéines du tégument externe diffusent dans le cytoplasme directement après la fusion de l'enveloppe virale avec la membrane plasmique lors de l'entrée, les protéines du tégument interne telles que pU_L36 et pU_L37, qui interagissent ensemble, restent étroitement liées à la capside et assurent son transport vers le noyau et son association au complexe de pores nucléaires « *Nuclear pore complexes* » (NPC) ainsi que l'injection de l'ADN viral (194, 199). Ces mêmes protéines vont assurer le transport des capsides nouvellement formées, lors de la sortie du noyau, vers le site d'enveloppement final (200). Après l'injection de l'ADN viral dans le noyau, la protéine tégumentaire VP16 initie la transcription des gènes immédiats-précoces ICP0, ICP4, ICP22, ICP27 et ICP47 (199). ICP0 module les réponses innées et intrinsèques de l'hôte à l'infection (201, 202). Elle interagit également avec la protéine de la leucémie pro-myélocytaire, « *Promyelocytic leukemia* » (PML) aussi connue sous le nom de domaine nucléaire 10 « *Nuclear domain 10* » (ND10), et induit la dissociation de cette dernière par le biais de l'activité d'ubiquitine ligase E3 empêchant ainsi la capacité de PML à bloquer l'expression des gènes viraux (201, 202). ICP0 cible plusieurs protéines cellulaires et virales pour la dégradation induite par le protéasome (203). La protéine ICP0 a aussi la capacité de bloquer la réponse antivirale induite par les interférons au cours des premiers stades de l'infection grâce à l'inhibition spécifique de la réponse cellulaire médiée par les facteurs 3 et 7 de l'interféron (IRF3 et IRF7) (199, 204, 205). La protéine ICP4 se lie à l'ADN viral et module la réplication et la transcription. Elle peut moduler son propre promoteur ainsi que les promoteurs associés à la latence (199, 206). Les protéines U_L31, Us3, ICP34.5, U_L36, U_L37, U_L51, U_L11, U_L20, U_L46, U_L47, U_L48 et U_L49 sont requis lors de la sortie du virus du noyau vers le cytoplasme jusqu'au TGN ainsi que lors de l'enveloppement (199).

Plus de détails sur le rôle des protéines du tégument et le processus de tégumentation seront donnés plus loin lors de la description du cycle viral.

I.2.4 L'enveloppe virale

L'enveloppe, qui recouvre le tégument, est une bicouche lipidique dans laquelle des glycoprotéines virales sont ancrées. Ces glycoprotéines virales jouent un rôle dans la fusion et l'entrée du virus dans la cellule hôte et également dans la propagation du virus d'une cellule à une autre. Les lipides de l'enveloppe proviennent essentiellement des membranes des compartiments de la cellule hôte (207). L'enveloppe contiendrait 12 glycoprotéines virales : gB, gC, gD, gE, gG, gH, gI, gJ, gK, gL, gM, et gN et 5 protéines virales membranaires non glycosylées pU_L20, pU_L43, pU_L45, pU_L56 et pU_S9 qui seraient présentes dans la partie intrinsèque de la bicouche lipidique de l'enveloppe (3). Les glycoprotéines ne sont pas toutes essentielles pour la réplication du virus, cependant elles assurent plusieurs fonctions durant le cycle viral et la neurovirulence (208-213). Les glycoprotéines gB, gC, gD et gH, qui forment un complexe avec gL, sont impliquées dans l'entrée du virus dans la cellule par un mécanisme de fusion (214). La glycoprotéine gE forme aussi un hétérodimère avec la glycoprotéine gI. Ce complexe est capable de se lier à la fraction Fc de l'immunoglobuline G (IgG) favorisant ainsi l'évasion au système immunitaire de l'hôte (215-218).

I.3 Cycle de réplication du virus herpès simplex de type 1

Le cycle viral du VHS-1 est caractérisé par son mode d'infection bimodal où le virus va osciller entre 2 types de cycles d'infection bien distincts : un cycle lytique dans les cellules épithéliales durant lequel tous les gènes viraux sont exprimés et un cycle latent dans les neurones durant lequel l'ADN viral persiste sous forme épisomale et les gènes viraux sont réprimés à l'exception des ARN non codants connus sous le nom de transcrits associées à la latence « *latency-associated transcript* » (LAT) (219, 220). L'orientation de l'infection vers un cycle lytique ou latent dépend de la réaction du virus face à la réponse de la cellule hôte, qui condense la chromatine autour de l'ADN viral nu dès son injection dans le noyau afin de bloquer la transcription des gènes viraux (221).

I.3.1 L'infection lytique

Le cycle lytique du VHS-1 peut être divisé en quatre étapes majeures : l'entrée dans la cellule hôte, l'expression des gènes viraux, la réplication de l'ADN viral puis l'assemblage et la sortie de particules virales nouvellement formées. Le cycle lytique prend environ 18-20 h (3, 222) (Figure 5).

Toutes ces étapes seront discutées plus en détail dans les prochaines sections.

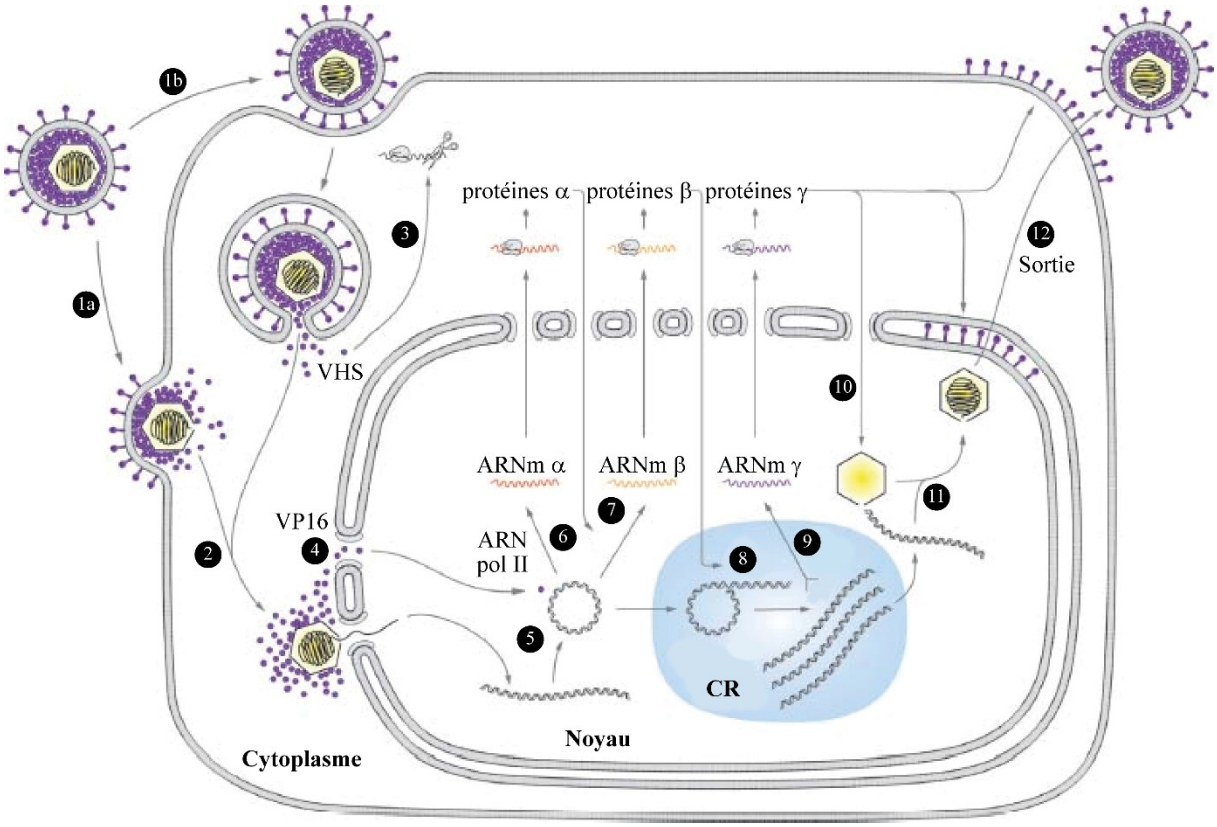

Figure 5: Cycle de réplication lytique de VHS-1.

Fixation du virus sur la membrane plasmique et internalisation soit par fusion de l'enveloppe virale avec la membrane plasmique (1a) ou par endocytose (1b) libérant ainsi la capside et les protéines de tégument dans le cytoplasme. 2 : Transport de la capside vers les pores nucléaires et injection de l'ADN viral dans le noyau. 3 : Dégradation des ARN messagers de l'hôte par la protéine vhs. 4 : La protéine transactivatrice VP16 se dirige vers le noyau pour la transcription des gènes α. 5 : circularisation de l'ADN viral. 6 : Démarrage de la transcription par l'ARN polymérase II de l'hôte. 7 : Les protéines α activent la transcription des gènes β. 8 : Les protéines β sont impliquées dans la réplication de l'ADN viral. 9 : L'expression des gènes γ stimule la synthèse de l'ADN viral. 10 : Assemblage de la capside dans le noyau. 11 : Encapsidation de l'ADN viral. 12 : Sortie. Adapté de Fields Virology (3).

I.3.1.1 L'attachement et l'entrée du virus

Le VHS-1 a la capacité d'entrer dans les cellules en utilisant plusieurs voies selon des cellules hôtes ciblées (3, 223). Ainsi, l'entrée dans les cellules Vero, Hep2 et les cellules neuronales se fait par la fusion de l'enveloppe virale avec la membrane plasmique (3, 223, 224). L'entrée du virus dans les cellules Vero par fusion entraîne une augmentation de la concentration intracellulaire de calcium (3, 225). Lorsqu'il s'agit des cellules HeLa, les CHO-K1 (« *Chinese hamster ovary* » ovaires du hamster de Chine) et les kératinocytes, le virus emprunte la voie de l'endocytose dépendante du pH (3, 226-228). Cependant, dans le cas des cellules de mélanome de souris B78H1, le virus emprunte plutôt la voie de l'endocytose indépendante du pH (229).

Cinq glycoprotéines virales sont impliquées dans le processus de l'entrée du virus: gB, gC, gD, et l'hétérodimère gH/gL (230-233). L'attachement du virion à la surface cellulaire est médié par gC et gB, qui interagissent avec les glycosaminoglycanes ou héparane sulfate protéoglycanes (HSPG) de la surface cellulaire, en particulier le sulfate d'héparane (222, 234). Cependant, bien que la fixation du virus à la surface des cellules montre une forte dépendance aux interactions de gB et gC avec l'héparane sulfate, des études ont également montré que les cellules déplétées pour l'héparane sulfate sont toujours sensibles à l'infection et conservent la capacité de lier la gB soluble (230, 235-237). La gB agit également comme un ligand pour le PILR-α (récepteur α couplé à l'immunoglobuline de type 2 « *paired immunoglobulin-like type 2 receptor* ») (230, 238). C'est l'interaction entre quatre glycoprotéines, gD, gB et l'hétérodimère gH / gL, qui est requise pour l'entrée du virus dans la cellule hôte (222, 239, 240). La glycoprotéine gD peut se lier aux récepteurs : la nectine-1 et la nectine-2, le médiateur d'entrée du virus de l'herpès (HVEM « *herpesvirus entry mediators* ») et l'héparane sulfate 3-O-sulfaté (3-O-S-HS). La région N-terminale de la gD interagit avec les récepteurs cellulaires induisant des changements conformationnels dans gD et la libération de son domaine C-

terminal, qui active les complexes gB et gH / gL, déclenchant ainsi la fusion membranaire (222, 230, 239, 241)(Figure 6).

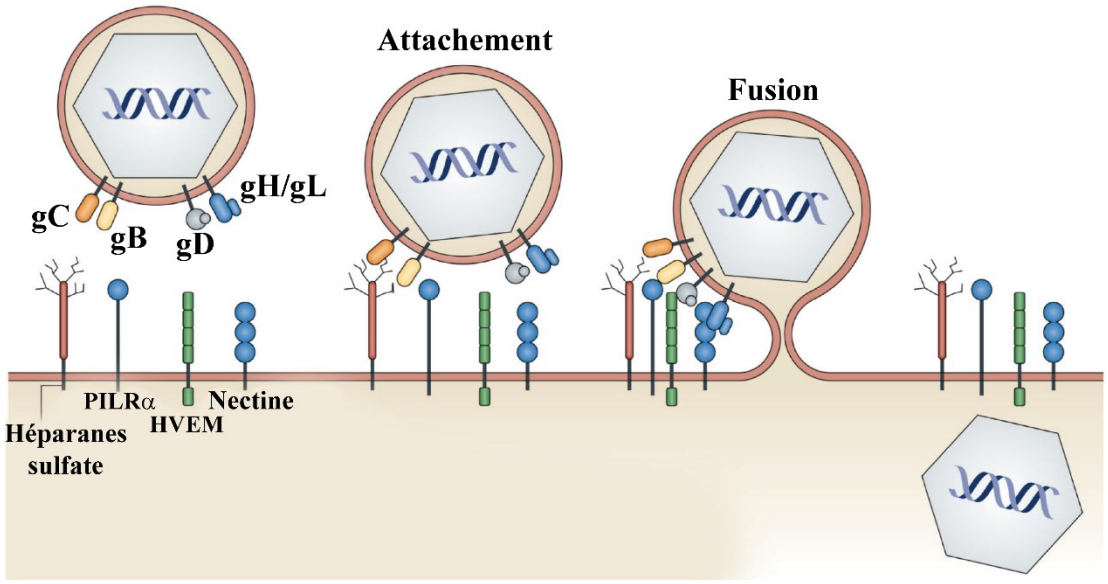

Figure 6 : Attachement et entrée du VHS-1.

L'attachement du VHS-1 implique cinq glycoprotéines: gB, gC, gD, et l'hétérodimère gH/gL. L'attachement est initié par gB et gC puis stabilisé par gD qui subit un changement conformationnel déclenchant la fusion de l'enveloppe virale avec la membrane plasmique via l'activation de gB et du complexe gH/gL. Adapté de *Sedy et al (214).*

I.3.1.2 Le transport du virus au noyau

Directement après la fusion de l'enveloppe virale avec la membrane plasmique, la grande majorité des protéines du tégument se dissocient de la capside et certaines d'entre elles (VP1/2, VP13/14, VP16 et VP22) vont être phosphorylées par les kinases virales et/ou cellulaires (242-247). Les protéines tégumentaires VP1/2 (U_L36), pU_L37 (U_L37) et VP11/12 (U_L46), restent associées à la capside (193, 245-248). Le complexe pU_L36/pU_L37, s'associe aux moteurs moléculaires kinésines et dynéine qui se trouvent aux extrémités des microtubules pour assurer le transport antérograde ou rétrograde respectivement des capsides (192, 193, 249-256). Les capsides vont être transportées jusqu'au noyau où elles vont se lier aux NPC. Les capside reste sur le côté cytoplasmique du NPC, tandis que l'ADN pénètre dans le noyau par translocation à travers les pores nucléaires (40, 257, 258). La protéine VP1/2 est nécessaire pour

la libération de l'ADN viral des capsides dans le noyau. Elle interagit avec la protéine de la capside pU_L25 ainsi que la protéine du vertex portale de la capside pU_L6 et la protéine du complexe CAN/Nup214 ce qui stimule la libération de l'ADN viral des capsides à travers les pores nucléaires dans le noyau des cellules nouvellement infectées (247, 259-262).

Les autres protéines du tégument vont assurer d'autres fonctions permettant au virus de mieux se répliquer, et ce en détriment des fonctions cellulaires, telles que la protéine kinase pU_S3 qui induit l'inactivation des facteurs pro-apoptotiques bloquant ainsi l'apoptose (263-265). La protéine vhs (U_L41) possède une activité endo-ribonucléase qui entrave l'expression des protéines cellulaires et virales en dégradant l'ARNm de l'hôte au cours des premiers stades de l'infection et l'ARNm viral plus tard dans l'infection (190, 266-268). La protéine ICP0 cible plusieurs protéines cellulaires et virales pour la dégradation induite par le protéasome permettant ainsi au virus d'échapper à l'immunité intrinsèque des cellules hôtes (199, 203-205).

I.3.1.3 La cascade d'expression des gènes viraux

La transcription et la réplication du génome viral ainsi que l'assemblage des capsides nouvellement formées ont lieu au noyau (222). Au cours de l'infection lytique, plus de 80 gènes viraux sont exprimés (3, 269). Cette expression est hautement régulée et se déroule en cascade de trois catégories de gènes dont les produits de chaque catégorie impactent l'expression des gènes de la catégorie suivante (3, 222, 269, 270) (Figure 7).

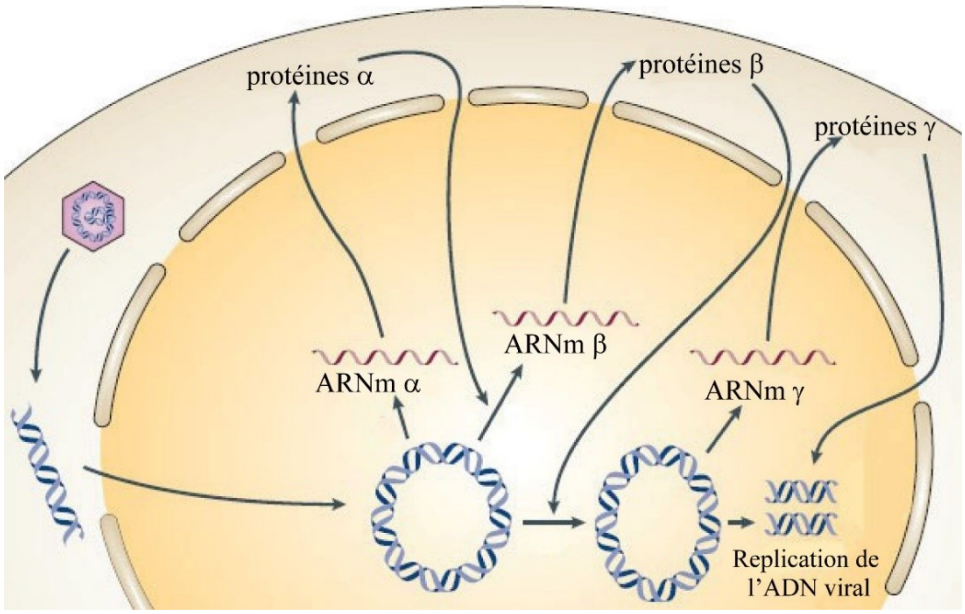

Figure 7: Cascade d'expression des gènes viraux.

L'expression des gènes viraux se déroule de façon séquentielle et les produites de chaque catégorie de gènes impactent l'expression des gènes de la séquence suivante. Une fois dans le noyau, l'ADN viral est transcrit par l'ARN pol II de l'hôte en 5 catégories de gènes. Les gènes immédiats précoces (α), les gènes immédiats (β1 et β2) et les gènes tardifs (γ1 et γ2). Les gènes α (immédiats-précoces) sont exprimés en premier, suivis de β1 (précoces-précoces), β2 (tardifs-précoces), γ1 (pseudo-tardif) et γ2 (tardif vrai). Adapté de *Knipe et al* (221)

Une fois relâché dans le noyau, l'ADN viral s'associe rapidement aux histones après la condensation de la chromatine autour de lui afin de bloquer la transcription des gènes viraux (221, 271-273). Les quatre protéines virales VP16, ICP0, ICP8 et pU_S3 semblent être impliquées dans la décondensation de la chromatine en favorisant des modifications actives sur les histones permettant ainsi le déclenchement de la transcription des gènes viraux (221, 274-282). L'ADN viral est transcrit par l'ARN pol II de l'hôte dans un ordre chronologique en 5 étapes qui impliquent les gènes immédiats précoces (α), les gènes précoces (β1 et β2) et les gènes tardifs (γ1 et γ2). Les gènes α (immédiats-précoces) sont exprimés en premier, suivis de β1 (précoces-précoces), β2 (tardifs-précoces), γ1 (pseudo-tardifs) et γ2 (tardifs vrais). Les gènes α (immédiats-précoces) codent pour 6 protéines : ICP0, ICP4, ICP22, ICP27, ICP47 et $pU_S1.5$. Ces gènes qui sont les premiers à être exprimés n'exigent pas une synthèse préalable des

protéines virales, mais nécessitent tout de même la présence de la protéine VP16 (U_L48) pour son activité transactivatrice. Les protéines α jouent un rôle important dans les premières étapes de l'infection notamment le contrôle et l'initiation de l'expression des autres gènes viraux, plus particulièrement, les gènes précoces grâce à leurs fonctions transcriptionnelles et post-transcriptionnelles (3). Les gènes α contiennent plusieurs copies de la séquence consensus: 5'-GyATGnTAATGArATTCyTTGnGGG-3' qui est le lieu de liaison du facteur de transcription cellulaire Oct-1 (222, 283). La protéine VP16 interagit spécifiquement avec Oct-1 et se complexe interagi avec le facteur de cellule hôte 1 (HCF-1 « *Host cell factor 1* ») ce qui active la transcription des gènes α (222).

Les gènes β codent pour sept protéines (pU_L5, pU_L8, pU_L9, pU_L29, pU_L30, pU_L42 et pU_L52) impliquées dans la synthèse et la réplication du génome viral (160, 269, 270, 284). La synthèse de cette catégorie de protéines nécessite la présence des protéines ICP4 et ICP0 (3). Les protéines produites suite à la traduction de gènes β provoquent un arrêt de la transcription des gènes α (3). Le déclenchement de la réplication de l'ADN viral provoque la diminution de l'expression des gènes précoces et l'augmentation de l'expression des gènes tardifs (3).

Les gènes tardifs γ codent principalement pour les protéines nécessaires à l'empaquetage et à l'assemblage des capsides ainsi que les glycoprotéines de l'enveloppe virale et les protéines du tégument (3, 48, 270). Leur transcription requiert la présence des protéines virales ICP4, ICP0, ICP22, ICP27 et US1.5 ainsi que la réplication de l'ADN viral (3, 270, 285, 286).

I.3.1.4 La transcription et la réplication de l'ADN viral

Parmi les protéines virales codées par le génome du VHS-1, sept assurent des fonctions essentielles à la réplication de l'ADN viral (3, 164, 222, 287). La protéine U_L9 se lie à l'origine de réplication de l'ADN (OBP « *origin-binding protein* »)(164, 222, 287-291). La protéine

ICP8 (U_L29) se lie à l'ADN simple brin et joue un rôle important dans la synthèse de l'ADN viral, le contrôle de l'expression des gènes viraux et la formation de sites pré-réplicatifs et de compartiments de réplication (164, 287, 292). Ensuite, il y a l'ADN polymérase virale avec ses deux sous unités, la sous unité catalytique Pol (U_L20) et la sous unité ou facteur de processivité (U_L42) (3, 164, 222, 287). Finalement, le complexe hélicase/primase H/P qui est formé par l'hétérotrimère pU_L5, pU_L8 et pU_L52 ($U_L5/U_L8/U_L52$) (3, 164, 222, 287, 293).

L'infection par le VHS-1 entraîne une réorganisation dramatique du noyau de la cellule infectée impliquant la relocalisation des protéines cellulaires et l'assemblage ordonné des compartiments de réplication dans lesquels l'expression génique, la réplication de l'ADN, et l'assemblage de nouvelles capsides se produisent (3, 164, 222, 287, 294). Après l'entrée des génomes viraux dans le noyau, le génome se circularise puis des complexes nucléoprotéiques ICP4/ ICP27 sont détectés dans des compartiments spécifiques appelés sites pré-réplicatifs (3, 295-297). Les protéines ND10 sont recrutées juste après dans des sites adjacents aux complexes nucléoprotéiques ICP4/ICP27 afin de réprimer l'expression des gènes viraux. Toutefois, ces sites de ND10 seront rapidement dissociés sous l'action de la protéine virale ICP0 (3, 287, 294, 298-303). Après la circularisation du génome viral linéaire, la réplication de l'ADN viral se déroule en deux phases: une phase initiale de réplication appelée thêta qui démarre dans l'une des origines de réplication Ori_L ou Ori_S, suivie d'une phase de réplication circulaire « *rolling circle* ». Cette dernière génère des concatémères qui sont clivés et empaquetés dans des particules virales infectieuses (164, 287, 297, 304, 305) (Figure 8).

Dans la première étape, deux homodimères de pU_L9 se fixent sur les sites spécifiques BOX I et BOX II se trouvant sur l'origine de réplication Ori_S, ce qui recrute la protéine ICP8 qui interagit avec pU_L9 au niveau d'une séquence de 13 acides aminés (AA) de l'extrémité carboxy terminale (164, 287, 288, 290, 291). Cette interaction ATP dépendante stimule les

activités hélicase et ATPase de pU_L9, ce qui amorce le déroulement des brins d'ADN et la formation de structures d'épingle à cheveux (164, 287, 288, 291, 306, 307). Cette étape est accompagnée de changements conformationnels dans pU_L9 qui commence à se lier de façon non spécifique à l'ADN simple brin (164, 288, 307). L'exposition de l'ADN provoque une modification conformationnelle de la protéine ICP8 qui la libère de pU_L9 et la positionne sur l'ADN monocaténaire afin d'empêcher l'hybridation des brins complémentaires (164). Une fois que les protéines pU_L9 et ICP8 ont amorcé la séparation des brins d'ADN complémentaires, le complexe hélicase/primase H/P (pU_L5/pU_L8/pU_L52) est recruté pour dérouler l'ADN et synthétiser de courtes amorces d'ARN pour initier la réplication (164, 222, 287, 308). Par la suite, l'ADN polymérase virale avec ses deux sous-unités Pol et pU_L42 est recruté à la fourche de réplication (164, 287). Le recrutement de la polymérase implique des interactions directes entre Pol et H/P (164, 287). En effet, les deux sous-unités pU_L5 et pU_L8 de H/P interagissent avec Pol ce qui entraine des changements conformationnels dans le complexe H/P amenant ainsi la polymérase à l'ADN viral pour commencer la synthèse de nouveaux brins d'ADN selon le modèle de réplication thêta (Θ) (164, 287, 309, 310).

Dans la deuxième étape, la réplication continue selon le modèle de réplication circulaire « *rolling circle* » qui génère des concatémères qui seront clivés et empaquetés dans des particules virales infectieuses (164, 287, 297, 304, 305) (Figure 8).

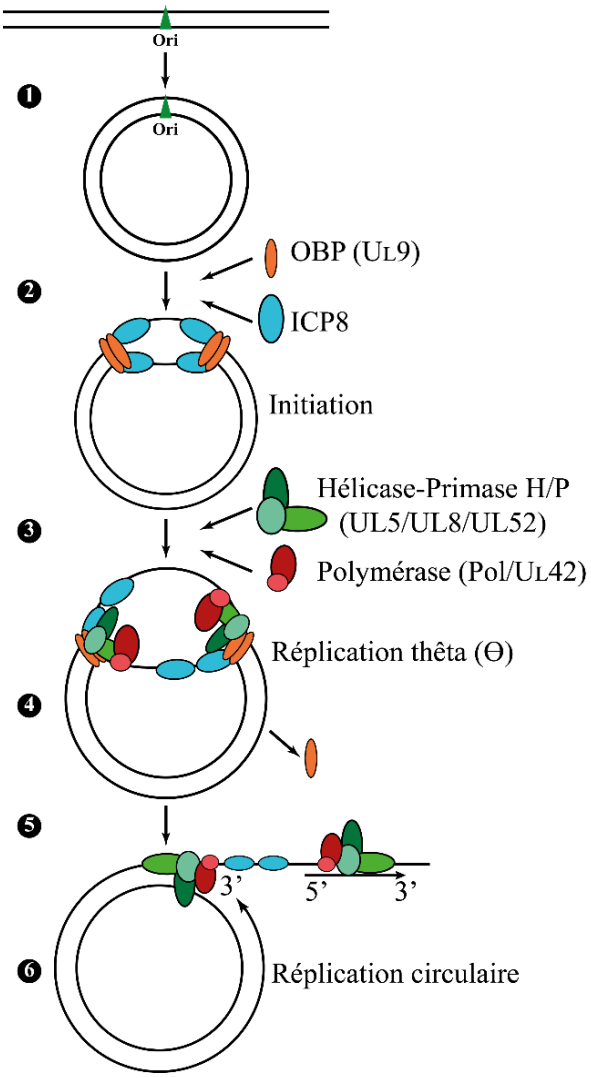

Figure 8 : Diagramme de réplication de l'ADN du VHS-1

(1) L'ADN viral linéaire se circularise à son entrée dans le noyau. (2) Les protéines virales UL9 puis ICP8 s'associent à l'une des origines de réplication pour initier le déroulement l'ADN. (3) Le complexe hélicase/primase H/P ($U_L5/U_L8/U_L52$) ainsi que l'ADN polymérase virale avec ses deux sous-unités Pol et U_L42 sont recrutés à la fourche de réplication. (4) La réplication débute selon le modèle thêta (Θ). (5-6) La réplication continue selon le modèle circulaire « *rolling circle* » générant des concatémères d'ADN qui seront clivés par la suite. Adapté de Fields Virology (3) et *Taylor et al (308).*

I.3.1.5 L'assemblage de la capside

Après l'initiation de la réplication de l'ADN viral, l'expression des gènes tardifs γ, en particulier ceux codant pour les protéines de la capside, augmente pour fournir les éléments nécessaires à l'assemblage des nouvelles capsides et l'encapsidation du génome viral (3).

L'assemblage de la capside est un processus très complexe qui implique beaucoup d'interactions protéiques ainsi que des réactions enzymatiques protéolytiques (3, 180, 311-321). Ce processus nécessite la présence des protéines structurales VP5 (U_L19), VP26 (U_L35), VP19C (U_L38), VP23 (U_L18), pU_L6 (U_L6), pU_L17 (U_L17) et pU_L25 (U_L25) (3, 145, 321). En plus des protéines structurales, l'assemblage des capsides nécessite la participation de la protéine de l'échafaudage pre-VP22a (U_L26.5) ainsi que la protéase pU_L26 (U_L26) essentielle à la maturation (3, 321-323).

Bien que l'assemblage de la capside et l'encapsidation du génome viral ont lieu dans le noyau, les premières étapes de l'assemblage semblent se produire dans le cytoplasme (3). En effet, la plupart des protéines impliquées dans l'assemblage de la capside possèdent des séquences de localisation nucléaires (NLS) « *nuclear localization sequences* » leur permettant de se relocaliser dans le noyau (3, 308). Toutefois, les protéines VP5 (U_L19), VP23 (U_L18) et VP26 (U_L35) étant dépourvues de séquences de localisation nucléaires (NLS), ne peuvent se relocaliser dans le noyau par elles-mêmes et doivent donc interagir et former des complexes - au niveau du cytoplasme - avec celles contenant du NLS pour être transportées dans le noyau (308). Pour cela, la protéine VP5 (U_L19) forme un complexe avec pre-VP22a (U_L26.5) et VP19C (U_L38) (324-328). La protéine VP23 (U_L18) interagit également avec VP19C (U_L38) et quant à VP26 (U_L35), elle atteint le noyau indirectement en interagissant avec VP5 déjà engagée avec pre-VP22a (324-328). Une fois que tous les composants nécessaires à l'assemblage des nouvelles capsides sont dans le noyau, le processus commence avec la formation de la structure dodécamérique en forme d'anneau (12 copies) nommée *portal* (178-181, 329-333). Les monomères pUL6 du portal interagissent avec les protéines de l'échafaudage pre-VP22a au niveau d'un domaine hydrophobe entre les acides aminés (AA) 143 à 151 dans le pre-VP22a (313, 331, 334-336). L'anneau du portal agit comme un nidus sur lequel pentons et hexons ainsi que les complexes VP19C/VP23 sont ajoutés de manière séquentielle jusqu'à finalement la

formation d'une sphère complète, mais immature, thermosensible et fragile nommée procapside (49, 316, 320, 321, 337, 338).

La transition d'une procapside sphérique immature à une capside angulaire mature dépend de l'activité de la protéase associée aux protéines de l'échafaudage (339-341). Au cours du processus de maturation, la protéase pU$_L$26 (U$_L$26) s'auto-protéolyse au niveau des résidus 247 et 610 pour donner deux nouvelles protéines : la VP21 de 363 AA qui sert d'échafaudage et la VP24 de 247 AA qui garde l'activité protéase (3, 339-341). La protéine d'échafaudage pre-VP22a (U$_L$26.5) subit à son tour l'action de la protéase VP24 qui la clive près de l'extrémité carboxy terminale pour donner la protéine d'échafaudage VP22a de 304 AA (3, 317, 339-341). L'ensemble de ces réactions protéolytiques mènent au changement conformationnel de la capside et lui procure sa forme icosaèdrale plus stable pouvant donner lieu à d'autres types de capsides (3, 317, 339-342) (Figure 9).

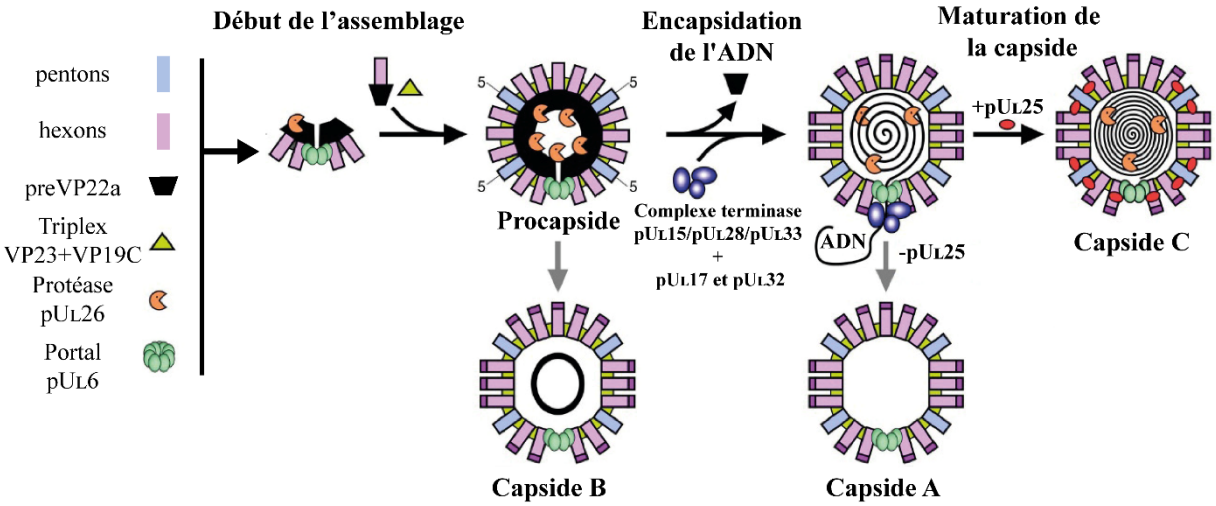

Figure 9 : Assemblage et maturation des capsides nucléaires.

L'assemblage des capsides nucléaires débute par l'association des pentons et des hexons (via le Triplex) autour des protéines de l'échafaudage pour former une procapside sphérique thermosensible et fragile. La procapside entame différentes étapes de maturation impliquant des réactions protéolytiques via pU$_L$26 et s'angularise pour adopter la forme icosaèdrale pour devenir une capside A ou une capside B, qui sont des produits incomplets, ou encore une capside C mature. Adapté de *Homa et al* (343) et *Heming et al* (145).

En plus des procapsides, on peut trouver trois autres types de capsides plus stables ayants des morphologies distinctes dans les noyaux des cellules infectées (145). (i) Les capsides A contiennent très peu de protéines dans leur cavité à la suite du relargage des protéines d'échafaudage VP21, VP22a ainsi que la majorité de la protéase VP24. Ces capsides se forment probablement à la suite de l'échec de l'incorporation de l'ADN (45, 145). (ii) Les capsides B retiennent les protéines de l'échafaudage dans leur cavité et ne parviennent donc pas à incorporer l'ADN viral à cause du manque d'espace (145). (iii) Les capsides C relâchent les protéines de l'échafaudage VP21 et VP22a, mais retiennent la protéase VP24. Les capsides C réussissent à incorporer l'ADN viral et parviennent préférentiellement à quitter le noyau pour un assemblage ultérieur en virions infectieux (144, 145).

L'encapsidation de l'ADN du VHS-1 nécessite la présence de sept protéines virales : pU_L6, pU_L15, pU_L17, pU_L25, pU_L28, pU_L32, et pU_L33 (145, 323, 331, 344-350). L'ADN concatémérique est incorporée dans les capsides C via le complexe portal (pU_L6) sous l'action des protéines pU_L17, pU_L25 et pU_L32 (145, 184, 351). Une fois l'encapsidation d'une copie intégrale d'ADN réalisée, les protéines du complexe terminase pU_L15/pU_L28 s'associent avec la protéine pU_L33 pour cliver l'ADN au niveau des séquences répétées libérant ainsi une seule copie de l'ADN du reste du concatémère (145, 352-355). La dernière étape de l'encapsidation pour une capside C consiste à garder l'ADN à l'intérieur de la capside pour donner finalement une capside C mature qui parait très dense et noirâtre en microscopie électronique (356, 357). Pour cela, la protéine pU_L25 formant un bouchon pour le complexe portal (pU_L6) empêchant ainsi la sortie de l'ADN (144-146). La protéine pU_L25 interagit avec la protéine pU_L17 avec laquelle elles forment un hétérodimère qui nécessite la présence de la protéine pU_L36 (VP1/2) pour stabiliser l'interaction avec la capside (145, 176, 358). Les trois protéines pU_L17, pU_L25 et pU_L36 forment le CVSC qui se lient spécifiquement aux triplex adjacents à chacun des onze pentons (145, 178, 182-187, 358).

I.3.1.6 La sortie du noyau

Une fois que la nucléocapside mature est formée dans le noyau, elle entame sa route vers l'espace extracellulaire via une voie spécialisée en traversant les membranes nucléaires, le cytoplasme et la membrane plasmique (3, 359). Ainsi, la première étape consiste à traverser l'enveloppe nucléaire qui représente une barrière physique beaucoup plus forte que la membrane plasmique du fait que cette dernière est constituée d'une seule membrane facilement accessible alors que l'enveloppe nucléaire est un système membranaire plus rigide et très complexe composé de deux membranes désignées comme membranes nucléaires internes et externes (MNI, MNE) qui sont séparées par un espace périnucléaire (360-362). Le mécanisme exact par lequel la capside mature traverse la barrière nucléaire a été débattu pendant plusieurs décennies (3, 359, 363-365). A ce stade, trois modèles généraux ont été proposés (le modèle luminal, le modèle des pores élargis et le modèle d'enveloppement / dé-enveloppement / ré-enveloppement) afin d'expliquer la sortie des capsides du noyau et leur transport jusqu'à la membrane plasmique (3, 359, 363) (Figure 10).

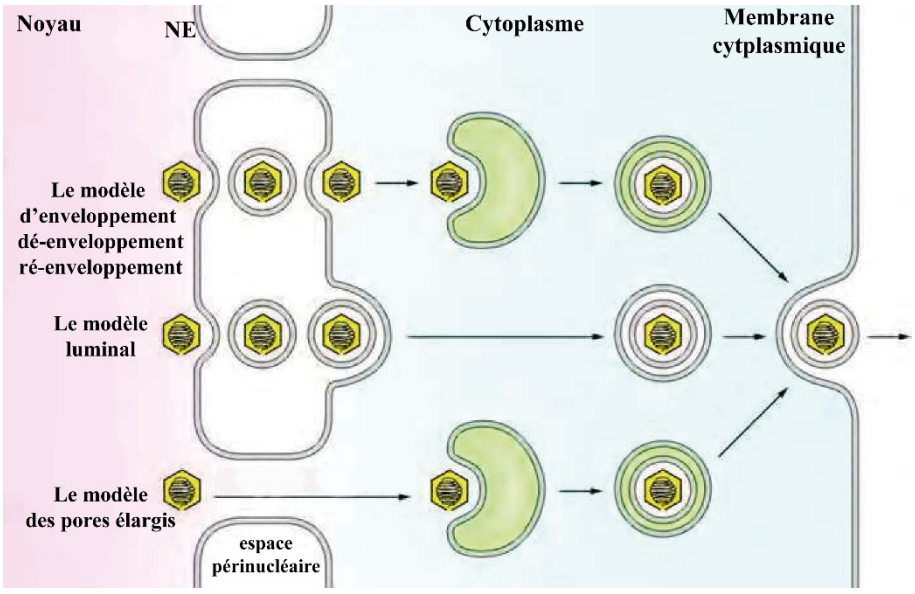

Figure 10 : Modèles proposés pour la sortie des capsides nucléaires et leur maturation.

Les capsides nucléaires nouvellement formées parviennent à quitter le noyau selon 3 modèles : le modèle luminal, le modèle des pores élargis et le modèle d'enveloppement / dé-enveloppement / ré-enveloppement Adapté de Fields Virology (3).

Le modèle luminal est un processus d'enveloppement unique qui comprend l'acquisition d'une enveloppe par le bourgeonnement des capsides nucléaires à la MNI suivie du transport luminal de ces particules enveloppées à travers le RE et la voie sécrétoire vers la surface cellulaire pour la libération des particules virales après la fusion des vésicules de secrétions et la membrane plasmique (MP) (359, 364, 366). Dans ce modèle, tous les composants du virion mature doivent déjà faire partie de la particule virale dans l'espace périnucléaire, et doivent aussi être conservés dans la particule virale mature suggérant ainsi la rétention de l'intégrité structurelle du virion primaire enveloppé pendant le transit par le transport vésiculaire hors du réticulum endoplasmique et à travers la voie sécrétoire (359, 364, 366). Cependant, ce modèle a été contesté du fait que les principaux composants des particules virales enveloppées se trouvant dans l'espace périnucléaire sont réellement absents des virions matures indiquant une discontinuité entre les virions nucléaires et extracellulaires du même que la composition en phospholipides des virions extracellulaire diffère de celle des noyaux des cellules infectées (207, 359, 364, 366-369).

Le modèle des pores élargis suggère que les capsides nucléaires peuvent accéder directement au cytosol par des pores nucléaires dilatés puis bourgeonner avec les compartiments cellulaires pour être sécrétées dans le milieu extracellulaire par la voie de sécrétion classique (370, 371). Cependant, les capsides nucléaires présentent un diamètre de 125 nm. Ceci est trop grand pour traverser les pores nucléaires intacts qui comprennent un panier central limitant le transport des particules jusqu'à une taille maximale d'environ 36 nm (359, 372-374). Un tel processus de transport affecterait donc l'intégrité des pores nucléaires. Cependant, l'élargissement des pores nucléaires lors des infections par le VHS-1 a été constaté sans pour autant affecter leur intégrité (359, 370, 371, 375, 376).

Le modèle d'enveloppement / dé-enveloppement / ré-enveloppement est le plus largement accepté et défendu par des modèles biologiques solides basés principalement sur des observations morphologiques et ultrastructurales (200, 359, 363, 365, 368, 369, 377-389). Dans ce modèle, les capsides nucléaires acquièrent une enveloppe primaire (l'enveloppement) en bourgeonnant à la membrane nucléaire interne entraînant la formation de virions enveloppés dans l'espace périnucléaire. Ces virus enveloppés fusionnent avec la MNE libérant ainsi des capsides nues dans le cytoplasme (le dé-enveloppement). Les capsides nues du cytoplasme seront transportées jusqu'au réseau trans-Golgi « *trans-Golgi network* » (TGN) où elles acquièrent leur enveloppe finale (le ré-enveloppement) (Figure 11).

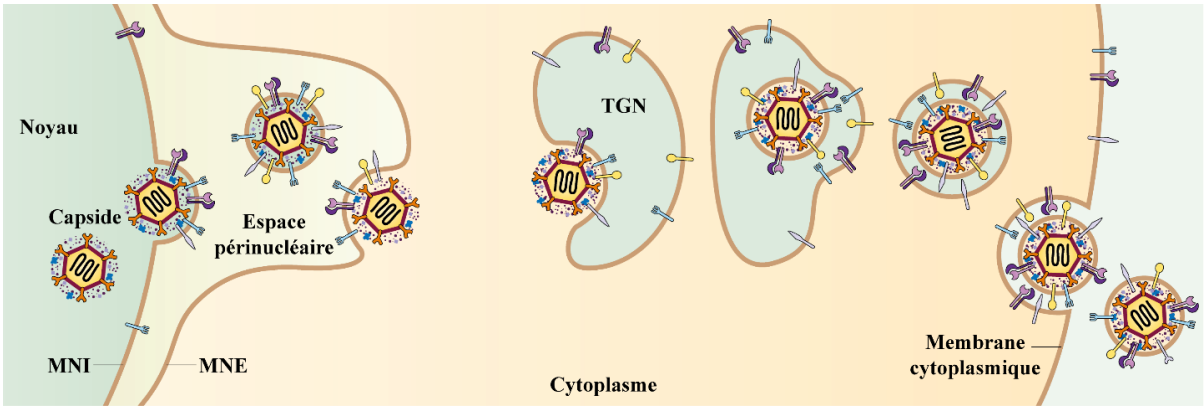

Figure 11 : Modèle d'enveloppement / dé-enveloppement / ré-enveloppement.

Après que les capsides se sont formées dans le noyau, elles bourgeonnent dans la MNI (enveloppement) pour former une particule enveloppée dans l'espace périnucléaire. Ces particules fusionnent avec la MNE (dé-enveloppement) et sont libérées nues dans le cytoplasme. Les capsides se lient et bourgeonnent dans les membranes du TGN (ré-enveloppement) et les virions enveloppés sont sécrétés dans le milieu extracellulaire. Adapté de *Johnson & Baines (383)*.

L'enveloppement primaire est principalement médié par deux protéines virales, la phosphoprotéine nucléaire pU_L31 et la protéine membranaire intégrale de type II pU_L34 (383, 390, 391). Ses deux protéines forment ensemble le complexe de sortie nucléaire « *nuclear egress complex* » (NEC) au niveau de la MNI. La protéine pU_L31 du NEC interagit avec la capside via la protéine pU_L25 du CVSC ou la protéine pU_L33 du complexe terminase (184, 383, 392-397). Cette interaction pU_L31-capside, est contrôlée via la phosphorylation de pU_L31 par

la sérine / thréonine kinase virale pUS3 (394, 398, 399). Les composants du NEC sont essentiels pour la sortie des capsides nucléaires et sont aussi incorporés dans les particules périnucléaires (369, 383, 385, 390, 391, 400-404). Mais avant d'atteindre la MNI, les capsides doivent contourner les lamines nucléaires qui forment un réseau dense de microfilaments nucléoplasmiques de type V qui tapissent la surface interne de la MNI faisant ainsi la liaison entre la chromatine et la membrane nucléaire et formant un composant structurel majeur du noyau (405). Le génome viral code pour deux kinases virales pUL13 et pUS3 que le virus utilise pour la phosphorylation et la dissociation des lamines A et C (406-412). Le virus exploite aussi les protéines kinases C de la cellule « *protein kinase C* » (PKC) qui sont recrutées à la membrane nucléaire d'une manière dépendante du NEC afin de phosphoryler les lamines B (383, 413-416) (figure 12).

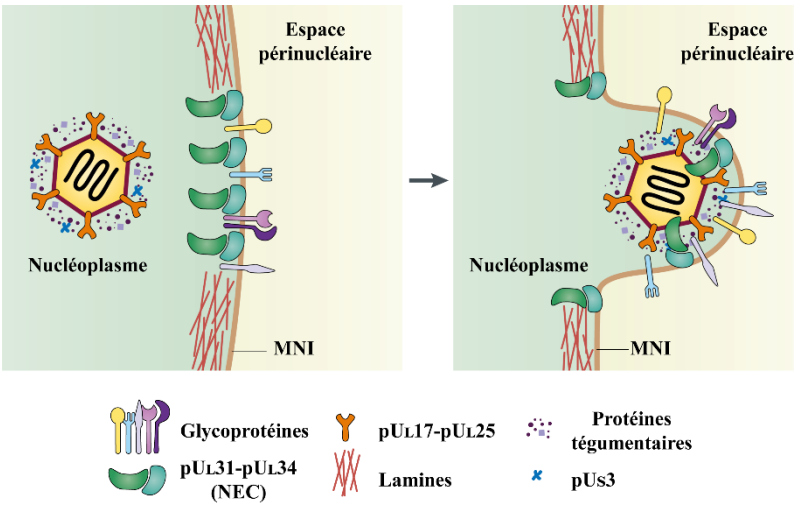

Figure 12 : L'enveloppement primaire.

La dissociation des lamines nucléaires de la membrane nucléaire interne (MNI) est favorisée par le complexe d'enveloppement nucléaire (NEC) avec la participation des kinases cellulaires et virales. Le NEC recrute des glycoprotéines virales qui sont incorporées dans la particule enveloppée. Une partie du tégument est déjà liée à la capside. Adapté de *Johnson & Baines (383)*.

En plus des protéines pUL31 et pUL34, des glycoprotéines virales telles que gB, gD, gH/gL et gM sont détectées au niveau la MNI et dans les particules virales périnucléaires ce qui

suggère leur rôle potentiel dans l'enveloppement ou même le dé-enveloppement. Le recrutement de ces glycoprotéines est favorisé par l'interaction avec le NEC (211, 213, 383, 401, 417, 418). L'analyse biochimique des capsides périnucléaires suggère que ces particules contiennent également quelques protéines du tégument telles que pUL11, pUL36 (VP1/2), pUL41 (vhs), pUL48 (VP16), pUL47 (VP13/14) et pUL49 (VP22) qui jouent des rôles importants dans l'enveloppement primaire (359, 395, 419-422). Toutefois, la densité du tégument de ces particules périnucléaires est moins importante que celle des virus extracellulaires suggérant que la majeure partie du tégument est ajoutée aux capsides durant le transport dans le cytoplasme et/ou pendant l'enveloppement final (188, 367, 422-424).

La deuxième étape dans le processus de la sortie des capsides nucléaires implique la fusion de l'enveloppe du virion périnucléaire avec la MNE libérant ainsi des capsides nues dans le cytoplasme (dé-enveloppement) (Figure 13).

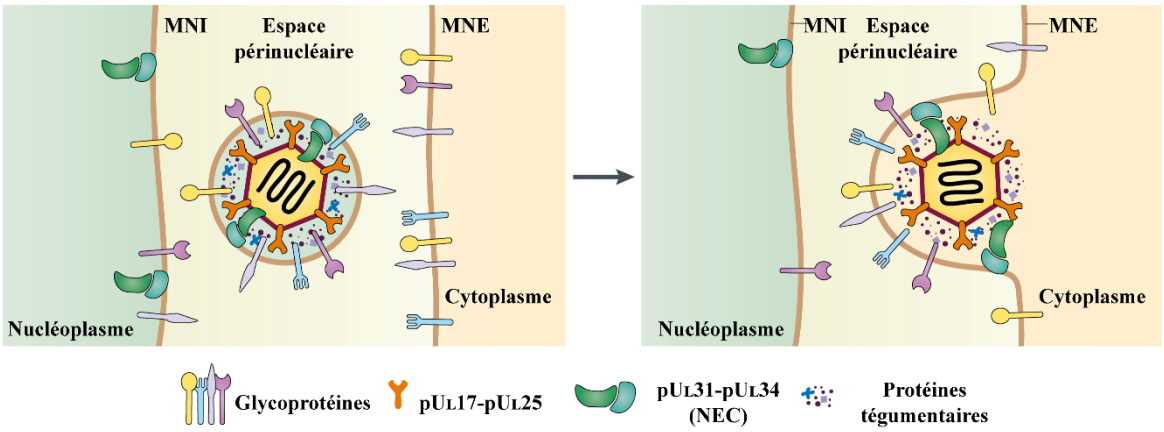

Figure 13: Le dé-enveloppement.

L'enveloppe primaire doit fusionner avec la membrane nucléaire externe (MNE) libérant des capsides nues dans le cytoplasme et laissant les protéines pUL31 et pUL34 du NEC dans la membrane nucléaire externe (MNE). Adapté de *Johnson & Baines (383)*.

Les mécanismes moléculaires qui régulent l'étape du dé-enveloppement ne sont toujours pas bien connus (359, 380, 381). Toutefois, des recherches rapportent l'implication de certaines protéines virales, notamment la protéine virale pUS3 dont l'activité sérine / thréonine

kinase est très importante pour un dé-enveloppement efficace (368, 406, 412, 425-427). En effet, une accumulation de virions enveloppés dans l'espace périnucléaire est observée lors de la mutation ou la délétion de la protéine pU_S3 (368, 398, 427). De la même façon que la phosphorylation de pU_L31 par pU_S3 induit l'interaction pU_L31-capside pour amorcer l'enveloppement primaire, la déphosphorylation de pU_L31 par pU_S3 induit le détachement du NEC de la capside au moment de la fusion de l'enveloppe des particules virales périnucléaires avec la MNE laissant ainsi les protéines pU_L31 et pU_L34 du NEC associés à la MNE (368, 369, 383, 389, 394, 428, 429).

Malgré la présence des glycoprotéines gB, gD et gH/gL dans la MNI et dans l'enveloppe des virions périnucléaires (383), leur implication dans le dé-enveloppement est très ambigüe du fait que la délétion simultanée de gB et de gH induit l'accumulation de virions enveloppés dans l'espace périnucléaire (211, 212), alors que la mutation individuelle de l'une ou de l'autre n'a pas d'effet important sur la sortie du noyau (430-432). La glycoprotéine gK semble aussi être impliquée dans la régulation du dé-enveloppement puisqu'une surexpression de gK provoque une accumulation de virions enveloppés dans l'espace périnucléaire (433). D'autres protéines virales telles que pU_L20, pU_L48 (VP16) et pU_L51 pourraient réguler positivement ou négativement cette étape (434-436).

En plus des facteurs viraux cités plus haut, des recherches suggèrent que des protéines cellulaires sont aussi responsables de la fusion de l'enveloppe du virion primaire et de la MNE (428, 429). Dans ce contexte, la déplétion de la chaîne lourde du CD98 (CD98hc) et de son partenaire intégrine β1 ainsi que la protéine p32 induisent des invaginations de la MNI dans le nucléoplasme et une accumulation aberrante de virions enveloppés aussi bien dans l'espace périnucléaire que dans les structures d'invagination (437-439). La surexpression de la Torsine A altère également le dé-enveloppement conduisant à l'accumulation de virions primaires dans

l'espace périnucléaire (440). Les interactions physiques à travers l'enveloppe nucléaire sont médiées par l'intermédiaire du complexe LINC « ***LI****nkers of* ***N****ucleoskeleton and* ***C****ytoskeleton* » qui relie le nucléosquelette au cytosquelette. Ce complexe est formé par les protéines à domaine KASH « *Klarsicht, ANC-1, SYNE homology* » situées dans la MNE, qui s'étendent dans le cytosol pour entrer en contact avec les filaments du cytosquelette, et les protéines à domaine SUN « Sad1/UNC-84 homology » incorporées dans la MNI qui s'ancrent dans les lamines nucléaires. Les protéines SUN et KASH interagissent étroitement dans l'espace périnucléaire pour former un pont entre les deux membranes nucléaires (441-449). Une surexpression de SUN induit une accumulation des virions enveloppés dans la lumière du réticulum endoplasmique et l'espace périnucléaire qui se dilate ce qui suggère son implication dans le dé-enveloppement (450).

L'utilisation de pU_L31 pour le dé-enveloppement dépend de la lignée cellulaire. De plus, les virus déplétés pour les protéines pU_L31 ou pU_L34 du NEC ont un faible niveau de réplication. Ceci suggère que le mécanisme qu'ils utilisent pour sortir du noyau est indépendant de pU_L34 et de pU_L31 (391, 402, 451, 452). Pour ce mécanisme, une nouvelle voie pour la sortie du noyau a été récemment décrite. En effet, l'infection des fibroblastes d'embryon de souris n'exprimant pas le gène TorA codant pour la torsine A induit une dégradation de l'enveloppe nucléaire (NEBD) « *Nuclear envelope breakdown* » (453).

I.3.1.7 La tégumentation

Le tégument constitue un réseau d'interactions protéine-protéine très dense et très complexe comprenant des milliers de copies de protéines de différentes tailles reliant la capside à l'enveloppe virale (198, 454-456). La distribution intracellulaire des protéines tégumentaires a été analysée afin de localiser le compartiment cellulaire dans lequel la tégumentation a lieu en évaluant la localisation des protéines tégumentaires. L'assemblage du tégument sur les

capsides se produit en majeure partie dans le cytoplasme, toutefois, la localisation nucléaire partielle de certaines protéines du tégument telles que pU$_L$36 (VP1/2), pU$_L$37, pU$_L$41 (vhs), pU$_L$46 (VP11/12), pU$_L$47 (VP13/14), pU$_L$48 (VP16), pU$_L$49 (VP22), ICP0 et ICP4 a été rapportée dans certaines études (190, 195, 383, 457-461).

En plus de son interaction avec les protéines pU$_L$17 et pU$_L$26 pour former le CVSC (145, 178, 182-187, 358), la protéine pU$_L$36 (VP1/2) interagit avec la capside nucléaire via la protéine majeure de la capside pU$_L$19 (VP5) (458, 462-465). Elle interagit avec une autre protéine de tégument (pU$_L$37) et ensemble, elles servent d'échafaudage sur lequel s'attacheront d'autres protéines tégumentaires (466-468). Contrairement à la plupart des autres protéines tégumentaires, pU$_L$36 et pU$_L$37 sont incorporées dans les virions avec une stœchiométrie fixe et la surexpression de pU$_L$37 dans les cellules infectées n'augmente pas son incorporation dans les virions (469-471). Toujours au niveau du noyau, la protéine pU$_L$48 (VP16) (faisant partie du tégument externe) s'ajoute en interagissant avec pU$_L$36 (454, 456, 472-474). A son tour, pU$_L$48 (VP16) interagit avec d'autres protéines du tégument externe pU$_L$41 (vhs), pU$_L$46 (VP11/12) et pU$_L$49 (VP22) (190, 456, 475-477). La délétion de pU$_L$48 (VP16) entraîne la production de grandes quantités de particules légères « *Light-Particles* » (ces particules non infectieuses sont composées principalement d'enveloppe et de protéines de tégument et sont dépourvues de capsides et d'ADN viral) qui contiennent les protéines pU$_L$46, pU$_L$47 et pU$_L$49, mais pas pU$_L$36 et pU$_L$37, suggérant que pU$_L$48 pourrait être un élément clé dans le lien entre le tégument interne et externe (478, 479). Les deux protéines pU$_L$46 et pU$_L$47 contribuent significativement à l'assemblage des virions. Or, le mécanisme régulant cette contribution reste mal connu (190). La protéine pU$_L$46 interagit aussi bien avec la capside qu'avec les protéines tégumentaires pU$_L$21, pU$_L$37, pU$_L$48, pU$_S$3, pU$_S$10 et ICP0 (190, 454, 456, 475, 480). De même, pU$_L$47 interagit avec de nombreuses protéines tégumentaires telles que pU$_L$14, pU$_L$17, pU$_L$21, pU$_L$48, pU$_L$49, pU$_S$11(190, 397, 481). D'autres interactions entre les protéines du

tégument ou le tégument et les glycoprotéines de l'enveloppe virale ont lieu dans le cytoplasme ou dans le TGN lors de l'enveloppement final faisant de la tégumentation un processus très complexe nécessitant encore beaucoup d'investigations pour comprendre comment ces protéines favorisent un assemblage efficace des virions (190, 194, 381).

I.3.1.8 L'enveloppement final ou le ré-enveloppement

Une fois qu'elles atteignent le cytoplasme, les capsides contenant les premières couches du tégument sont transportées jusqu'au site d'enveloppement où elles acquièrent l'enveloppe finale sur laquelle des glycoprotéines sont ancrées (Figure 14).

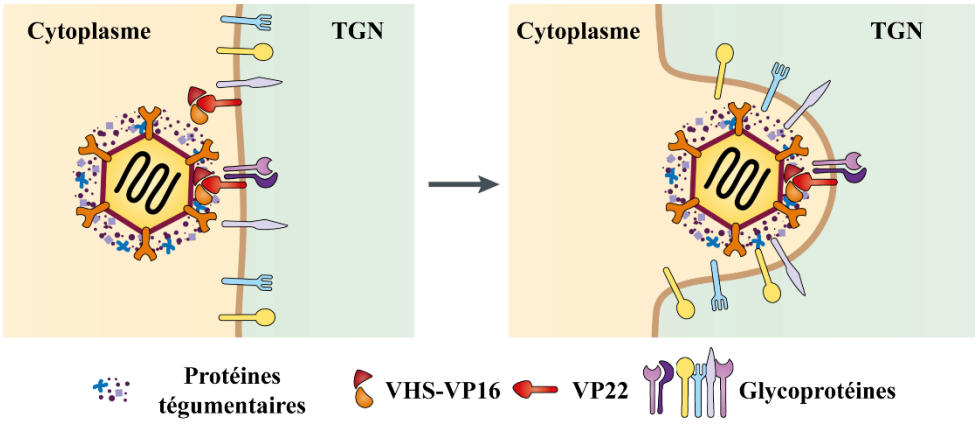

Figure 14: Le ré-enveloppement.

Dans le cytosol, les capsides contenant les premières couches du tégument se lient à la membrane du TGN qui contient des glycoprotéines virales. Les interactions entre le tégument et les glycoprotéines favorisent l'enveloppement. Adapté de *Johnson & Baines (383)*.

L'identité précise du ou des compartiments cytoplasmiques où l'enveloppement final a lieu a soulevé plusieurs débats. Cependant, de nombreuses études définissent le TGN comme étant le site de l'enveloppement final du VHS-1 (190, 200, 367, 387, 482-485). Les protéines de tégument contribuent au processus de ré-enveloppement en formant un réseau d'interactions très complexe reliant la capside à l'enveloppe virale. En effet, en plus de leurs interactions directes avec les protéines de la capside, les protéines du tégument interne interagissent également avec d'autres protéines solubles du tégument ainsi que les queues cytoplasmiques

des glycoprotéines virales ou des protéines associées à la membrane (190, 194, 198, 381, 383, 395, 486-489). Parmi les interactions tégument-tégument les plus caractérisées et ayant un impact direct sur l'enveloppement secondaire on trouve trois complexes pU_L7/pU_L51, pU_L11/pU_L16 et pU_L36/pU_L37 (190, 194, 381, 490). La protéine du tégument pU_L51 est localisée dans l'appareil de Golgi dans le cas de transfection alors qu'elle est périnucléaire dans le cas de l'infection (491). La délétion de pU_L51 induit une accumulation de capsides non enveloppées dans le cytoplasme (436, 492). Elle co-localise partiellement avec la protéine du tégument pU_L7 ainsi que gE au niveau de la MP, mais cette colocalisation est perdue lors de la déplétion de pU_L51 indiquant son implication dans le recrutement de pU_L7 au niveau de la membrane plasmique (493, 494). La délétion de pU_L7 a un effet similaire à celui de pU_L51 induisant une accumulation de capsides non enveloppées dans le cytoplasme (490, 495). Pris ensemble, ces résultats suggèrent que pUL7 et pUL51 fonctionnent comme un complexe qui favorise l'enveloppement secondaire au cours de la maturation. Le complexe $pU_L11/pU_L16/pU_L21$ est capable d'interagir avec les membranes en s'associant sur la queue cytoplasmique de gE via pU_L11 et pU_L16, avec une liaison directe de pU_L11 à gE favorisant l'interaction gE/pU_L16 (496-500). La délétion de pU_L11 ou de pU_L16 a pour résultat une réduction de l'enveloppement secondaire avec une accumulation de capsides non développées dans le cytoplasme (501-505). Le complexe pU_L36/pU_L37 assure le transport des capsides jusqu'au TGN via les moteurs moléculaires kinésines qui se trouvent aux extrémités des microtubules (192, 193, 200, 249, 251-256, 482, 506). La délétion de pU_L36 entraîne l'accumulation de capsides nues dans le cytoplasme (507). La protéine pU_L37 interagit avec gK et pU_L20 son partenaire de liaison associé à la membrane (488). Le complexe gK/pU_L20 est impliqué dans l'enveloppement secondaire et la localisation de gD et de gH/gL dans les sites d'assemblage (190, 508, 509). La déplétion de pU_L20 ou de gK induisent une accumulation des capsides non enveloppées dans le cytoplasme (510). La protéine pU_L36 (VP1/2) interagit

également avec pU_L48 (VP16) et la déplétion de cette dernière réduit l'enveloppement secondaire de manière drastique (478). La protéine pU_L49 contribue également à l'enveloppement secondaire par la formation d'un complexe tégument-glycoprotéine comprenant pU_L49, gE/gI, gM et ICP0, par lequel l'extrémité C-terminale de pU_L49 relie les extrémités cytoplasmiques de gE et gM alors que l'extrémité N-terminale recrute ICP0 (190, 511).

Les 16 protéines de l'enveloppe virale (gB, gC, gD, gE, gG, gH, gI, gJ, gK, gM, gN, pU_L20, pU_L43, pU_L45, pU_L56 et pU_S9) destinées à faire partie du virion mature devraient aussi être acheminées vers le TGN afin de rencontrer les capsides cytoplasmiques. La plupart de ces protéines contiennent des motifs dileucine, tyrosine dans leurs domaines cytoplasmiques qui prédispose leur localisation au TGN via des interactions avec la machinerie de tri cellulaire (512-521). Cependant, les autres protéines qui ne contiennent aucun de ces motifs sollicitent l'interaction avec d'autres protéines virales pour leur recrutement dans le TGN et leur incorporation dans les virions (190, 383). Par exemple, la localisation de l'hétérodimère gE/gI au TGN repose sur des motifs de trafic dans le domaine cytoplasmique de gE (506), et la localisation de gD et l'hétérodimère gH/gL au TGN est dépendante de gM et/ou de gK/pUL20 (190, 509, 522, 523).

Un nombre croissant de publications soulève l'implication des protéines Rab GTPases dans les derniers stades de la réplication de plusieurs virus enveloppés notamment l'assemblage et l'enveloppement final (524-530). Les protéines Rab GTPase jouent un rôle clé dans la régulation du trafic membranaire à différents endroits du système endomembranaire (531-535). La déplétion Rab1a/b, Rab5, Rab11 et Rab43 prévient l'enveloppement du VHS-1 (536, 537).

Une étude récente a démontré l'implication des microARN (miARN) dans l'enveloppement secondaire du VHS-1. Les microARN (miARN) sont une classe de petits ARN

non codants qui régulent post-transcriptionnellement les gènes en se liant à des séquences partiellement complémentaires dans la région 3' (3'UTR) des ARNm cibles. Dans cette étude, les miR-199a-5p et miR-199a-3p préviennent l'enveloppement secondaire en régulant négativement la protéine d'activation de la GTPase spécifique de Cdc42 (538).

I.3.1.9 Transport et sortie du virus

La première étape dans le transport des virions vers la membrane cytoplasmique consiste à la scission de la vésicule de transport - contenant dans sa lumière un virion enveloppé – du TGN. De nombreux virus enveloppés utilisent l'activité de scission du complexe de tri endosomal cellulaire nécessaire au transport « *endosomal sorting complex required for transport* » (ESCRT) pour cette étape cruciale de leur cycle viral (539-541). Ce complexe joue un rôle primordial dans le transport du VHS-1 via les corps multivésiculaires (MVB) et la protéine Vps4 (542-547). Le VHS-1 utilise également des protéines impliquées dans la voie de sécrétion, afin de faciliter la sortie à travers membrane plasmique, telles que Rab3A, Rab6A, Rab8a, Rab11a, GAP-43, kinésine-1 et SNAP-25 (190, 548). La déplétion de Rab6A, Rab10, Rab13 et Annexin1 par des siRNA est préjudiciable à la réplication du VHS-1 et la déplétion de Rab27a réduit la production de particules virales suggérant ainsi son rôle dans le transport des vésicules contenant les virions et la fusion avec la membrane cytoplasmique (549-551). La protéine Kinase D (PKD3) joue aussi un rôle très important durant cette étape du fait que sa déplétion empêche le transport du TGN vers la membrane cytoplasmique (552).

I.3.2 L’infection latente

La latence est décrite comme une infection durant laquelle le génome viral persiste dans les neurones de l'hôte sans production de protéines virales ou particules virales infectieuses (3, 219, 304, 553-557). Les neurones sensoriels des ganglions trigéminaux qui innervent les lèvres, la gencive et les yeux sont le principal site de latence du VHS-1 chez les humains (3). Toutefois,

les neurones sympathiques et sensoriels des ganglions vestibulaires, géniculés, spiraux et sacrés peuvent également être des sites de latence (553, 558, 559). La latence peut persister pendant toute la vie sans manifestations symptomatiques, avec possibilité de réactivation à tout moment suite à un stimulus (3). L'infection latente peut être divisée en trois phases: l'établissement, le maintien et la réactivation (3, 219, 304, 553-557).

Dans une infection lytique, la protéine du tégument VP16 (pU_L48) est relâchée en même temps que la capside dans le cytoplasme ou elle interagit avec le facteur de cellule hôte 1 « *Host cell factor 1* » (HCF-1) qui contient une séquence de localisation nucléaire (NLS), et à la suite de cette association, VP16 est transportée vers le noyau (560). Dans le noyau, les deux protéines (VP16/HCF-1) interagissent avec la protéine Oct-1 « *Octamer binding protein-1* » pour former un complexe trimérique (VP16/HCF-1/Oct-1) qui interagit à son tour avec les promoteurs des gènes immédiats précoces favorisant leur association avec des histones acétyltransférases et des lysine déméthylases qui entrainent la modification des histones activant ainsi la transcription et la synthèse des protéines immédiates-précoces (219, 278, 279, 556, 561-563). Cependant, lors d'une infection latente, les mécanismes qui contrôlent le cycle viral lytique ne sont pas adéquatement respectés. Les particules virales libérées lors du cycle lytique dans les cellules épithéliales infectent les neurones sensoriels au niveau des terminaisons nerveuses. Les capsides libérées dans le cytoplasme sont transportées le long des axones via la dynéine cytoplasmique associée aux microtubules qui fournit la force motrice pour les mouvements rétrogrades vers le noyau au niveau du corps cellulaire (219, 564). Cette longue distance (axone) parcourue par les capsides, entrave le transport efficace de VP16 jusqu'au noyau et semble jouer un rôle très important dans l'établissement de la latence du fait que l'infection des corps cellulaires conduit à un cycle lytique, alors que l'infection des terminaisons nerveuses mène à une infection latente (553, 565). En plus, dans les neurones, Oct-1 n'est pas exprimée et HCF-1 est exclusivement cytoplasmique ce qui va à l'encontre de la formation du complexe

trimérique (VP16/HCF-1/Oct-1) et donc à la transcription des gènes immédiats précoces (219, 553, 556, 566-569). Pendant la latence, le génome viral persiste sous une forme épisomale associée à la chromatine ce qui empêche la transcription des gènes viraux à l'exception d'un ARN non codant connu sous le nom de transcrit associé à la latence « *latency-associated transcript* » (LAT) (220, 221, 275, 570, 571) (Figure 15).

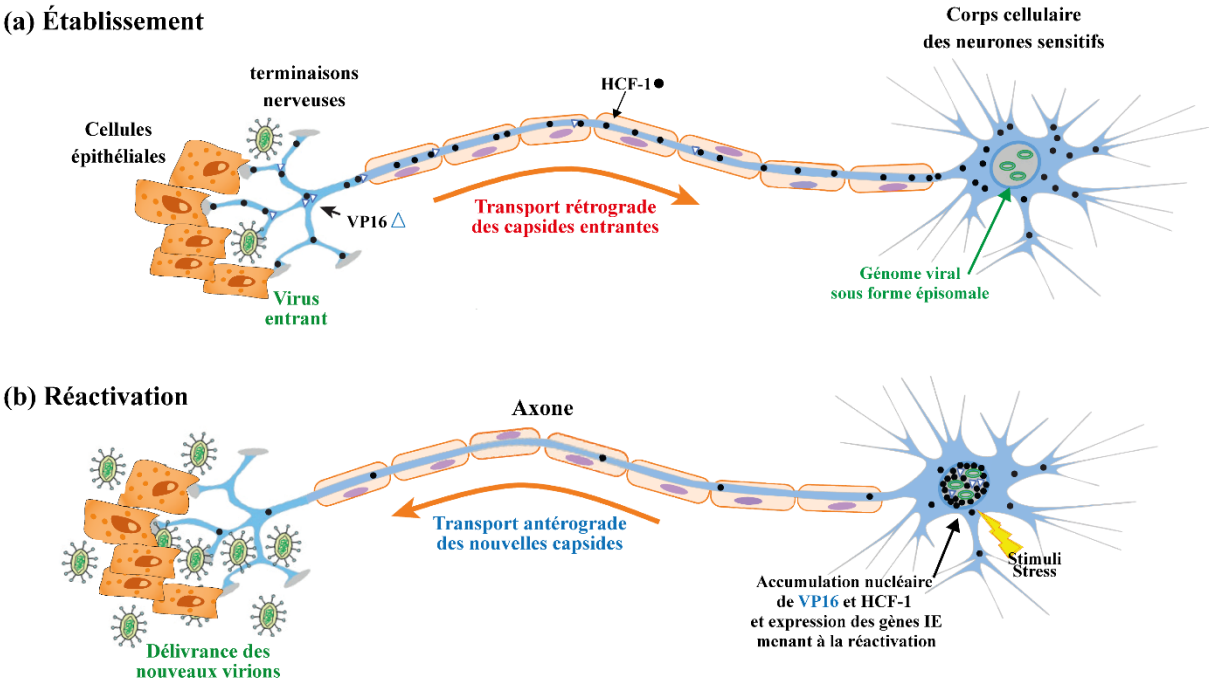

Figure 15: Établissement de la latence et réactivation.

(a) Le VHS-1 pénètre dans les neurones via les terminaisons nerveuses innervant les cellules épithéliales. Les capsides sont transportées le long des axones par un mouvement rétrograde vers le noyau au niveau du corps cellulaire. La protéine du tégument VP16 (triangles bleus) se dissocie de la capside presque immédiatement après sa libération dans le cytoplasme, et migre vers le noyau avec une très faible efficacité entravant ainsi la formation du complexe trimérique (VP16/HCF-1/Oct-1) et donc la transcription des gènes immédiats précoces. **(b)** Les stimuli de réactivation favorisent l'accumulation nucléaire de HCF-1(cercles noirs) et VP16, qui est synthétisée *de novo* stimulant ainsi la réplication de l'ADN viral et la transcription des gènes viraux. Les capsides nouvellement formées sont transportées par un mouvement antérograde vers les terminaisons nerveuses des axones où elles arrivent à maturité et sont ensuite libérées pour assurer un nouveau cycle infectieux lytique dans les cellules épithéliales. Adapté de *Wilson & Mohr (553).*

Le LAT est un transcrit primaire de 8,3 kb, qui est épissé en introns LAT majeurs stables de 1,5 et 2 kb qui s'accumulent abondamment dans les noyaux des neurones infectés (572), ainsi qu'un exon mineur très instable de 6,3 kb difficile à détecter de manière fiable sans l'utilisation

de techniques très sensibles du fait qu'il est rapidement excisé en plusieurs miARN (573-576). Le LAT et les miARN associés semblent limiter l'expression des gènes immédiats-précoces *in vitro* en apportant des modifications post-traductionnelles aux histones associées aux promoteurs des gènes viraux maintenant ainsi l'état de latence (275, 577-581). LAT favorise la survie des neurones après l'infection par le VHS-1 en réduisant l'apoptose. Ceci est soutenu par des études qui démontrent que les mutants LAT$^-$ établissent la latence de façon moins efficace que le type sauvage et que leur neurovirulence est plus forte (582-584).

Le génome du VHS-1 contient 18 structures en tige-boucle qui aboutissent à 27 séquences de miRNA matures miR-H1 à miR-H27 dont 6 sont localisés dans le LAT (miR-H2, H3, H4, H5, H7 et H8) (569, 585). Les fonctions de la majorité de ces miRNA restent inconnues. Toutefois, Les miR-H6, miR-H2, miR-H3 et miR-H4 régulent négativement l'expression des gènes viraux ICP0, ICP6 et ICP34.5 respectivement et leur expression est élevée lors de la latence indiquant leur implication dans l'établissement et le maintien de la latence (585). Le niveau d'expression de miR-H15, miR-H17, miR-H18, miR-H26 et miR-H27 augmente significativement lors de la réactivation suggérant un rôle potentiel de ces miRNA dans cette étape (585, 586). Les microARN cellulaires semblent aussi jouer un rôle dans la latence. Le microARN cellulaire miR-101, qui cible la région non traduite 3' de la sous-unité bêta de l'ATP synthase mitochondriale (ATP5B), agit comme une défense cellulaire qui empêche la réplication lytique du VHS-1 ce qui peut favoriser son entrée dans la latence (585, 587).

À la suite d'un stimulus (stress, fatigue, température, traumatisme, exposition aux UV…etc), le VHS-1 est susceptible de se réactiver. Pendant la réactivation, les niveaux du transcrits LAT diminuent et les histones qui lui sont associées deviennent désacétylées. (221, 588). L'accumulation du HCF-1 dans le noyau en même temps que de VP16 nouvellement

produite, stimule la réplication de l'ADN viral de même que la transcription des gènes viraux tels que ICP0. Cette dernière s'associe à des histones acétylées favorisant ainsi la transcription des gènes lytiques et l'accumulation de leurs transcrits. (221, 553). Les capsides nouvellement formées sont transportées par un mouvement antérograde vers les terminaisons nerveuses des axones où elles arrivent à maturité et sont ensuite libérées pour assurer un nouveau cycle infectieux lytique dans les cellules épithéliales adjacentes.

I.4 Détection et analyse des particules virales

I.4.1 Les techniques quotidiennes de laboratoire

Les virus ne sont généralement détectés que de manière indirecte et les principales méthodes d'étude des virus animaux sont centrées sur la croissance des cellules vivantes, la réaction avec des anticorps spécifiques (comme le cas pour les tests ELISA pour détecter des antigènes viraux ou des anticorps spécifiques au virus), le dosage par plaque « *plaque assay* » pour quantifier les particules infectieuses ainsi que la réaction en chaîne de la polymérase « *polymerase chain reaction* » (PCR) (589-591). De plus, il est difficile d'étudier un virus qui n'atteint pas un titre élevé dans des cellules en culture (*in vitro*) ou dans un modèle animal (*in vivo*) (592). Toutes les techniques classiques pour la détection des virus ont leurs forces et leurs limites, et devraient être choisies avec soin en prenant en considération la vitesse, l'automatisation, la fiabilité et le coût de chaque technique (593-595).

I.4.2 La protéomique virale

La connaissance de la composition protéique des particules virales matures ou des intermédiaires cellulaires lors de l'infection est un élément très important pour les études fonctionnelles de la pathogenèse virale. Ceci permet de comprendre de nombreux aspects tels que l'abondance et la localisation des protéines virales et de concentrer l'analyse sur des protéines spécifiques afin de déterminer leurs rôles au cours de l'infection. La protéomique est

une technologie à haut débit qui complète l'exploration génomique pour évaluer les interactions protéine-protéine (596). Les progrès de la protéomique basés sur l'utilisation des techniques d'identification des protéines telles que la spectrométrie de masse « *mass spectrometry* » (SM) ont révolutionné l'étude des protéines en permettant l'analyse de leur expression globale, ce qui a contribué à notre compréhension des interactions hôte-virus, en mettant l'accent sur les virus qui ont un impact sur la santé humaine (596, 597). Au cours des dernières années, la SM a connu des avancées significatives, ce qui a permis d'améliorer la résolution, la détection et la quantification des peptides/protéines. Ainsi, dans un seul et même échantillon, on peut observer plusieurs milliers de protéines de tailles différentes (3 - 300 kDa) avec des quantités aussi faibles qu'une copie (596-599). Depuis les années 1990, la SM a permis d'analyser la composition protéique de plusieurs virions purifiés, et a conduit à l'identification de composants jusqu'alors inconnus. Ainsi l'étude de la composition protéique de plusieurs virus herpétiques a été possible grâce à la SM. Tel est le cas pour le cytomégalovirus humain (HCMV), le cytomégalovirus murin (MCMV) le virus d'Epstein-Barr (EBV), le virus de l'herpès associé au sarcome de Kaposi (KSHV), etc. (600-606). Le VHS-1 ne fait pas l'exception. En effet, l'analyse par SM de virus extracellulaires matures hautement purifiés a déterminé que ces particules virales contiennent 8 protéines de capsides, 13 glycoprotéines virales, 23 protéines tégumentaires et au moins 49 protéines cellulaires (188). Une autre étude toute récente a identifié une nouvelle protéine cellulaire capable d'interagir avec la glycoprotéine virale M (gM) et de moduler les processus de fusion membranaires induites par le virus (607). Malgré le fait que la protéomique virale soit victime de sa grande sensibilité (la présence de quantités infimes de contaminants peut être détecté), elle demeure une technique très performante dans l'identification et l'analyse des protéines virales (597).

I.4.3 La cytométrie de flux

La cytométrie en flux implique la détection de cellules, et la caractérisation des populations cellulaires selon leur taille et leur granulosité. Elle a permis la différenciation de plusieurs populations cellulaires et d'examiner et d'analyser leurs processus internes (608, 609). Les progrès récents dans le domaine de la cytométrie de flux ont favorisé l'amélioration de la détection en ajoutant des photomultiplicateurs au cytomètres ce qui a permis la détection de particules aussi petites que 100 nm. Ces petites particules peuvent être des composants cellulaires comme des exosomes, ou même extracellulaires, tels que de petites bactéries ou des virus (610-613). La virométrie en flux fait référence à l'utilisation d'un cytomètre de flux pour détecter des particules virales. Les virus sont couramment analysés par des techniques telles que la microscopie électronique (ME), l'ELISA, le Western blot, la PCR...etc. Cependant, ces méthodes analysent les préparations virales en vrac (incapacité d'analyser des virions individuels ou leurs proportions dans des préparations virales et le manque de discrimination entre les virions et les particules virales non infectieuses) et nécessitent souvent une préparation d'échantillons qui est dans certains cas très difficile (614). Tandis que, la virométrie de flux permet la détection et l'analyse directe des particules virales individuelles (612, 615-617). Comme pour le cas des cellules, les particules virales sont d'abord isolées puis incubées soit avec des anticorps spécifiques ou avec des molécules fluorophores puis analysées individuellement à travers un cytomètre de flux.

I.5 Hypothèses et objectifs de recherche

Le VHS-1 est un agent infectieux responsable de plusieurs pathologies allant des moins graves comme les lésions orolabiales plus connues sous le nom des feux sauvages, au plus sérieuses telles que les encéphalites et les kératites. Il n'y a pas de traitement curatif ni de vaccin contre les infections au VHS-1. Afin de pouvoir mieux contrôler ces maladies, il faut être capable de bien comprendre et de maîtriser le cycle de réplication viral, de l'entrée du virus jusqu'à la sortie des nouveaux virions en passant par la maturation des capsides nucléaires et les mécanismes sous-jacents ainsi que le processus de tégumentation. Cependant, bien que les nombreuses recherches aient apporté considérablement d'éléments de réponses sur ces points, beaucoup de questions se posent toujours concernant la sortie du noyau ainsi que la couche du tégument et le processus de tégumentation.

Dans un premier temps, l'analyse protéomique des particules virales matures du VHS-1 par SM a déterminé que la majeure partie des protéines qui les composent se trouve dans la couche du tégument (188). Cette couche est très complexe et sa formation dépend de multiples interactions entre les diverses protéines du tégument avec les protéines de la capside et de l'enveloppe virale (190, 192-194). Des analyses des particules virales ont montré que les protéines formant la capside sont hautement structurées et ont une stœchiométrie stable (618). Cependant, d'autres études estiment que les protéines constituant le tégument sont moins structurées (191, 471, 619, 620). La déplétion des protéines du tégument affecte directement l'infectiosité et la réplication du virus (189, 621). L'analyse de la couche tégumentaire et de l'importance de la quantité relative des protéines qui la constituent ainsi que son impact sur l'infectiosité permet d'évaluer directement l'impact biologique de la variabilité de ces protéines au niveau individuel des particules virales. Or, une telle analyse a été difficile car la plupart des méthodes évaluent généralement la composition moyenne des populations virales entières et non pas la teneur pour chaque particule individuelle. Comme hypothèse, nous pensons que

certaines protéines de tégument ont une stœchiométrie rigoureusement contrôlée, tandis que d'autres ont une stœchiométrie flexible. Nous pensons aussi qu'il est très probable qu'en plus de leur présence qualitative, la quantité relative des protéines du tégument modulent également l'infectiosité. L'objectif donc est d'évaluer, par virométrie de flux, la variabilité des protéines de tégument du VHS-1 entre les particules virales individuelles ainsi que d'évaluer la pertinence biologique de cette variabilité sur les particules virales.

Dans un second temps, lors de la maturation des capsides nucléaires, les capsides C sont préférentiellement libérées par le noyau (383, 388, 622). On pensait que cette sélection était dû à la présence du complexe pU_L17/pU_L25 sur les capsides C (145, 184, 395). Or, il a été observé par la suite que ce complexe est présent également sur les capsides A et B (145, 186, 187). Ceci laisse penser à l'implication des protéines de l'hôte dans ce processus. Aussi, le recrutement des premières protéines du tégument semble avoir lieu dans le noyau (196). Toutefois, malgré les connaissances cumulées jusqu'à nos jours et les efforts colossaux en recherche, les mécanismes responsables de la maturation des capsides et l'acquisition des protéines du tégument restent ambigus. Pour cela, la caractérisation de la composition protéique précise des capsides nucléaires A, B et C serait très informative. Comme hypothèse, nous pensons que les protéines virales qui composent les capsides C seraient légèrement ou pas différentes de celles qui composent les capsides A et B. Ceci suggèrerait que la sélection des capsides C par le noyau serait la conséquence d'un processus plus complexe impliquant les protéines de l'hôte. Aussi, nous pensons que les protéines du tégument interne seraient acquises au niveau du noyau. Malheureusement la séparation des capsides nucléaires sur un gradient de densité nous procure des capsides C contaminées a 30% par les B (356). Or, la combinaison du gradient de densité à la virométrie de flux semble résoudre ce problème (356). Le premier objectif serait donc de produire des enchantions de haute pureté en combinant le gradient de densité à la virométrie de flux. Le second objectif est d'analyser les capsides nucléaires par spectrométrie de masse afin

de déterminer la composition protéique exacte pour les trois types de capsides (A, B et C) présentes dans les noyaux des cellules infectées incluant les protéines cellulaires qui leur sont associées. Cette analyse nous permettra également de déterminer si l'acquisition des protéines du tégument débute effectivement au noyau à un stade précoce du cycle viral.

Ce projet de recherche constitue un point de convergence entre plusieurs techniques classiques et innovatrices en virologie, biologie cellulaire et protéomique. Il permet d'ajouter de nouveaux éléments quant à la maturation des capsides virales ainsi que le processus de tégumentation et la modulation des protéines du tégument et son impact sur l'infectiosité. Finalement, il contribue à l'accumulation de nouvelles données qui permettront probablement d'ouvrir de nouvelles voies de recherche pour mieux comprendre et contrôler le cycle viral ainsi que d'exporter la technologie de la virométrie en flux pour étudier d'autres virus.

Chapitre II - Résultats – présentation par articles

II.1 Article 1: Quantitative Evaluation of Protein Heterogeneity within Herpes Simplex Type I Viral Particles

Auteurs : Nabil El Bilali, Johanne Duron, Diane Gingras et Roger Lippé

Publié dans : Journal of Virology. May 2017 ; volume 91, n°10.

Contribution des auteurs :

Nabil El Bilali* : Conception, planification et réalisation des expériences, analyse des données, montage des figures et rédaction de l'article.

Johanne Duron : Préparation des stocks des virus déplétés pour VP16 et VP22.

Diane Gingras : Contribution dans l'optimisation et la réalisation des expériences de microscopie électronique.

Roger Lippé : Création et supervision du projet, conception des expériences, analyse des données et rédaction de l'article.

* Premier auteur

Note sur le texte :

Cette section reproduit le texte intégral de l'article mentionné ci-dessus.

Certaines modifications ont toutefois été apportées à la mise en page du manuscrit afin de mieux l'intégrer à la présente thèse.

Quantitative evaluation of Protein Heterogeneity within Herpes simplex type I Viral Particles

by

Nabil El Bilali, Johanne Duron, Diane Gingras and Roger Lippé

Department of Pathology and Cell biology, University of Montreal.

Succursale Centre-Ville, Montreal, Quebec, Canada

Running title: HSV-1 Tegument Heterogeneity Impacts Infectivity

Corresponding author

roger.lippe@umontreal.ca

II.1.1 Abstract

Several virulence genes have been identified thus far in the herpes simplex virus type 1 genome. It is also generally accepted that protein heterogeneity among virions further impacts viral fitness. However, linking this variability directly with infectivity has been challenging at the individual viral particle level. To address this issue, we resorted to flow cytometry (flow virometry), a powerful approach we recently employed to analyze individual viral particles, to identify which tegument proteins vary and directly address if such variability is biologically relevant. We found that the stoichiometry of the U_L37, ICP0 and VP11/12 tegument proteins in virions is more stable than the VP16 and VP22 tegument proteins which varied significantly among viral particles. Most interestingly, viruses sorted for their high VP16 or VP22 content yielded modest but reproducible increases in infectivity when compared to their corresponding low containing VP16 or VP22 counterparts. These findings were corroborated for VP16 in siRNA experiments but proved intriguingly more complex for VP22. An analysis by quantitative Western blotting revealed substantial alterations of virion composition upon manipulation of individual tegument proteins and suggests that VP22 protein levels acted indirectly on viral fitness. These findings reaffirm the interdependence of the virion components and corroborate that viral fitness is not only influenced by the genome of viruses but also by the stoichiometry of proteins within each virion.

Importance

The ability of viruses to spread in animals has been mapped to several viral genes but other factors are clearly involved, including virion heterogeneity. To directly probe whether the latter influences viral fitness, we analyzed the protein content of individual herpes simplex virus type 1

particles using an innovative flow cytometry approach. The data confirm that some viral proteins are incorporated in more controlled amounts, while others vary substantially. Interestingly, this correlates with a trans-activating viral protein and indirectly to a second virion component, whose modulation profoundly alters virion composition. This reaffirms that not only the presence but also the amount of specific tegument proteins is an important determinant of viral fitness.

II.1.2 Introduction

Over the years, virulence genes that modulate the ability of viruses to propagate have been identified. Given their parasitic nature, viruses are also largely influenced by their hosts. This relates, for example, to both the innate and acquired immune responses and the presence of specific cellular receptors that contribute to tropism. However, many reports suggest that protein heterogeneity among viral particles additionally impacts viral fitness, but it has been challenging to probe at the individual virion level. One important reason is that most methods typically evaluate the average composition of whole viral particle populations and rarely address individual particle content. On the other hand, techniques such as immuno-EM and fluorescence microscopy, do evaluate particle to particle variation but not infectivity. Thus, no tool existed until now to directly evaluate the biological relevance of protein variability among individual virions. The present work attempts to tackle this issue.

Mature herpes simplex virus type 1 (HSV-1) virions are composed of 4 distinct layers encompassing the double stranded DNA viral genome, a capsid, a so-called tegument and a host-derived lipid envelope. Altogether, at least 44 different viral proteins and potentially as many cellular proteins are incorporated in mature extracellular HSV-1 viruses (1). Interestingly, the bulk of these proteins are contained within the tegument, an intricate layer whose composition is dependent on multiple interactions among the various tegument proteins as well as with capsid and

envelope proteins (2). As for other viruses, virulence varies within and among HSV-1 stocks, while viral preparations typically contain a vast array of heterogeneous particles dominated by the presence of non-infectious particles (3). These properties make HSV-1 an ideal candidate to study protein variability among viral particles and probe the impact of this variability on the ability of the virus to infect cells.

The HSV-1 tegument structurally bridges the viral envelope to the capsid. It is multifunctional and is implicated in capsid transport, targeting of the incoming capsids to the nuclear pores, egress of newly made viral particles and acquisition of the final envelope (4, 5). Among the tegument proteins are trans-activating molecules that modulate the expression of other viral proteins. These include ICP0, ICP4 and VP16 that are all present in virions, presumably to jump start the infection cycle (6-8). Not surprisingly, depleting or altering these proteins genetically or by RNA interference leads to reduced viral yields (9-13). Thus, the tegument proteins are not merely structural but also active participants in most aspects of the viral life cycle and are important determinants of viral fitness. It is very likely that, in addition to their qualitative presence, their relative amounts in a given viral particle also modulate the infection, but evaluating this relationship has been difficult.

While the stoichiometry of the components forming the highly structured HSV-1 capsid has been determined with good accuracy (14), only rough estimates prevail for the more loosely organized tegument layer. These last estimates were originally derived from semi-quantitative sypro red or coomassie staining of protein gels and autoradiograms (15-17). More recently, tegument abundance has also been monitored by coincidence fluorescence spectroscopy and, in the case of pseudorabies herpesvirions (PRV), by fluorescence microscopy of GFP tagged components (18, 19). Several pieces of evidence suggest that some tegument proteins have a tightly controlled

stoichiometry, while others may be more flexible. For instance, overexpression of the abundant VP22 tegument leads to its greater incorporation in mature virions (20). This contrasts with U_L37, whose quantity remains stable in virions even when exogenously overexpressed (21). Moreover, an analysis by quantitative mass spectrometry of deletion mutants of the related pseudovirus hinted that VP1/2 and VP13/14 are incorporated in virions in fixed amounts, while VP11/12, VP16, and VP22 are present in variable quantities (22). These findings are consistent with work by Smith and colleagues who found some heterogeneity of specific tegument proteins among viral particles (19). However, none of the above studies addressed whether this heterogeneity is mirrored by corresponding changes in infectivity at the individual particle level. Interestingly, the addition of extraneous tegument proteins in the form of so-called L-particles, which contain an envelope and tegument proteins but are devoid of viral capsid and genome, enhances the ability of transfected viral DNA to generate infectious particles (23), pointing to the importance of the relative amount of tegument proteins.

The goal of the present study was to quantitatively evaluate the variability of the HSV-1 tegument proteins among viral particles and to evaluate the biological relevance of that particle-to-particle variability. To this end, we resorted to flow cytometry, a powerful method we recently employed to characterize and purify HSV-1 nuclear capsids (24). The present study shows that flow cytometry can also be used to study naturally occurring heterologous populations of mature extracellular HSV-1 virions. It further confirms that some tegument proteins are more stable in their stoichiometry from viral particle to the next while others, such as VP16 and VP22, are incorporated in greatly more flexible amounts. Interestingly, the sorting by flow cytometry of virions based on their VP16 or VP22 content translated into a modest but reproducible modulation of infectivity with particles containing more VP16 or VP22 being slightly more infectious.

Interestingly, RNA interference studies targeting VP16 corroborated these findings, while virion depletion of VP22 hinted at a more complex scenario. Quantitative Western blot analyses of the viral tegument layer thus indicated that this latter phenotype is likely multifactorial and indirectly related to VP22 protein levels. They also revealed that altering one tegument component, for instance by changing its stoichiometry or by tagging it with GFP, can have profound implications for the overall composition of the virions. We ultimately confirmed at the individual viral particle level that the amount of individual tegument proteins in the virions, as opposed to merely their presence, is indeed a contributing factor that modulates infectivity of the viral particles. Thus, not only the presence but also the amount of specific proteins in mature virions constitutes a *bona fide* viral fitness factor.

II.1.3 Materials and Methods

Cells and viruses. African green monkey kidney Vero cells (ATCC CCL-81) were cultured at 37°C in 5% CO_2 in Dulbecco's modified Eagle's medium (Sigma-Aldrich) supplemented with 10% fetal bovine serum (FBS; HyClone®), 2 mM L-glutamine (Life Technologies), and antibiotics (100 U/ml penicillin and 100 µg/ml streptomycin). 143B cells (ATCC CRL-8303) were also supplemented with 15 mg/ml 5-bromo-2 deoxyuridine (BrdU; Sigma).

The GFP tagged and corresponding wild type HSV-1 viral stocks used in this study are summarized in Table 1. These include the parental strains KOS, F and 17+ that were kindly provided by Beate Sodeik. The K26GFP and K37eGFP recombinant viruses, both in the strain KOS background and carrying a GFP tag on the capsid protein VP26 and the tegument protein U_L37 respectively, were kindly provided by Prashant Desai (25, 26). The HSV-1 GS4677, GS3351, GS3330 and GS2971 recombinant viruses carrying a GFP tag on the capsid protein U_L25, the tegument proteins VP11/12 and VP16 and the envelope glycoprotein B (gB) respectively (all strain

F derived) were generously provided by Gregory Smith (27, 28). The 0+ GFP 12 and 0+ GFP 105 recombinant viruses, obtained from William Halford, are in the KOS background and carry a GFP tag on the tegument protein ICP0 between the amino acids 11-12 and 104-105 respectively (29). The GHSV-U_L46 recombinant virus tagging VP11/12 (strain KOS) was kindly provided by Jim Smiley (30), while the HSV-1 VP16-GFP recombinant virus (strain 17+) carrying a GFP tag on the aforementioned protein was obtained from Peter O'Hare (31). Finally, the HSV-1 GFP VP22 recombinant virus (strain 17+) carrying a GFP tag on the tegument protein VP22 was kindly provided by Gill Elliott (32). All viruses were amplified on BHK, 143B or Vero cells and tittered on Vero cells by plaque assay as previously described (33). Please note that, for clarity, all figures in this study refer to the tagged proteins rather than the official names of the viruses (see Table 1).

Purification of extracellular virions. Vero cells freshly passaged the day before were grown on 500 cm^2 dishes until 80% confluent. Cells were mock treated or infected with wild type or recombinant HSV-1 at a multiplicity of infection (MOI) of 5. At 18 hours post infection (hpi), the extracellular medium was harvested and clarified by centrifugation at 300 x g for 5 min at 4°C. The samples were then filtered through a 0.45 µm filter to eliminate intact cells and large cellular debris. Extracellular virions were subsequently pelleted by centrifugation at 20,000 x g for 1 hour at 4°C in a Beckman SW32-Ti rotor. The viral pellets were resuspended in MNT buffer (30 mM MES, 100 mM NaCl, 20 mM Tris HCl pH 7.4) and treated for 30 min at 10°C with 500 U/mL of DNAse I (Roche) and 2 mg/ml of RNAse A (Invitrogen) to digest both cellular and non-encapsidated viral nucleic acids. The viral preparations were then stored at -80°C.

Antibodies. Primary antibodies for Western blotting were graciously provided by various sources (and diluted) as follows. Anti-VP1/2 (1:300) provided by R. Courtney (34); anti-U_L37 (1:1000) provided by F. J. Jenkins (35); anti-U_S3 (1:4000) provided by B. Roizman (36); anti-VP16 (1:1000) provided by H. Browne (37); anti-VP13/14 (1:5000) and anti-VP22 (1:10000) provided by G. Elliot (38, 39). Commercial antibodies against VP5 (1:1000; Cedarlane), ICP0 (1:5000; Abcam), ICP4 (1:1000; Abcam) and calnexin (1:1000; Enzo Life Sciences) were also used. Horseradish peroxidase-coupled secondary antibodies (goat anti-mouse or anti-rabbit) were used at 1:10000 and were purchased from Jackson ImmunoResearch.

Gel electrophoresis and quantitative Western blotting. Five micrograms of extracellular virions were boiled for 10 min in loading buffer (50 mM Tris-HCl pH 6.8, 2% SDS, 0.1% bromophenol blue, 10% glycerol, and 2% β-mercaptoethanol) and separated on 10% SDS-PAGE gels. Proteins were electrophoretically transferred from the gels to polyvinylidene difluoride (PVDF) membranes, and the membranes incubated for 30 min in blocking buffer (10% nonfat dry milk, 13.7 mM NaCl, 0.27 mM KCl, 0.2 mM KH_2PO_4, 1 mM Na_2HPO_4, and 0.1% Tween 20). All primary antibodies were diluted in blocking buffer and added to blots for 1 to 2 h. Blots were then washed three times in blocking buffer and probed with secondary antibodies conjugated to horseradish peroxidase. The detection was done on a ChemiDoc MP System (Bio-Rad), which has a 4 orders of magnitude dynamic range, and Clarity Western ECL Substrate (Bio-Rad). Images were acquired and analyzed with the Image Lab Software Version 5 (Bio-Rad). The volume intensity of each tegument band was divided by that of the Calnexin (in case of cell lysates) or VP5 capsid protein (in case of extracellular virions) for each sample to normalize for gel loading. These

tegument/VP5 ratios were finally compared to that of wild type of each strain, arbitrarily set at 1, to avoid biases among viral strains.

Syto 13 and Syto 61 fluorescence labeling of viral particles. Five microliters of a diluted fraction of DNAse/RNAse treated virions were incubated for 1 h at 4°C with 1 µM Syto 13 (green fluorescence) or Syto 61 (red fluorescence; Invitrogen), unless otherwise indicated. Note that either Syto signal is minimal as a free molecule but strongly stimulated when bound to nucleic acid. Consequently, unwashed labeled virions were directly analyzed by flow cytometry (see below). To measure the impact of the Syto dyes on the viability of the virus, the stained samples were directly assessed in plaque assays as described below.

Flow cytometry analysis. Flow cytometry was performed as previously described (24). Briefly, Syto 13 or 61 labeled particles and/or GFP recombinant viruses diluted 1:500 in 0.2 µm filtered MNT were analyzed on a FACSAria II sorter (BD Biosciences) equipped with a 100 µm nozzle and 405, 488, and 633 nm lasers. The 100 µm nozzle, rather than a smaller one, was used to reduce the pressure and hence maximize the excitation time and signal strength (24). Analysis and sorting were performed in PBS at low pressure (23 psi) and a flow rate between 1 and 3 for a maximum of 3000 events/sec to minimize coincidental events. For GFP and Syto 13, the samples were excited with a 488 nm laser coupled to an emission filter allowing the 515-545 nm wavelengths to go through. Syto 61 fluorescence was detected with the 633 nm laser coupled to a 660-670 nm bandpass. In all cases, a minimal threshold of 200 for the SSC channel was applied to remove the background signal and 100,000 particles analyzed. They were then analyzed in the fluorescence channel, gating on GFP tagged, Syto 13 and/or Syto 61 labeled virions as indicated. To insure the

approach only monitored single viral particles, as opposed to virion aggregates, several tools were used. First, as mentioned above, the samples were all pre-filtered through a 0.45 µm filter. Secondly, the filtered virions were initially analyzed by light scattering, where FSC is a measure of size and SSC an indication of granularity and internal complexity. In all cases, a gate was applied on the bulk of the particles (> 95 %; see corresponding figures) which excluded large aggregates. Third, a purity mask of 16 was applied upon sorting, meaning that each drop being scanned could not be sorted if a non-target particle fell within the first or last 8/32 of the leading or trailing drop, thus effectively preventing doublets to be sorted and only allowing single event sorting. The data were initially acquired with the FACSDiva software version 6.1.3 (BD Biosciences) and then processed with FlowJo version 10.0.7r2 (TreeStar). Note that only fluorescent viral particles were considered for the histograms and the calculation of the mean fluorescence intensity (MFI). Upon sorting, the diluted virions were aliquoted and frozen at -80°C and subsequently tittered on Vero cells as detailed below. The robust Coefficient of variability (% rCV) corresponds to the robust standard deviation divided by the median. Bilateral Student's T-tests were used to determine any statistically significant differences between the samples.

AcGFP Flow Cytometer Calibration Beads. AcGFP (Clontech, cat Nº 632594) beads are a mixture of six distinct populations with a different amount of attached AcGFP molecules and thus a distinct fluorescence signature. Molecular Equivalent of Soluble Fluorophore (MESF) per peak is obtained by correlating the Mean Fluorescence Intensity (MFI) of each population with the amount of soluble AcGFP yielding the same fluorescence intensity. Twenty microliters of AcGFP Calibration Beads were resuspended in 1 ml of 1X flow cytometer calibration beads dilution buffer according to the manufacturer's instructions.

Plaque assays. To assess viral particle infectivity, Vero cells were plated on 6 well plates and grown to confluency. The growth medium was removed and 250 µl aliquots of 10 fold serial dilutions of virions in RPMI + 0.1% BSA were placed on the cells in duplicates. After 1 h adsorption to cells at 37°C, 2X DMEM media mixed with 2% agarose (1:1) was added and the cells further incubated at 37°C. The media/agarose mix was typically removed 72 hpi later, the cells fixed with methanol and the plaques revealed with crystal violet as before (33).

Quantitative PCR (qPCR) analysis of sorted virions. To determine genome copy numbers, 200 µl of FACS sorted virus were first treated for 10 min at 37°C with 500 U/mL of DNAse I (Roche) to digest non-encapsidated viral DNA. The encapsidated viral DNA was extracted using GenElute Mammalian Genomic DNA Miniprep Kits (Sigma-Aldrich) as per the manufacturer's instructions. These samples were then analyzed by quantitative PCR using HSV-1 glycoprotein B (gB) specific primers (forward: 5' CCACGAGACCGACATGGAGC 3'; reverse: 5' GTGTTCGGTGTGCGACCCCTC 3'). The q-PCR was performed with a LightCycler 480 (Roche) using the PerfeCTa SYBR Green SuperMix (Quanta BIOSCIENCES). The data were analyzed using LightCycler1 480 software version 1.5.

Electron Microscopy. Sorted viruses were firstly fixed in 2% glutaraldehyde in 0.1 M phosphate buffer (PB, pH 7.3) for 1 h on ice. Viruses were then concentrated by passing them through a 13 mm Swinny stainless steel holder (EMD Millipore) containing an 0.1 µm Omnipore PTFE hydrophobic membrane filter (EMD Millipore). The filter containing sorted viruses was washed with PB and post-fixed in 1% OsO_4 in PB for 1h at 4ºC. The filter was then rinsed, dehydrated in

increased concentrations of ethanol and embedded in Epon (40). Ultrathin sections of filter containing viruses were done using a Reichert ultracut microtome and placed on naked nickel grids. The grids were then contrasted with 3% aqueous uranyl acetate (Canemco & Marivac). Samples were examined on a Philips CM100 transmission electron microscope and digital micrographs were captured using an AMT XR80 CCD digital camera.

Production of depleted virus using siRNA. 143B cells were seeded in 6-well plates at a concentration of 5×10^4 cells/well 24 hours before transfection. Cells were transfected for 48 hours using PepMute^{TM} siRNA Transfection Reagent (SignaGen® Laboratories) according to the manufacturer's instructions. RNA interference reagents (Dharmacon) used at 25-100 nM/well included a unique siRNA against VP16 (12, 13) and two distinct siRNA against VP22. Cells were then either mock treated or infected with HSV-1 KOS at a MOI of 5. After the one hour adsorption time, cells were washed with phosphate-buffered saline (PBS) then complete DMEM without BrdU was added to the wells and infection was continued for another 24 hours. The supernatant was then harvested and cleared from cell debris by centrifugation at 500g for 5 minutes at 4 C°. Extracellular virions were then titrated on Vero cells and/or concentrated 2 hours at 18,000g and the viral pellets were resuspended in MNT then analyzed by Western blotting.

II.1.4 Results

Successful detection of mature HSV-1 enveloped virions by flow cytometry. We previously showed that we can detect HSV-1 non-enveloped nuclear capsids by flow cytometry despite being smaller than the theoretical resolution limit of 0.5 µm of most instruments (24). Since it is not possible to discern 100 µm from 200 µm particles, whether commercial beads or viruses, or the

background signal based on light scattering, we circumvented this issue in the past by GFP tagging nuclear capsids or by staining the viral genome with the nucleic acid Syto 13 dye, whose fluorescence is strongly stimulated when bound to nucleic acids. This not only allowed us to tell the capsids apart from the background but proved to be an efficient tool to efficiently enrich for so-called C nuclear capsids, reaching 90% purity in a single purification step (24).

To evaluate if mature enveloped virions could also be monitored by flow cytometry, we labelled them with the membrane-permeable Syto 13 along with control nuclear capsids or buffer alone. Figure 1A depicts our analysis strategy. As previously reported (24), background particles present in the 0.22 µm filtered PBS shield buffer were detected by light scattering, but were otherwise devoid of any intrinsic fluorescence (fig. 1B, panels a, b). Similarly, no significant fluorescent signal was detected when Syto 13 was added to buffer alone (4% of particles emitted light with a mean fluorescence intensity (MFI) of 780; fig. 1B, panels c-d). In contrast, the addition of Syto 13 to nuclear capsids nearly labelled 90% of the capsids and gave rise to 23 fold increase in fluorescence with a MFI of 17589 (fig. 1B, panels e-h). Interestingly, addition of Syto 13 to extracellular virions was equally efficient (87% efficiency) but only resulted in a 3 fold increase in fluorescence for a MFI of 2093 (fig. 1B, panels i-l). These results suggested that the viral envelope or density of the tegument layer partially perturbed the entry of Syto 13 in the viral particles and/or quenched its fluorescence. However, the signal was amply sufficient to detect, analyze and sort enveloped HSV-1 virions by flow cytometry.

Since it was possible to detect Syto-stained virions by flow cytometry, we reasoned we could employ a different strategy to detect them by GFP tagging diverse virion components. As indicated in figure 2, extracellular mature virions encoding GFP tagged capsids (U_L25-GFP), tegument proteins (VP11/12-GFP) or envelope proteins (GFP-gB) were all readily detectable by flow

cytometry over the background signal. Albeit this seemed less efficient than with Syto 13 stained virions, these findings paved the way for the analysis of the distinct tegument proteins present in extracellular virions.

Flow cytometry quantification of viral particles. To define the usefulness of our flow cytometry approach, we fist confirmed that the GFP signals could quantitatively be detected. Not surprisingly, commercials beads using known relative amounts of GFP signal lead to a very linear detection by the flow cytometer (fig. 3A). This was largely expected since these beads are commonly used to calibrate those instruments. Thus, we could use flow cytometry to measure GFP signals embedded in virions. Next, we probed a battery of recombinant viruses coding for various GFP-tagged tegument proteins that are incorporated in virions (see Table 1 and fig. 3C). We also used two capsid controls, i.e. the K26GFP virus which tags the VP26 protein as well as GS4677, which encodes for U_L25-GFP (Fig. 3B). Cells were infected with these recombinant viruses and the extracellular virions collected 18 hours later and analyzed by FACS. In all cases, the virions were initially detected by light scattering, gating on the bulk of the particles using the same gating strategies that excludes large aggregates as for figures 1 and 2. All individual particles were subsequently analyzed in the fluorescence channel (see Fig. 3B and C, dot blots), then focusing on the GFP positive particles (see Fig. 3B and C, histograms). For all recombinant viruses, clear signals were detected above the control untagged wild type virions. This was in full agreement with our previous report that particles as small as 100 μm could indeed be detected by flow cytometry (24). Note that U_L25, which has previously been estimated at 60 copies (41) could also be detected. We concluded that flow cytometry can be used to analyze individual virions tagged for various components, even when low copy proteins are tagged.

Individual viral particles vary in their tegument content. Having established a method to individually analyze large numbers of HSV-1 virions, we proceeded to compare the tegument content of extracellular particles using the aforementioned battery of GFP tagged viruses. To this end, we characterized by flow cytometry 100 000 extracellular virions of each recombinant virus and calculated the variance of the GFP signals. Rather than employing the coefficient of variation of the mean (CV), we instead used that of the median (rCV), a more robust approach that naturally excludes outlying points that can strongly skew results. As control, we evaluated the rCV of U_L25-GFP tagged capsid component, since this capsid component is believed to be invariant in the virions (41). We finally performed statistical comparisons between the rCV obtained for various samples with that for the U_L25-GFP virus to detect tegument proteins that may vary significantly among viral particles. Figure 4 reveals that the capsid and tegument components VP26, ICP0, U_L37 and VP11/12 did not significantly differ from U_L25 in variance. In contrast, VP16 and VP22 were much more variable among viral particles ($p<0.01$ and $p<0.001$ respectively). Thus, while some tegument proteins are incorporated in similar amounts among viral particles, VP16 and VP22 vary considerably from particle to particle. This was consistent with their much broader distributions in the GFP profiles, as opposed to the tight distribution for U_L25 and VP26 (fig. 3A).

VP16 and VP22 levels in virions appear to correlate with infectivity. The most critical question was whether the higher variability in VP16 or VP22 content in virions had any biological relevance or simply reflected a reduced stringency in copy numbers. We therefore exploited the power of flow cytometry to sort viruses based on tegument abundance. To this end, we harvested viral populations at the extreme ends of the tegument distribution curves and got viral stocks incorporating either the lowest or top 10% amounts of VP16 or VP22 (see schematic of this analysis

in fig. 5A). We then measured their efficacy to infect Vero cells in plaque assays, initially using the same number of FACS events to infect cells. Under these conditions, no differences were noted in plaque size, indicating that cell-cell spread was not impaired (fig 5B). However, modest but reproducible 2.5 to 4 fold differences in the number of plaque forming units were found (fig. 5C). In contrast, when the same experiment was done for the invariant U_L37 tegument protein, selecting once again for viruses incorporating the lowest and top 10% levels of U_L37, no differences in plaque size or infectivity were observed (fig. 5B-C). As expected, virions with high VP22 content appeared to contain an increased proportion of infectious particles (fig. 5D). Oddly, such difference was not statistically significant for VP16 but was reproducibly detected.

In an effort to better understand why virions containing different amounts of VP16 or VP22 differed, we considered the presence of doublets, aggregates and coincidental events in the high sorted fractions. Although sorting was performed under technical conditions that typically excludes such events (see materials and methods), we nonetheless used three independent approaches to rule them out. Given that forward scattering is an indication of size, while side scattering is rather suggestive of sample granularity and internal complexity, we first compared the light scattering profiles of the high/low fractions of VP16 and VP22 samples. Figure 6A (panels a, d and g) shows the typical profiles of viral particles prior to their sorting into high and low GFP content. To evaluate the properties of these sorted viral particles, we examined their light scattering profiles Panels b, e and h highlight the forward light scattering of these sorted particles, which is color coded for ease of analysis (orange for the lowest 10% GFP^+ viral particles, blue for the highest 10% GFP^+ viral particles, while black dots represent unselected particles not belonging to these two groups). Clearly, both GFP populations displayed similar forward scattering properties and thus were likely of similar size. Interestingly, viral particles containing more VP16/VP22 exhibited an

increased side scattering profile, presumably reflecting a greater complexity than their low counterparts (Fig. 6A, panels c, f and i). We conclude that viral particles containing high levels of tegument proteins are, by this criteria, of similar sizes as their low counterpart. We next performed a classical flow cytometry dilution analysis, which is based on the assumption that coincidental events would be detected at low sample dilution but would disappear when samples are highly diluted. In that case, the mean fluorescence intensities of the recorded events would be reduced by simply diluting the samples. Figure 6B shows that, as expected, diluting the viral stocks reduced the number of events recording by the instrument during the fixed 60 second analysis but only marginally altered the fluorescence levels of each of those events. These results are once again consistent with the conclusion that the analysis of individual viral particles was achieved. Finally, sorted viruses were analyzed by electron microscopy. As shown in fig. 6C, individual viral particles were readily detected with no evidence for viral aggregates. As expected, the bulk of these viruses shared the characteristics of mature virions with a DNA containing capsid and an envelope. We conclude that the higher FACS signals measured in the high fractions were unlikely attributed to aggregates, virion doublets or coincidental events.

Higher infectivity of sorted viral particles is not explained by L-particles. Typical HSV-1 preparations contain a proportion of so-called L-particles, non-infectious enveloped viral entities that are loaded with tegument proteins but lack a viral capsid or genome. It was therefore possible that the viral particles sorted above for their high tegument content proportionally contained less L-particles than their corresponding low tegument counterpart, which would therefore be less infectious. To rule out this scenario, we performed dual labelling of the tegument and viral genome using the GFP tagged viral strains and Syto dyes. Since GFP and Syto 13 share similar excitation

and emission profiles, we screened a panel of red emitting Syto dyes and identified Syto 61 as the best candidate (fig. 7A and data not shown). Since we wanted to isolate intact virions, we first examined if the membrane-permeable Syto 61 perturbs the virus. We consequently compared the plaque forming capacity of untreated or Syto 61 stained virions with various concentrations of the dye and found that it was well tolerated by the virions and had no impact on the ability of the viruses to propagate (fig. 7B), as did Syto 13 (data not shown). It was therefore possible to label with Syto 61 the viral genome of the above GFP recombinants and eliminate L-particles by first selecting Syto 61 positive events, then sorting GFP positive viral particles (see cartoon of the approach in fig. 7C). Syto 61 positive viral particles sorted for their high content of VP16 or VP22 (fig. 7D) were again significantly more infectious than their low VP16 or VP22 virion counterparts (fig. 7E), reiterating the above findings and ruling out a significant implication of L-particles in the above results. We therefore concluded that particles sorted for their high VP16 or VP22 content seemed more infectious than particles containing lower amounts of the same proteins.

Depletion of VP16 or VP22 in virions hints at a complex scenario. To orthogonally confirm our findings, we used a RNA interference strategy to lower the amounts of the proteins in the virions and assessed their infectivity, an approach we successfully used in the past for VP16 and several host proteins incorporated in virions (13, 42). As anticipated, siRNA targeting VP16 or VP22 significantly reduced the level of expression of these proteins in infected cell lysates (fig. 8A). Not surprisingly, this resulted in a concomitant depletion of the proteins in viral particles produced on siRNA-treated cells (fig. 8B). Individual testing of the two siRNA used to block VP22 expression also led to reduced levels of VP22, albeit with different efficacies suggesting off target effect were not an issue (data not shown). We then proceeded to evaluate the infectivity of these extracellular

virions and found that the depletion of VP16 from the virus had a profound impact on its ability to form plaques (fig. 8C), in full agreement with the flow cytometry data. Unexpectedly, VP22 depleted virions had the opposite effect on viral infectivity and exhibited an improved plaque forming capacity. Thus, while the amount of VP16 in virions directly correlated with the infectivity of the viral particles, a more complex situation seemed to prevail for VP22.

The overall composition of the tegument can be altered by modulating single components. The tegument layer is the result of an intricate interconnectivity of its components, with the deletion of one tegument protein often impacting the incorporation of other viral proteins. We therefore asked whether tagging of the tegument proteins affected their level of incorporation but also that of other virion components. This was achieved by quantitative Western blotting of all the recombinant virions used in this study using a battery of antibodies (fig. 9). To insure equal numbers of viral particles were loaded, all values were normalized for VP5. These tegument/VP5 ratios were then compared to their corresponding wild type strains (arbitrarily set at 1) to insure the data were not biased by strain considerations. Interestingly, tagging of the capsid protein VP26 with GFP had no noticeable impact on its incorporation or any of the tegument proteins examined (fig. 9). Similarly, tagging of U_L25 seemed to incorporate slightly less U_L37 but had an otherwise normal complement of other tegument proteins. In sharp contrast, tagging of most other tegument proteins drastically reduced their incorporation and that of multiple other virion components. Interestingly, while tagging of VP11/12 at either the carboxyl or amino-terminal end yielded similar results, this was clearly not the case for ICP0, with the ICP0-GFP_{105} virus seemingly having a normal composition while the ICPO-GFP_{12} virus had a profoundly distinct virion content, suggesting a positional effect of the GFP moiety. Altogether, these results indicated that large tags

such as GFP can impair the incorporation of the labelled proteins but can also alter the overall composition of viruses. We consequently conclude the observed impact of VP22 on infectivity was likely indirect and due to several factors subsequent to the overall change in virion composition.

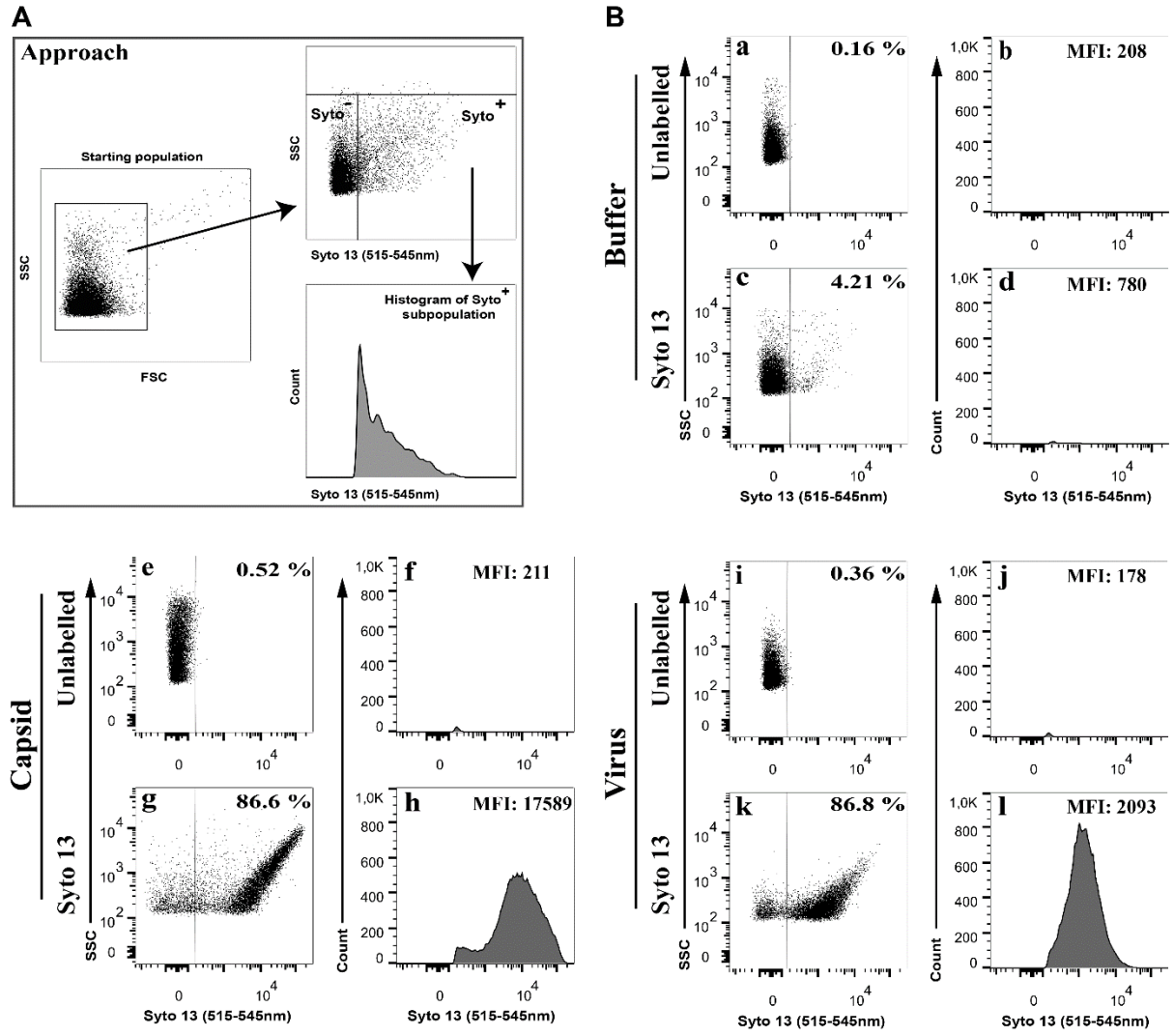

Figure. 1 : Analysis of syto stained HSV-1 virions by FACS.

Vero cells were infected with wild type HSV-1 at an MOI of 5 for 18 hpi. Extracellular virions were stained with 1 µM Syto 13 and analyzed by flow cytometry. **(A)** Schematic description of the gating strategy. Note that aggregated particles were first excluded by gating them out in the SSC versus FSC plots and by specific flow cytometry parameters (see materials and methods). **(B)** The left panels for each condition (dot plots) show the fluorescence profiles of all non-aggregated particles while only Syto 13+ samples (fluorescence above the buffer control) were considered in the right panels (histograms). Percentages in the panels denote the amount of Syto 13 positive

particles relative to the starting population, which includes inert particles inherently present in the FACS buffer (356). Meanwhile, the mean fluorescence signal (MFI) is only that of the Syto 13+ viral particles.

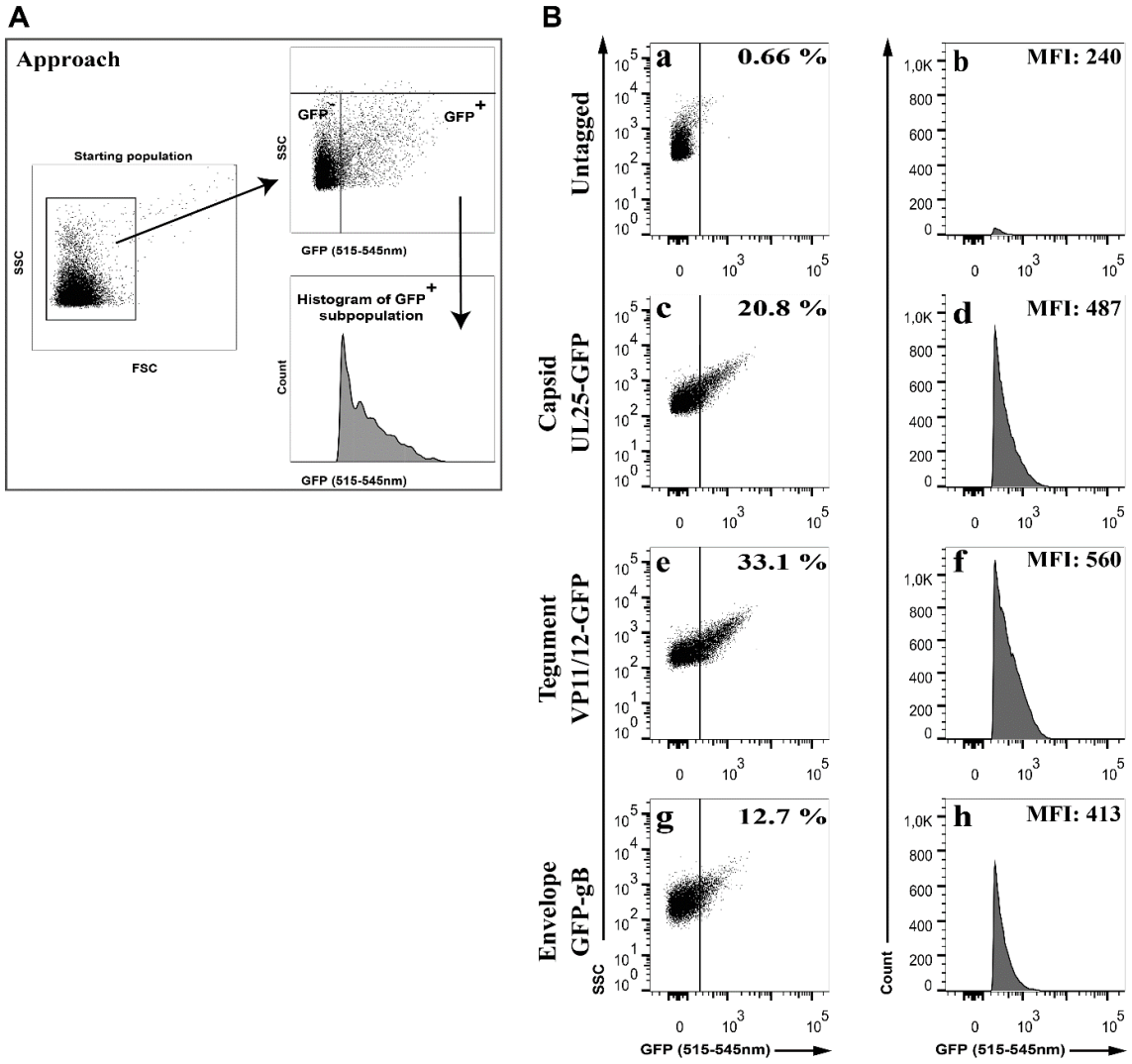

Figure. 2: Analysis of GFP tagged virions by FACS.

Vero cells were infected with wild type HSV-1 (untagged) or fluorescent recombinant viruses tagging the viral capsid (UL25-GFP), the tegument (VP11/12-GFP) or envelope (GFP-gB) at an MOI of 5 for 18 hpi. Virions were diluted and directly analyzed by flow cytometry. (A) Schematic description of the gating strategy. Virion aggregates were first removed by gating them out and

GFP+ particles analyzed. (B) The proportion (%) and mean fluorescence levels (MFI) of the GFP particles are indicated in each panel (average of 3 independent experiments). As above, these percentages denote the amount of GFP positive particles relative to the starting population, which includes inert particles inherently present in the FACS buffer (24). Meanwhile, the mean fluorescence signal (MFI) is only that of the GFP+ viral particles. Note the sharp edge of the left f the GFP histograms, a direct consequence of the gating.

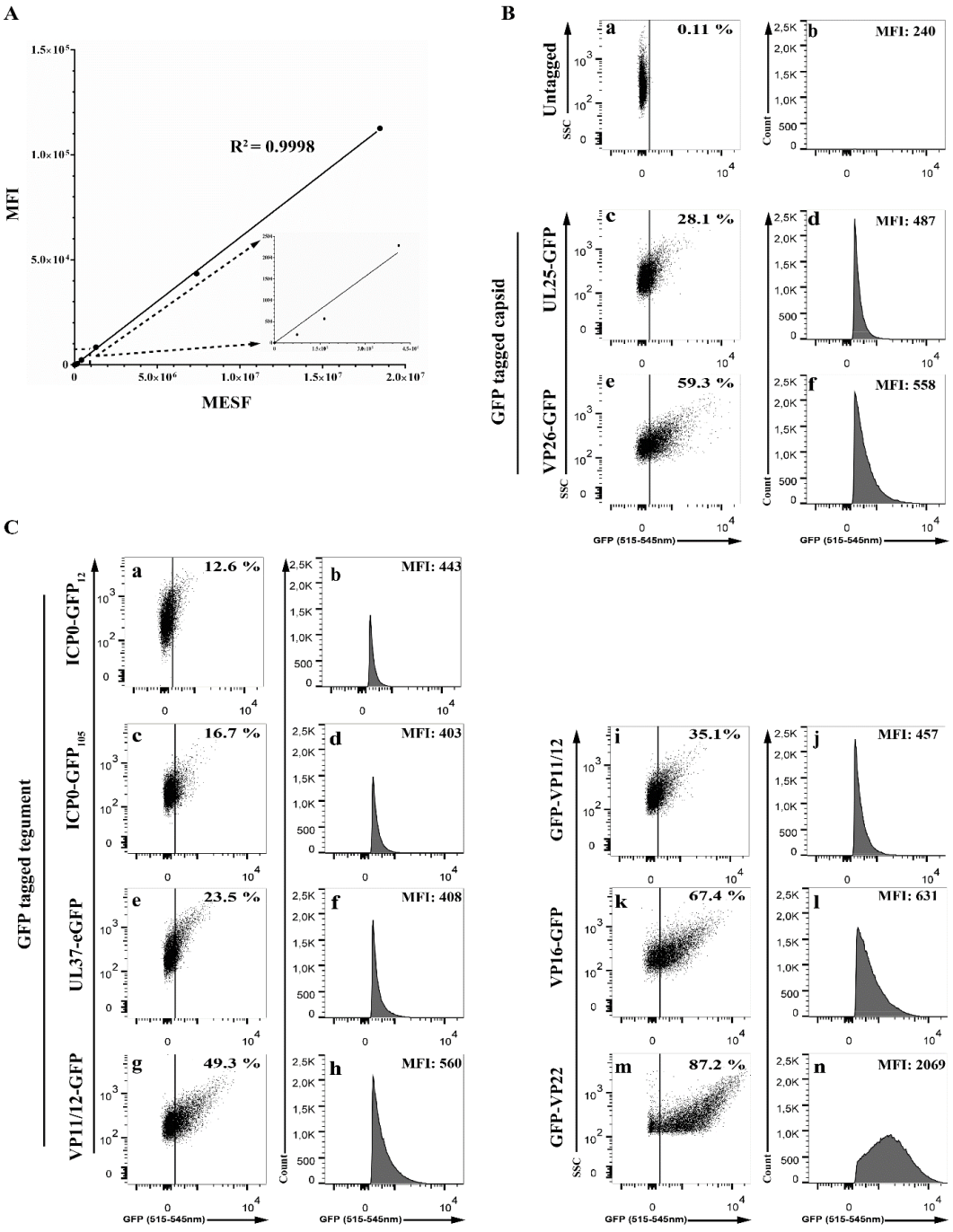

Figure. 3: Flow cytometry detects all structural constituents of the virus.

(A) Linear detection of AcGFP Flow Cytometer Calibration Beads analyzed by flow cytometry using a 488 nm laser line. **(B, C)** Extracellular virions were purified from wild type (i.e., non-fluorescent) infected cells or from cells infected with fluorescent recombinants viruses and

examined by flow cytometry as above. The left panels show total individual particles (i.e. excluding aggregates) while the right panels show the histograms profiles of the GFP-positive gated material for each virus. The mean fluorescence signal (MFI) and the proportion (%) in each panel is the average of 4 independent experiments. Once again, these percentages denote the amount of GFP positive particles relative to the starting population, which includes inert particles inherently present in the FACS buffer (24). Meanwhile, the MFI is only that of the GFP+ viral particles. Once again, the sharp edge of the left of the GFP histograms is a direct consequence of the gating rather than a binomial distribution of the signal.

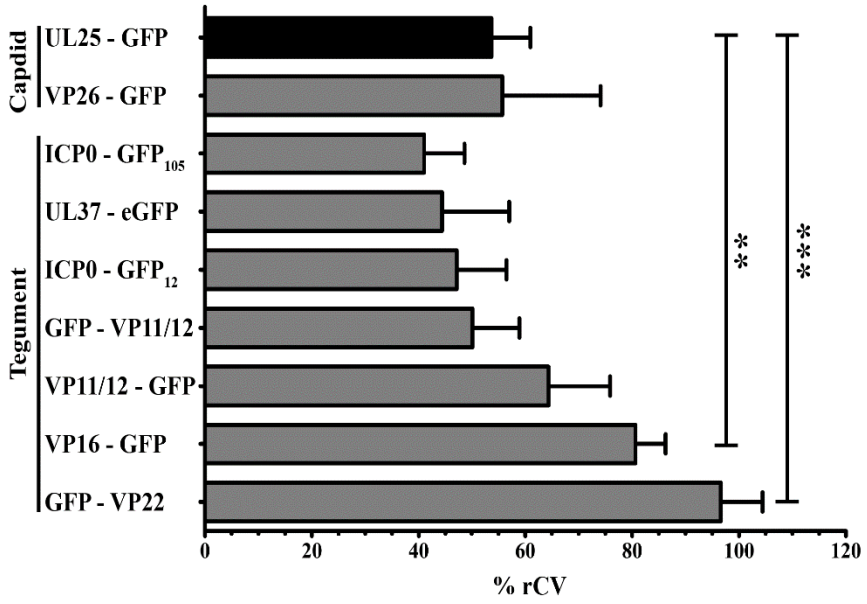

Figure. 4: Variability of the tegument among individual viral particles.

Extracellular virions were purified from wild type (i.e., non-fluorescent) infected cells or from cells infected with the indicated fluorescent recombinant viruses and analyzed by flow cytometry. Tegument variability was measured by the coefficient of variability based on the medians (% rCV). Error bars represent the standard deviation of 4 independent experiments. Student T tests were performed to analyze the significance of the data (** $p<0.01$; *** $p<0.001$).

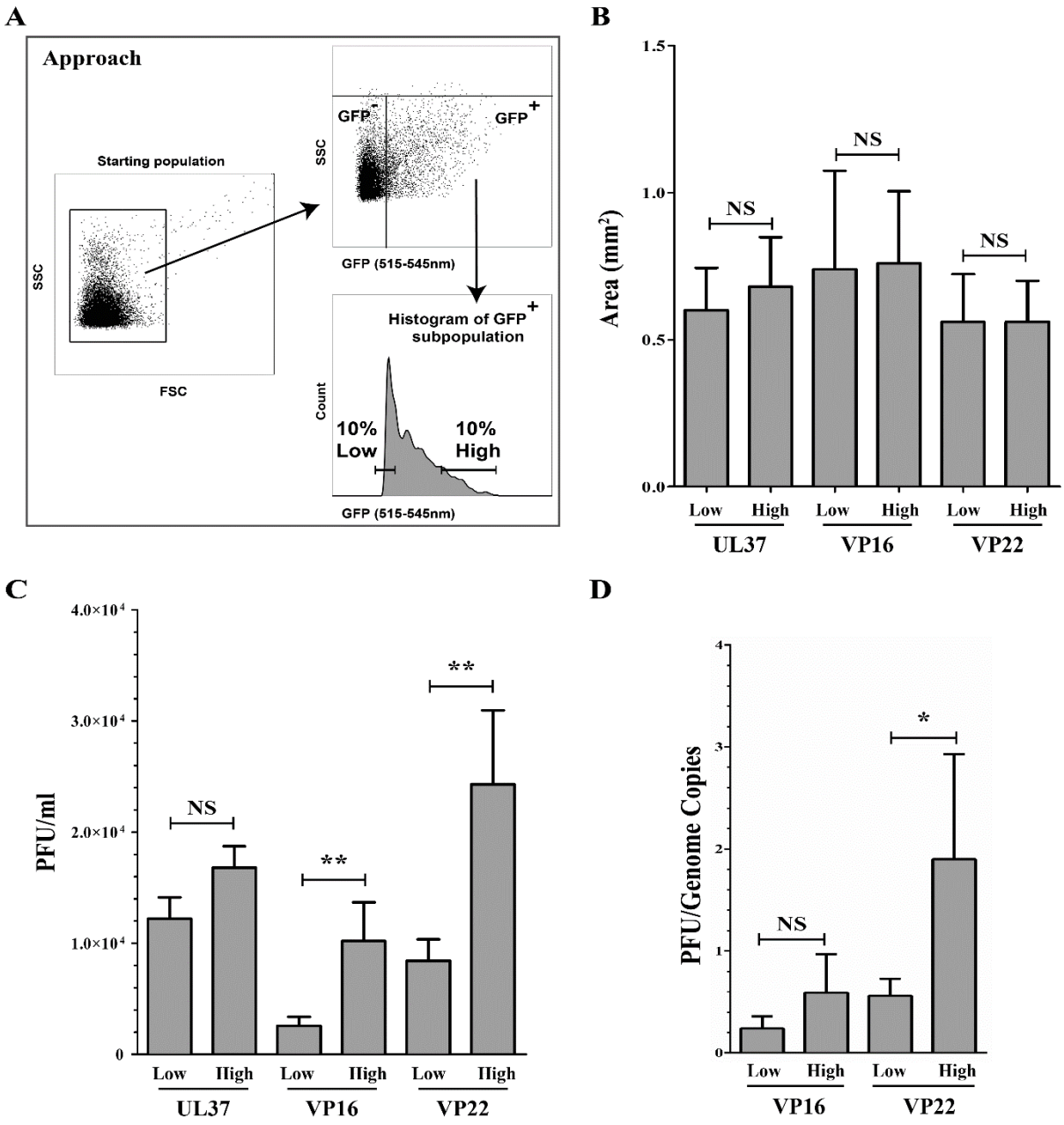

Figure. 5: VP16 and VP22 abundance correlate with infectivity.

Extracellular virions were purified from cells infected with K37eGFP, VP16-GFP or GFP-VP22 viruses and sorted by flow cytometry as above for their low or high levels of U_L37, VP16 or VP22 respectively. **(A)** Schematic description of the gating strategy applied for Sorting of viruses by FACS**.** Virion aggregates were first removed by gating them out. **(B, C)** Viral spread of the sorted viruses. The infectivity of the sorted virions was assessed by plaque assays on Vero cells and plaque

size (B) and abundance (C) were evaluated. **(D)** PFU to genome copy ratios. The ratio of PFU/Genome Copies was obtained by dividing the PFU values obtained above by the corresponding values of genome copies measured by q-PCR for the same viral samples. Error bars represent the standard deviation derived from 3 independent experiments and analyzed with the Student T test (NS not significant, i.e. $p > 0.05$; ** $p < 0.01$).

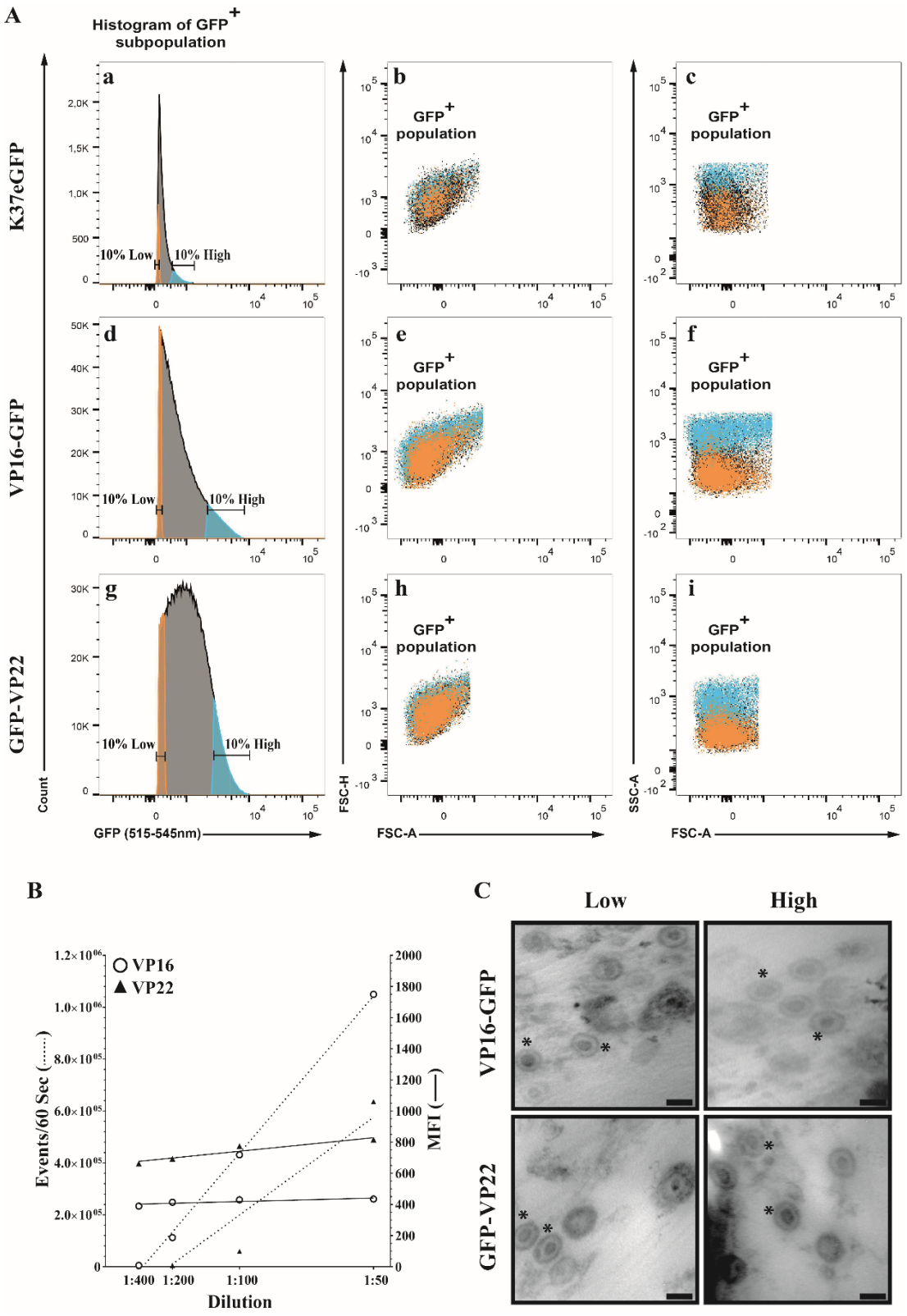

Figure. 6: Sorted viruses are single viral particles.

(A) Extracellular virions were purified from cells infected with VP16-GFP or GFP-VP22 viruses

and then sorted by flow cytometry as above for their low or high levels of VP16 or VP22 content respectively. All panels are only GFP+ particles, i.e. already depleted of aggregates and non-fluorescent components. FSC-H and FSC-A are respectively the height and area under the curve of the forward scattering signal, while SSC-A measures the area under the side scattering signal. (Orange: particles with the lowest 10% GFP signal, blue: particles with the top 10% GFP signal; black: particles exhibiting an intermediate GFP signal and not subsequently analyzed). The linear edges around the dot blots reflect the gate used to sort the samples. **(B)** Extracellular virions purified from infected cells were first diluted 1:50 then serial dilutions of 1:2 were prepared and analyzed by flow cytometry by continuous recording of events during a fixed time (60 sec in these experiments). **(C)** Sorted viruses were concentrated on 0.1 µm filter and the filter then embedded and processed for electron microscopy (see Materials and Methods). For clarity, the presence of a capsid with its envelope is indicated by asterisks. Bars represent 100 nm.

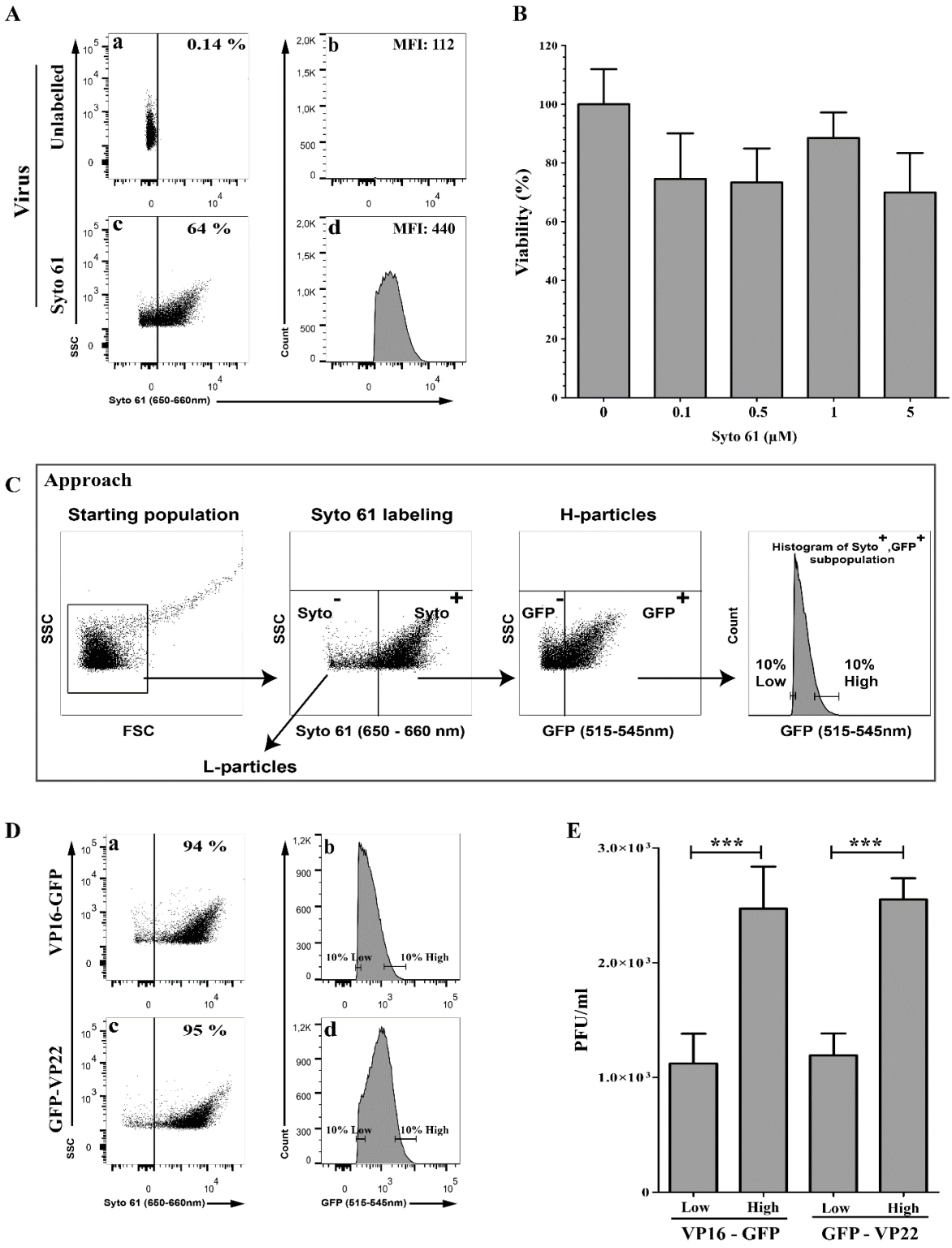

Figure. 7: Difference in infectivity is not linked to L-Particles.

(A) Staining of virions with Syto 61. Vero cells were infected with untagged wild type viruses at

an MOI of 5 for 18 hpi. Purified extracellular virions were stained with 1 μM Syto 61 or mock treated and analyzed by flow cytometry. Aggregates were gated out and Syto 61 fluorescence evaluated. The percentages denote the amount of Syto 61+ particles relative to the starting population, which includes inert particles inherently present in the FACS buffer (356). Meanwhile, the mean fluorescence signal (MFI) is only that of the Syto 61+ viral particles. **(B)** Syto 61 does not affect the viability of the stained virions. Wild type strain F extracellular virions were stained with 0 to 5 μM Syto 61 for 1h at 4°C. The viability of the Syto 61 labeled virions was assessed by standard plaque assays. For comparison, the number of plaques obtained for the untreated sample was set at 100%. Error bars represent the standard deviation of 2 independent experiments. **(C)** Schematic description of the approach to deplete L-particles and enrich for heavy particles (H-particles). Once aggregates were gated out (left most panel) VP16-GFP or GFP-VP22 Syto 61 positive events were selected to exclude L-particles (second panel from the left). A second gating was then applied to select GFP positive particles (third panel from the left). The samples were finally sorted on the basis of their low or high levels of VP16 or VP22 (right most panel). As before, all sorting took place under conditions where only single individual viral particles were present (see materials and methods). **(D)** Sorting of DNA containing GFP positive virions. High and low containing viral particles were sorted according to the scheme depicted in panel C. Percentages denote the amount of GFP+ particles, which only includes heavy particles with a potential contamination by a mere 5-6% by L-particles. Alternatively, these values could also be H-particles that were not labelled with the Syto 61 dye. **(E)** Infectivity of the sorted virions. The infectivity of the Syto 61+/GFP+ sorted virions were assessed by plaque assay on Vero cells. Error bars represent the standard deviation of 2 independent experiments and analyzed with the Student T test (*** $p<0.001$).

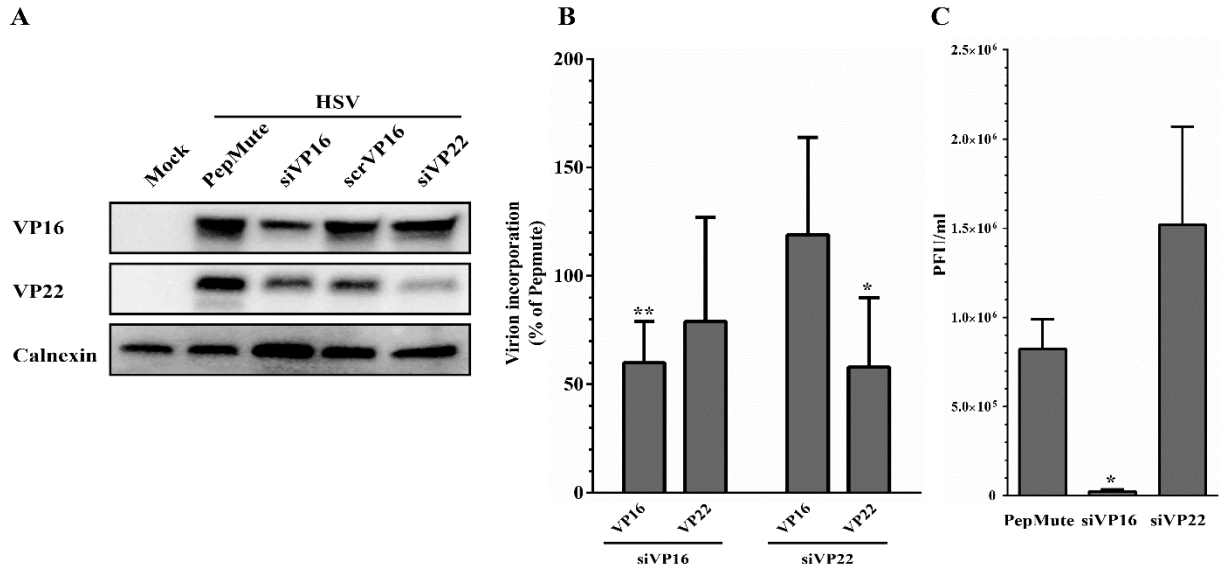

Figure. 8: Analysis of VP16 and VP22 siRNA depleted virions.

143B cells were transfected for 48 hours using pepmute with a unique RNAi against VP16 or two pooled siRNA targeting VP22. Cells were then infected with HSV-1 KOS at an MOI of 5 for 24 hours. **(A)** Immunoblot of mock treated or siRNA transfected and HSV-1 infected cell lysate. Thirty micrograms of cell lysate were separated by SDS-PAGE, transferred to PVDF membrane and probed with antibodies against VP16 and VP22. Calnexin was used as a loading control**. (B)** Impact on VP16/VP22 incorporation in virions. The amount of VP16 or VP22 in extracellular virions produced by cells transfected with the indicated siRNA was evaluated by Western blotting in 5 independent experiments, each normalized to the untreated sample (i.e. pepmute set at 100%). **(C)** Impact on infectivity. The infectivity of the VP16 or VP22 depleted extracellular virions was assessed in standard plaque assays. Error bars represent the standard deviation of 3 independent experiments (* $p<0.05$; ** $p<0.01$).

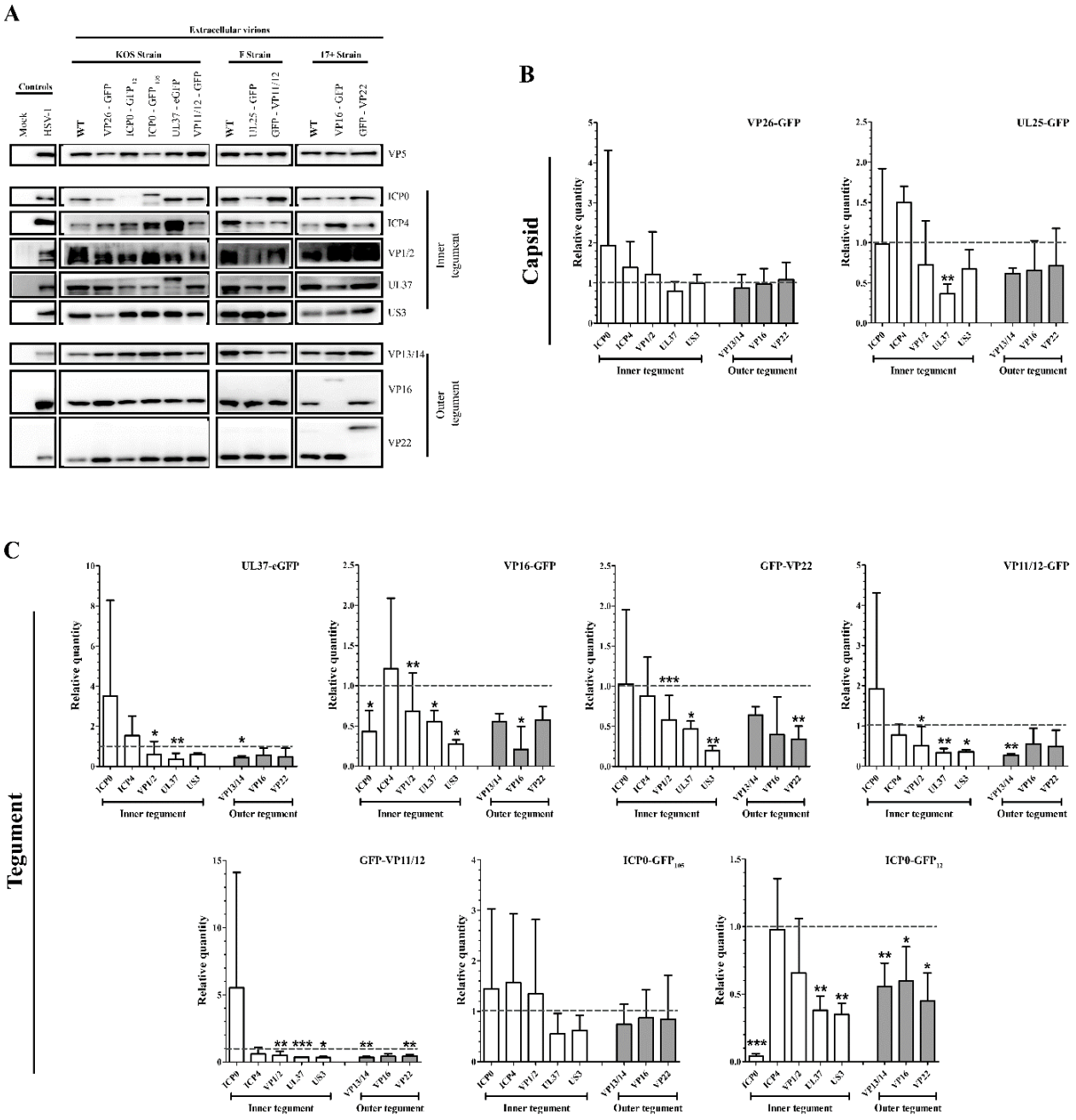

Figure 9: Interconnectivity of the virion components.

(A) Western blot analyses. Extracellular virions indicated at the top of the blots were purified from infected cells and analyzed by Western blotting using antibodies indicated to the right of each blot. **(B, C)** Tegument quantification. The amounts of various tegument proteins present in virions tagged on the capsid **(B)** or the tegument **(C)** were determined by quantitative Western blots. The

data were normalized to VP5 to insure even loading of the gels. These tegument/VP5 ratios were finally compared to those of wild type of each strain, arbitrarily set at 1, to avoid biases among viral strains. Error bars represent the standard deviation of 3 independent experiments. Student T tests were performed to analyze the significance of the data (* $p<0.05$; ** $p<0.01$; *** $p<0.001$). Note that throughout this study, a ChemiDoc was used, not film which is notoriously non-linear.

II.1.5 Discussion

The power of flow cytometry. One limitation to characterize the heterogeneity of viral particles has been the limited tools to examine them individually, with the notable exception of labor-intensive electron microscopy and more recently fluorescence microscopy. The present study meaningfully contributes to these past findings in several ways. First, we probed by flow cytometry 100,000 particles, adding a significant level of power to such analysis. Secondly, we quantitatively looked at the protein content of individual viral particles, not entire viral populations as is typically the case for Western blotting, biochemical assays or mass spectrometry. Third, unlike the above studies, we could directly correlate protein content changes to individual virion infectivity. Finally, the present work looks at a large picture by probing the impact of the modified protein on the overall composition of the virus. This, in principle, enables a much better view of the real consequence of manipulating virion content even if only altering one viral protein. Thus, our flow cytometry analysis of individual viral particles is clearly a very useful technical advancement, but also leads to very relevant information.

Our previous (24) and present work shows that it is possible to detect, analyze and sort individual viral intermediates, including mature virions, despite their limited size below the theoretical detection limit of most FACS instruments. These viral particles can either be labelled

with membrane permeable Syto reagents, which emit fluorescence when bound to nucleic acid, or by genetically tagging various virion components with a fluorescent molecule. Interestingly, flow cytometry appears insensitive to the location of the tags in the virions as DNA, capsid, tegument and envelope proteins could all be detected. This is not surprising since this methodology has been used to monitor both cell surface markers as well as internal molecules, either fluorescently labelled or through detection with antibodies following permeabilization of the cells. Consequently, the location of a given GFP tagged protein in the virion, for instance an inner or outer tegument protein, should have no bearing on its detection. These findings enabled us to individually and statistically probe the relative amounts of tegument proteins among very large numbers of viral particles. This unique advantage over existing methods is a very useful tool to explore the variability of virions in terms of their protein content, in addition to being a very efficient way to purify viral intermediates.

Variability of the tegument. The HSV-1 tegument proteins U_L37, ICP0 and VP11/12 did not statistically vary any more that the U_L25 capsid proteins or VP26 for that matter. Nonetheless, the data suggest some level of variability. Whether this reflects real biological variability is not known. Intuitively, one expected no variation at all for VP26 if it is incorporated in a unique stoichiometry into the capsid. We were thus initially surprised by its rCV values. However, we find the same variability as Smith and colleagues (19) using fluorescence microscopy, who reported a variance of 0.48 while we got 0.53 (i.e. 53%). On the other hand, the variance of VP26 is clearly more restricted than that of VP22 and VP16 (see the tight bell curves for VP26 in figure 3B, panel D compared to others). The question remains though. Why this variation? Perhaps, the stoichiometry of VP26 is not as fixed as expected, as evidenced by the lower incorporation of GFP tagged the corresponding U_L25 in PRV particles (43) or alternatively, that the technology we both used (i.e.

fluorescence) has limitations. Albeit unanticipated from past findings, this may nonetheless be significant. One case in point is the U_L17/U_L25 complex, which was first thought to specifically label C-capsids, but has since been found on other nuclear capsids, albeit at lower levels (44-46). Interestingly, VP22, and to a lesser extent VP16, fluctuated significantly more among viral particles than the above proteins. This is in agreement with a quantitative mass spectrometry study of VP13/14, VP22 and U_S3 PRV deletion mutants, which hinted that VP1/2 and VP13/14 are incorporated in virions in fixed amounts, while VP11/12, VP16, and VP22 are present in variable quantities (22). This scenario is also consistent with work by Smith and colleagues who found by fluorescence microscopy some heterogeneity of specific PRV tegument proteins among viral particles (19). Finally, our data are in line with various reports that indicate VP22 varies much more than other tegument proteins, with wildly ranging estimates of 450 to 2640 copies per HSV-1 viral particles (15, 17, 18). Altogether, this reiterates the value of flow cytometry to quantitatively assess virion content.

The variability of some tegument proteins and not others is intriguing. Interestingly, tegument variability map to abundant tegument proteins but it is difficult to ascertain whether this is purely coincidental. A potential scenario may be that the outer tegument is spatially less stringent in the outskirt of the viral particles and/or is less organized there, allowing for more versatility in the copy number of proteins such as VP16 and VP22. This would contrast with inner tegument proteins, which interact with the highly structured viral capsid. This is consistent with the reported greater incorporation of the outer VP22 tegument protein in virions when overexpressed and the stable incorporation of the inner U_L37 tegument protein under similar conditions (20, 21). Clearly, more spatial information on the arrangement of the tegument layer is required to fully assess this possibility. An alternative view is that some of the tegument variability is caused by unspecified

mutations in some of the viral strains used in this study, particularly bacmid-derived strains. While most of them have been characterized (see references in Table 1), full sequencing data is not yet available. An interesting and additional aspect is tegument variability and overall protein composition of virions produced in various cell lines, which clearly add another layer of complexity to the present findings (47).

Interdependence of tegument components. Tagging virions with GFP often impacts viral fitness to the point that some proteins cannot readily be tagged without consequences (48, 49). This implies a negative effect of the tag on the organization of the virions and/or function of the labelled proteins. The present study confirms this and shows that the GFP moiety can have consequences for other tegument components. Hence, while GFP labelling of VP26, U_L25, or ICP0 at position 105 but not position 12, had minimal impacts on the composition of the viruses, the coupling of GFP to most tegument proteins clearly reduced their recruitment and limited the incorporation of several other viral proteins. Moreover, this does not even take into account untested viral tegument proteins as well as the many host proteins that are incorporated in mature viruses (1, 13). Thus, the impact of one molecule on other virion proteins may even be greater than reported here. An interesting point is the low incorporation of GFP tagged ICP0. It might mean that its incorporation into virions is optional or that it is not rate limiting and consequently little is required to initiate the infection.

Absolute values of individual tegument proteins. The present study reports the relative amounts of tegument proteins, which has proved very useful to evaluate tegument variability among viral particles. Unfortunately, it has not been possible to define absolute copy numbers, albeit it was one

of our original goals. Apparently, GFP fluorescence varies by as much as 10 fold depending on the size of the tagged proteins, with large proteins being comparatively less fluorescent (personal communication by John Nolan). For this reason, commercial beads with defined absolute GFP copy numbers cannot be used as standards to determine absolute tegument copy numbers. Consequently, it would not be possible to tag one viral component, for example VP26, to evaluate the precise numbers of another virion component. However, as shown in figure 3B, it is readily possible to monitor abundance by measuring relative copy numbers of a given protein under different conditions, which is precisely what we did. It remains to be seen whether a different tagging strategy could circumvent this limitation.

Biological relevance of tegument heterogeneity. Our flow cytometry and RNA interference findings show a clear correlation between VP16 abundance in virions and infectivity. One plausible explanation rests with the trans-activating properties of VP16, where presumably more of the protein in the incoming virions should stimulate the infection if it is rate limiting. This is consistent with the boosting impact that L-particles, which contain tegument proteins, have on the "infectivity" of transfected viral DNA (i.e. devoid of tegument), but their lack of stimulation when used in parallel with viruses containing a full set of tegument proteins, especially at high multiplicities of infection (23). Given the 73% reduced levels of VP16 in the VP16-GFP recombinant viruses compared to its wild type counterpart, VP16 levels in this recombinant virus may indeed be suboptimal. Rather than being a caveat, this instead allowed us to appreciate its critical role in the incoming viruses early during the infection, particularly since it is otherwise a late protein. Alternatively, or perhaps additionally, this study may point to the contribution of other virion components whose levels are indeed altered in the VP16-GFP viruses (this study) or the

many host and viral proteins that have recently been shown to interact with VP16 (50). However, resolving this issue constitutes a significant challenge that will require multi-parametric approaches.

Regarding the HSV-1 VP22 tegument protein, our flow cytometry data initially suggested a direct link between infectivity and VP22 abundance. However, down regulating VP22 in virions by RNA interference resulted in a surprising increase in infectivity, in apparent contradiction with the above findings. The simplest interpretation is thus that VP22 abundance per se is not the main or sole contributing factor to viral fitness. In the present context, it is worth noting that although the levels of VP16 were statistically unaltered in the GFP-VP22 recombinant viruses, they nonetheless were reproducibly reduced. That VP22 interacts with the trans-activating domain of VP16 and has been postulated to modulate its function is also of particular interest (51). Moreover, VP22 has been implicated in the optimal localization and expression of several viral proteins or their incorporation into mature virions, including VP16 (52-54). Furthermore, it is possible that viruses sorted for their high levels of VP22 also contained more VP16, hence promoting viral infectivity. To address this latter possibility, we attempted to compare by Western blotting the compositions of the flow cytometry sorted VP16-GFP or GFP-VP22 with that of untagged virions. Unfortunately, this proves technically problematic as we estimated that 6 days of continuous sorting were required to produce sufficient material, since this approach generates highly diluted samples and significant losses of material in subsequent concentration steps (data not shown). We therefore cannot tell at this point if viral particles loaded with more VP22 were more infectious based on their VP16 content or activity and/or other proteins.

The minimal differences reported here in infectivity may seem unconvincing to some used to log differences. However, such small differences may nonetheless be significant. One appealing

outcome of the present work is the potentially preferential infection of cells by the fittest viral particles. This would be consistent with reports indicating that both neuronal and non-neuronal cells are typically infected by only a few HSV-1 virions (55-57). Similarly, a 2-3 fold advantage may be sufficient to preferentially promote the spread of the fittest virions in their hosts. However, an open question is how such a selection might operate, but resolving this issue may be challenging given the complex interconnectivity of the tegument proteins and the impact of GFP tags on the overall composition of virions. One other major difficulty is to evaluate the impact of tegument variability *in vivo*, i.e. in animal models, since every new round of infection will generate some diversity among the viral particles even if we infect the animals with homogenous viral stocks. Thus the infection of animals with FACS sorted virions would quickly lead to a heterogeneous viral population, likely masking any phenotype linked to tegument amounts. Some ingenuity would therefore be required to solve this difficult puzzle.

Concluding remarks

Overall, the present study quantifies the generally accepted concept whereby viral fitness is not merely dependent on the genetic makeup of viruses but also in the precise levels of proteins that are incorporated into the viral particles. A second important aspect of this work is that modulating a single virion component can have profound impacts on the overall composition of a virus. Although the present study focuses on HSV-1, it likely applies to other members of the herpesvirus family, all complex entities containing a great number of components in their mature particles. Altogether, this opens up new research avenues to address the virulence of HSV-1 and potentially of other viruses.

Virus	Strain	Tagged protein	Reference
HSV-1 GS4677	F	UL25 – GFP	unpublished
HSV-1 GS3351	F	GFP - VP11/12	(256, 623)
HSV-1 GS2971	F	GFP - gB	(623)
HSV-1 0+ GFP 12	KOS	ICP0 - GFP 12	(624)
HSV-1 0+ GFP 105	KOS	ICP0 - GFP 105	(624)
HSV-1 K26GFP	KOS	VP26GFP	(625)
HSV-1 K37eGFP	KOS	UL37eGFP	(626)
GHSV-UL46	KOS	VP11/12 - GFP	(627)
HSV-1 VP16-GFP	17	VP16 - GFP	(628)
HSV-1 GFP VP22	17	GFP - VP22	(629)

Table 1:Viruses used in this study.

II.1.6 Acknowledgements

We would like to acknowledge the significant contribution of Dr Kerstin Radtke in the early stages of this project. We also wish to thank John Nolan for judicious advice on the analysis of small particles by flow cytometry. We are particularly indebted to Danièle Gagné, who provided first class advice and service at the flow cytometry platform of IRIC. Finally, we wish to thank Drs Beate Sodeik, Prashant Desai, Gregory A Smith, William Halford, Jim Smiley, Steve Weinheimer, Peter O'Hare, Gill Elliott, Richard Courtney, Frank Jenkins, Bernard Roizman and Helena Browne for providing viral strains and antibodies without which this work would not have been possible. This study was funded by the Canadian Institutes of Health Research to RL (grant # MOP258030). The authors have no conflict of interest to report.

II.1.7 References

1. **Loret S, Guay G, Lippé R.** 2008. Comprehensive characterization of extracellular herpes simplex virus type 1 virions. J Virol **82:**8605-18.
2. **Mettenleiter TC.** 2006. Intriguing interplay between viral proteins during herpesvirus assembly or: the herpesvirus assembly puzzle. Vet Microbiol **113:**163-9.
3. **Taha MY, Brown SM, Clements GB.** 1988. Neurovirulence of individual plaque stocks of Herpes simplex virus type 2 strain HG 52. Arch Virol **103:**15-25.
4. **Johnson DC, Baines JD.** 2011. Herpesviruses remodel host membranes for virus egress. Nat Rev Microbiol **9:**382-94.
5. **Smith G.** 2012. Herpesvirus transport to the nervous system and back again. Annu Rev Microbiol **66:**153-76.
6. **Kelly BJ, Fraefel C, Cunningham AL, Diefenbach RJ.** 2009. Functional roles of the tegument proteins of herpes simplex virus type 1. Virus Res **145:**173-86.
7. **Loret S, Lippé R.** 2012. Biochemical analysis of infected cell polypeptide (ICP)0, ICP4, UL7 and UL23 incorporated into extracellular herpes simplex virus type 1 virions. J Gen Virol **93:**624-34.
8. **Henaff D, Remillard-Labrosse G, Loret S, Lippé R.** 2013. Analysis of the early steps of herpes simplex virus 1 capsid tegumentation. J Virol **87:**4895-906.
9. **Preston CM.** 1979. Control of herpes simplex virus type 1 mRNA synthesis in cells infected with wild-type virus or the temperature-sensitive mutant tsK. J Virol **29:**275-84.
10. **Sacks WR, Schaffer PA.** 1987. Deletion mutants in the gene encoding the herpes simplex virus type 1 immediate-early protein ICP0 exhibit impaired growth in cell culture. J Virol **61:**829-39.

11. **Weinheimer SP, Boyd BA, Durham SK, Resnick JL, O'Boyle DR, 2nd.** 1992. Deletion of the VP16 open reading frame of herpes simplex virus type 1. J Virol **66:**258-69.

12. **Zhang YQ, Lai W, Li H, Li G.** 2008. Inhibition of herpes simplex virus type 1 by small interfering RNA. Clin Exp Dermatol **33:**56-61.

13. **Stegen C, Yakova Y, Henaff D, Nadjar J, Duron J, Lippé R.** 2013. Analysis of virion-incorporated host proteins required for herpes simplex virus type 1 infection through a RNA interference screen. PLoS One **8:**e53276.

14. **Baines J, Duffy C.** 2006. Nucleocapsid Assembly and Envelopment of Herpes Simplex Virus, p 175-204. *In* Sandri-Goldin RM (ed), Alpha Herpesviruses. Caister Academic Press, Norfolk.

15. **Heine JW, Honess RW, Cassai E, Roizman B.** 1974. Proteins specified by herpes simplex virus. XII. The virion polypeptides of type 1 strains. J Virol **14:**640-51.

16. **Roller RJ, Roizman B.** 1992. The herpes simplex virus 1 RNA binding protein US11 is a virion component and associates with ribosomal 60S subunits. J Virol **66:**3624-32.

17. **Newcomb WW, Jones LM, Dee A, Chaudhry F, Brown JC.** 2012. Role of a reducing environment in disassembly of the herpesvirus tegument. Virology **431:**71-9.

18. **Clarke RW, Monnier N, Li H, Zhou D, Browne H, Klenerman D.** 2007. Two-color fluorescence analysis of individual virions determines the distribution of the copy number of proteins in herpes simplex virus particles. Biophys J **93:**1329-37.

19. **Bohannon KP, Jun Y, Gross SP, Smith GA.** 2013. Differential protein partitioning within the herpesvirus tegument and envelope underlies a complex and variable virion architecture. Proc Natl Acad Sci U S A **110:**E1613-20.

20. **Leslie J, Rixon FJ, McLauchlan J.** 1996. Overexpression of the herpes simplex virus type 1 tegument protein VP22 increases its incorporation into virus particles. Virology **220:**60-8.

21. **McLauchlan J.** 1997. The abundance of the herpes simplex virus type 1 UL37 tegument protein in virus particles is closely controlled. J Gen Virol **78:**189-94.

22. **Michael K, Klupp BG, Mettenleiter TC, Karger A.** 2006. Composition of Pseudorabies Virus Particles Lacking Tegument Protein US3, UL47, or UL49 or Envelope Glycoprotein E. J Virol **80:**1332-9.

23. **Dargan DJ, Subak-Sharpe JH.** 1997. The effect of herpes simplex virus type 1 L-particles on virus entry, replication, and the infectivity of naked herpesvirus DNA. Virology **239:**378-88.

24. **Loret S, El Bilali N, Lippé R.** 2012. Analysis of herpes simplex virus type I nuclear particles by flow cytometry. Cytometry A **81:**950-9.

25. **Desai P, Person S.** 1998. Incorporation of the green fluorescent protein into the herpes simplex virus type 1 capsid. J Virol **72:**7563-8.

26. **Desai P, Sexton GL, Huang E, Person S.** 2008. Localization of herpes simplex virus type 1 UL37 in the Golgi complex requires UL36 but not capsid structures. J Virol **82:**11354-61.

27. **Antinone SE, Smith GA.** 2010. Retrograde axon transport of herpes simplex virus and pseudorabies virus: a live-cell comparative analysis. J Virol **84:**1504-12.

28. **Antinone SE, Zaichick SV, Smith GA.** 2010. Resolving the assembly state of herpes simplex virus during axon transport by live-cell imaging. J Virol **84:**13019-30.

29. **Liu M, Schmidt EE, Halford WP.** 2010. ICP0 dismantles microtubule networks in herpes simplex virus-infected cells. PLoS One **5:**e10975.

30. **Willard M.** 2002. Rapid directional translocations in virus replication. J Virol **76:**5220-32.

31. **La Boissiere S, Izeta A, Malcomber S, O'Hare P.** 2004. Compartmentalization of VP16 in cells infected with recombinant herpes simplex virus expressing VP16-green fluorescent protein fusion proteins. J Virol **78:**8002-14.

32. **Elliott G, O'Hare P.** 1999. Live-cell analysis of a green fluorescent protein-tagged herpes simplex virus infection. J Virol **73:**4110-9.

33. **Turcotte S, Letellier J, Lippé R.** 2005. Herpes simplex virus type 1 capsids transit by the trans-Golgi network, where viral glycoproteins accumulate independently of capsid egress. J Virol **79:**8847-60.

34. **McNabb DS, Courtney RJ.** 1992. Characterization of the large tegument protein (ICP1/2) of herpes simplex virus type 1. Virology **190:**221-32.

35. **Schmitz JB, Albright AG, Kinchington PR, Jenkins FJ.** 1995. The UL37 protein of herpes simplex virus type 1 is associated with the tegument of purified virions. Virology **206:**1055-65.

36. **Munger J, Chee AV, Roizman B.** 2001. The U(S)3 protein kinase blocks apoptosis induced by the d120 mutant of herpes simplex virus 1 at a premitochondrial stage. J Virol **75:**5491-7.

37. **McLean C, Buckmaster A, Hancock D, Buchan A, Fuller A, Minson A.** 1982. Monoclonal antibodies to three non-glycosylated antigens of herpes simplex virus type 2. J Gen Virol **63:**297-305.

38. **Donnelly M, Verhagen J, Elliott G.** 2007. RNA binding by the herpes simplex virus type 1 nucleocytoplasmic shuttling protein UL47 is mediated by an N-terminal arginine-rich domain that also functions as its nuclear localization signal. J Virol **81:**2283-96.

39. **Elliott G, O'Reilly D, O'Hare P.** 1996. Phosphorylation of the herpes simplex virus type 1 tegument protein VP22. Virology **226:**140-5.

40. **Luft JH.** 1961. Improvements in epoxy resin embedding methods. J Biophys Biochem Cytol **9:**409-14.

41. **Conway JF, Cockrell SK, Copeland AM, Newcomb WW, Brown JC, Homa FL.** 2010. Labeling and localization of the herpes simplex virus capsid protein UL25 and its interaction with the two triplexes closest to the penton. J Mol Biol **397:**575-86.

42. **Khadivjam B, Stegen C, Hogue-Racine MA, El Bilali N, Dohner K, Sodeik B, Lippe R.** 2017. The ATP-dependent RNA Helicase DDX3X modulates Herpes Simplex Virus Type 1 Gene Expression. J Virol doi:10.1128/JVI.02411-16.

43. **Bohannon KP, Sollars PJ, Pickard GE, Smith GA.** 2012. Fusion of a fluorescent protein to the pUL25 minor capsid protein of pseudorabies virus allows live-cell capsid imaging with negligible impact on infection. J Gen Virol **93:**124-9.

44. **Trus BL, Newcomb WW, Cheng N, Cardone G, Marekov L, Homa FL, Brown JC, Steven AC.** 2007. Allosteric signaling and a nuclear exit strategy: binding of UL25/UL17 heterodimers to DNA-Filled HSV-1 capsids. Mol Cell **26:**479-89.

45. **Yang K, Baines JD.** 2011. Selection of HSV capsids for envelopment involves interaction between capsid surface components pUL31, pUL17, and pUL25. Proc Natl Acad Sci U S A **108:**14276-81.

46. **Toropova K, Huffman JB, Homa FL, Conway JF.** 2011. The herpes simplex virus 1 UL17 protein is the second constituent of the capsid vertex-specific component required for DNA packaging and retention. J Virol **85:**7513-22.

47. **Yang TY, Courtney RJ.** 1995. Influence of the host cell on the association of ICP4 and ICP0 with herpes simplex virus type 1. Virology **211:**209-17.

48. **Jambunathan N, Chouljenko D, Desai P, Charles AS, Subramanian R, Chouljenko VN, Kousoulas KG.** 2014. Herpes Simplex Virus 1 Protein UL37 Interacts with Viral Glycoprotein gK and Membrane Protein UL20 and Functions in Cytoplasmic Virion Envelopment. J Virol **88:**5927-35.

49. **Nagel CH, Döhner K, Fathollahy M, Strive T, Borst EM, Messerle M, Sodeik B.** 2008. Nuclear egress and envelopment of herpes simplex virus capsids analyzed with dual-color fluorescence HSV1(17+). J Virol **82:**3109-24.

50. **Oh HS, Knipe DM, Oh HS, Bryant KF, Nieland TJ, Mazumder A, Bagul M, Bathe M, Root DE, Knipe DM.** 2015. Proteomic analysis of the herpes simplex Virus 1 virion protein 16 transactivator protein in infected cells. . Proteomics **5:**e01086-13.

51. **Elliott G, Mouzakitis G, O'Hare P.** 1995. VP16 interacts via its activation domain with VP22, a tegument protein of herpes simplex virus, and is relocated to a novel macromolecular assembly in coexpressing cells. J Virol **69:**7932-41.

52. **Elliott G, Hafezi W, Whiteley A, Bernard E.** 2005. Deletion of the herpes simplex virus VP22-encoding gene (UL49) alters the expression, localization, and virion incorporation of ICP0. J Virol **79:**9735-45.

53. **Duffy C, Lavail JH, Tauscher AN, Wills EG, Blaho JA, Baines JD.** 2006. Characterization of a UL49-null mutant: VP22 of herpes simplex virus type 1 facilitates viral spread in cultured cells and the mouse cornea. J Virol **80:**8664-75.

54. **Tanaka M, Kato A, Satoh Y, Ide T, Sagou K, Kimura K, Hasegawa H, Kawaguchi Y.** 2012. Herpes simplex virus 1 VP22 regulates translocation of multiple viral and cellular proteins and promotes neurovirulence. J Virol **86:**5264-77.

55. **Kobiler O, Lipman Y, Therkelsen K, Daubechies I, Enquist LW.** 2010. Herpesviruses carrying a Brainbow cassette reveal replication and expression of limited numbers of incoming genomes. Nat Commun **1 (article # 146):**1-8.

56. **Kobiler O, Brodersen P, Taylor MP, Ludmir EB, Enquist LW.** 2011. Herpesvirus replication compartments originate with single incoming viral genomes. MBio **2:**e00278-11.

57. **Taylor MP, Kobiler O, Enquist LW.** 2012. Alphaherpesvirus axon-to-cell spread involves limited virion transmission. Proc Natl Acad Sci U S A **109:**17046-51.

II.2 Article 2: Proteomics of Herpes Simplex Virus Type 1 Nuclear Capsids

Auteurs : Nabil El Bilali, Bita Khadivjam, Eric Bonneil, Pierre Thibault et Roger Lippé

Article en révision

Contribution des auteurs :

Nabil El Bilali* : Conception, planification et réalisation des expériences, analyse des données, montage des figures et rédaction de l'article.

Bita Khadivjam : Réalisation des expériences de coloration à l'argent (Silver Staining).

Eric Bonneil : Analyse des échantillons par MS-MS.

Pierre Thibault : Analyse des échantillons par MS-MS.

Roger Lippé : Création et supervision du projet, conception des expériences, analyse des données et rédaction de l'article.

* Premier auteur

Note sur le texte :

Cette section reproduit le texte intégral de l'article mentionné ci-dessus.

Certaines modifications ont toutefois été apportées à la mise en page du manuscrit afin de mieux l'intégrer à la présente thèse.

Proteomics of Herpes simplex virus type 1 nuclear capsids

By

Nabil El Bilali[1], Bita Khadivjam[1], Eric Bonneil[2], Pierre Thibault[2] and Roger Lippé[1]

[1]Department of Pathology and Cell biology, University of Montreal, C.P. 6128, Succursale Centre-Ville, Montréal, Québec, Canada H3C 3J7

[2]Institute for Research in Immunology and Cancer, ‡Department of Chemistry, Université de Montréal, C.P. 6128, Succursale Centre-Ville, Montréal, Québec, Canada H3C 3J7

Running title: Proteomics of HSV-1 nuclear capsids

Keywords: HSV / nuclear capsids / mass spectrometry / flow virometry / flow cytometry / proteomics / egress

Corresponding author:
Roger Lippé
Email: roger.lippe@umontreal.ca
Tel.: (+1) 514 343-5616

II.2.1 Abstract

Herpes simplex virus has a complex life cycle that includes the production of distinct particles in the nucleus, where new capsids are assembled. Among these nuclear capsids, procapsids are devoid of nucleic acid but contain large amounts of the preVP22a scaffold protein. These thermo-unstable particles then mature into A-, B- or C-nuclear icosahedral capsids, depending on their ability to shed the proteolytically processed scaffold and incorporate the viral genome. Interestingly, C-capsids are preferentially exported to the cytoplasm and ultimately give rise to infectious virions. While A-, B- and C-capsids share several components, their distinct fate hints at meaningful differences. To probe them, we performed proteomics studies of highly enriched nuclear capsids, relying in part on flow virometry to purify C-nuclear capsids. We found that while many proteins are indeed common among these nuclear capsids, they exhibit unique sets of proteins. These naturally include viral proteins but also many cellular proteins.

Importance

Much is known about the biology of herpesviruses. This includes their unique ability to traverse the two nuclear envelopes by budding and fusion respectively. For HSV-1, this implies the involvement of the pUL31/pUL34 and pUL17/pUL25 complexes that may favor C-capsid egress. However, this selection process is not clear, nor are all the differences that distinguish A-, B- and C-capsids. The present study unveils what proteins compose these capsids, including many unexpected host proteins. This should open up new research avenues to clarify the biology of this most interesting family of viruses. It also reiterates the use of flow virometry as an innovative tool to purify viral particles.

II.2.2 Introduction

Herpesviruses replicate their genome and assemble new capsids in the nucleus. Given their large dimension and the restrictive size of nuclear pores, these capsids reach the cytoplasm by non-conventional means implicating a budding step through the inner nuclear membrane that produces primary enveloped virions in the perinuclear space (1). These transient viral intermediates rapidly fuse with the outer nuclear envelope to yield naked cytoplasmic capsids. Ultimately, those capsids are re-enveloped and acquire their mature envelope from the cell (2). For herpes simplex virus type 1 (HSV-1) and the related pseudorabies virus (PRV), the viral proteins pUL31, pUL34 and pUS3 as well as the host proteins PKC, torsin A and SUN2 play a role in nuclear egress (3-9). However, very little is known of this viral egress pathway and additional research is required to decipher how these viruses escape the nucleus. A better understanding of the proteins present on the nuclear and perinuclear capsids may be very useful in this respect.

A relevant issue regarding HSV-1 propagation is the generation of parallel forms of viral particles in the nucleus, namely procapsids as well as A-, B- and C-capsids. These all share the basic components of the capsids, in particular the major capsid protein VP5 (encoded by the viral gene UL19), the minor VP19C (UL38), VP23 (UL18), VP26 (UL35) proteins as well as the pUL6 portal protein (10, 11). However, these capsids differ in a number of ways. As recently reviewed (12), procapsids are spherical and thermo-unstable entities devoid of DNA but containing the pre-VP22a scaffold protein (10, 13). They are believed to be the precursors of the other three-capsid types, which arise when the newly duplicated concatemeric viral genome is cut into monomers, incorporated in the newly synthesized capsids and the capsid harbors an icosahedral shape (10, 14). Concomitantly, the viral protease PRA cleaves the scaffold into VP22a and a small 25 amino acid carboxyl terminal peptide (15, 16). PRA, which is co-expressed in frame with pre-VP22a using a

preceding start codon and consequently sharing many amino acids, cleaves itself into VP24, VP21 and the aforementioned carboxyl terminal fragment (15, 17). While A-, B- and C-nuclear capsids co-exist, A-capsids are considered abortive as they fail to incorporate the viral genome (18). They do nonetheless process and shed the scaffold and PRA but may contain some VP24 (11). For these reasons, A-capsids are somewhat translucid by electron microscopy when negatively stained (19). On the other hand, the scaffold and viral protease are also processed in B-capsids but without shedding or viral DNA incorporation (20). They arise when DNA cleavage and packaging are aberrant (12) and, upon negative staining, these capsids are rather greyish by electron microscopy (19). Finally, C-capsids, which are electron dense, are nuclear capsids that shed their cleaved scaffold, retain the VP24 protease fragment and incorporate viral DNA monomers (11, 19, 21). Only nuclear C-capsids ultimately give rise to fully mature and infectious virions. One open issue is whether the C-capsids differ from A- and B-capsids in other ways and whether they might specifically interact with cellular proteins within the nucleus.

Work by several laboratories including ours has indicated that C-capsids are preferentially released by the nucleus in infected cells as well as in an in vitro nuclear egress assay (1, 22, 23). This raises the question as to why they are favored over A- or B-capsids. Initial findings by Baines and colleagues suggested that the pUL17/pUL25 complex, initially dubbed C-capsid specific complex (CCSC) (24), may promote the interaction of C-capsids with pUL31 (25), a member of the nuclear egress complex (NEC) that is essential for nuclear viral exit (3, 4). Subsequent work, though, revealed the concomitant presence of pUL17/pUL25 on A- and B-nuclear capsids, albeit in lower stoichiometry than on C-capsids, leading to the renaming of the CCSC into the capsid vertex-specific complex (CVSC) (26, 27). Meanwhile, the pUL36 tegument protein has been shown to stably anchor the pUL17/pUL25 complex onto the capsids and is now considered a

member of the CVSC (12, 28, 29). Given the presence of the CVSC complex on all three nuclear capsid types, this implies the participation of molecules other than pUL17, pUL25 or pUL36 in the preferential egress of C-capsids. Clearly, HSV-1 nuclear egress is not yet fully understood. Determining the precise composition of the A-, B- and C-nuclear capsids may therefore be informative.

Along its egress pathway, HSV-1 sequentially recruits some two dozen distinct viral proteins and possibly as many as 49 host proteins (30, 31). While it is not clear where the aforementioned host proteins are recruited onto the capsids, most viral proteins that constitute the so-called tegument layer are likely incorporated on the maturing viral particles while they transit in the cytoplasm. Many of these tegument proteins may additionally be recruited onto the capsids during their final envelopment by virtue of their interactions with the viral glycoproteins accumulating, for instance, at the TGN (32). In contrast, some viral tegument proteins, such as ICP0, ICP4, pUL36 and pUL37, have been reported on nuclear capsids and may constitute the "primary" nuclear tegument (33). This does not, however, exclude that these molecules may be coating the capsids in more than one cellular compartments. Greater scrutiny of the tegumentation process is therefore required to determine where each tegument component is targeted to the viral capsids.

To address how newly assembled C-capsids selectively escape the nucleus, define how they may differ from A- and B-nuclear capsids, probe their primary nuclear tegument and how they mature in the course of an infection, we evaluated by proteomics the protein content of all three thermostable forms of nuclear capsids from wild-type HSV-1 infections. While A- and B-nuclear capsids isolated from classical sucrose gradients were relatively pure, C-capsids were substantially contaminated by B-capsids by this approach. We therefore combined those density gradients with a novel flow virometry approach we developed for HSV-1 to enrich the DNA containing C-capsids

to high purity. We now report a mass spectrometry analysis of the composition of these capsids from three independent experiments and stringent scoring conditions. By and large, the viral protein content of the A-, B- and C-capsids was similar in many respects and in agreement with past findings. Unexpectedly, a few viral proteins were only reproducibly seen in A- or C-capsids and sixty-four host proteins were additionally detected on the various capsids, nineteen of which were present on all three nuclear capsid types. These included several ribosomal and RNA binding proteins as well as histones and hnRNP components. While the biological significance of these proteins must be orthogonally validated, the present findings open many interesting and future research avenues

II.2.3 Results

Purification of HSV-1 nuclear capsids. Given our interest in the human proteins that could be present in the nuclear capsid samples, the nuclear capsids were prepared from wild-type HSV-1 infected HeLa cells, as for our previous proteomic study of mature extracellular virions (30). Naturally, it was imperative that the samples be as pure as possible. To achieve this, we first purified intact nuclei from infected cells to limit cytoplasmic and extracellular contaminants, an approach we successfully used in the past (22, 23, 33). Second, we relied on 20-50% sucrose density gradients, a classical approach to purify HSV-1 A-, B- and C-nuclear capsids (34). Third, to insure that these were not stripped of their tegument (33, 35, 36), we prepared the gradients in physiological salt concentrations using a so-called low-salt TNE buffer (33). Isolated nuclei were therefore resuspended in low-salt TNE and broken mechanically by freeze-thawing, DNase treated and sonicated. To further improve purity, the samples were first overlaid onto a 35% sucrose cushion prior to being separated onto a 20-50% continuous sucrose gradient. This overall strategy

is detailed in figure 1. As expected, the gradients exhibited A, B and C bands for infected samples, while no such band was visible for an equal number of mock-infected cells (fig. 2A and data not shown).

The viral bands were carefully picked and, as controls, the same locations were harvested from identical gradients prepared from uninfected cells. To monitor sample purity, all samples were analyzed by SDS-PAGE and silver staining, loading equal protein amounts in the case of the infected samples. For the mock samples, the same volumes were used as the corresponding infected bands, since we anticipated much lower protein levels (e.g. same volume of mock A as for A-capsids and so on). As shown in the figure 2B, some host proteins with similar density as the viral capsids were detected by silver staining. However, more intense and numerous bands were seen in the viral samples, suggesting a good capsid enrichment. Moreover, many common bands were visible in the infected samples, including the expected capsid components pUL19 (VP5), pUL38 (VP19c), pUL18 (VP23) and pUL35 (VP26) (10). To evaluate the purity of these capsid preparations, the three sucrose bands were examined and quantified by negative staining and transmission electron microscopy. The data revealed that the A- and B- fractions were in fact relatively pure in terms of capsids but also of large contaminants (fig. 2C; Table 1). In contrast, nearly 30% of the capsids in the C- fractions were in fact B-capsids. It was therefore essential to further purify the C-capsids prior to analyzing them by mass spectrometry.

Flow virometry enrichment of C-nuclear capsids. Flow virometry, a term coined by Grivel and colleagues (37), is an innovative and efficient method to characterize and purify individual viral particles, as recently reviewed (38). We previously reported that HSV-1 nuclear C-capsids can indeed be sorted to 90% purity by GFP tagging one of the viral structural proteins or by

labelling the viral genome with Syto 13, a membrane-permeable nucleic acid dye with low fluorescence when unbound (39). The same strategy successfully works for fully mature extracellular virions (40). To validate the usefulness of this approach in the present study, the A-, B- and C- sucrose gradient fractions were briefly incubated with Syto 13 and analyzed by flow virometry. Under these conditions, only background fluorescence was noted in the A- and B-fractions, in agreement with the above EM results (fig. 3A, panels a-d) with mean fluorescence intensities (MFI) of 2,396 and 2,459 without Syto 13 and 3,173 to 3,240 in the presence of Syto 13 respectively. Similarly, less than 1% of the C-capsids were only weakly fluorescent in the absence of Syto 13 (MFI = 6,099). By comparison, incubation of PBS with Syto 13 without any capsids led to an MFI of 829. In contrast, 82% of the particles from the C-fraction were strongly fluorescent when incubated with Syto 13 (MFI = 33,258; fig. 3A, panels e and f). To isolate C-nuclear capsids with the highest possible purity, we therefore opted to combine the sucrose gradients with flow virometry, gating on the Syto fluorescent signal as schematically depicted in figure 3B. Hence, C-capsids harvested from the gradients were incubated with Syto 13 and sorted by flow cytometry. Upon quantification of the negatively stained capsids by electron microscopy (fig. 3C), nearly all capsids were C-type capsids (96%), with few contamination (A-capsid: 0%; B-capsids: 4%; n=508). With this level of purity, it was now possible to proceed to mass spectrometry.

Mass spectrometry of A-, B- and C-nuclear capsids. To circumvent possible differences among sample preparations, the three nuclear capsid types were prepared on sucrose gradients from three independent experiments, followed by flow virometry in the case of C-capsids. It should be noted that the Syto 13 dye is not protein-based and consequently did not “contaminate” our proteomics analyses. Despite the presence of minor amounts of proteins in the mock samples (fig.

2B), the latter were prepared in parallel using the corresponding sucrose fractions. However, the "mock C-fraction" was not processed by flow virometry since unstainable with Syto 13. All triplicate samples (7 µg per sample) and mock controls (same volume as the infected samples) were sequentially injected into a LC-MS/MS spectrometer and their protein content identified using a hybrid human/HSV-1 database (see materials and methods). Stringent conditions were used to limit false negatives (95% protein and peptide probabilities and a minimum of 2 peptides). Under these conditions, 87 different host proteins were identified in the uninfected samples (fig. 4). Oddly, 55% of those contaminants (48 out of 87) were common to the various mock samples despite coming from different portions of the density gradients (fig. 4). These contaminants included a vast array of proteins with distinct functions (e.g. annexins, integrins, keratins, protein disulfide-isomerases and many others; Table S1). It should be noted that these proteins were overall 10 fold less abundant than the proteins in the viral samples (average of 2,160 total spectra for each mock sample compared to an average of 20,748 for each infected sample). While present, these irrelevant cellular proteins were consequently only minimally abundant.

As anticipated, no viral protein was identified in any of the mock samples. Upon examining the viral protein content of each capsid type, a good reproducibility was observed among the triplicate experiments (fig. 5A). For instance, 76.5% of the proteins (26 out of 34) were noted in the three A-capsid isolates (A1, A2, A3). Similarly, 65.6% and 69.7% of the proteins were identified the B- and C-capsid isolates respectively (B1, B2, B3 or C1, C2, C3). For host proteins, these values were slightly lower at 43.2% (38 out of 88 in A1, A2, A3), 52.0% (B1, B2, B3) and 48.6% (C1, C2, C3) (fig. 5B). Most notably, 86-92% of the proteins found in the mock A (73 out of 79), B (72 out of 84) or C (60 out of 68) fractions were absent in the viral samples, hinting at their good purity (fig. 5B).

Viral protein content of the nuclear capsids. For maximal stringency, we opted to consider only the proteins consistently found in all three independent replicates. When doing so, a total of 26 viral proteins were reproducibly identified in A-capsids, while 21 and 23 viral proteins were reproducibly found in B- and C-capsids (fig. 5A). Most interestingly, 62.1% of those proteins were common to all three capsid types (18 out of 29; fig. 5A, rightmost Venn diagram). Those included the expected capsid components pUL18 (VP23), pUL19 (VP5), pUL35 (VP26), pUL38 (VP19c) as well as the pUL25 capsid vertex component and pUL6 portal (fig. 6 and supplementary Table S2). To our surprise, the capsid vertex component pUL17 partner was only consistently detected on A- and C-capsids. As mass spectrometry cannot distinguish the highly related viral PRA and scaffold proteins and fragments thereof, all peptides were combined and found on all capsid types.

Several tegument proteins were identified on all three nuclear capsid types, including pUL21, pUL36, pUL49 (VP22), pUL50, pUL51 and pUS10 (fig. 6 and Table S2). In contrast, pRL2 (ICP0) and pUL37, previously reported to be present on nuclear C-capsids (33, 41), were barely detected in this study, while pUS3 was not seen at all. Interestingly, the pUL15, pUL28 and pUL33 viral DNA terminase complex known to bind procapsids (42) were absent from C-capsids and only partially found on A- and B-capsids, corroborating previous reports that it falls off when the viral genome is successfully encapsidated (43, 44). Oddly, pRS1 (ICP4) was only consistently detected on A-capsids. Similarly, pUL2, pUL3, pUL12, pUL39 (ICP6), pUL42, pUL46, pUL47 (VP13/14), pUL48 and pUS1 (ICP22) were found on all or some of the capsids (fig. 6, Table S2). Finally, both components of the nuclear egress complex (NEC; pUL31 and pUL34) were reproducibly uncovered on A-, B- and C-nuclear capsids. Though only a few spectra were detected for pUL31 and pUL34 in each sample, suggesting a potential low abundance, pUL31 levels were similar in

A- and B-capsids and more abundant than in C-capsids. Meanwhile, pUL34 amounts were similar for A- and C-capsids and less abundant in B-capsids (Table S2). Thus, a complex arrangement of expected and unexpected proteins were uncovered on A-, B- and/or C-capsids.

Host protein content of the nuclear capsids. The correct identification of host proteins in the viral particles required an additional bioinformatics step, since host proteins were identified not only in the viral samples but also in the mock controls. Although in much smaller amounts in the latter case, these cellular proteins were purposely ignored for the viral particles, albeit they could *de facto* be real components of the nuclear capsids. Interestingly, nearly a third of the remaining positive hits consistently found in the three replicates were common to the three-capsid types (19 out of 64 proteins; fig. 5B). This included a vast array of proteins and associated functions (fig. 7 and supplementary Table S3). Overall, proteins falling under RNA metabolism were prevalent (ribosomal, hnRNP, RNA binding and translation), in addition to select histones, heat shock components and proteins with other cellular roles. Though several of those proteins did not have associated "Go-Terms", between 82 and 88% of the documented proteins were either nuclear or known to transit by the nucleus, highlighting that their detection on nuclear capsids may be biologically relevant. As with any proteomics study, these protein hits will require orthogonal validation to understand how, if at all, they interact with the viral capsids and perhaps modulate their assembly or egress.

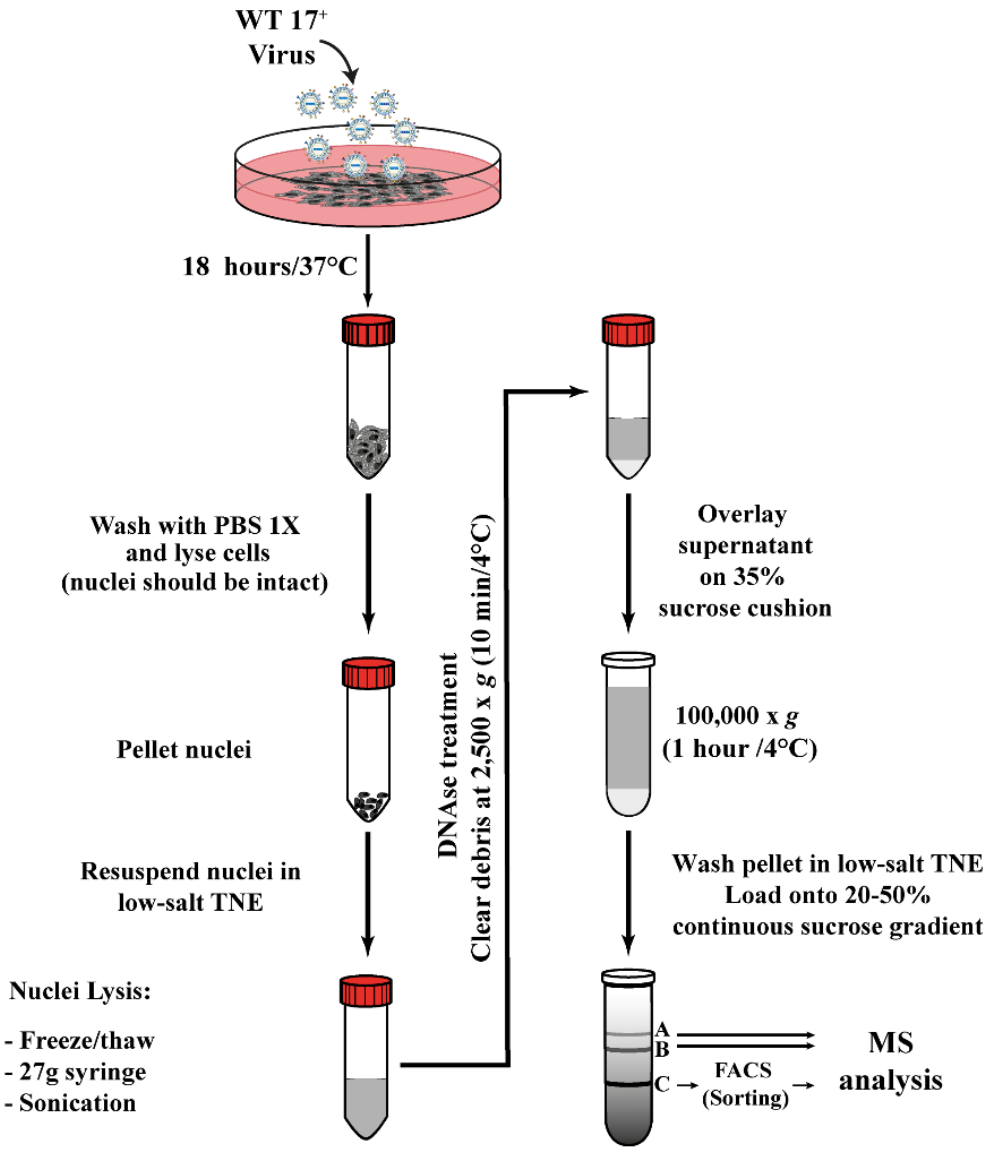

Figure. 1: Purification scheme.

Schematic illustration of the different steps used to purify HSV-1 nuclear capsids. This includes the preparation of nuclei from infected cells, the recovery of the nuclear capsids from these nuclei and their separation on linear sucrose gradients. For C-capsids, a subsequent purification step by flow cytometry was applied for maximal purity. See text and Materials and Methods for details.

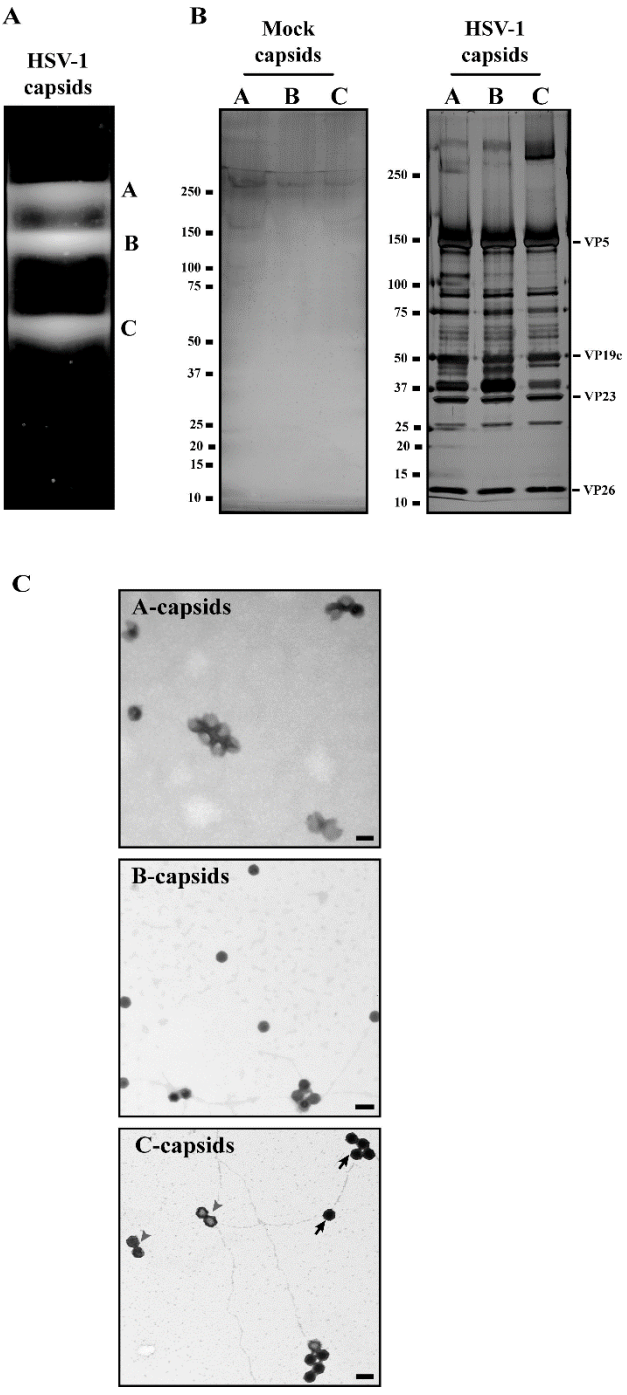

Figure. 2: Silver staining and electron microscopy analysis of isolated nuclear capsids.

A) Hela cells were infected with HSV-1 strain 17 and cells were harvested 18 hours post infection. They were washed and lysed to isolate the nuclei. The latter were then mechanically broken up, DNAse treated and sonicated and the nuclear capsids separated on a sucrose cushion then a 20-

50% linear sucrose gradient prepared in the presence of 150 mM NaCl (low salt TNE). The “A”, “B”, and “C” labels on the right side of the gradient refers to the different nuclear capsid types. **B)** Two micrograms of the gradient-purified capsids and equivalent volumes from the uninfected gradients were loaded onto a 5-15% SDS-polyacrylamide gels and the overall protein composition determined by silver staining. Though many bands are visible, proteins with molecular weights corresponding to the main constituents of the capsids were detectable, as indicated to the right of the stained gels. **C)** The purity of each capsid fraction was accessed by negative staining and EM (see Table 1 for quantification). Bars represent 100 nm. While A- and B-capsids were quite pure, C-capsids (dark arrows) were substantially cross-contaminated by B-capsids (arrowheads).

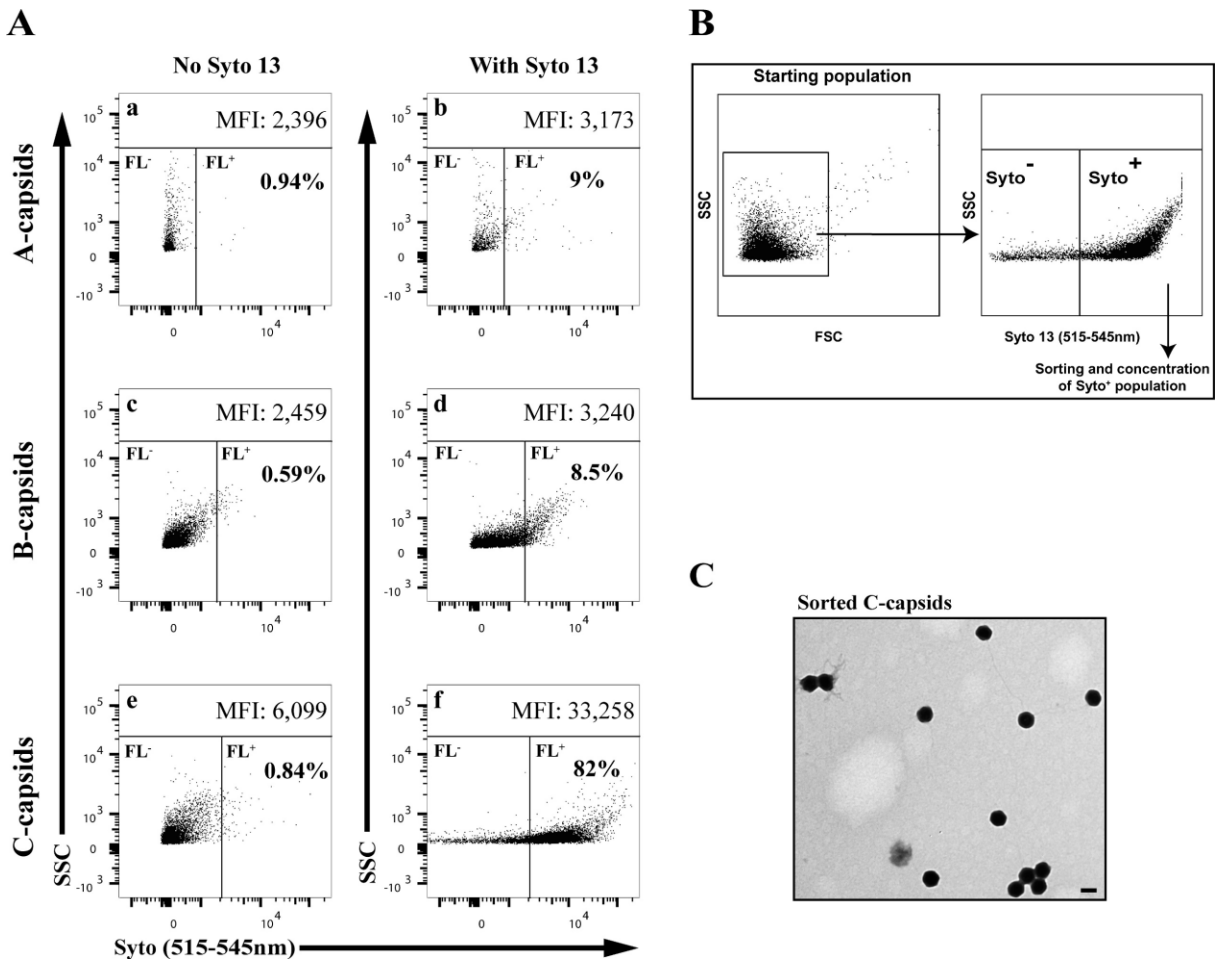

Figure. 3: Analysis of nuclear capsids by flow virometry.

A) Nuclear capsids collected from 20-50% linear sucrose gradients were stained with 1 μM Syto 13 and analyzed by flow cytometry. Aggregated particles were excluded by gating them out in the SSC versus FSC plots. The percentages of Syto 13-positive particles, relative to the starting population, are indicated in each graph. Mean fluorescence intensities of the Syto 13 positive particles are noted at the top of each sample. As a reference point, the buffer alone had no fluorescence (MFI of 0), while the buffer mixed with Syto 13 had a MFI of 829. **B)** Schematic description of the gating strategy applied for the sorting of Syto 13 labeled C capsids by FACS. **C)** EM analysis of sorted C-capsids. Ninety-six percent of the capsids were C-capsids (see text). The bar represents 100 nm.

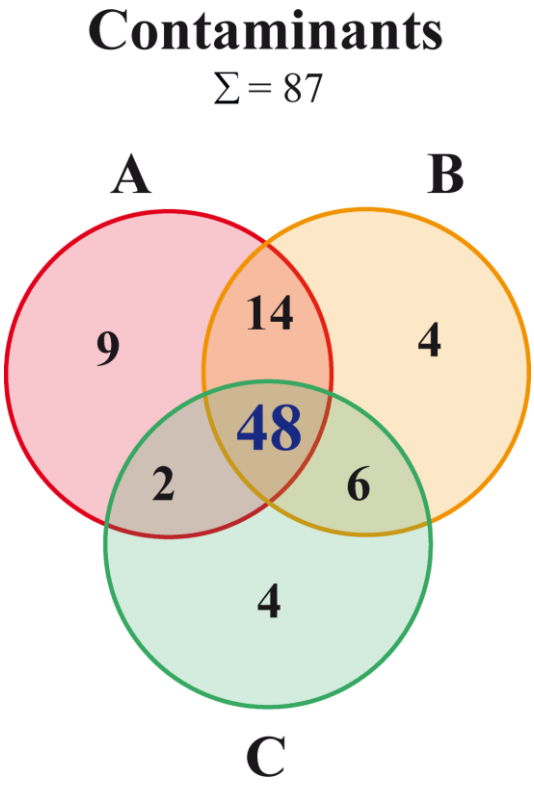

Figure. 4: Contaminants.

The Venn diagram represents the number of distinct proteins identified by mass spectrometry in the non-infected mock samples. A, B and C refer to the same sucrose fractions where A-, B- and C-capsids migrated in the infected samples. To limit false negatives, a threshold of 95% protein and peptide probabilities and a minimum of 2 peptides was applied. A total of 87 different proteins were found (see Σ), 48 of which were common to the three fractions. See Table S1 for a list of these proteins.

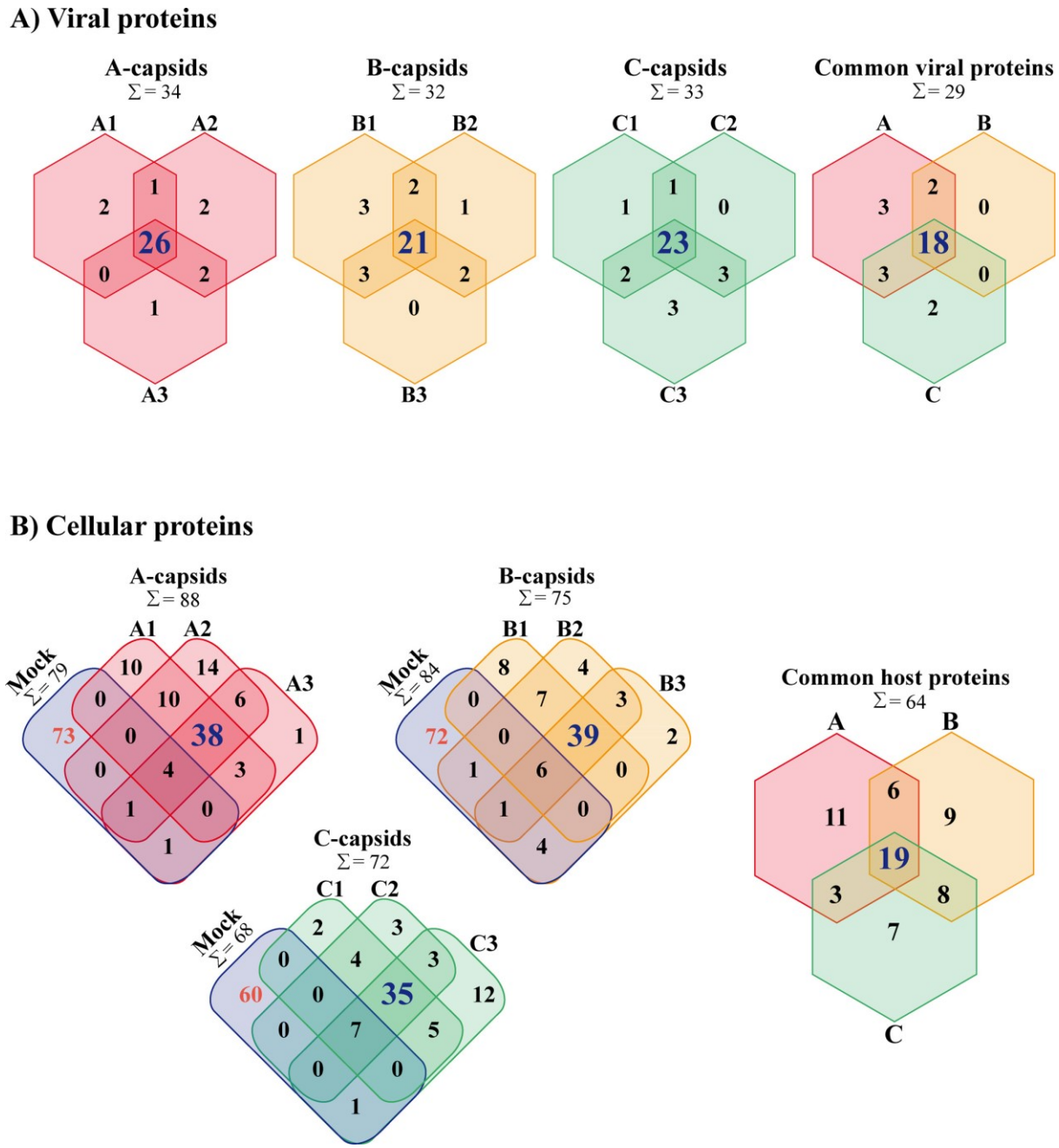

Figure. 5: Analysis of protein content of the nuclear capsids by proteomics.

The Venn diagrams show the overlap of proteins identified by mass spectrometry in three independent samples prepared on different days but analyzed simultaneously (ex: A1, A2 and A3). As above, a threshold of 95% protein and peptide probabilities and a minimum of 2 peptides were applied. **A)** Viral proteins and **B)** Cellular proteins identified by mass spectrometry. Note that for

the cellular proteins, the mock samples are additionally depicted (Mock), since several cellular proteins co-fractionated with the viral capsids. Those contaminants uniquely found in the mock samples (red values) correspond to those depicted in Fig. 4. In contrast, no viral protein was found in the mock samples. Common proteins (right-most Venn Diagrams) were those that were found in all three independent replicates and capsid types (dark blue values). The sums (Σ) of proteins of each sample are indicated at the top of each diagram as well as for the Mock samples.

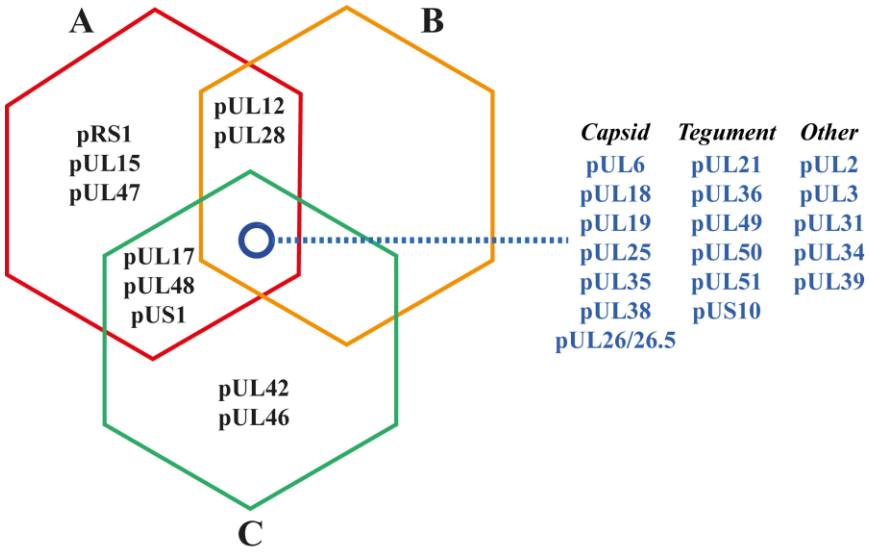

Figure. 6: Reproducible viral proteins found in the nuclear capsids.

All viral proteins identified by mass spectrometry and reproducibly found in the independent replicates are listed. For simplicity and conciseness, the gene names were used. Note that no viral protein was uniquely associated with B-capsids (Refer to Table S2 for details). As discussed in text, pUL26 and pUL26.5 cannot be distinguished by mass spectrometry and were consequently amalgamated.

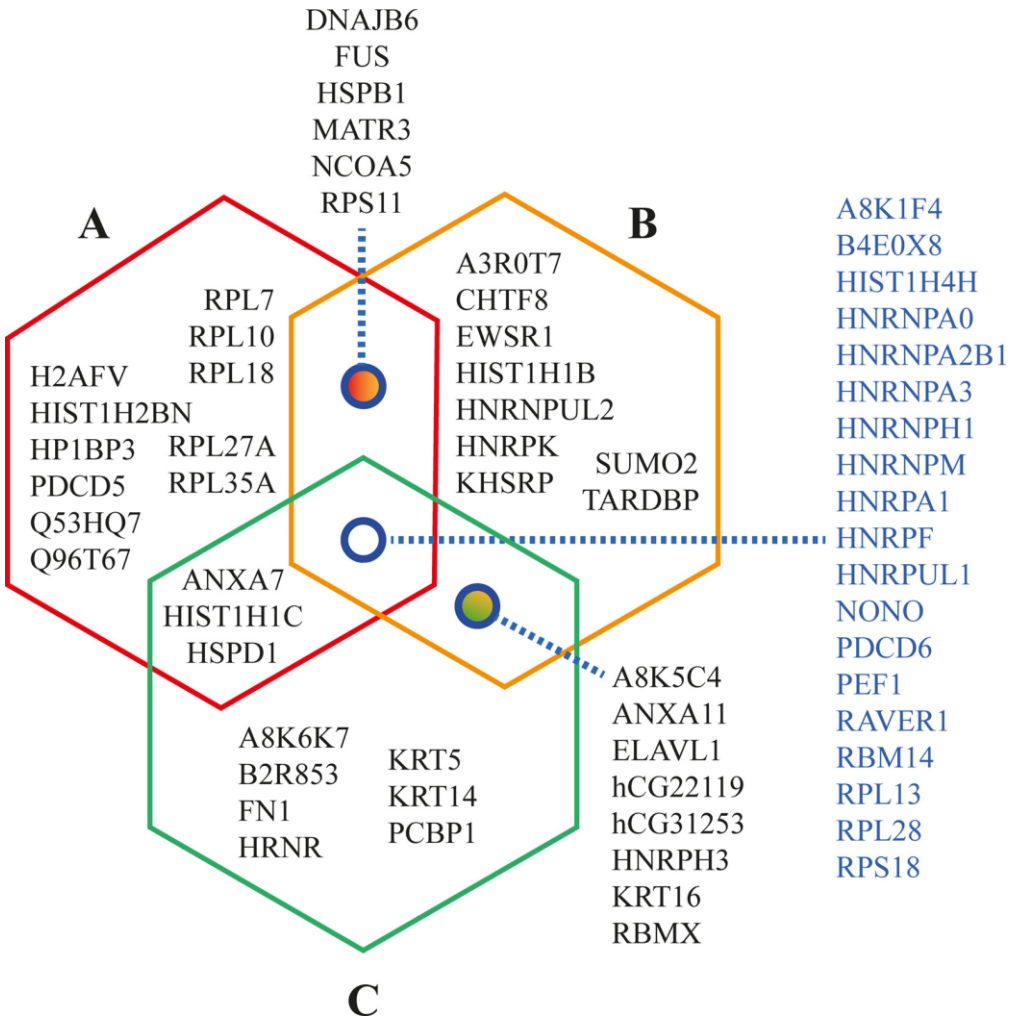

Figure. 7: Reproducible host proteins found in the nuclear capsids.

All cellular proteins identified by mass spectrometry, absent from the mock samples and reproducibly found in the independent replicates are listed. For simplicity and conciseness, the alternative IDs were used when available. Otherwise, the Uniprot accession IDs were used (Refer to Table S3 for details).

II.2.4 Discussion

Strategy. Proteomics is a powerful technique to identify complex protein contents, but sample purity is critical. While it is impossible to rule out contaminants, substantial efforts were made to insure our preparations of nuclear capsids were strongly enriched. This first included the isolation of the nuclear capsids from infected nuclei, rather than purifying the capsids from total cell lysates, to remove as many cytoplasmic and other contaminants as possible. That we primarily detected nuclear proteins is a good indication that this strategy was successful. Second, cross-contamination of the capsids was assessed by electron microscopy, which revealed a greater than 90% purity for A- and B-capsids harvested from the sucrose gradients. Third, given the significant contamination of the gradient purified C- capsids with B-capsids, we resorted to an innovative method to further enrich them using our recently published flow virometry approach (38-40). This yielded C-capsids with a 96% purity level, as measured by electron microscopy. Forth, while no evidence for cellular debris or otherwise large contaminants were noted, electron microscopy cannot of course exclude small impurities. For this reason, uninfected cells were analyzed in parallel by mass spectrometry to reduce the contribution of host proteins that might inadvertently co-fractionate with the viral capsids. We then systematically removed all proteins identified in the mock samples from the corresponding capsid fraction, even though this possibly removed proteins that truly interact with the viral capsids. Finally, we only considered proteins that were detected in all three independent experiments for the greatest stringency. While this overall approach most likely led to false negatives and a protein list that may not be as exhaustive as it could be, it strengthened the quality of our positive hits.

Data reproducibility. While imperfect, most proteins were reproducibly identified in the independent triplicates with rates ranging from 66-77% for viral proteins and 43-52% for host proteins. It should be noted that for host proteins, this lower reproducibly might result from the compounded detection of the proteins in both the viral samples and mock controls, i.e. in more than three samples. Interestingly, many host proteins found in the A-, B- or C-mock fractions proved common to all three samples. This was a bit unexpected since it suggests the proteins interact with large entities that exhibit different densities. Alternatively, it may be that these proteins non-specifically stick to capsid components. Whatever the case, their common detection in the mock samples suggests these are truly negative hits that should be removed from our final lists. Most critically, this demonstrates the importance of analyzing control mock samples when assessing the cellular protein content of viral particles.

Nuclear capsid components. HSV-1 replication results in the production of four types of nuclear capsids that can be distinguished based on their DNA and protein content. In the present study, procapsids were not characterized since thermolabile (13). In contrast, A-, B- and C-capsids were individually probed to better define them molecularly. As expected, they all shared the basic components of the capsid shell, including the major capsid protein pUL19 (VP5), but also pUL18 (VP23), pUL35 (VP26), pUL38 (VP19c) and the pUL6 portal (10). This strongly validated our proteomics approach, even for lower abundance proteins.

Capsid egress from the nucleus. The pUL31/pUL34 NEC complex plays a critical role in the release of newly assembled HSV-1 capsids, in the absence of which the viral particles accumulate in the nucleus (3, 4). pUL34 is a transmembrane protein that recruits pUL31 to the

inner nuclear envelope (3, 45), while pUL31 has additionally been found on nuclear capsids and at DNA damage sites (46, 47). Furthermore, pUL31 has recently been implicated in the packaging of the viral DNA into the capsids (19). It is therefore not surprising to detect pUL31 on all nuclear capsids or pUL47, since an interactor of the NEC and modulator of nuclear viral egress (48). However, the reproducible detection of the normally membrane bound pUL34 was puzzling. This was not overtly due to the contamination of the preparation by nuclear membranes as none of the viral glycoproteins were detected (only rare gB peptides were non reproducibly found – see Table S2). In fact, our protocols minimized the use of detergents and limited them to the very first step where lysis of the cells took place in the presence of NP40 in conditions that do not lyse nuclei. These nuclei were subsequently washed, broken mechanically and the capsids loaded onto sucrose gradients. Despite this, we cannot completely rule out nuclear membrane contaminants. The alternative is that some minor amounts of pUL34 indeed coat the nuclear capsids, presumably by interacting with pUL31. Noteworthy, pUL51, a palmitoylated viral protein that is needed for viral nuclear egress and is found in both the cytoplasm and on membranes (49-52), was also reproducibly detected on all nuclear capsids. Albeit counterintuitive at first, this would not be a first when detecting membrane-associated proteins in soluble fractions. For example, Rab proteins are soluble molecules that are covalently isoprenylated to enable membrane anchoring (53). Nonetheless, the GDP dissociation inhibitor (GDI), a Rab specific protein that binds this isoprenyl tail, masks its hydrophobic properties and can extract Rab proteins from membranes, a central and critical aspect of the normal cycling of this family of proteins (54). Whether pUL34 and/or pUL51 use a similar machinery would be an exciting prospect worth exploring.

It is valuable to note the lack of pUS3 on any of the nuclear capsids. This is not trivial as this viral kinase phosphorylates both NEC members (55, 56), which are present on all nuclear capsid

types. Thus, if pUS3 acts on pUL31 and pUL34 within the nucleus (57, 58) but is absent on the nuclear capsids yet present on perinuclear and mature extracellular virions (30, 59), it must then be recruited to the capsids as they bud through the inner nuclear envelope. We would also expect that the second viral kinase pUL13 should be nearby, since it phosphorylates and activates pUS3 and is also implicated in viral nuclear egress (60, 61).

In addition to the NEC complex, the CVSC is also believed to modulate viral egress from the nucleus by interacting with the viral capsid triplexes in the proximity of the pentons (28, 29). The present study confirms that pUL25 indeed coats A-, B- and C-nuclear capsids. Although care should be taken when comparing total spectra, pUL25 appeared more abundant on C-capsids followed by A- and B-capsids (Table S2), in agreement with others (12). In contrast, only A- and C-capsids harbored pUL17 in the current study, while absent in the B-fraction, unlike previous claims (25, 27, 29). This was surprising given the presence of the other CVSC components and the pUL17 dependent recruitment of pUL25 onto the capsids (29, 62, 63). Whether this is due to impure sample purity in the past, the inability of mass spectrometry to detect pUL17 on B-capsids in the current study or a putatively lower abundance of pUL17 on these capsids needs to be addressed. It may also be a consequence, as previously suggested, of the observation that CVSC components are not as tightly bound to A- or B-capsids (26). Finally, the third member of the CVSC, pUL36, was present on all three capsid types. Given that the spectra covered the entire length of the protein, this would be interpreted as full-length pUL36. This is not inconsistent, however, with the reported presence of the carboxyl terminal portion of pUL36 is the nucleus for PRV (64) as mass spectrometry cannot tell apart a full-length protein from its proteolytic fragments. Overall, it is clear that the CVSC at least partially decorates A-, B- and C-nuclear capsids.

It was originally reported that the NEC may specifically enhance the egress of nuclear C-capsids via pUL25, a model that is incompatible with the presence of both NEC and CVSC components on the three thermostable nuclear capsid types (24-27). The molecular basis of the preferential release of C-capsids from the nucleus consequently remains unclear. From the present study, only pUL42 and pUL46 seem C-capsid specific, but it is unclear how they could direct such egress. However, a plethora of host proteins that interact with these capsids were also detected. It remains to be seen whether one or some of them could contribute to viral egress.

Primary tegumentation and capsid maturation. We previously reported that the primary tegument (i.e. onto nuclear C-capsids) includes pUL36, pUL37, ICP0 and ICP4 (33). The present study corroborated this observation for pUL36. However, pUL36 was also found on A- and B-nuclear capsids, albeit in 35-40% of the amounts seen on C-capsids (Table S2). While this fits its recent identification as a member of the CVSC (12, 28, 29), this was strikingly distinct from our previous report that pUL36 is absent on B-capsids by Western blotting and immuno-EM (33). Similarly, pUL37 was not found in this study, contrary to our previous report that it is detectable on C-capsids (33). While ICP4 reached our stringent thresholds in all A-capsid samples, it was only detected on some of the B- and C-triplicates and ICP0 was only identified in one of the three C-capsid samples. Whether this means that these proteins are absent on the nuclear capsids or that the previously used antibody-mediated detection was better or conversely non-specific remains to be clarified. The true constituents of the primary tegument remain therefore an open question.

The process of tegumentation results from the complex and multiple interactions between capsid, tegument and viral glycoproteins whereby up to 24 different viral proteins coat the capsids (30, 32). Common dogma stipulates that the bulk of this tegument is recruited onto the maturing

capsids while in the cytoplasm and/or during final envelopment. The limited space in perinuclear virions to accommodate the tegument is compatible with this concept (65). However, the present study revealed the detection of numerous tegument proteins common to A-, B- and C-capsids (i.e. pUL21, pUL49, pUL50, pUL51, pUS10) in addition to the aforementioned pUL31, pUL34 and pUL36 proteins. Moreover, viral proteins involved in genome duplication and metabolism such as pUL2, pUL12, pUL39 (ICP6), pUL42 and pUL50 (66-71) were also detected on some or all of the nuclear capsid types (Table S2). This may corroborate past findings that viral DNA replication, cleavage and packaging are intimately linked and required to incorporate the viral genome into the capsids (12), as recently noted for pUL12 (72). Finally, pUL17, pUL42, pUL46, pUL48 and pUS1 were also present on C capsids. Altogether, this amounts to quite a few viral proteins interacting with the nuclear capsids. It should be noted though that, as for pUL31 and pUL34, many of these proteins are shed from the maturing capsids since they are absent in mature extracellular virions (30), as seen in Table 2. All told, this entails a scenario whereby unique proteins may coat nuclear capsids that are released upon their egress across the nuclear envelopes, while others are retained in mature virions. It is worth speculating that the proteins uniquely coating nuclear capsids but absent in mature virions may play a significant role during nuclear egress. At the very least, a complex scenario seems to emerge where multiple proteins may coat the nuclear capsids.

Incorporation of cellular components. Not surprisingly, host proteins were identified in the nuclear capsid fractions, in line with the detection of numerous cellular proteins in several mature extracellular herpes virions (30, 73). It is most interesting that the bulk of these cellular proteins are either nuclear proteins or proteins that transit through the nucleus, based on the analysis of their Go-Terms. While some may merely be contaminants, much effort was done to limit them by

subtracting all the proteins detected in the mock samples. It remains possible, of course, that some proteins stick non-specifically to the viral capsids. This would be surprising given that many of them differentially associated with A-, B- or C-capsids, despite their similar compositions. Furthermore, these proteins were not detected in mature extracellular virions, suggesting they do play a role during viral nuclear egress and later on fall off the capsids. Alternatively, it may be that those proteins are components of higher molecular weight complexes with similar density as the viral capsids. The presence of numerous hnRNPs may be evidence in that direction. Similarly, ribosomal proteins, which can bind rRNA in the nucleus and form the large ribosomal subunit (74), could co-fractionate with the viral capsids. Only functional assays will resolve whether the presence of these numerous cellular proteins is fortuitous or biologically relevant for HSV-1 nuclear egress.

Content of fraction A (%)		
A-capsids	**B-capsids**	**C-capsids**
91.8 ± 0.7	**6.0 ± 1.2**	**2.2 ± 1.9**
(n = 333)	**(n = 23)**	**(n = 6)**
Content of fraction B (%)		
A-capsids	**B-capsids**	**C-capsids**
2.9 ± 1.2	**92.9 ± 1.8**	**4.2 ± 2.1**
(n = 23)	**(n = 717)**	**(n = 32)**
Content of fraction C (%)		
A-capsids	**B-capsids**	**C-capsids**
0.4 ± 0.4	**28.9 ± 3.6**	**70.7 ± 3.6**
(n = 3)	**(n = 223)**	**(n= 503)**

Table. 1: Purity of capsid fractions

Sample purity was assessed by negative staining and EM. The values represent the mean from three independent experiments ± sem. N = Total of capsids counted in the three independent experiments.

Table. 2: Comparison of protein content of C-nuclear capsids and mature extracellular virions.

Protein group	mw (kDa)	C-capsids	Virus*
Capsid-associated			
UL6	74.1	Yes	Yes
UL15	80.9	No	No
UL17	74.6	Yes	Yes
UL18	34.3	Yes	Yes
UL19	149.1	Yes	Yes
UL25	62.7	Yes	Yes
UL26/26.5		Yes**	Yes
UL28	85.6	No	No
UL33	14.4	No	No
UL35	12.1	Yes	Yes
UL38	50.3	Yes	Yes
Envelope			
UL1	24.9	No	Yes
UL10	51.4	No	Yes
UL20	24.2	No	No
UL22	90.4	No	Yes
UL27	100.3	No	Yes
UL43	44.9	No	No
UL44	55.0	No	Yes
UL45	18.2	No	Yes
UL49A	9.2	No	No
UL53	37.6	No	No
UL56	21.2	No	Yes
US4	25.2	No	Yes
US5	9.6	No	No
US6	43.3	No	Yes
US7	41.4	No	Yes
US8	59.1	No	Yes
US8A	16.8	No	No
US9	10.0	No	Yes
Tegument			
RL1	26.2	No	Yes
RL2	78.5	No	Yes
RS1	132.8	No	Yes
UL7	33.1	No	Yes
UL11	10.5	No	Yes

	UL13	57.2	No	Yes
	UL14	23.9	No	Yes
	UL16	40.4	No	Yes
	UL21	57.6	Yes	Yes
	UL23	41.0	No	Yes
	UL36	335.9	Yes	Yes
	UL37	120.6	No	Yes
	UL41	54.9	No	Yes
	UL46	78.2	Yes	Yes
	UL47	73.8	No	Yes
	UL48	54.3	Yes	Yes
	UL49	32.3	Yes	Yes
	UL50	39.1	Yes	Yes
	UL51	25.5	Yes	Yes
	UL55	20.5	No	Yes
	US2	32.5	No	Yes
	US3	52.8	No	Yes
	US10	34.1	Yes	Yes
	US11	17.8	No	No
Other				
	UL2	36.3	Yes	No
	UL3	25.6	Yes	No
	UL4	78.2	No	No
	UL5	98.7	No	No
	UL8	79.9	No	No
	UL9	94.3	No	No
	UL12	67.5	No	No
	UL24	29.5	No	No
	UL29	128.4	No	No
	UL30	136.4	No	No
	UL31	34.0	Yes	No
	UL32	64.0	No	No
	UL34	29.8	Yes	No
	UL39	124.1	Yes	No
	UL40	38.0	No	No
	UL42	51.2	Yes	No
	UL52	114.4	No	No
	UL54	55.3	No	No
	US1	46.5	Yes	No
	US12	9.8	No	No

* From *Loret et al* (30). **Cannot tell apart or from cleaved products. In blue: Common to C-capsids and mature virions;

In red: Unique to C-capsids; In green: Unique to mature virions.

II.2.5 Materials and Methods

Cells and virus. Hela cells (ATCC CCL-2) were cultured at 37°C in the presence of 5% CO2 in Dulbecco's modified Eagle's medium (Sigma-Aldrich) containing 10% fetal bovine serum (FBS; HyClone®), 2 mM L-glutamine (Life Technologies), 100 U/ml penicillin and 100 µg/ml streptomycin. The HSV-1 parental wild-type strain 17+, which Beate Sodeik generously provided (Hannover Medical School, Germany), was amplified and titered by plaque assay on BHK and Vero cells, respectively, as before (75).

Purification of nuclear capsids.

Hela cells passaged one day earlier were grown on 500 cm2 dishes until subconfluent. They were subsequently infected with HSV-1 wild-type virus at a multiplicity of infection (MOI) of 5. Eighteen hours post infection (hpi), capsids were purified as previously described (33) with some minor modifications. Briefly, infected cells were scraped from dishes and washed with phosphate-buffered saline (PBS) then resuspended at a concentration of 1 × 107 cells/ml. They were then incubated for 30 min on ice in NP-40 lysis buffer (150 mM NaCl, 10 mM Tris-HCl, pH 7.5, 2 mM MgCl2, 1% Igepal, 5 mM dithiothreitol). Cell lysates were spun at 225 × *g* for 10 min and the nuclei resuspended in modified (low-salt) TNE (20 mM Tris, pH 7.5, 150 mM NaCl, 1 mM EDTA), cracked by 3 cycles of freeze-thaw in liquid nitrogen and a 37°C bath, treated for 1 hour at 10°C with 500 U/mL of DNAse I (Roche) and sonicated with 10 x 1 sec pulses at intensity of 8 in a Microcup-horn sonicator at 4°C. The resulting nuclear lysates were cleared at 2500 × *g* for 10 min, and nuclear capsids were recovered using a 35% sucrose cushion. A-, B- and C-capsids were finally

separated on a 20-50% linear sucrose gradient prepared in low-salt TNE at 100,000 × *g* for 1 h. The three nuclear capsid fractions were individually collected, pelleted at 100,000 × *g* and stored at −80°C. Parallel gradients were prepared from non-infected cells using the same number of starting cells and samples collected at exactly the same locations as the corresponding A-, B- and C-bands.

Gel electrophoresis and silver staining. Three micrograms of each capsid fraction were boiled for 10 min in loading buffer (50 mM Tris-HCl pH 6.8, 2% SDS, 0.1% bromophenol blue, 10% glycerol, and 2% β-mercaptoethanol) and separated by SDS-PAGE. For the mock controls, equal volumes as the corresponding viral fractions were used to prevent the artificial boosting of the total protein content of these samples. Following electrophoresis, gels were fixed overnight (5% acetic acid-50% methanol solution), washed for 10 min (50% methanol solution) then extensively rinsed in Milli-Q water. To stain the proteins, the gels were incubated with a 0.02% thiosulfate sodium solution, in 0.1% silver nitrate and in a reaction buffer (0.04% formaldehyde and 2% carbonate sodium) with rinsing with water between each step. The gels were finally incubated in 5% acetic acid solution to stop the reaction then scanned on a ChemiDoc station (BioRad).

Syto 13 fluorescence labeling of C-capsids. Ten microliters of sucrose-purified capsids were incubated for 1 h at 4°C with 1 μM Syto 13 (green fluorescence). Unwashed labeled virions were directly analyzed by flow cytometry as described below.

Flow virometry. Analysis of the samples by flow cytometry was performed as previously described (38-40) using Syto 13 labeled capsids diluted 500 fold in 0.2 µm filtered MNT. The samples were processed on a standard FACSAria II sorter (BD Biosciences) equipped with a 100 µm nozzle and 405, 488, and 633 nm lasers. Analysis and sorting were performed in PBS at low pressure (23 psi) and a flow rate between 1 and 3 for a maximum of 3000 events/s. Samples were excited with a 488 nm laser coupled to an emission filter allowing the 515-545 nm wavelengths to go through. A minimal threshold of 200 for the SSC channel was applied to minimize the background signal. One hundred thousand particles were analyzed in the fluorescence channel, gating on Syto 13 labeled capsids, using a gate that includes the bulk of the particles (> 95 %) but which excluded large aggregates. A yield mask of 32 was applied upon sorting to increase purity. The data were acquired with FACSDiva software (version 6.1.3, BD Biosciences) and processed with FlowJo version 10.0.7r2 (TreeStar). Sorted C-capsids were concentrated by ultracentrifugation at 100,000 × *g* for 1 hour, and stored at −80°C.

Mass spectrometry. Seven micrograms of each viral sample (or equivalent volumes of the corresponding mock samples) were diluted with 100 mM ammonium bicarbonate and 5 mM TCEP then vortexed at 37°C for 30 min. Chloroacetamide (110 mM in ammonium bicarbonate) was added to the samples to get a final concentration of 55 mM, and vigorously mixed again for another 30 min at 37°C. The samples were then digested overnight with trypsin with an enzyme to protein ratio of 1/50. Samples were then dried down in a Speed-Vac and reconstituted in 40 µl of 0.2% formic acid. The tryptic peptides were loaded on a C18 stem trap from New Objective and separated on a home-made C18 column (15 cm * 150 um id) at a flow rate of 600 nl/min with a gradient of 5-30% of A (0.2% formic acid in water and B (0.2% formic acid in acetonitrile). The analytical

column was coupled to a Q-Exactive Plus (Thermo Fisher Scientific). The resolution was set at 70000 for the survey scan and 17500 for the tandem mass spectrum acquisition. A maximum of 12 precursors were sequenced for each duty cycle. AGC target values for MS and MS/MS scans were set to 3e6 (max fill time 50 ms) and 2e4 (max fill time 150 ms), respectively. The precursor isolation window was set to m/z 1.6 with a high energy dissociation normalized collision energy of 25 and the dynamic exclusion window was set to 30 s. Tandem mass spectra were searched against the combined human and HSV1 17+ Uniprot databases with carbamidomethylation (C) as fixed modifications, deamidation (NQ) oxidation (M) and acetylation (N-ter) as variable modifications. Tolerance was set at 10 ppm on precursor mass and 0.01 Da on the fragments.

Electron Microscopy. The purity of the capsids was analyzed by negative staining as previously described (30). Briefly, 10 µL of purified A, B and C capsids or flow cytometry sorted and concentrated C capsids were adsorbed on hexagonal 200-mesh copper grids coated with Formvar and carbon (Canemco & Marivac). Excess liquid was removed with a filter paper then samples were contrasted with 2% uranyl acetate (Canemco & Marivac), washed in distilled water, and dried on filter paper. Samples were examined on a Philips CM100 transmission electron microscope and digital micrographs were captured using an AMT XR80 CCD digital camera. Quantification of the types of nuclear capsids (A, B or C) was done from randomly selected fields from at least three independent experiments.

II.2.6 Acknowledgements

We are indebted to Gael Dulude and Annie Gosselin of the nearby IRIC research center for their invaluable help with flow virometry and to Dr. Beate Sodeik for providing wild-type virus. We

also wish to thank Diane Gingras for expertise, advice and support in electron microscopy. We are also grateful to Dr Richard Roller (University of Iowa Health Care) and Dr Fred Homa (University of Pittsburgh) for insightful comments and suggestions. The present study was funded by the Canadian Institutes of Health Research (MOP 82921) and Canadian Foundation for Innovation (FCI #6908) to RL. Proteomics analyses were performed by the Center for Advanced Proteomics Analyses, a Node of the Canadian Genomic Innovation Network that is supported by the Canadian Government through Genome Canada.

Table S 1: Cellular contaminants.

								Exp 1				Exp 2				Exp 3	
Uniprot	**Alternate ID**	**mw (kDa)**	***Total spectra***	**Mock A**	**Mock B**	**Mock C**	**A-capsids**	**B-capsids**	**C-capsids**	**A-capsids**	**B-capsids**	**C-capsids**	**A-capsids**	**B-capsids**	**C-capsids**
A0A0B4J2A4_HUMAN	ACAA2	42 kDa	A0A0B4J2A4_HUMAN	1	3	3	0	0	0	0	0	0	0	0	0
ACTG_HUMAN	ACTG1	42 kDa	ACTG_HUMAN	6	4	3	10	8	8	8	5	7	2	2	10
ALBU_HUMAN	ALB	69 kDa	ALBU_HUMAN	8	10	4	0	0	4	0	0	3	0	0	5
ANXA1_HUMAN	ANXA1	39 kDa	ANXA1_HUMAN	6	3	4	0	0	0	0	0	0	0	0	0
A0A024R5Z7_HUMAN	ANXA2	39 kDa	A0A024R5Z7_HUMAN	3	2	2	0	0	0	0	0	0	0	0	0
ANXA4_HUMAN	ANXA4	36 kDa	ANXA4_HUMAN	3	7	3	0	0	0	0	0	0	0	0	0
ANXA5_HUMAN	ANXA5	36 kDa	ANXA5_HUMAN	2	1	0	0	0	0	0	0	0	0	0	0
ANXA7_HUMAN	ANXA7	53 kDa	ANXA7_HUMAN	1	2	0	5	5	9	6	5	7	5	7	8
AT1A1_HUMAN	ATP1A1	113 kDa	AT1A1_HUMAN	14	10	7	0	0	0	0	0	0	0	0	0
A0A0S2Z3L2_HUMAN	ATP2A2	115 kDa	A0A0S2Z3L2_HUMAN	3	4	3	0	0	0	0	0	0	0	0	0
ATPA_HUMAN	ATP5A1	60 kDa	ATPA_HUMAN	30	33	27	0	0	0	0	0	0	0	0	0
ATPB_HUMAN	ATP5B	57 kDa	ATPB_HUMAN	24	21	14	1	0	0	0	0	0	0	0	0
BAP31_HUMAN	BCAP31	28 kDa	BAP31_HUMAN	4	3	2	0	0	0	0	0	0	0	0	0
CALR_HUMAN	CALR	48 kDa	CALR_HUMAN	1	1	3	0	0	0	0	0	0	0	0	0
A0A024RBH2_HUMAN	CKAP4	66 kDa	A0A024RBH2_HUMAN	5	4	1	0	0	0	0	0	0	0	0	0
A0A024R2W4_HUMAN	DAG1	98 kDa	A0A024R2W4_HUMAN	11	10	8	0	0	0	0	0	0	0	0	0
A0A024RAD5_HUMAN	DDOST	51 kDa	A0A024RAD5_HUMAN	6	5	4	0	0	0	0	0	0	0	0	0
A0A024R9D7_HUMAN	DECR1	36 kDa	A0A024R9D7_HUMAN	5	3	3	0	0	0	0	0	0	0	0	0
A0A024R713_HUMAN	DLD	54 kDa	A0A024R713_HUMAN	2	0	0	0	0	0	0	0	0	0	0	0
ECH1_HUMAN	ECH1	36 kDa	ECH1_HUMAN	3	2	1	0	0	0	0	0	0	0	0	0
ECHM_HUMAN	ECHS1	31 kDa	ECHM_HUMAN	5	5	8	0	0	0	0	0	0	0	0	0
A0A024R4F1_HUMAN	ENO1	47 kDa	A0A024R4F1_HUMAN	23	23	16	0	1	0	0	0	0	0	0	0
ERP29_HUMAN	ERP29	29 kDa	ERP29_HUMAN	10	9	11	0	0	0	0	0	0	0	0	0
A0A090N8Y2_HUMAN	ERP70	73 kDa	A0A090N8Y2_HUMAN	16	11	13	0	0	0	0	0	0	0	0	0
A0A0S2Z4C3_HUMAN	FH	55 kDa	A0A0S2Z4C3_HUMAN	5	6	3	0	0	0	0	0	0	0	0	0
A0A024R6W0_HUMAN	GOT2	47 kDa	A0A024R6W0_HUMAN	4	3	1	0	0	0	0	0	0	0	0	0
A0A0K2BMD8_HUMAN	HBA2	15 kDa	A0A0K2BMD8_HUMAN	90	33	18	1	1	2	0	0	2	0	2	3
D9YZU5_HUMAN	HBB	16 kDa	D9YZU5_HUMAN	19	21	15	0	0	0	0	0	0	0	1	0
A0A024R1F4_HUMAN	hCG_2010666	61 kDa	A0A024R1F4_HUMAN	18	12	9	0	0	0	0	0	0	0	0	0
A0A0K0K1L1_HUMAN	HEL-S-282	29 kDa	A0A0K0K1L1_HUMAN	7	2	1	0	0	0	0	0	0	0	0	0
A0A0K0K1H8_HUMAN	HEL-S-71p	77 kDa	A0A0K0K1H8_HUMAN	13	5	3	0	0	1	0	0	0	0	0	1
A0A024R017_HUMAN	HIST1H2AC	14 kDa	A0A024R017_HUMAN	0	1	1	4	0	2	2	1	2	1	0	0
A0A024RD80_HUMAN	HSP90AB1	83 kDa	A0A024RD80_HUMAN	4	5	6	0	0	0	0	0	0	0	2	5
ENPL_HUMAN	HSP90B1	92 kDa	ENPL_HUMAN	49	54	42	1	0	0	1	0	0	1	0	0
GRP78_HUMAN	HSPA5	72 kDa	GRP78_HUMAN	23	20	17	1	0	0	1	0	0	0	0	0
CH10_HUMAN	HSPE1	11 kDa	CH10_HUMAN	3	2	0	0	0	0	0	0	0	0	0	0
E7EMF1_HUMAN	ITGA2	89 kDa	E7EMF1_HUMAN	12	12	8	0	0	0	0	0	0	0	0	0
A5YM53_HUMAN	ITGAV	116 kDa	A5YM53_HUMAN	13	9	10	0	0	0	0	0	0	0	0	0
ITB1_HUMAN	ITGB1	88 kDa	ITB1_HUMAN	17	20	22	0	0	0	0	0	0	0	0	0
ITB5_HUMAN	ITGB5	88 kDa	ITB5_HUMAN	14	16	15	0	0	0	0	0	0	0	0	0
H6VRF8_HUMAN	KRT1	66 kDa	H6VRF8_HUMAN	14	46	29	42	20	58	19	36	62	27	16	49
K1C10_HUMAN	KRT10	59 kDa	K1C10_HUMAN	10	11	15	18	9	28	5	13	21	13	6	30
K22E_HUMAN	KRT2	65 kDa	K22E_HUMAN	0	4	9	19	8	29	1	9	23	6	2	32
K1C9_HUMAN	KRT9	62 kDa	K1C9_HUMAN	11	34	15	28	17	38	11	22	44	22	10	38
LEG1_HUMAN	LGALS1	15 kDa	LEG1_HUMAN	4	3	1	0	0	0	0	0	0	0	0	0
A6XGP7_HUMAN	NOGOC	22 kDa	A6XGP7_HUMAN	30	31	30	0	0	0	0	0	0	0	0	0
A0A024R8S5_HUMAN	P4HB	57 kDa	A0A024R8S5_HUMAN	6	5	3	0	0	1	0	0	0	0	0	0
A0A1B0GU58_HUMAN	PCCA	67 kDa	A0A1B0GU58_HUMAN	4	3	1	0	0	0	0	0	0	0	0	0
PDIA6_HUMAN	PDIA6	48 kDa	PDIA6_HUMAN	10	6	4	1	0	0	0	0	0	0	0	0
A8K401_HUMAN	PHB	30 kDa	A8K401_HUMAN	2	3	3	0	0	0	0	0	0	0	0	0

B4DNK4_HUMAN	PKM	50 kDa		B4DNK4_HUMAN	9	3	3		0	0	0		0	0	0		0	0	0
A0PK02_HUMAN	PLXNB2	56 kDa		A0PK02_HUMAN	12	9	9		0	0	0		0	0	0		0	0	0
A8K3B4_HUMAN	POR	77 kDa		A8K3B4_HUMAN	1	9	8		0	0	0		0	0	0		0	0	0
A1A508_HUMAN	PRSS3	26 kDa		A1A508_HUMAN	4	6	2		0	1	1		0	0	1		0	0	1
PTK7_HUMAN	PTK7	118 kDa		PTK7_HUMAN	9	5	4		0	0	0		0	0	0		0	0	0
A0A024R1U4_HUMAN	RAB5C	23 kDa		A0A024R1U4_HUMAN	3	2	4		0	0	0		0	0	0		0	0	0
A0A024RBE8_HUMAN	SLC25A3	40 kDa		A0A024RBE8_HUMAN	2	1	0		0	0	0		0	0	0		0	0	0
ADT2_HUMAN	SLC25A5	33 kDa		ADT2_HUMAN	6	6	3		1	0	1		0	0	0		0	0	0
S26A2_HUMAN	SLC26A2	82 kDa		S26A2_HUMAN	2	2	4		0	0	0		0	0	0		0	0	0
4F2_HUMAN	SLC3A2	68 kDa		4F2_HUMAN	3	4	1		0	0	0		0	0	0		0	0	0
B3A2_HUMAN	SLC4A2	137 kDa		B3A2_HUMAN	2	1	0		0	0	0		0	0	0		0	0	0
SMC5_HUMAN	SMC5	129 kDa		SMC5_HUMAN	0	2	1		0	0	0		0	0	0		0	0	0
C9JMN1_HUMAN	SMC6	85 kDa		C9JMN1_HUMAN	2	3	2		0	0	0		0	0	0		0	0	0
A0A024R229_HUMAN	TMEM2	154 kDa		A0A024R229_HUMAN	1	4	2		0	0	0		0	0	0		0	0	0
TBA1A_HUMAN	TUBA1A	50 kDa		TBA1A_HUMAN	15	11	8		1	1	1		3	0	0		2	0	0
L8B4J3_HUMAN	UbC	77 kDa		L8B4J3_HUMAN	6	4	2		0	1	1		0	0	0		2	2	1
H3BRG4_HUMAN	UQCRC2	45 kDa		H3BRG4_HUMAN	5	1	3		0	0	0		0	0	0		0	0	0
A0A024QZN9_HUMAN	VDAC2	34 kDa		A0A024QZN9_HUMAN	7	7	8		0	0	0		0	0	0		0	0	0
B0YJC4_HUMAN	VIM	50 kDa		B0YJC4_HUMAN	5	4	4		1	1	1		1	0	1		0	0	1
A0A140VJM0_HUMAN		117 kDa		A0A140VJM0_HUMAN	38	38	32		0	0	0		0	0	0		0	0	0
A8K309_HUMAN		39 kDa		A8K309_HUMAN	13	13	8		0	0	0		0	0	0		0	0	0
A8K486_HUMAN		18 kDa		A8K486_HUMAN	1	0	0		1	0	2		3	0	1		3	0	1
A8K4W2_HUMAN		29 kDa		A8K4W2_HUMAN	1	2	3		0	0	0		0	0	0		0	0	0
A8K6Q8_HUMAN		85 kDa		A8K6Q8_HUMAN	19	12	7		0	0	0		0	0	0		0	0	0
B2RE46_HUMAN		69 kDa		B2RE46_HUMAN	2	2	1		0	0	0		0	0	0		0	0	0
B3KQT9_HUMAN		54 kDa		B3KQT9_HUMAN	21	23	17		0	0	0		0	0	0		0	0	0
B3KRN4_HUMAN		48 kDa		B3KRN4_HUMAN	11	13	8		0	0	0		0	0	0		0	0	0
B3KTS5_HUMAN		31 kDa		B3KTS5_HUMAN	19	22	16		0	0	0		0	0	0		0	0	0
B4DJ30_HUMAN		113 kDa		B4DJ30_HUMAN	0	2	1		0	0	0		0	0	0		0	0	0
B4DL99_HUMAN		66 kDa		B4DL99_HUMAN	6	5	9		0	0	0		0	0	0		0	0	0
B4DMF5_HUMAN		57 kDa		B4DMF5_HUMAN	3	2	2		0	0	0		0	0	0		0	0	0
B4DTY9_HUMAN		84 kDa		B4DTY9_HUMAN	15	9	1		0	0	0		0	0	0		0	0	0
B4DUL5_HUMAN		40 kDa		B4DUL5_HUMAN	12	10	10		0	0	0		0	0	0		0	0	0
B4DW05_HUMAN		24 kDa		B4DW05_HUMAN	4	2	1		0	0	0		0	0	0		0	0	0
In blue: Proteins present in some of the viral caps																			

Table S 2: Viral proteins found with HSV-1 nuclear capsids.

Uniprot	Description	mw (kDa)	A-capsids		B-capsids		C-capsids	
			Average	SEM	Average	SEM	Average	SEM
Capsid								
B9VQD3_HHV11	UL6 (Portal protein)	74	61,0	11,2	40,7	5,7	72,7	7,1
G8H8D9_HHV1	UL18 (VP23; Triplex capsid protein 2)	34	68,7	9,2	31,3	9,2	52,7	6,4
G8HBD2_HHV1	UL19 (VP5 Major capsid protein)	149	377,0	43,7	278,3	13,6	393,3	35,0
A0A181ZHX9_HHV11	UL35 (VP26; SCP; Small capsomere-interacting protein)	12	110,0	18,0	81,7	5,5	98,7	11,6
B9VQG6_HHV11	UL38 (VP19C; Triplex capsid protein 1)	50	169,7	5,8	150,7	11,7	190,0	21,7
CVSC								
A0A0X8E9Y0_HHV1	UL17 (Capsid vertex component 1)	75	58,3	27,0	19,7	16,8	68,7	3,5
B9VQF2_HHV11	UL25 (Capsid vertex component 2)	63	70,0	3,1	50,0	9,2	102,0	0,6
LTP_HHV1	UL36 (Large tegument protein deneddylase)	333	6,7	1,2	7,7	0,9	19,0	1,2
Terminase complex								
A0A193GSF3_HHV1	UL15 (Tripartite terminase subunit 3)	81	6,3	0,9	2,7	1,2	1,3	0,7
A0A0S1TJ41_HHV1	UL28 (Tripartite terminase subunit 1)	86	6,7	2,9	5,7	1,7	0,3	0,3
B9VQG1_HHV11	UL33	15	1,3	0,9	0,0	0,0	0,0	0,0
PRA/Scaffold*								
G8HBD9_HHV1	UL26 (Protease)	66	170,3	36,9	203,7	37,4	165,0	87,9
A0A0B5E5D4_HHV1	UL26.5 (Scaffold)	34	1,0	1,0	11,7	9,7	4,7	0,7
	Combined Protease/Scaffold		*171,3*	*36,7*	*215,3*	*27,8*	*169,7*	*87,3*
NEC								
A0A181ZGN3_HHV11	UL31 (Nuclear egress protein 1)	34	5,3	1,9	5,3	2,8	2,3	0,3
A0A0F7GQM8_HHV1	UL34 (Nuclear egress protein 2)	30	6,3	0,9	3,3	0,9	6,3	0,3
Replication / DNA metabolism								
G8HBB5_HHV1	UL2 (Uracil-DNA glycosylase)	36	6,3	0,7	7,7	1,2	5,3	0,3
A0A0S1TJ35_HHV1	UL5 (DNA replication helicase)	99	0,7	0,3	0,7	0,3	0,0	0,0
A0A181ZGG2_HHV11	UL12 (Alkaline nuclease)	67	11,7	1,8	15,0	3,1	4,3	4,3
A0A0S1TES2_HHV1	UL29 (major DNA binding protein)	128	0,0	0,0	0,0	0,0	0,7	0,7
A0A0S1TEL8_HHV1	UL39 (Ribonucleoside-diphosphate reductase large subunit)	124	14,0	2,6	4,3	0,9	6,0	1,5
G8HBF6_HHV1	UL42 (DNA polymerase processivity subunit)	51	9,3	4,8	6,3	2,7	7,3	1,2
DUT_HHV11	UL50 (Deoxyuridine 5'-triphosphate nucleotidohydrolase)	39	4,3	0,9	6,0	1,0	6,3	0,3
Tegument								
A0A0S1TJG0_HHV1	RL2 (ICP0)	79	0,0	0,0	0,0	0,0	1,3	0,3
A0A0B5E5S4_HHV1	RS1 (ICP4)	133	8,3	1,9	3,0	2,5	2,3	0,9
A0A0S1TJL6_HHV1	UL3 (Nuclear protein)	24	9,0	2,0	8,7	1,7	6,7	0,3
A0A181ZH20_HHV11	UL14	24	1,3	1,3	9,3	9,3	5,0	2,5
A0A0B5E481_HHV1	UL21	58	6,7	0,7	7,3	0,9	6,7	0,3
LTP_HHV1	UL36 (Large tegument protein deneddylase)	333	6,7	1,2	7,7	0,9	19,0	1,2
A0A0S1TER6_HHV1	UL37	121	0,0	0,0	0,7	0,7	0,3	0,3
A0A181ZH33_HHV11	UL41 (VHS)	55	1,3	0,9	0,0	0,0	0,0	0,0
G8HBG0_HHV1	UL46 (VP11/12 Tegument protein)	78	3,3	1,8	0,0	0,0	3,0	0,6
A0A181ZGV0_HHV11	UL47 (Tegument protein)	74	38,0	5,5	13,7	8,8	10,7	6,4
G8HBG2_HHV1	UL48 (VP16 Transactivating tegument protein)	54	4,3	0,3	4,0	2,3	5,3	0,9
A0A181ZGW0_HHV11	UL49 (VP22 Tegument protein)	32	3,0	0,6	7,0	0,6	10,3	1,2
DUT_HHV11	UL50 (Deoxyuridine 5'-triphosphate nucleotidohydrolase)	39	4,3	0,9	6,0	1,0	6,3	0,3
A0A181ZG15_HHV11	UL51 (Tegument protein)	25	13,0	2,5	18,0	1,2	14,7	0,9
G8HBG9_HHV1	UL54 (Multifunctional expression regulator)	55	1,3	0,3	3,0	1,0	2,3	0,9
A0A181ZFX4_HHV11	US1 (ICP22 transcriptional regulator)	47	6,3	2,4	1,7	0,3	2,7	0,3
A0A0B5E9X1_HHV1	US10	33	5,0	1,5	7,7	0,9	3,3	0,3
A0A0B5EA79_HHV1	US11	17	0,3	0,3	1,7	1,2	0,0	0,0
Others								
A0A181ZH10_HHV11	UL27 (gB)	100	2,0	0,6	0,0	0,0	1,3	0,3
* As originally assigned by Mascot								

	Exp 1			Exp 2			Exp 3		
Total spectra assigned	**A-capsids**	**B-capsids**	**C-capsids**	**A-capsids**	**B-capsids**	**C-capsids**	**A-capsids**	**B-capsids**	**C-capsids**
B9VQD3_HHV11	54	35	70	83	52	86	46	35	62
G8H8D9_HHV1	87	15	63	59	32	54	60	47	41
G8HBD2_HHV1	444	260	461	392	270	344	295	305	375
A0A181ZHX9_HHV11	117	71	119	137	89	98	76	85	79
B9VQG6_HHV11	159	141	223	179	137	149	171	174	198
A0A0X8E9Y0_HHV1	96	6	74	6	0	70	73	53	62
B9VQF2_HHV11	68	38	102	76	68	101	66	44	103
G8HBF0_HHV1	6	9	17	9	6	21	5	8	19
A0A193GSF3_HHV1	5	1	2	8	5	0	6	2	2
A0A0S1TJ41_HHV1	2	4	0	12	9	0	6	4	1
B9VQG1_HHV11	3	0	0	1	0	0	0	0	0
G8HBD9_HHV1	150	129	0	242	245	300	119	237	195
A0A0B5E5D4_HHV1	3	31	6	0	2	4	0	2	4
	153	*160*	*6*	*242*	*247*	*304*	*119*	*239*	*199*
A0A181ZGN3_HHV11	9	11	3	4	3	2	3	2	2
A0A0F7GQM8_HHV1	6	5	6	8	3	6	5	2	7
G8HBB5_HHV1	7	6	5	7	10	5	5	7	6
A0A0S1TJ35_HHV1	0	0	0	1	1	0	1	1	0
A0A181ZGG2_HHV11	11	21	0	15	11	0	9	13	13
A0A0S1TES2_HHV1	0	0	0	0	0	0	0	0	2
A0A0S1TEL8_HHV1	15	6	4	18	4	5	9	3	9
G8HBF6_HHV1	0	1	9	16	9	8	12	9	5
DUT_HHV11	4	7	6	6	7	7	3	4	6
A0A0S1TJG0_HHV1	0	0	2	0	0	1	0	0	1
A0A0B5E5S4_HHV1	6	8	2	12	0	1	7	1	4
A0A0S1TJL6_HHV1	7	7	7	13	12	6	7	7	7
A0A181ZH20_HHV11	0	28	8	0	0	7	4	0	0
A0A0B5E481_HHV1	6	6	7	8	9	7	6	7	6
G8HBF0_HHV1	6	9	17	9	6	21	5	8	19
A0A0S1TER6_HHV1	0	2	0	0	0	0	0	0	1
A0A181ZH33_HHV11	1	0	0	3	0	0	0	0	0
G8HBG0_HHV1	0	0	2	6	0	4	4	0	3
A0A181ZGV0_HHV11	39	30	0	47	0	22	28	11	10
G8HBG2_HHV1	5	8	5	4	4	4	4	0	7
A0A181ZGW0_HHV11	2	8	8	4	6	11	3	7	12
DUT_HHV11	4	7	6	6	7	7	3	4	6
A0A181ZG15_HHV11	11	20	16	18	18	15	10	16	13
G8HBG9_HHV1	1	4	1	2	4	2	1	1	4
A0A181ZFX4_HHV11	5	2	3	11	1	3	3	2	2
A0A0B5E9X1_HHV1	2	9	3	7	8	3	6	6	4
A0A0B5EA79_HHV1	0	0	0	1	4	0	0	1	0
A0A181ZH10_HHV11	2	0	1	3	0	1	1	0	2

	Exp 1			Exp 2			Exp 3		
Percent coverage of the protein	**A-capsids**	**B-capsids**	**C-capsids**	**A-capsids**	**B-capsids**	**C-capsids**	**A-capsids**	**B-capsids**	**C-capsids**
B9VQD3_HHV11	35,2%	21,3%	33,6%	40,4%	31,8%	43,5%	24,4%	19,4%	27,1%
G8H8D9_HHV1	62,9%	0,0%	51,3%	52,8%	59,4%	62,6%	60,7%	38,7%	37,1%
G8HBD2_HHV1	48,3%	40,8%	52,8%	48,4%	43,1%	52,0%	51,2%	41,9%	44,6%
A0A181ZHX9_HHV11	80,4%	83,9%	85,7%	84,8%	84,8%	85,7%	82,1%	79,5%	84,8%
B9VQG6_HHV11	50,3%	45,4%	53,8%	52,0%	46,2%	52,3%	51,2%	54,6%	55,5%
A0A0X8E9Y0_HHV1	39,3%	0,0%	45,0%	0,0%	0,0%	34,7%	33,0%	23,6%	42,1%
B9VQF2_HHV11	38,8%	28,3%	45,7%	37,6%	41,0%	51,7%	45,2%	31,4%	35,9%
G8HBF0_HHV1	1,5%	2,0%	2,5%	2,2%	0,8%	3,4%	0,9%	0,6%	3,6%
A0A193GSF3_HHV1	6,0%	1,6%	3,1%	11,4%	6,7%	0,0%	8,3%	3,7%	3,1%
A0A0S1TJ41_HHV1	1,4%	5,5%	0,0%	6,9%	10,4%	0,0%	9,8%	6,5%	2,3%
B9VQG1_HHV11	16,9%	0,0%	0,0%	7,7%	0,0%	0,0%	0,0%	0,0%	0,0%
G8HBD9_HHV1	62,7%	60,2%	0,0%	58,9%	73,9%	63,6%	60,3%	67,7%	59,2%
A0A0B5E5D4_HHV1	57,1%	61,1%	4,3%	0.0	60,8%	45,0%	0.0	55,9%	40,4%
A0A181ZGN3_HHV11	12,7%	12,7%	6,5%	6,5%	6,5%	3,9%	9,2%	3,9%	6,5%
A0A0F7GQM8_HHV1	18,2%	12,4%	12,4%	12,4%	6,2%	12,4%	12,4%	6,2%	12,4%
G8HBB5_HHV1	8,1%	5,7%	5,7%	5,7%	8,4%	5,7%	8,4%	8,4%	5,7%
A0A0S1TJ35_HHV1	0,0%	0,0%	0,0%	0,9%	1,3%	0,0%	1,3%	1,3%	0,0%
A0A181ZGG2_HHV11	13,7%	22,4%	0,0%	15,7%	14,5%	0,0%	8,8%	13,1%	15,2%
A0A0S1TES2_HHV1	0,0%	0,0%	0,0%	0,0%	0,0%	0,0%	0,0%	0,0%	1,7%
A0A0S1TEL8_HHV1	9,0%	4,3%	4,1%	12,0%	4,1%	5,5%	4,4%	3,0%	7,4%
G8HBF6_HHV1	0,0%	0,0%	5,1%	15,0%	15,2%	9,8%	14,3%	8,6%	5,1%
DUT_HHV11	8,6%	19,1%	15,4%	15,4%	19,1%	15,4%	12,1%	11,3%	15,4%
A0A0S1TJG0_HHV1	0,0%	0,0%	4,0%	0,0%	0,0%	2,8%	0,0%	0,0%	2,8%
A0A0B5E5S4_HHV1	3,7%	5,5%	0,0%	5,4%	0,0%	0,9%	4,9%	0,7%	0,0%
A0A0S1TJL6_HHV1	17,4%	21,4%	17,0%	25,4%	26,3%	12,1%	17,4%	22,3%	12,1%
A0A181ZH20_HHV11	0,0%	41,1%	18,3%	0,0%	0,0%	22,4%	18,3%	0,0%	0,0%
A0A0B5E481_HHV1	12,7%	8,0%	6,4%	11,6%	8,6%	8,4%	9,5%	8,0%	6,4%
G8HBF0_HHV1	1,5%	2,0%	2,5%	2,2%	0,8%	3,4%	0,9%	0,6%	3,6%
A0A0S1TER6_HHV1	0,0%	2,0%	0,0%	0,0%	0,0%	0,0%	0,0%	0,0%	1,0%
A0A181ZH33_HHV11	2,0%	0,0%	0,0%	8,2%	0,0%	0,0%	0,0%	0,0%	0,0%
G8HBG0_HHV1	1,1%	0,0%	2,4%	6,7%	0,0%	2,8%	5,7%	0,0%	2,8%
A0A181ZGV0_HHV11	28,0%	16,6%	0,0%	35,4%	0,0%	18,8%	24,1%	12,4%	10,2%
G8HBG2_HHV1	9,2%	14,1%	14,5%	11,8%	10,2%	9,4%	9,2%	0,0%	13,5%
A0A181ZGW0_HHV11	8,6%	18,6%	19,9%	14,6%	19,3%	24,9%	12,3%	15,0%	19,9%
DUT_HHV11	8,6%	19,1%	15,4%	15,4%	19,1%	15,4%	12,1%	11,3%	15,4%
A0A181ZG15_HHV11	28,7%	28,7%	29,9%	42,6%	30,7%	30,7%	23,0%	25,0%	23,0%
G8HBG9_HHV1	2,5%	11,7%	2,3%	4,9%	8,0%	4,9%	2,5%	2,5%	8,0%
A0A181ZFX4_HHV11	8,8%	3,3%	5,5%	11,4%	3,3%	5,5%	3,3%	3,3%	3,3%
A0A0B5E9X1_HHV1	3,0%	19,7%	9,7%	14,0%	17,0%	9,7%	11,3%	14,0%	8,3%
A0A0B5EA79_HHV1	0,0%	0,0%	0,0%	5,3%	24,3%	0,0%	0,0%	5,3%	0,0%
A0A181ZH10_HHV11	2,1%	0,0%	0,9%	2,1%	0,0%	0,9%	1,1%	0,0%	1,9%

Legend	
	3 out of 3 experiments (2 peptides minimum)
	2 out of 3 experiments (2 peptides minimum)
	1 out of 3 experiments (2 peptides minimum)
	0 out of 3 experiments (2 peptides minimum)

Table S 3: Cellular proteins found with HSV-1 nuclear capsids.

				A-capsids		B-capsids		C-capsids	
Uniprot	**Alternate ID**	**Description**	**mw (kDa)**	Average	SEM	Average	SEM	Average	SEM
Ribosomal									
RL10_HUMAN	RPL10	60S ribosomal protein L10	25 kDa	2,3	0,3	0,7	0,3	1,0	0,0
A8K4C8_HUMAN	RPL13	60S ribosomal protein L13	24 kDa	11,3	4,4	4,7	0,9	6,3	0,3
A0A024QZD1_HUMAN	RPL18	Ribosomal protein L18, isoform CRA_c	22 kDa	3,0	1,0	0,7	0,7	0,7	0,3
RL18A_HUMAN	RPL18A	60S ribosomal protein L18a	21 kDa	3,0	1,5	1,7	0,9	0,0	0,0
J3KTE4_HUMAN	RPL19	Ribosomal protein L19	23 kDa	2,7	0,9	0,0	0,0	0,0	0,0
K7EJT5_HUMAN	RPL22	60S ribosomal protein L22 (Fragment)	5 kDa	1,7	0,7	0,0	0,0	0,0	0,0
C9JNW5_HUMAN	RPL24	60S ribosomal protein L24	18 kDa	2,3	1,5	1,0	0,6	0,0	0,0
E9PLL6_HUMAN	RPL27A	60S ribosomal protein L27a	12 kDa	3,3	1,3	0,3	0,3	1,0	0,6
RL28_HUMAN	RPL28	60S ribosomal protein L28	16 kDa	5,0	1,0	2,3	0,3	4,0	0,6
RL35A_HUMAN	RPL35A	60S ribosomal protein L35a	13 kDa	3,7	0,7	2,3	0,7	0,7	0,3
A0A024RBK3_HUMAN	RPL6	60S ribosomal protein L6	33 kDa	1,7	0,7	0,7	0,7	0,3	0,3
A0A024R814_HUMAN	RPL7	Ribosomal protein L7, isoform CRA_a	30 kDa	2,7	0,7	0,0	0,0	0,0	0,0
RS11_HUMAN	RPS11	40S ribosomal protein S11	18 kDa	4,0	1,0	3,0	0,6	0,0	0,0
RS18_HUMAN	RPS18	40S ribosomal protein S18	18 kDa	15,7	4,7	9,3	1,5	8,3	0,7
H0YEN5_HUMAN	RPS2	40S ribosomal protein S2 (Fragment)	21 kDa	2,0	0,6	1,3	0,7	0,3	0,3
hnRNP									
ROA0_HUMAN	HNRNPA0	Heterogeneous nuclear ribonucleoprotein A0	31 kDa	6,7	3,2	5,7	1,2	8,7	0,3
ROA2_HUMAN	HNRNPA2B1	Heterogeneous nuclear ribonucleoproteins A2/B1	37 kDa	17,7	2,0	24,7	5,2	23,7	3,4
ROA3_HUMAN	HNRNPA3	Heterogeneous nuclear ribonucleoprotein A3	40 kDa	3,3	0,9	3,7	0,3	4,0	0,6
E9PCY7_HUMAN	HNRNPH1	Heterogeneous nuclear ribonucleoprotein H	47 kDa	8,3	2,3	9,3	1,8	6,7	0,9
HNRPM_HUMAN	HNRNPM	Heterogeneous nuclear ribonucleoprotein M	78 kDa	42,7	10,4	43,0	6,5	35,0	1,7
HNRL2_HUMAN	HNRNPUL2	Heterogeneous nuclear ribonucleoprotein U-like protein 2	85 kDa	0,7	0,3	3,3	1,3	1,3	0,9
A0A024RAZ7_HUMAN	HNRPA1	Heterogeneous nuclear ribonucleoprotein A1, isoform CRA_b	39 kDa	8,0	1,2	7,0	1,2	8,7	0,3
A0A024R7T3_HUMAN	HNRPF	Heterogeneous nuclear ribonucleoprotein F, isoform CRA_a	46 kDa	7,7	2,0	7,0	0,0	6,3	0,9
A0A024QZK8_HUMAN	HNRPH3	Heterogeneous nuclear ribonucleoprotein H3 (2H9), isoform CRA_a	37 kDa	1,3	0,7	5,7	0,3	5,3	1,9
A0A024R228_HUMAN	HNRPK	Heterogeneous nuclear ribonucleoprotein K, isoform CRA_d	51 kDa	1,7	0,7	4,3	1,5	1,3	0,3
A0A024R0J9_HUMAN	HNRPUL1	Heterogeneous nuclear ribonucleoprotein U-like 1, isoform CRA_a	85 kDa	3,3	0,7	5,7	1,8	4,0	0,6
HP1B3_HUMAN	HP1BP3	Heterochromatin protein 1-binding protein 3	61 kDa	5,7	2,2	1,0	0,6	0,3	0,3
A0A087WZ13_HUMAN	RAVER1	Ribonucleoprotein PTB-binding 1	78 kDa	7,3	0,3	8,3	2,6	4,3	0,3
RNA binding									
A8K5C4_HUMAN		cDNA FLJ76290, highly similar to Homo sapiens TIA1 cytotoxic granule-associated RNA bindingprotein-like 1 (TIAL1), transcript variant 1, mRNA	42 kDa	1,3	0,9	2,3	0,3	2,7	0,3
B0QYK0_HUMAN	EWSR1	RNA-binding protein EWS	65 kDa	0,0	0,0	7,0	1,5	1,7	0,9
FUS_HUMAN	FUS	RNA-binding protein FUS	53 kDa	4,3	1,2	11,3	1,2	3,3	1,2
A0A0S2Z4Z0_HUMAN	RBM14	RNA binding motif protein 14 isoform 1 (Fragment)	69 kDa	12,7	2,3	21,0	4,4	11,3	0,9
RBM4_HUMAN	RBM4	RNA-binding protein 4	40 kDa	0,7	0,7	2,3	1,5	2,0	1,2
RBMX_HUMAN	RBMX	RNA-binding motif protein, X chromosome	42 kDa	0,7	0,3	4,3	1,3	5,7	0,9
Translation									
Q53HQ7_HUMAN		Elongation factor 1-alpha (Fragment)	50 kDa	3,3	0,3	1,3	0,9	0,7	0,3
Heat shock									
HSPB1_HUMAN	HSPB1	Heat shock protein beta-1	23 kDa	6,0	2,5	5,3	1,5	1,7	0,7
B3GQS7_HUMAN	HSPD1	Mitochondrial heat shock 60kD protein 1 variant 1	61 kDa	2,7	0,7	2,0	0,6	3,0	0,6
Histones									
A3R0T7_HUMAN		Liver histone H1e	22 kDa	1,7	1,7	6,0	0,0	2,3	2,3
H2AV_HUMAN	H2AFV	Histone H2A.V	14 kDa	5,3	0,9	1,3	0,9	1,3	1,3
H15_HUMAN	HIST1H1B	Histone H1.5	23 kDa	2,7	1,3	3,3	0,3	0,7	0,7
H12_HUMAN	HIST1H1C	Histone H1.2	21 kDa	10,3	4,3	4,7	2,3	7,3	0,9
U3KQK0_HUMAN	HIST1H2BN	Histone H2B	19 kDa	3,3	0,9	0,3	0,3	0,3	0,3
B2R4R0_HUMAN	HIST1H4H	Histone H4	11 kDa	28,0	7,9	16,0	2,6	20,0	1,2
DNA/chromosomes									
CTF8A_HUMAN	CHTF8	Chromosome transmission fidelity protein 8 homolog isoform 2	51 kDa	0,0	0,0	3,3	0,9	0,0	0,0
A0A024R4E2_HUMAN	TARDBP	TAR DNA binding protein, isoform CRA_b	45 kDa	1,7	0,9	5,3	0,9	1,7	0,9
Others									
A8K1F4_HUMAN		cDNA FLJ78094, highly similar to Homo sapiens myeloid leukemia factor 2, mRNA	28 kDa	12,0	3,6	9,7	2,4	7,0	0,6
A8K6K7_HUMAN		Glycogen synthase	84 kDa	0,7	0,3	0,3	0,3	4,3	0,3
B2R853_HUMAN		cDNA, FLJ93744, highly similar to Homo sapiens keratin 6E (KRT6E), mRNA	60 kDa	3,3	2,0	2,7	1,8	10,7	2,7
B4E0X8_HUMAN		cDNA FLJ61021, highly similar to Far upstream element-binding protein 1	66 kDa	4,0	0,6	14,3	1,8	6,7	1,2
Q96T67_HUMAN		TOB3	65 kDa	11,3	4,5	0,3	0,3	0,3	0,3
ANX11_HUMAN	ANXA11	Annexin A11	54 kDa		1,5	4,7	1,8	8,7	1,2
ANXA7_HUMAN	ANXA7	Annexin A7	53 kDa	5,3	0,3	5,7	0,7	8,0	0,6
A0A0S2Z3B6_HUMAN	ASS1	Argininosuccinate synthase 1 isoform 2 (Fragment)	24 kDa	1,3	0,3	0,0	0,0	0,0	0,0
A0A0S2Z569_HUMAN	DAZAP1	DAZ associated protein 1 isoform 1	43 kDa	0,3	0,3	2,0	0,6	1,3	0,3
A0A0J9YX62_HUMAN	DNAJB6	DnaJ homolog subfamily B member 6	37 kDa	4,7	0,3	5,0	2,5	1,7	0,3
ELAV1_HUMAN	ELAVL1	ELAV-like protein 1	36 kDa	2,3	0,7	2,7	0,3	3,7	0,3
A0A024R462_HUMAN	FN1	Fibronectin 1, isoform CRA_n	259 kDa	0,0	0,0	0,0	0,0	3,3	0,7
A0A024R693_HUMAN	hCG_22119	Galectin	26 kDa	1,7	1,2	2,0	0,0	4,7	0,9
A0A024R261_HUMAN	hCG_24487	HCG24487, isoform CRA_c	21 kDa	4,3	2,0	2,0	0,6	0,7	0,3
A0A024R8A7_HUMAN	hCG_31253	HCG31253, isoform CRA_a	62 kDa	2,3	1,2	7,0	1,0	6,7	0,7
HORN_HUMAN	HRNR	Hornerin OS=Homo sapiens	282 kDa	3,3	1,8	0,7	0,3	4,7	1,5
A0A087WTP3_HUMAN	KHSRP	Far upstream element-binding protein 2	73 kDa	0,0	0,0	9,7	0,9	1,3	1,3
K1C14_HUMAN	KRT14	Keratin, type I cytoskeletal 14 OS=Homo sapiens GN=KRT14 PE=1 SV=4	52 kDA	4,3	2,6	2,7	1,5	7,7	1,3
K1C16_HUMAN	KRT16	Keratin, type I cytoskeletal 16	51 kDa	5,3	2,9	3,3	1,3	6,0	1,5
K2C5_HUMAN	KRT5	Keratin, type II cytoskeletal 5	62 kDa	3,3	2,4	2,0	1,0	11,0	1,5
A0A0R4J2E8_HUMAN	MATR3	Matrin-3	95 kDa	5,3	0,9	11,7	5,8	2,3	0,7
NCOA5_HUMAN	NCOA5	Nuclear receptor coactivator 5	66 kDa	2,0	0,0	2,7	0,7	1,3	1,3
A0A0S2Z4Z9_HUMAN	NONO	Non-POU domain containing octamer-binding isoform 1 (Fragment)	54 kDa	7,0	2,0	12,7	2,6	8,0	0,6
PCBP1_HUMAN	PCBP1	Poly(rC)-binding protein 1	37 kDa	0,3	0,3	0,3	0,3	2,3	0,3
PDCD5_HUMAN	PDCD5	Programmed cell death protein 5	14 kDa	4,3	1,5	1,3	0,9	1,3	0,3
PDCD6_HUMAN	PDCD6	Programmed cell death protein 6	22 kDa	13,7	3,8	11,3	3,0	14,3	2,9
PEF1_HUMAN	PEF1	Peflin	30 kDa	4,7	0,7	5,7	0,7	6,3	0,3
K7EJ44_HUMAN	PFN1	Profilin	11 kDa	0,3	0,3	0,0	0,0	1,7	0,9
SORCN_HUMAN	SRI	Sorcin	22 kDa	1,3	0,7	1,0	0,6	2,3	0,7
A0A024R8S3_HUMAN	SUMO2		11 kDa	1,3	0,3	3,3	0,9	1,0	0,0

	Exp 1			Exp 2			Exp 3					
Total spectra	**A-capsids**	**B-capsids**	**C-capsids**	**A-capsids**	**B-capsids**	**C-capsids**	**A-capsids**	**B-capsids**	**C-capsids**	**Mock A**	**Mock B**	**Mock C**
RL10_HUMAN	3	1	1	2	1	1	2	0	1	0	0	0
A8K4C8_HUMAN	6	3	7	20	6	6	8	5	6	0	0	0
A0A024QZD1_HUMAN	2	0	1	5	0	0	2	2	1	0	0	0
RL18A_HUMAN	2	2	0	6	3	0	1	0	0	0	0	0
J3KTE4_HUMAN	1	0	0	4	0	0	3	0	0	0	0	0
K7EJT5_HUMAN	1	0	0	3	0	0	1	0	0	0	0	0
C9JNW5_HUMAN	0	0	0	5	2	0	2	1	0	0	0	0
E9PLL6_HUMAN	2	0	1	6	0	2	2	1	0	0	0	0
RL28_HUMAN	4	2	4	7	3	5	4	2	3	0	0	0
RL35A_HUMAN	3	3	1	5	3	0	3	1	1	0	0	0
A0A024RBK3_HUMAN	1	2	0	3	0	0	1	0	1	0	0	0
A0A024R814_HUMAN	4	0	0	2	0	0	2	0	0	0	0	0
RS11_HUMAN	3	4	0	6	3	0	3	2	0	0	0	0
RS18_HUMAN	12	9	7	25	12	9	10	7	9	0	0	0
H0YEN5_HUMAN	2	2	1	3	2	0	1	0	0	0	0	0
ROA0_HUMAN	3	4	9	13	8	8	4	5	9	0	0	0
ROA2_HUMAN	18	24	28	21	34	26	14	16	17	0	0	0
ROA3_HUMAN	5	4	4	3	3	3	2	4	5	0	0	0
E9PCY7_HUMAN	6	10	8	13	12	5	6	6	7	1	0	0
HNRPM_HUMAN	29	36	38	63	56	32	36	37	35	0	0	0
HNRL2_HUMAN	1	2	1	1	6	0	0	2	3	0	0	0
A0A024RAZ7_HUMAN	6	9	9	10	7	8	8	5	9	0	0	0
A0A024R7T3_HUMAN	8	7	8	11	7	5	4	7	6	0	0	0
A0A024QZK8_HUMAN	2	6	4	2	5	3	0	6	9	0	0	0
A0A024R228_HUMAN	3	2	1	1	7	1	1	4	2	0	0	0
A0A024R0J9_HUMAN	2	9	3	4	5	4	4	3	5	0	0	0
HP1B3_HUMAN	4	2	0	10	1	0	3	0	1	0	0	0
A0A087WZI3_HUMAN	8	4	4	7	13	4	7	8	5	0	0	0
A8K5C4_HUMAN	1	2	3	3	3	2	0	2	3	0	0	0
B0QYK0_HUMAN	0	6	2	0	10	0	0	5	3	0	0	0
FUS_HUMAN	5	9	4	6	12	1	2	13	5	0	0	0
A0A0S2Z4Z0_HUMAN	12	28	13	17	22	10	9	13	11	0	0	0
RBM4_HUMAN	0	5	0	2	2	2	0	0	4	0	0	0
RBMX_HUMAN	0	3	4	1	7	6	1	3	7	0	0	0
Q53HQ7_HUMAN	3	3	1	4	0	1	3	1	0	0	0	0
HSPB1_HUMAN	4	8	1	11	5	1	3	3	3	0	0	0
B3GQS7_HUMAN	4	1	3	2	3	4	2	2	2	0	35	0
A3R0T7_HUMAN	5	6	7	0	6	0	0	6	0	0	0	0
H2AV_HUMAN	5	3	0	7	0	4	4	1	0	0	0	0
H15_HUMAN	4	3	2	4	4	0	0	3	0	0	0	0
H12_HUMAN	6	7	7	19	7	9	6	0	6	0	0	0
U3KQK0_HUMAN	3	0	0	5	0	1	2	1	0	0	0	0
B2R4R0_HUMAN	25	12	18	43	21	22	16	15	20	0	0	0
CTF8A_HUMAN	0	2	0	0	5	0	0	3	0	0	0	0
A0A024R4E2_HUMAN	3	7	3	2	5	0	0	4	2	0	0	0
A8K1F4_HUMAN	7	5	6	19	13	7	10	11	8	0	0	0
A8K6K7_HUMAN	1	1	4	1	0	5	0	0	4	0	0	0
B2R853_HUMAN	7	0	9	0	6	16	3	2	7	0	0	0
B4E0X8_HUMAN	3	15	6	4	17	5	5	11	9	0	0	0
Q96T67_HUMAN	9	0	0	20	0	0	5	1	1	0	0	0
ANX11_HUMAN	4	4	11	6	8	7	1	2	8	0	0	0
ANXA7_HUMAN	5	5	9	6	5	7	5	7	8	1	2	0
A0A0S2Z3B6_HUMAN	2	0	0	1	0	0	1	0	0	0	0	0
A0A0S2Z569_HUMAN	0	1	1	0	2	1	1	3	2	0	0	0
A0A0J9YX62_HUMAN	4	3	1	5	10	2	5	2	2	0	0	0
ELAV1_HUMAN	1	2	3	3	3	4	3	3	4	0	0	0
A0A024R462_HUMAN	0	0	2	0	0	4	0	0	4	0	0	0
A0A024R693_HUMAN	1	2	5	4	2	6	0	2	3	0	0	0
A0A024R261_HUMAN	1	3	1	8	2	0	4	1	1	0	0	0
A0A024R8A7_HUMAN	0	8	6	4	8	6	3	5	8	0	0	0
HORN_HUMAN	6	1	2	0	0	5	4	1	7	0	0	0
A0A087WTP3_HUMAN	0	11	0	0	10	0	0	8	4	0	0	0
K1C14_HUMAN	9	0	9	0	5	9	4	3	5	2	4	0
K1C16_HUMAN	10	2	8	0	6	7	6	2	3	0	0	0
ANXA7_HUMAN	8	3	9	0	3	14	2	0	10	0	4	1
A0A0R4J2E8_HUMAN	5	23	3	7	8	1	4	4	3	0	0	0
NCOA5_HUMAN	2	4	0	2	2	0	2	2	4	0	0	0
A0A0S2Z4Z9_HUMAN	5	17	8	11	13	9	5	8	7	0	0	0
PCBP1_HUMAN	0	0	3	1	1	2	0	0	2	0	0	0
PDCD5_HUMAN	4	1	1	7	3	1	2	0	2	0	0	0
PDCD6_HUMAN	12	10	15	21	17	19	8	7	9	0	0	0
PEF1_HUMAN	4	5	6	6	7	7	4	5	6	0	0	0
K7EJ44_HUMAN	0	0	2	0	0	3	1	0	0	0	0	0
SORCN_HUMAN	2	0	1	2	2	3	0	1	3	0	0	0
A0A024R8S3_HUMAN	1	5	1	2	3	1	1	2	1	0	0	0

	Exp 1			Exp 2			Exp 3		
Percent coverage of the protein	**A-capsids**	**B-capsids**	**C-capsids**	**A-capsids**	**B-capsids**	**C-capsids**	**A-capsids**	**B-capsids**	**C-capsids**
RL10_HUMAN	9,4%	3,7%	3,7%	9,8%	3,7%	3,7%	9,4%	0.0	3,7%
A8K4C8_HUMAN	18,0%	9,5%	18,5%	40,8%	19,4%	18,5%	15,2%	14,2%	14,2%
A0A024QZD1_HUMAN	11,2%	0,0%	5,9%	11,7%	0,0%	0.0	6,4%	11,2%	5,9%
RL18A_HUMAN	5,7%	5,7%	0,0%	14,8%	14,8%	0,0%	5,7%	0.0	0,0%
J3KTE4_HUMAN	4,1%	0.0	0.0	13,9%	0.0	0.0	4,6%	0.0	0.0
K7EJT5_HUMAN	23,4%	0.0	0.0	51,1%	0.0	0.0	27,7%	0.0	0.0
C9JNW5_HUMAN	0,0%	0,0%	0,0%	26,0%	5,3%	0,0%	14,0%	5,3%	0,0%
E9PLL6_HUMAN	10,2%	0,0%	10,2%	12,0%	0.0	10,2%	18,5%	8,3%	0.0
RL28_HUMAN	16,1%	8,0%	16,1%	17,5%	13,9%	23,4%	16,1%	8,0%	16,1%
RL35A_HUMAN	19,1%	19,1%	10,9%	20,9%	19,1%	0.0	10,9%	10,9%	8,2%
A0A024RBK3_HUMAN	2,8%	5,9%	0.0	8,7%	0.0	0.0	2,8%	0.0	3,1%
A0A024R814_HUMAN	14,7%	0.0	0.0	11,6%	0.0	0.0	7,0%	0.0	0.0
RS11_HUMAN	10,1%	15,2%	0.0	22,2%	10,1%	0.0	16,5%	10,1%	0.0
RS18_HUMAN	36,2%	25,0%	27,0%	49,3%	25,0%	32,2%	25,0%	25,0%	32,9%
H0YEN5_HUMAN	9,7%	9,7%	4,1%	9,7%	9,7%	0.0	5,6%	0.0	0.0
ROA0_HUMAN	9,5%	14,4%	10,8%	19,7%	15,7%	10,8%	14,4%	13,1%	15,7%
ROA2_HUMAN	40,8%	43,3%	45,9%	36,3%	43,1%	45,9%	23,2%	32,0%	36,5%
ROA3_HUMAN	13,8%	13,8%	13,8%	10,3%	11,4%	11,4%	11,4%	13,8%	13,8%
E9PCY7_HUMAN	8,2%	11,9%	8,2%	12,4%	11,9%	8,2%	6,3%	8,2%	8,2%
HNRPM_HUMAN	33,6%	27,4%	26,2%	36,7%	27,8%	27,4%	25,9%	24,2%	25,8%
HNRL2_HUMAN	1,7%	3,0%	1,7%	1,7%	3,0%	0,0%	0,0%	3,0%	3,0%
A0A024RAZ7_HUMAN	19,9%	22,3%	22,0%	25,0%	22,3%	23,9%	22,3%	13,7%	18,8%
A0A024R7T3_HUMAN	10,1%	6,3%	6,3%	12,3%	6,3%	6,3%	6,3%	6,3%	6,3%
A0A024QZK8_HUMAN	6,9%	17,1%	13,0%	6,9%	14,5%	6,9%	0,0%	18,2%	24,3%
A0A024R228_HUMAN	5,8%	3,7%	3,7%	3,7%	13,8%	3,7%	1,9%	10,6%	6,7%
A0A024R0J9_HUMAN	2,8%	9,7%	3,8%	5,2%	6,2%	4,9%	4,0%	4,9%	4,9%
HP1B3_HUMAN	5,1%	3,6%	0.0	13,6%	2,0%	0.0	4,0%	0.0	2,0%
A0A087WZ13_HUMAN	12,7%	6,1%	4,6%	9,3%	6,4%	4,6%	8,4%	6,1%	6,9%
A8K5C4_HUMAN	2,9%	5,3%	7,5%	7,5%	8,3%	4,5%	0,0%	5,3%	8,3%
B0QYK0_HUMAN	0,0%	8,6%	3,9%	0,0%	13,1%	0,0%	0,0%	8,6%	6,8%
FUS_HUMAN	10,8%	11,6%	9,3%	9,3%	13,3%	3,0%	6,8%	15,8%	9,1%
A0A0S2Z4Z0_HUMAN	11,2%	24,1%	16,4%	19,1%	19,6%	15,7%	13,8%	15,2%	11,8%
RBM4_HUMAN	0,0%	14,3%	2,2%	6,6%	6,6%	7,7%	0,0%	0,0%	7,7%
RBMX_HUMAN	0,0%	6,7%	12,3%	2,1%	16,6%	11,8%	2,1%	9,5%	14,3%
Q53HQ7_HUMAN	3,5%	3,5%	1,7%	3,5%	0.0	1,7%	3,5%	1,7%	1,7%
HSPB1_HUMAN	14,1%	22,9%	5,4%	34,6%	9,8%	4,9%	9,8%	9,8%	10,2%
B3GQS7_HUMAN	7,6%	3,7%	8,6%	6,3%	7,6%	8,6%	6,5%	8,8%	6,5%
A3R0T7_HUMAN	15,1%	22,4%	15,5%	0,0%	26,9%	0,0%	0,0%	20,1%	0,0%
H2AV_HUMAN	25,8%	18,0%	0.0	25,8%	18,0%	18,0%	18,0%	10,9%	0.0
H15_HUMAN	14,2%	14,2%	5,8%	13,7%	9,7%	0,0%	0,0%	14,6%	0,0%
H12_HUMAN	19,7%	19,7%	16,0%	32,4%	24,4%	17,8%	23,0%	0.0	18,8%
U3KQK0_HUMAN	12,7%	0,0%	0,0%	12,7%	0,0%	5,4%	6,0%	6,6%	0,0%
B2R4R0_HUMAN	39,8%	32,0%	39,8%	56,3%	39,8%	47,6%	33,0%	33,0%	32,0%
CTF8A_HUMAN	0,0%	4,8%	0,0%	0,0%	6,3%	0,0%	0,0%	4,2%	2,1%
A0A024R4E2_HUMAN	6,3%	11,8%	4,1%	4,8%	9,2%	0,0%	0,0%	11,8%	7,0%
A8K1F4_HUMAN	18,5%	19,0%	13,3%	30,6%	26,6%	14,1%	23,4%	23,4%	18,1%
A8K6K7_HUMAN	1,4%	1,1%	8,3%	1,4%	0,0%	8,6%	0,0%	0,0%	5,2%
B2R853_HUMAN	9,8%	0,0%	8,3%	0,0%	8,5%	17,2%	5,0%	3,4%	5,0%
B4E0X8_HUMAN	6,5%	13,0%	9,7%	7,6%	22,1%	6,0%	7,8%	14,5%	9,7%
Q96T67_HUMAN	13,1%	0.0	0.0	13,1%	0.0	0.0	4,7%	2,1%	1,4%
ANX11_HUMAN	9,1%	8,1%	18,6%	9,1%	9,9%	9,1%	3,2%	5,5%	11,7%
ANXA7_HUMAN	8,6%	7,4%	16,0%	8,6%	7,6%	13,0%	10,0%	12,0%	9,0%
A0A0S2Z3B6_HUMAN	5,1%	0.0	0.0	4,6%	0.0	0.0	5,1%	0.0	0.0
A0A0S2Z569_HUMAN	0,0%	3,7%	3,7%	0,0%	3,7%	3,7%	3,7%	5,9%	3,7%
A0A0J9YX62_HUMAN	5,1%	5,1%	3,0%	5,1%	8,4%	5,4%	5,1%	7,8%	5,4%
ELAV1_HUMAN	3,4%	6,1%	6,1%	6,1%	6,1%	13,8%	9,5%	13,8%	13,8%
A0A024R462_HUMAN	0,0%	0,0%	1,1%	0,0%	0,0%	1,6%	0,0%	0,0%	1,6%
A0A024R693_HUMAN	4,4%	10,0%	14,4%	14,4%	10,0%	14,4%	0,0%	10,0%	10,0%
A0A024R261_HUMAN	4,9%	17,9%	5,4%	22,8%	10,3%	0.0	14,7%	4,9%	5,4%
A0A024R8A7_HUMAN	0,0%	9,4%	7,0%	7,2%	7,9%	7,9%	5,6%	7,0%	7,0%
HORN_HUMAN	3,7%	0,7%	1,1%	0,0%	0,0%	1,9%	2,1%	0,7%	3,4%
A0A087WTP3_HUMAN	0,0%	13,8%	0,0%	0,0%	14,5%	0,0%	0,0%	12,8%	3,0%
K1C14_HUMAN	12,1%	0,0%	16,5%	0,0%	7,0%	16,7%	6,6%	7,8%	9,8%
K1C16_HUMAN	16,1%	3,8%	16,3%	0,0%	6,8%	11,6%	11,4%	4,9%	6,8%
K2C5_HUMAN	8,5%	3,4%	8,5%	0,0%	4,9%	14,0%	3,2%	0,0%	10,0%
A0A0R4J2E8_HUMAN	3,8%	14,6%	3,9%	4,7%	4,5%	1,7%	2,6%	5,3%	4,0%
NCOA5_HUMAN	3,3%	4,5%	0.0	3,3%	1,7%	0.0	3,1%	3,3%	6,0%
A0A0S2Z4Z9_HUMAN	3,4%	16,3%	8,3%	11,9%	12,1%	11,9%	7,4%	11,9%	8,3%
PCBP1_HUMAN	0,0%	0,0%	8,7%	2,5%	2,5%	5,6%	0,0%	0,0%	3,1%
PDCD5_HUMAN	19,2%	10,4%	8,8%	28,0%	19,2%	8,8%	10,4%	0.0	19,2%
PDCD6_HUMAN	39,8%	18,8%	30,9%	35,1%	39,8%	36,6%	15,7%	13,1%	13,1%
PEF1_HUMAN	10,2%	7,4%	10,2%	10,2%	7,4%	10,2%	7,4%	7,4%	10,2%
K7EJ44_HUMAN	0,0%	0,0%	18,3%	0,0%	0,0%	18,3%	13,5%	0,0%	0,0%
SORCN_HUMAN	11,6%	0,0%	5,6%	12,6%	9,6%	11,6%	0,0%	4,0%	9,6%
A0A024R8S3_HUMAN	12,6%	23,2%	12,6%	12,6%	23,2%	12,6%	12,6%	23,2%	12,6%

Legend	
	3 out of 3 experiments (2 peptides minimum)
	2 out of 3 experiments (2 peptides minimum)
	1 out of 3 experiments (2 peptides minimum)
	0 out of 3 experiments (2 peptides minimum)

II.2.7 References

1. **Johnson DC, Baines JD.** 2011. Herpesviruses remodel host membranes for virus egress. Nat Rev Microbiol **9:**382-94.
2. **Henaff D, Radtke K, Lippé R.** 2012. Herpesviruses exploit several host compartments for envelopment. Traffic **13:**1443-9.
3. **Reynolds AE, Ryckman BJ, Baines JD, Zhou Y, Liang L, Roller RJ.** 2001. U(L)31 and U(L)34 proteins of herpes simplex virus type 1 form a complex that accumulates at the nuclear rim and is required for envelopment of nucleocapsids. J Virol **75:**8803-17.
4. **Simpson-Holley M, Baines J, Roller R, Knipe DM.** 2004. Herpes simplex virus 1 U(L)31 and U(L)34 gene products promote the late maturation of viral replication compartments to the nuclear periphery. J Virol **78:**5591-600.
5. **Park R, Baines JD.** 2006. Herpes simplex virus type 1 infection induces activation and recruitment of protein kinase C to the nuclear membrane and increased phosphorylation of lamin B. J Virol **80:**494-504.
6. **Mou F, Forest T, Baines JD.** 2007. US3 of herpes simplex virus type 1 encodes a promiscuous protein kinase that phosphorylates and alters localization of lamin A/C in infected cells. J Virol **81:**6459-70.
7. **Turner EM, Brown RS, Laudermilch E, Tsai PL, Schlieker C, Rose AE, Zhao C, Turner EM, Steyer AM, Schlieker C.** 2015. The Torsin Activator LULL1 Is Required

for Efficient Growth of Herpes Simplex Virus 1 : Arresting a Torsin ATPase reshapes the endoplasmic reticulum. J Virol **89:**8444-52.

8. **Klupp BG, Hellberg T, Granzow H, Franzke K, Dominguez Gonzalez B, Goodchild RE, Mettenleiter TC.** 2017. Integrity of the Linker of Nucleoskeleton and Cytoskeleton Is Required for Efficient Herpesvirus Nuclear Egress. J Virol **91**.

9. **Ronfeldt S, Klupp BG, Franzke K, Mettenleiter TC.** 2017. Lysine 242 within helix 10 of the pseudorabies virus nuclear egress complex pUL31 component is critical for primary envelopment of nucleocapsids. J Virol doi:10.1128/JVI.01182-17.

10. **Newcomb WW, Homa FL, Thomsen DR, Booy FP, Trus BL, Steven AC, Spencer JV, Brown JC.** 1996. Assembly of the herpes simplex virus capsid: characterization of intermediates observed during cell-free capsid formation. J Mol Biol **263:**432-46.

11. **Baines J, Duffy C.** 2006. Nucleocapsid Assembly and Envelopment of Herpes Simplex Virus, p 175-204. *In* Sandri-Goldin RM (ed), Alpha Herpesviruses. Caister Academic Press, Norfolk.

12. **Heming JD, Conway JF, Homa FL.** 2017. Herpesvirus Capsid Assembly and DNA Packaging. Adv Anat Embryol Cell Biol **223:**119-142.

13. **Newcomb WW, Trus BL, Cheng N, Steven AC, Sheaffer AK, Tenney DJ, Weller SK, Brown JC.** 2000. Isolation of herpes simplex virus procapsids from cells infected with a protease-deficient mutant virus. J Virol **74:**1663-73.

14. **Heymann JB, Cheng N, Newcomb WW, Trus BL, Brown JC, Steven AC.** 2003. Dynamics of herpes simplex virus capsid maturation visualized by time-lapse cryo-electron microscopy. Nat Struct Biol **10:**334-41.

15. **Liu FY, Roizman B.** 1991. The herpes simplex virus 1 gene encoding a protease also contains within its coding domain the gene encoding the more abundant substrate. J Virol **65:**5149-56.

16. **Liu F, Roizman B.** 1993. Characterization of the protease and other products of amino-terminus- proximal cleavage of the herpes simplex virus 1 UL26 protein. J Virol **67:**1300-9.

17. **Davison MD, Rixon FJ, Davison AJ.** 1992. Identification of genes encoding two capsid proteins (VP24 and VP26) of herpes simplex virus type 1. J Gen Virol **73:**2709-13.

18. **Sherman G, Bachenheimer SL.** 1988. Characterization of intranuclear capsids made by ts morphogenic mutants of HSV-1. Virology **163:**471-80.

19. **Chang YE, Van Sant C, Krug PW, Sears AE, Roizman B.** 1997. The null mutant of the U(L)31 gene of herpes simplex virus 1: construction and phenotype in infected cells. J Virol **71:**8307-15.

20. **Newcomb WW, Brown JC.** 1991. Structure of the herpes simplex virus capsid: effects of extraction with guanidine hydrochloride and partial reconstitution of extracted capsids. J Virol **65:**613-20.

21. **Booy FP, Newcomb WW, Trus BL, Brown JC, Baker TS, Steven AC.** 1991. Liquid-crystalline, phage-like packing of encapsidated DNA in herpes simplex virus. Cell **64:**1007-15.

22. **Rémillard-Labrosse G, Guay G, Lippé R.** 2006. Reconstitution of herpes simplex virus type 1 nuclear capsid egress in vitro. J Virol **80:**9741-53.

23. **Rémillard-Labrosse G, Lippé R.** 2011. In vitro nuclear egress of herpes simplex virus type 1 capsids. Methods **55:**153-9.

24. **Trus BL, Newcomb WW, Cheng N, Cardone G, Marekov L, Homa FL, Brown JC, Steven AC.** 2007. Allosteric signaling and a nuclear exit strategy: binding of UL25/UL17 heterodimers to DNA-Filled HSV-1 capsids. Mol Cell **26:**479-89.

25. **Yang K, Baines JD.** 2011. Selection of HSV capsids for envelopment involves interaction between capsid surface components pUL31, pUL17, and pUL25. Proc Natl Acad Sci U S A **108:**14276-81.

26. **Cockrell SK, Huffman JB, Toropova K, Conway JF, Homa FL.** 2011. Residues of the UL25 protein of herpes simplex virus that are required for its stable interaction with capsids. J Virol **85:**4875-87.

27. **Toropova K, Huffman JB, Homa FL, Conway JF.** 2011. The herpes simplex virus 1 UL17 protein is the second constituent of the capsid vertex-specific component required for DNA packaging and retention. J Virol **85:**7513-22.

28. **Fan WH, Roberts AP, McElwee M, Bhella D, Rixon FJ, Lauder R.** 2015. The large tegument protein pUL36 is essential for formation of the capsid vertex-specific component at the capsid-tegument interface of herpes simplex virus 1. J Virol **89:**1502-11.

29. **Huet A, Makhov AM, Huffman JB, Vos M, Homa FL, Conway JF.** 2016. Extensive subunit contacts underpin herpesvirus capsid stability and interior-to-exterior allostery. Nat Struct Mol Biol **23:**531-9.

30. **Loret S, Guay G, Lippé R.** 2008. Comprehensive characterization of extracellular herpes simplex virus type 1 virions. J Virol **82:**8605-18.

31. **Stegen C, Yakova Y, Henaff D, Nadjar J, Duron J, Lippé R.** 2013. Analysis of virion-incorporated host proteins required for herpes simplex virus type 1 infection through a RNA interference screen. PLoS One **8:**e53276.

32. **Mettenleiter TC.** 2006. Intriguing interplay between viral proteins during herpesvirus assembly or: the herpesvirus assembly puzzle. Vet Microbiol **113:**163-9.

33. **Henaff D, Remillard-Labrosse G, Loret S, Lippé R.** 2013. Analysis of the early steps of herpes simplex virus 1 capsid tegumentation. J Virol **87:**4895-906.

34. **Gibson W, Roizman B.** 1972. Proteins specified by herpes simplex virus. VIII. Characterization and composition of multiple capsid forms of subtypes 1 and 2. J Virol **10:**1044-52.

35. **Wolfstein A, Nagel CH, Radtke K, Dohner K, Allan VJ, Sodeik B.** 2006. The inner tegument promotes herpes simplex virus capsid motility along microtubules in vitro. Traffic **7:**227-37.

36. **Radtke K, Kieneke D, Wolfstein A, Michael K, Steffen W, Scholz T, Karger A, Sodeik B.** 2010. Plus- and minus-end directed microtubule motors bind simultaneously to herpes simplex virus capsids using different inner tegument structures. PLoS Pathog **6:**e1000991.

37. **Arakelyan A, Fitzgerald W, Margolis L, Grivel JC.** 2013. Nanoparticle-based flow virometry for the analysis of individual virions. J Clin Invest **123:**3716-27.

38. **Lippe R.** 2018. Flow Virometry: a Powerful Tool To Functionally Characterize Viruses. J Virol **92**.

39. **Loret S, El Bilali N, Lippé R.** 2012. Analysis of herpes simplex virus type I nuclear particles by flow cytometry. Cytometry A **81:**950-9.

40. **El Bilali N, Duron J, Gingras D, Lippe R.** 2017. Quantitative Evaluation of Protein Heterogeneity within Herpes Simplex Virus 1 Particles. J Virol **91**.

41. **Bucks MA, O'Regan KJ, Murphy MA, Wills JW, Courtney RJ.** 2007. Herpes simplex virus type 1 tegument proteins VP1/2 and UL37 are associated with intranuclear capsids. Virology **361:**316-24.

42. **Sheaffer AK, Newcomb WW, Gao M, Yu D, Weller SK, Brown JC, Tenney DJ.** 2001. Herpes simplex virus DNA cleavage and packaging proteins associate with the procapsid prior to its maturation. J Virol **75:**687-98.

43. **Taus NS, Baines JD.** 1998. Herpes simplex virus 1 DNA cleavage/packaging: the UL28 gene encodes a minor component of B capsids. Virology **252:**443-9.

44. **Yu D, Weller SK.** 1998. Herpes simplex virus type 1 cleavage and packaging proteins UL15 and UL28 are associated with B but not C capsids during packaging. J Virol **72:**7428-39.

45. **Roller RJ, Zhou Y, Schnetzer R, Ferguson J, DeSalvo D.** 2000. Herpes simplex virus type 1 U(L)34 gene product is required for viral envelopment. J Virol **74:**117-29.

46. **Yang K, Wills E, Lim HY, Zhou ZH, Baines JD.** 2014. Association of Herpes Simplex Virus pUL31 with Capsid Vertices and Components of the Capsid Vertex Specific Complex. J Virol doi:10.1128/JVI.03175-13.

47. **Sherry MR, Hay TJM, Gulak MA, Nassiri A, Finnen RL, Banfield BW.** 2017. The Herpesvirus Nuclear Egress Complex Component, UL31, Can Be Recruited to Sites of DNA Damage Through Poly-ADP Ribose Binding. Sci Rep **7:**1882.

48. **Maruzuru Y, Shindo K, Liu Z, Oyama M, Kozuka-Hata H, Arii J, Kato A, Kawaguchi Y.** 2014. Role of herpes simplex virus 1 immediate early protein ICP22 in viral nuclear egress. J Virol **88:**7445-54.

49. **Koshizuka T, Kawaguchi Y, Nozawa N, Mori I, Nishiyama Y.** 2007. Herpes simplex virus protein UL11 but not UL51 is associated with lipid rafts. Virus Genes **35:**571-5.

50. **Daikoku T, Ikenoya K, Yamada H, Goshima F, Nishiyama Y.** 1998. Identification and characterization of the herpes simplex virus type 1 UL51 gene product. J Gen Virol **79 (Pt 12):**3027-31.

51. **Nozawa N, Daikoku T, Koshizuka T, Yamauchi Y, Yoshikawa T, Nishiyama Y.** 2003. Subcellular localization of herpes simplex virus type 1 UL51 protein and role of palmitoylation in Golgi apparatus targeting. J Virol **77:**3204-16.

52. **Nozawa N, Kawaguchi Y, Tanaka M, Kato A, Kimura H, Nishiyama Y.** 2005. Herpes simplex virus type 1 UL51 protein is involved in maturation and egress of virus particles. J Virol **79:**6947-56.

53. **Shinde SR, Maddika S.** 2018. Post translational modifications of Rab GTPases. Small GTPases **9:**49-56.

54. **Edler E, Stein M.** 2017. Recognition and stabilization of geranylgeranylated human Rab5 by the GDP Dissociation Inhibitor (GDI). Small GTPases doi:10.1080/21541248.2017.1371268**:**1-16.

55. **Ryckman BJ, Roller RJ.** 2004. Herpes simplex virus type 1 primary envelopment: UL34 protein modification and the US3-UL34 catalytic relationship. J Virol **78:**399-412.

56. **Mou F, Wills E, Baines JD.** 2009. Phosphorylation of the UL31 protein of herpes simplex virus 1 by the US3 encoded kinase regulates localization of the nuclear envelopment complex and egress of nucleocapsids. J Virol **83:**5181-91.

57. **Klupp BG, Granzow H, Mettenleiter TC.** 2001. Effect of the pseudorabies virus US3 protein on nuclear membrane localization of the UL34 protein and virus egress from the nucleus. J Gen Virol **82:**2363-71.

58. **Mou F, Wills EG, Park R, Baines JD.** 2008. Effects of lamin A/C, lamin B1, and viral US3 kinase activity on viral infectivity, virion egress, and the targeting of herpes simplex virus UL34 encoded protein to the inner nuclear membrane. J Virol **82:**8094-104.

59. **Reynolds AE, Wills EG, Roller RJ, Ryckman BJ, Baines JD.** 2002. Ultrastructural localization of the herpes simplex virus type 1 UL31, UL34, and US3 proteins suggests specific roles in primary envelopment and egress of nucleocapsids. J Virol **76:**8939-52.

60. **Cano-Monreal GL, Wylie KM, Cao F, Tavis JE, Morrison LA.** 2009. Herpes simplex virus 2 UL13 protein kinase disrupts nuclear lamins. Virology doi:10.1016/j.virol.2009.06.051.

61. **Kato A, Yamamoto M, Ohno T, Tanaka M, Sata T, Nishiyama Y, Kawaguchi Y.** 2006. Herpes simplex virus 1-encoded protein kinase UL13 phosphorylates viral Us3 protein kinase and regulates nuclear localization of viral envelopment factors UL34 and UL31. J Virol **80:**1476-86.

62. **Thurlow JK, Murphy M, Stow ND, Preston VG.** 2006. Herpes simplex virus type 1 DNA-packaging protein UL17 is required for efficient binding of UL25 to capsids. J Virol **80:**2118-26.

63. **Dai X, Gong D, Wu TT, Sun R, Zhou ZH.** 2014. Organization of capsid-associated tegument components in Kaposi's sarcoma-associated herpesvirus. J Virol **88:**12694-702.

64. **Lee JI, Luxton GW, Smith GA.** 2006. Identification of an essential domain in the herpesvirus VP1/2 tegument protein: the carboxy terminus directs incorporation into capsid assemblons. J Virol **80:**12086-94.

65. **Newcomb WW, Fontana J, Winkler DC, Cheng N, Heymann JB, Steven AC.** 2017. The Primary Enveloped Virion of Herpes Simplex Virus 1: Its Role in Nuclear Egress. MBio **8**.

66. **Gallo ML, Dorsky DI, Crumpacker CS, Parris DS.** 1989. The essential 65-kilodalton DNA-binding protein of herpes simplex virus stimulates the virus-encoded DNA polymerase. J Virol **63:**5023-9.

67. **Mullaney J, Moss HW, McGeoch DJ.** 1989. Gene UL2 of herpes simplex virus type 1 encodes a uracil-DNA glycosylase. J Gen Virol **70:**449-54.

68. **Hernandez TR, Lehman IR.** 1990. Functional interaction between the herpes simplex-1 DNA polymerase and UL42 protein. J Biol Chem **265:**11227-32.

69. **Pyles RB, Thompson RL.** 1994. Evidence that the herpes simplex virus type 1 uracil DNA glycosylase is required for efficient viral replication and latency in the murine nervous system. J Virol **68:**4963-72.

70. **Cooper J, Conner J, Clements JB.** 1995. Characterization of the novel protein kinase activity present in the R1 subunit of herpes simplex virus ribonucleotide reductase. J Virol **69:**4979-85.

71. **Balasubramanian N, Bai P, Buchek G, Korza G, Weller SK.** 2010. Physical interaction between the herpes simplex virus type 1 exonuclease, UL12, and the DNA double-strand break-sensing MRN complex. J Virol **84:**12504-14.

72. **Grady LM, Szczepaniak R, Murelli RP, Masaoka T, Le Grice SFJ, Wright DL, Weller SK.** 2017. The exonuclease activity of HSV-1 UL12 is required for the production of viral DNA that can be packaged to produce infectious virus. J Virol doi:10.1128/JVI.01380-17.

73. **Lippé R.** 2012. Deciphering novel host–herpesvirus interactions by virion proteomics. Front Microbio **3:**1-14.

74. **Pena C, Hurt E, Panse VG.** 2017. Eukaryotic ribosome assembly, transport and quality control. Nat Struct Mol Biol **24:**689-699.

75. **Turcotte S, Letellier J, Lippé R.** 2005. Herpes simplex virus type 1 capsids transit by the trans-Golgi network, where viral glycoproteins accumulate independently of capsid egress. J Virol **79:**8847-60.

Chapitre III - Discussion générale

L'analyse protéomique des virions extracellulaires par spectrométrie de masse a identifié 23 protéines virales comme étant du tégument, et quelques 49 protéines cellulaires incluant des protéines impliquées dans le trafic cellulaire et l'exocytose (188, 189). Cependant, aucune étude comparable n'a permis de caractériser la composition complète des capsides nucléaires. De plus, la séquence et les mécanismes responsables de l'acquisition des protéines du tégument ne sont pas très clairs et nécessitent beaucoup d'investissements. Les protéines du tégument ont fait l'objet de nombreuses études afin de déterminer leurs rôles dans l'infection et la virulence. Cependant, étant limitées par les techniques conventionnelles telles que le dosage par plaque « *plaque assay* », la plupart de ces études considèrent l'ensemble d'une population virale comme étant la responsable du phénotype d'infection sans prendre en considération une éventuelle variabilité au sein d'une même population (189, 621, 630, 631). En effet, jusqu'à nos jours, aucune technique ne permet d'évaluer directement l'impact biologique d'une variabilité quantitative des protéines du tégument d'une façon individuelle entre les particules virales.

III.1 La virométrie de flux : avantages et limites

Les virus sont de très petites particules qui sont en dessous de la limite de détection de la plupart des instruments de cytométrie de flux. En effet, la taille des particules à analyser par cytométrie de flux constitue un facteur limitant pour cette technologie. Cependant, cette limite de détection est améliorée lors de l'utilisation de la lumière diffractée mesurée en face et sur le côté (FSC / SSC) « *Forward Scatter / Side Scatter* » conjointement avec un marquage fluorescent. Dans le cas de notre étude, la combinaison de SSC avec la protéine fluorescente verte GFP « *Green Fluorescent Protein* » ou le Syto 13 qui est une molécule fluorescente qui se lie spécifiquement aux acides nucléiques (632), nous a permis dans le premier article de détecter les particules virales matures et de les trier selon l'intensité du signal GFP afin de déterminer l'impact biologique de la variabilité du tégument pour les protéines tégumentaires

VP16 (pUL48) et VP22 (pUL49). Dans le deuxième article, l'emploi de la virométrie en flux nous a permis de détecter les capsides nucléaires et d'évaluer leur pureté, mais surtout d'enrichir la pureté des capsides C afin de les analyser par la suite par spectrométrie de masse. L'utilisation de la virométrie en flux constitue un atout quant à la petite quantité de matériel nécessaire qui nous permet d'analyser un nombre de particules statistiquement pertinent. Elle permet la détection et l'analyse de toutes les composantes virales (capside, tégument, enveloppe). Cependant, il est primordial de contrôler certains paramètres tels que le type d'instrument utilisé, la détermination du bruit de fond, la calibration, la préparation du virus et la technique de coloration (614). Finalement, la virométrie de flux fournit ainsi de nouveaux outils pour répondre à des questions biologiques et quantitatives sur des virus qui ont subsisté très longtemps sans réponses.

III.2 L'hétérogénéité du tégument et son impact sur l'infectiosité

La couche protéique du tégument est située dans l'espace entre l'enveloppe et la capside et occupe environ les deux tiers du volume à l'intérieur du virion (145). L'analyse des particules virales matures par tomographie cryo-électronique a révélé que les protéines du tégument sont distribuées de façon non symétrique et adoptent une structure polaire (633). Cette asymétrie a également été observée par microscopie à super-résolution ainsi que par l'imagerie par fluorescence des particules individuelles (471, 634). En plus de cette hétérogénéité structurale, nous avons démontré qu'il y a aussi une hétérogénéité quantitative et qualitative dans les protéines du tégument dont la pertinence biologique varie d'une protéine à une autre et d'une particule virale à une autre. En effet, l'analyse par virométrie de flux de particules virales marquées au niveau de différentes protéines (capsides, tégument et enveloppe) par le GFP nous a permis de conclure que pendant que certaines protéines du tégument démontrent une stœchiométrie étroitement contrôlée, d'autres peuvent être plus flexibles. Ceci est vrai pour les

protéines du tégument ICP0, pU_L37 et VP11/12 (pU_L46) qui ne varient statistiquement pas plus que les protéines structurales de la capside pU_L25 ou VP26 (pU_L35) dont le nombre est fortement contrôlé lors de l'assemblage des capsides (145). Ces résultats sont en parfaite concordance avec une étude dans laquelle la quantité de pU_L37 incorporée dans les particules virales reste la même après la surexpression de cette protéine dans les cellules infectées (469). Cependant, l'incorporation des protéines VP16 (pU_L48) et VP22 (pU_L49) varie de façon très significative entre les particules virales et ceci est en accord avec une étude par spectrométrie de masse qui démontre que la quantité de ces deux protéines varie considérablement lors de l'infection des cellules par des mutants VP13/14 (pU_L47), VP22 (pU_L47), U_S3 et gE (470). Cette variabilité a été aussi remarquée par spectrofluorométrie et par microscopie à fluorescence (471, 619).

La déplétion de VP16 provoque une agrégation des nucléocapsides ainsi qu'un défaut dans l'enveloppement des particules virales (435), alors que la délétion réduit la réplication et induit la production de beaucoup de particules légères (L-particules) contenant de grandes quantités de pU_L46, pU_L47 et pU_L49, mais pas pU_L36 et pU_L37 (478, 635). L'infection par des mutants déplétés pour VP22 réduit la sortie virale et l'absence de VP22 est compensée par une augmentation de la quantité d'actine incorporée (636).

Toutefois, l'impact biologique de la variation des protéines tégumentaires VP16 et VP22 n'a jamais été déterminé au niveau individuel des particules virales. À cette fin, nous avons récolté des populations virales aux extrémités des courbes de répartition des téguments et obtenu des stocks viraux en incorporant les quantités les plus faibles ou les plus élevées de VP16 ou VP22 puis nous avons déterminé l'infectiosité de ces particules. Les résultats obtenus montrent une corrélation évidente entre l'abondance de VP16 ou VP22 dans les virions et l'infectiosité. Ceci est confirmé lors de l'utilisation des siRNA pour produire des particules

virales contenant très peu de VP16 ce qui suggère que la quantité de VP16 a un impact direct sur l'infectiosité des particules virales. Pour VP22 la contradiction entre les résultats de dosage par plaque et les déplétions par siRNA suggère que la quantité de VP22 affecte indirectement l'infectiosité virale. La quantité de VP22 incorporée dans les particules virales pourrait probablement affecter l'incorporation d'autres protéines virales qui sont des partenaires directes comme ICP0 ou VP16 ou indirectes comme VHS (511).

Un autre aspect de la modulation de la quantité des protéines du tégument et son impact sur l'ensemble du protéome viral est la modification de ces protéines en leur introduisant des marqueurs tels que la GFP. L'analyse quantitative des protéines du tégument par western blot nous indique clairement que certaines protéines sont très sensibles à l'ajout de marqueur comme la GFP et que ce dernier provoque un changement dans le taux d'incorporation non seulement de la protéine marquée, mais aussi des autres protéines susceptibles d'interagir de façon directe ou indirecte avec elle. Ceci étant en accord avec les observations que le marquage des virions avec la GFP affecte souvent l'organisation des virions et / ou les fonctions des protéines marquées (488, 637). De plus, la GFP a tendance à oligomériser et cela peut affecter la fonction biologique de la protéine (638, 639). Par conséquent, il est recommandé de marquer les protéines par des marqueurs monomériques qui sont généralement désignés par «m» comme première lettre du nom de la protéine, par exemple mCherry (638, 639).

L'ensemble de ces résultats nous indique que l'infectiosité des particules virales est directement liée à la quantité de tégument dans le cas de VP16 alors qu'il s'agit d'un processus plutôt multifactoriel et indirectement lié au niveau d'incorporation de la protéine VP22 (Figure 16)

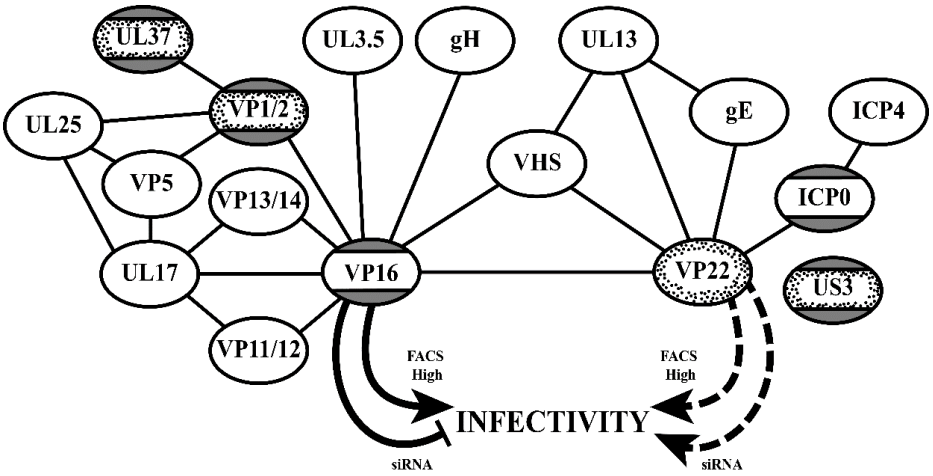

Figure 16. Impact de la modulation des VP16 et VP22 sur le protéome viral

Les différences dans l'infectiosité des particules incorporant les quantités les plus faibles ou les plus élevées de VP16 ou VP22 pourraient être dues au fait que les particules ayant plus de VP16 ou VP22 soient plus stables que leurs homologues ayant les quantités les plus faibles. Toutefois, l'analyse de la stabilité des particules virales triées pour leur haute ou faible teneur en pU_L37, VP16 ou VP22 démontre que les deux populations sont affectées de façon similaire lorsqu'elles sont chauffées préalablement à la température de l'éjection de l'ADN viral de la capside (37°C) (640). Ceci suggère que la stabilité des deux populations est comparable ce qui consolide l'hypothèse que la quantité du tégument impacte directement l'infectiosité (résultats non publiés).

III.3 Analyse protéomique des capsides nucléaires

III.3.1 Approche expérimentale

Tel que discuté plus lors du cycle lytique, les capsides nucléaires nouvellement formées acquièrent les premières protéines du tégument au niveau du noyau puis séquentiellement au niveau du cytoplasme et du TGN. Cette acquisition est favorisée par un réseau très complexe d'interactions protéiques entre les protéines de la capside et les protéines du tégument, mais

aussi entre les protéines de la couche tégumentaire elles-mêmes. Cependant, la séquence exacte d'addition de ces protéines est encore mal définie. Afin d'apporter plus de lumière sur ce processus, nous avons analysé la composition protéique des capsides nucléaires A, B et C par spectrométrie de masse. Avant de procéder à l'analyse protéomique, il fallait résoudre le problème de contamination des capsides par d'éventuelles protéines cellulaires et la contamination croisée des capsides, car étant séparées sur un gradient continu de sucrose, cette technique ne permet pas d'avoir des capsides C hautement purifiées contrairement aux A et B (49, 641). Pour remédier à ce problème, nous avons exploité les différences morphologiques basées sur les contenus des capsides afin d'évaluer leur pureté par microscopie électronique, mais surtout pour purifier les capsides C. Les capsides A et B ont une pureté d'un peu plus que 90% (minium toléré pour la SM) tandis que les capsides C sont contaminées a 30% par des capsides B, ce qui constitue un problème pour l'analyse par spectrométrie de masse pour les capsides C. Pour cela, nous avons marqué les capsides C par le Syto 13 de la même façon que nous avons procédé dans le premier article. Cette approche, nous a permis d'enrichir la pureté des capsides C a plus que 95%. De plus l'utilisation d'un contrôle de cellules non infectées nous a permis d'éliminer beaucoup de contaminants cellulaires.

III.3.2 Les protéines des capsides nucléaires

Les résultats de la spectrométrie de masse ont révélé que les capsides nucléaires A, B et C possèdent toutes les composantes protéiques majeures d'une capside mature à savoir VP5 (pU_L19), VP19c (pU_L38), VP23 (pU_L18), VP26 (pU_L35), la protéine portale pU_L6, pU_L25 et la protéine d'échafaudage pU_L26 quoique cette dernière soit présente en faible quantité pour les capsides C (145). Toutefois, nous avons noté que la protéine pU_L17 est détectée dans les capsides A et C et absente dans les B, ce qui confirme que les capsides A sont le produit des capsides C qui n'ont pas pu incorporer l'ADN. La protéine pU_L17 est indispensable pour la

fixation de pU_L25 sur la portale pU_L6 et ensembles, ces trois protéines sont impliquées dans l'encapsidation de l'ADN viral (145, 178, 182-187).

En plus des protéines de la capside, l'analyse a permis la détection de plusieurs autres protéines tégumentaires et non tégumentaires ce qui suggère l'incorporation de ces protéines à un stade hâtif du cycle viral. La détection des protéines pU_L31 et pU_L34 du NEC confirme leur rôle essentiel pour la sortie des capsides du noyau (369, 383, 385, 390, 391, 400-404). La présence de la protéine du tégument interne pU_L36 confirme l'acquisition de cette protéine au niveau du noyau (458). L'absence du pU_L37, qui est un partenaire de pU_L36, suggère que cette protéine est acquise plus tard ce qui est contradictoire avec l'étude qui démontre que l'association de pU_L36 et pU_L37 se fait au niveau du noyau (458). Il faut donc plus d'investissement pour déterminer si cette protéine est associée aux capsides au niveau du noyau. D'autres protéines du tégument telles que pU_L21, pU_L49, pU_L50, pU_L51 et pU_s10 ont été détectées dans les capsides nucléaires suggérant leurs rôles probables dans la sortie du noyau. Seules les protéines pU_L42 et pU_L46 sont spécifiques aux capsides C. Toutefois, le rôle exact de ces protéines dans le cycle viral reste à déterminer (190). Ceci suggèrerait que la sélection des capsides C par le noyau serait la conséquence d'un processus plus complexe impliquant probablement les protéines de l'hôte.

La présence de protéines cellulaires a également été constatée. Leur présence n'est pas une contamination vue l'utilisation du contrôle de cellules non infectées qui a permis l'élimination des contaminants. Il est à noter que ces protéines ne sont pas incorporées dans le virus mature (188) ce qui suggère leurs rôles possibles dans le processus de sortie des capsides du noyau. Il est donc primordial de pousser la recherche dans ce sens afin de déterminer leurs rôles exacts dans ce processus notamment, en déplétant les gènes codant pour ces protéines, par des ARN interférences.

Toutes ces données confirment l'hypothèse de l'acquisition de certaines protéines du tégument au niveau du noyau ce qui suggère l'implication probable de ces protéines dans l'enveloppement primaire des capsides. De plus, la présence de protéines cellulaires suggère fortement l'implication des protéines de l'hôte dans les premières étapes de la maturation des capsides.

III.4 Perspectives de recherche

Maintenant que nous savons que la variabilité de l'incorporation de VP16 ou VP22 module l'infectiosité du virus, il serait très intéressant d'analyser *in vitro* l'ensemble des protéines du tégument sans oublier les protéines cellulaires. Une telle étude nous permettra de mieux comprendre le cycle d'infection lytique ainsi que de déterminer le rôle des protéines virales et cellulaires dans ce processus. Pour cela, il faudrait générer des virus ayant chacun une seule protéine marquée avec des marqueurs monomériques tels que le mCherry afin de surmonter les problèmes liés à l'utilisation de la GFP.

L'analyse des virus marqués à la GFP par western blot révèle que la modification d'une protéine affecte l'incorporation des autres protéines virales. Cependant, il serait très important de vérifier l'impact de la modulation de la quantité de VP16 ou VP22 sur l'incorporation des autres protéines tégumentaires.

III.4.1 Impact de la modulation du tégument sur la virulence dans l'hôte

Les résultats du premier article nous ont permis de déterminer qu'il existe une hétérogénéité dans les populations virales qui est due au fait que les particules virales n'incorporent pas toutes forcement la même quantité d'une protéine donnée. Cette hétérogénéité se traduit par une variabilité de l'infectiosité sur les lignées cellulaires *in vitro*. Cependant, on ignore si le même scénario se reproduirait chez les animaux *in vivo*. Une telle étude nous permettra d'apporter plus de lumière sur la virulence chez l'hôte et contribuera

probablement au développement de nouveaux vaccins thérapeutiques et/ou préventifs. Ceci serait possible en utilisant la même approche expérimentale à savoir, l'emploie la cytométrie en flux pour le tri des particules virales selon leur teneur en tégument puis la concentration de ces virions dans un volume minimum pour les injecter aux souris.

III.4.2 Protéomique des intermédiaires viraux du VHS-1

L'analyse protéomique des particules virales matures par spectrométrie de masse a permis de caractériser la composition protéique intégrale du VHS-1 (188). Dans le deuxième article, nous avons fait la même chose pour les capsides nucléaires. Afin d'apporter plus de lumière sur le processus de la maturation et mieux comprendre les mécanismes sous-jacents, il serait judicieux de suivre les capsides tout au long de la cellule et de déterminer la composition protéique des différents intermédiaires comme, les capsides enveloppées périnucléaires, capsides cytoplasmiques nues, les capsides associées au TGN et les virus enveloppés dans les vésicules de transport. La comparaison de la composition protéique de toutes ces particules permettra d'établir l'incontestable séquence d'addition des protéines du tégument et de déterminer les rôles probables de chaque protéine virale et/ou cellulaire dans chaque étape du cycle viral.

Conclusions

Les travaux de recherche présentés dans cette thèse font le point de convergence entre plusieurs techniques classiques et innovatrices en virologie, biologie cellulaire et protéomique afin d'apporter de nouveaux éléments de réponses pour tenter de résoudre les énigmes entourant le cycle de vie du VHS-1.

En utilisant une méthodologie innovante que nous avons développée et qui exploite les vertus de la cytométrie en flux, nous avons pu démontrer que si la stœchiométrie pour certaines protéines du tégument est étroitement contrôlée, elle peut être beaucoup plus flexible pour d'autres. Ceci voudrait dire que la quantité de tégument incorporée varie considérablement d'une particule virale à une autre. La modulation de la quantité de tégument incorporée pourrait affecter de façon directe ou indirecte l'infectiosité du virus, mais pourrait également avoir des impacts profonds sur la composition globale du virus. De façon générale, on pourrait considérer que le comportement du virus lors de l'infection ne dépend pas uniquement de son matériel génétique, mais également des niveaux d'incorporation des protéines virales.

L'emploi de la virométrie en flux nous a également permis non seulement d'analyser les capsides nucléaires, mais aussi d'enrichir la pureté les capsides C. Pour la première fois, on était capable d'analyser trois types de capsides nucléaires (A, B et C) par spectrométrie de masse et déterminer leur composition protéique globale. Ceci appuie fortement la doctrine selon laquelle l'acquisition du tégument démarre hâtivement au niveau du noyau et soutien l'implication probable de ces protéines dans l'enveloppement primaire des capsides.

Les résultats de cette thèse ont permis d'ajouter de nouvelles informations qui contribueront sans doute à l'accroissement de la compréhension du cycle viral notamment, la maturation des capsides nucléaires ainsi que le processus de tégumentation et la modulation des protéines du tégument et son impact sur l'infectiosité. Toutefois, malgré tous les efforts des

différentes équipes de recherche, on est toujours loin de saisir l'ensemble des aspects de l'infection par le VHS-1. Il est à dire que la recherche devrait se poursuivre afin de développer de nouveaux médicaments qui permettront d'éliminer le virus et aussi de développer de nouveaux vaccins thérapeutiques et/ou préventifs.

Finalement, la virométrie en flux est une technique très puissante qui permet d'analyser les particules virales au niveau individuel. Et même si les travaux de recherche de cette thèse sont dédiés au VHS-1, cela n'empêcherait pas d'exporter la technologie de la virométrie en flux pour étudier d'autres virus.

Bibliographie

1. Ed R, Russell K. A Short History of the Discovery of Viruses2015.
2. Roizman B, Whitley RJ. The nine ages of herpes simplex virus. Herpes. 2001;8(1):23-27.
3. Roizman B, Knipe DM, Whitley RJ. Herpes Simplex Virus. In: Fields BN, Knipe DM, Howley PM, Cohen JI, Griffin DE, Lamb RA, et al., editors. Fields virology. 6 ed. Philadelphia: Wolters Kluwer Health/Lippincott Williams & Wilkins; 2013. p. 1823-1897.
4. Ebbell B. The Papyrus Ebers, the greatest Egyptian medical document. Copenhagen, London.: Levin & Munksgaard; H. Milford, Oxford university press; 1937. 135 p. p.
5. Wildy P. Herpes: history and classification. In: Kaplan AS, ed. The herpes-viruses New York: Academic Press; 1973. 1–25 p.
6. Beswick TSL. The origin and the use of the word herpes. Medical History. 1962;6(3):214-232.
7. Hutfield DC. History of herpes genitalis. British Journal of Venereal Diseases. 1966;42(4):263-268.
8. Cumston C. The history of herpes from the earliest times to the nineteenth century. Ann Med Hist. 1926;8:284-291.
9. Garzetti A. From Tiberius to the Antonines. A history of the roman empire AD 14-192. LTD MaC, editor. London: Taylor & Francis; 1974. 861 p. p.
10. ANDROUTSOS G. L'urologie dans l'oeuvre De re medica d'Aulus-Cornelius Celsus (1er siècle après JC). Progrès en Urologie. 2005;15:344-352.
11. Androutsos G, Diamantis A, Vladimiros L. Aulus-Cornelius Celse (1ers. après J.-C.) : L'andrologie dans l'œuvre médicale d'un grand encyclopédiste. Andrologie. 2007;17(3):246-252.

12. Villey R. La médecine latine. Histoire de la médecine de la pharmacie, de l'art dentaire et de l'art vétérinaire Paris, Albin Michel. 1977;8:17-24.
13. Morton R. Pyretologias, pars altera; sive, Exercitatio de febribus inflammatoriis universalibus: Sam. Smith & Benj. Walford; 1694.
14. Loewenthal LA. Daniel turner and "de morbis cutaneis". Archives of Dermatology. 1962;85(4):517-523.
15. Turner D. De morbis cutaneis. A treatise of diseases incident to the skin. In two parts. With a short appendix concerning the efficacy of local remedies, and the manner of some of their operations: Bonnwicke; 1714.
16. Astruc J. De morbis venereis libri sex.1736.
17. Willan R. On Cutaneous Diseases.: Kimber and Conrad.; 1809.
18. Bateman T, Willan R. A Practical Synopsis of Cutaneous Diseases According to the Arrangement of Dr. Willan: Longman; 1824.
19. Willan R, Bateman T. Delineations of Cutaneous Diseases Comprised in the Classification of Dr. Willan: Longman; 1817.
20. Stanberry LR. Understanding herpes: Univ. Press of Mississippi; 2006.
21. Unna PG. On herpes progenitalis, especially in women1883.
22. Diday P, Doyon A. Les herpes genitaux. Therapeutique des maladies veneriennes et des maladies cutanees. Paris: V Mason Paris; 1886.
23. Fournier J. Diagnostic et traitment de l'herpes genital. Rev Gen de Clinique et de Therapeutique. 1896;10:177-178.
24. Gruter W. Das herpesvirus, seine atiologische und klinische bedeutung. Munch Med Wschr 1924;71:1058.
25. Stanberry LR. Understanding herpes: Univ. Press of Mississippi; 2006. 136 p.

26. Andrews CH, Carmichael EA. A note on the presence of antibodies to herpesvirus in post-encephalitic and other human sera. Lancet. 1930;1:857–858.

27. Roizman B. The Herpesviruses. Roizman B, editor. New York: Plenum Press; 1982.

28. Doerr R. In: Handbuck der Virusforschung (Doerr R, Hallauer C, eds). Vienna: Springer. 1938.

29. Burnet FM, Williams SW. Herpes Simplex: a New Point of View. Medical Journal of Australia. 1939;1:637-642.

30. Stevens JG, Cook ML. Latent herpes simplex virus in spinal ganglia of mice. Science. 1971;173(3999):843-845.

31. Weller TH, Stoddard MB. Intranuclear inclusion bodies in cultures of human tissue inoculated with varicella vesicle fluid. J Immunol 1952;68:311–319.

32. Smith MG. Propagation in tissue cultures of a cytopathogenic virus from human salivary gland virus disease. Proc Soc Exp Biol Med 1956;92:424–430.

33. Rowe WP, Hartley JW, Waterman Sea. Cytopathogenic agent resembling human salivary gland virus recovered from tissue cultures of human adenoids. Proc Soc Exp Biol Med 1956;92:418–424.

34. Weller TH, Macauley JC, Craig JM, Wirth P. Isolation of intranuclear inclusion producing agents from infants with illnesses resembling cytomegalic inclusion disease. . Proc Soc Exp Biol Med 1957;94:4-12.

35. Epstein MA, Achong BG, Barr YM. Virus Particles in Cultured Lymphoblasts from Burkitt's Lymphoma. Lancet. 1964;1(7335):702-703.

36. Lopez C, Pellett P, Stewart J, Goldsmith C, Sanderlin K, Black J, et al. Characteristics of human herpesvirus-6. J Infect Dis. 1988;157(6):1271-1273.

37. Frenkel N, Schirmer EC, Wyatt LS, Katsafanas G, Roffman E, Danovich RM, et al. Isolation of a new herpesvirus from human CD4+ T cells. Proc Natl Acad Sci U S A. 1990;87(2):748-752.

38. Schneweis KE, Nahmias AJ. Antigens of herpes simplex virus types 1 and 2 – immunodiffusion and inhibition passive hemagglutination studies. . Z Immunitaetsforsch Exp Klin Immunol 1971;141:471–487.

39. Wildy P, Watson DH. Electron microscopic studies on the architecture of animal viruses. Cold Spring Harb Symp Quant Biol. 1963;27:25–47.

40. Tognon M, Furlong D, Conley AJ, Roizman B. Molecular genetics of herpes simplex virus. V. Characterization of a mutant defective in ability to form plaques at low temperatures and in a viral fraction which prevents accumulation of coreless capsids at nuclear pores late in infection. J Virol. 1981;40(3):870-880.

41. Mocarski ES, Roizman B. Site-specific inversion sequence of the herpes simplex virus genome: domain and structural features. Proc Natl Acad Sci U S A. 1981;78(11):7047-7051.

42. Mackem S, Roizman B. Regulation of herpesvirus macromolecular synthesis: temporal order of transcription of alpha genes is not dependent on the stringency of inhibition of protein synthesis. J Virol. 1981;40(1):319-322.

43. Post LE, Mackem S, Roizman B. Regulation of alpha genes of herpes simplex virus: expression of chimeric genes produced by fusion of thymidine kinase with alpha gene promoters. Cell. 1981;24(2):555-565.

44. Roizman B, Carmichael LE, Deinhardt F, de-The G, Nahmias AJ, Plowright W, et al. Herpesviridae. Definition, provisional nomenclature, and taxonomy. The Herpesvirus Study Group, the International Committee on Taxonomy of Viruses. Intervirology. 1981;16(4):201-217.

45. Gibson W, Roizman B. Proteins specified by herpes simplex virus. VIII. Characterization and composition of multiple capsid forms of subtypes 1 and 2. J Virol. 1972;10(5):1044-1052.

46. Kieff E, Hoyer B, Bachenheimer S, Roizman B. Genetic relatedness of type 1 and type 2 herpes simplex viruses. J Virol. 1972;9(5):738-745.

47. Heine JW, Spear PG, Roizman B. Proteins specified by herpes simplex virus. VI. Viral proteins in the plasma membrane. J Virol. 1972;9(3):431-439.

48. Spear PG, Roizman B. Proteins specified by herpes simplex virus. V. Purification and structural proteins of the herpesvirion. J Virol. 1972;9(1):143-159.

49. Gibson W, Roizman B. Proteins specified by herpes simplex virus. 8. Characterization and composition of multiple capsid forms of subtypes 1 and 2. J Virol. 1972;10(5):1044-1052.

50. Sherman G, Bachenheimer SL. Characterization of intranuclear capsids made by ts morphogenic mutants of HSV-1. Virology. 1988;163(2):471-480.

51. Whitley RJ, Soong SJ, Dolin R, Galasso GJ, Ch'ien LT, Alford CA. Adenine arabinoside therapy of biopsy-proved herpes simplex encephalitis. National Institute of Allergy and Infectious Diseases collaborative antiviral study. N Engl J Med. 1977;297(6):289-294.

52. Elion GB, Furman PA, Fyfe JA, de Miranda P, Beauchamp L, Schaeffer HJ. Selectivity of action of an antiherpetic agent, 9-(2-hydroxyethoxymethyl) guanine. Proc Natl Acad Sci U S A. 1977;74(12):5716-5720.

53. Schaeffer HJ, Beauchamp L, de Miranda P, Elion GB, Bauer DJ, Collins P. 9-(2-hydroxyethoxymethyl) guanine activity against viruses of the herpes group. Nature. 1978;272(5654):583-585.

54. Whitley RJ, Gnann JW, Jr. Acyclovir: a decade later. N Engl J Med. 1992;327(11):782-789.

55. Andreansky S, He B, van Cott J, McGhee J, Markert JM, Gillespie GY, et al. Treatment of intracranial gliomas in immunocompetent mice using herpes simplex viruses that express murine interleukins. Gene Ther. 1998;5(1):121-130.

56. Markert JM, Gillespie GY, Weichselbaum RR, Roizman B, Whitley RJ. Genetically engineered HSV in the treatment of glioma: a review. Rev Med Virol. 2000;10(1):17-30.

57. Friedman GK, Pressey JG, Reddy AT, Markert JM, Gillespie GY. Herpes Simplex Virus Oncolytic Therapy for Pediatric Malignancies. Mol Ther. 2009;17(7):1125-1135.

58. Todo T. Oncolytic virus therapy using genetically engineered herpes simplex viruses. Front Biosci. 2008;13:2060-2064.

59. Pol J, Kroemer G, Galluzzi L. First oncolytic virus approved for melanoma immunotherapy. Oncoimmunology. 2016;5(1):e1115641.

60. Goins WF, Huang S, Cohen JB, Glorioso JC. Engineering HSV-1 vectors for gene therapy. Methods Mol Biol. 2014;1144:63-79.

61. Liu BL, Robinson M, Han ZQ, Branston RH, English C, Reay P, et al. ICP34.5 deleted herpes simplex virus with enhanced oncolytic, immune stimulating, and anti-tumour properties. Gene Ther. 2003;10(4):292-303.

62. Wildy P. The viruses. Classification and Nomenclature of Viruses. 5: Karger Publishers; 1971. p. 27-75.

63. Davison AJ. Overview of classification. In: Arvin A, Campadelli-Fiume G, Mocarski E, Moore PS, Roizman B, Whitley R, et al., editors. Human Herpesviruses: Biology, Therapy, and Immunoprophylaxis. Cambridge2007.

64. Davison A, Eberle R, Ehlers B, Hayward G, McGeoch D, Minson A, et al. The order Herpesvirales. Archives of Virology. 2009;154(1):171-177.

65. Davison AJ. Herpesvirus systematics. Veterinary Microbiology. 2010;143(1-2):52-69.

66. Pelllett PE, Roizman B. Herpesviridae. In: Fields BN, Knipe DM, Howley PM, Cohen JI, Griffin DE, Lamb RA, et al., editors. Fields virology. 6 ed. Philadelphia: Wolters Kluwer Health/Lippincott Williams & Wilkins; 2013. p. 1802-1822.

67. Boutier M, Ronsmans M, Rakus K, Jazowiecka-Rakus J, Vancsok C, Morvan L, et al. Chapter Three - Cyprinid Herpesvirus 3: An Archetype of Fish Alloherpesviruses. In: Kielian M, Maramorosch K, Mettenleiter TC, editors. Advances in Virus Research. 93: Academic Press; 2015. p. 161-256.

68. Davison AJ. Channel catfish virus: a new type of herpesvirus. Virology. 1992;186(1):9-14.

69. Pellett PE, Davison AJ, Eberle R, Ehlers B, Hayward GS, Lacoste V. Alloherpesviridae. Virus taxonomy: Ninth report of the International Committee on Taxonomy of Viruses. 2011:108-110.

70. Pellett PE, Davison AJ, Eberle R, Ehlers B, Hayward GS, Lacoste V. Herpesviridae. Virus taxonomy: Ninth report of the International Committee on Taxonomy of Viruses. 2011:111-122.

71. Pellett PE, Davison AJ, Eberle R, Ehlers B, Hayward GS, Lacoste V. Malacoherpesviridae. Virus taxonomy: Ninth report of the International Committee on Taxonomy of Viruses. 2011:123.

72. Rechenchoski DZ, Faccin-Galhardi LC, Linhares REC, Nozawa C. Herpesvirus: an underestimated virus. Folia Microbiol (Praha). 2017;62(2):151-156.

73. Looker KJ, Magaret AS, May MT, Turner KM, Vickerman P, Gottlieb SL, et al. Global and Regional Estimates of Prevalent and Incident Herpes Simplex Virus Type 1 Infections in 2012. PLoS One. 2015;10(10):e0140765.

74. Knaup B, Schunemann S, Wolff MH. Subclinical reactivation of herpes simplex virus type 1 in the oral cavity. Oral Microbiol Immunol. 2000;15(5):281-283.

75. Looker KJ, Magaret AS, May MT, Turner KME, Vickerman P, Newman LM, et al. First estimates of the global and regional incidence of neonatal herpes infection. Lancet Glob Health. 2017;5(3):e300-e309.

76. Gottlieb SL, Giersing BK, Hickling J, Jones R, Deal C, Kaslow DC, et al. Meeting report: Initial World Health Organization consultation on herpes simplex virus (HSV) vaccine preferred product characteristics, March 2017. Vaccine. 2017.

77. Azher TN, Yin XT, Tajfirouz D, Huang AJ, Stuart PM. Herpes simplex keratitis: challenges in diagnosis and clinical management. Clin Ophthalmol. 2017;11:185-191.

78. Liesegang TJ. Herpes simplex virus epidemiology and ocular importance. Cornea. 2001;20(1):1-13.

79. Tsatsos M, MacGregor C, Athanasiadis I, Moschos MM, Hossain P, Anderson D. Herpes simplex virus keratitis: an update of the pathogenesis and current treatment with oral and topical antiviral agents - response. Clin Exp Ophthalmol. 2017;45(3):317.

80. Sarnoff DS. Treatment of recurrent herpes labialis. J Drugs Dermatol. 2014;13(9):1016-1018.

81. Jaques DA, Bagetakou S, L'Huillier AG, Bartoli A, Vargas MI, Fluss J, et al. Herpes simplex encephalitis as a complication of neurosurgical procedures: report of 3 cases and review of the literature. Virol J. 2016;13:83.

82. Rabinstein AA. Herpes Virus Encephalitis in Adults: Current Knowledge and Old Myths. Neurol Clin. 2017;35(4):695-705.

83. Vakharia K, Vakharia K. Bell's Palsy. Facial Plast Surg Clin North Am. 2016;24(1):1-10.

84. Tiemstra JD, Khatkhate N. Bell's palsy: diagnosis and management. Am Fam Physician. 2007;76(7):997-1002.

85. Furuta Y, Fukuda S, Chida E, Takasu T, Ohtani F, Inuyama Y, et al. Reactivation of herpes simplex virus type 1 in patients with Bell's palsy. J Med Virol. 1998;54(3):162-166.

86. Le Page A, Dupuis G, Frost EH, Larbi A, Pawelec G, Witkowski JM, et al. Role of the peripheral innate immune system in the development of Alzheimer's disease. Exp Gerontol. 2017.

87. Ridge PG, Ebbert MT, Kauwe JS. Genetics of Alzheimer's disease. Biomed Res Int. 2013;2013:254954.

88. Ballard C, Corbett A. Agitation and aggression in people with Alzheimer's disease. Curr Opin Psychiatry. 2013;26(3):252-259.

89. Sun X, Chen WD, Wang YD. beta-Amyloid: the key peptide in the pathogenesis of Alzheimer's disease. Front Pharmacol. 2015;6:221.

90. Hanger DP, Lau DH, Phillips EC, Bondulich MK, Guo T, Woodward BW, et al. Intracellular and extracellular roles for tau in neurodegenerative disease. J Alzheimers Dis. 2014;40 Suppl 1:S37-45.

91. Bloom GS. Amyloid-beta and tau: the trigger and bullet in Alzheimer disease pathogenesis. JAMA Neurol. 2014;71(4):505-508.

92. Wang J, Gu BJ, Masters CL, Wang YJ. A systemic view of Alzheimer disease - insights from amyloid-beta metabolism beyond the brain. Nat Rev Neurol. 2017;13(11):703.

93. Chong FP, Ng KY, Koh RY, Chye SM. Tau Proteins and Tauopathies in Alzheimer's Disease. Cell Mol Neurobiol. 2018.

94. Prince MJ. World Alzheimer Report 2015: the global impact of dementia: an analysis of prevalence, incidence, cost and trends: Alzheimer's Disease International; 2015.

95. Wong SL, Gilmour H, Ramage-Morin PL. La maladie d'Alzheimer et les autres formes de démence au Canada. Rapports sur la santé. 2016;27(5).

96. Hill JM, Gebhardt BM, Azcuy AM, Matthews KE, Lukiw WJ, Steiner I, et al. Can a herpes simplex virus type 1 neuroinvasive score be correlated to other risk factors in Alzheimer's disease? Med Hypotheses. 2005;64(2):320-327.

97. Ball MJ. "Limbic predilection in Alzheimer dementia: is reactivated herpesvirus involved?". Can J Neurol Sci. 1982;9(3):303-306.

98. Itzhaki RF. Herpes simplex virus type 1 and Alzheimer's disease: increasing evidence for a major role of the virus. Front Aging Neurosci. 2014;6:202.

99. Itzhaki RF, Wozniak MA. Herpes simplex virus type 1 in Alzheimer's disease: the enemy within. J Alzheimers Dis. 2008;13(4):393-405.

100. Mori I, Yokochi T, Koide N, Sugiyama T, Yoshida T, Kimura Y, et al. PCR search for the herpes simplex virus type 1 genome in brain sections of patients with familial Alzheimer's disease. J Clin Microbiol. 2004;42(2):936-937.

101. Mori I, Kimura Y, Naiki H, Matsubara R, Takeuchi T, Yokochi T, et al. Reactivation of HSV-1 in the brain of patients with familial Alzheimer's disease. J Med Virol. 2004;73(4):605-611.

102. Wozniak MA, Mee AP, Itzhaki RF. Herpes simplex virus type 1 DNA is located within Alzheimer's disease amyloid plaques. J Pathol. 2009;217(1):131-138.

103. Wozniak MA, Shipley SJ, Combrinck M, Wilcock GK, Itzhaki RF. Productive herpes simplex virus in brain of elderly normal subjects and Alzheimer's disease patients. J Med Virol. 2005;75(2):300-306.

104. Cheng SB, Ferland P, Webster P, Bearer EL. Herpes simplex virus dances with amyloid precursor protein while exiting the cell. PLoS One. 2011;6(3):e17966.

105. Piacentini R, Civitelli L, Ripoli C, Marcocci ME, De Chiara G, Garaci E, et al. HSV-1 promotes Ca2+ -mediated APP phosphorylation and Abeta accumulation in rat cortical neurons. Neurobiol Aging. 2011;32(12):2323 e2313-2326.

106. De Chiara G, Marcocci ME, Civitelli L, Argnani R, Piacentini R, Ripoli C, et al. APP processing induced by herpes simplex virus type 1 (HSV-1) yields several APP fragments in human and rat neuronal cells. PLoS One. 2010;5(11):e13989.

107. Wozniak MA, Itzhaki RF, Shipley SJ, Dobson CB. Herpes simplex virus infection causes cellular beta-amyloid accumulation and secretase upregulation. Neurosci Lett. 2007;429(2-3):95-100.

108. Itzhaki RF. Herpes simplex virus type 1 and Alzheimer's disease: possible mechanisms and signposts. FASEB J. 2017;31(8):3216-3226.

109. Alvarez G, Aldudo J, Alonso M, Santana S, Valdivieso F. Herpes simplex virus type 1 induces nuclear accumulation of hyperphosphorylated tau in neuronal cells. J Neurosci Res. 2012;90(5):1020-1029.

110. Lerchundi R, Neira R, Valdivia S, Vio K, Concha MI, Zambrano A, et al. Tau cleavage at D421 by caspase-3 is induced in neurons and astrocytes infected with herpes simplex virus type 1. J Alzheimers Dis. 2011;23(3):513-520.

111. Wozniak MA, Frost AL, Itzhaki RF. Alzheimer's disease-specific tau phosphorylation is induced by herpes simplex virus type 1. J Alzheimers Dis. 2009;16(2):341-350.

112. Zambrano A, Solis L, Salvadores N, Cortes M, Lerchundi R, Otth C. Neuronal cytoskeletal dynamic modification and neurodegeneration induced by infection with herpes simplex virus type 1. J Alzheimers Dis. 2008;14(3):259-269.

113. Lisco A, Munawwar A, Introini A, Vanpouille C, Saba E, Feng X, et al. Semen of HIV-1-infected individuals: local shedding of herpesviruses and reprogrammed cytokine network. J Infect Dis. 2012;205(1):97-105.

114. Suligoi B, Dorrucci M, Uccella I, Andreoni M, Rezza G, Italian Seroconversion S. Effect of multiple herpesvirus infections on the progression of HIV disease in a cohort of HIV seroconverters. J Med Virol. 2003;69(2):182-187.

115. Munawwar A, Singh S. Human Herpesviruses as Copathogens of HIV Infection, Their Role in HIV Transmission, and Disease Progression. J Lab Physicians. 2016;8(1):5-18.

116. Dinotta F, De Pasquale R, Nasca MR, Tedeschi A, Micali G. Disseminated herpes simplex infection in a HIV+ patient. G Ital Dermatol Venereol. 2009;144(2):205-209.

117. Root-Bernstein RS, Hobbs SH. Does HIV "piggyback" on CD4-like surface proteins of sperm, viruses, and bacteria? Implications for co-transmission, cellular tropism and the induction of autoimmunity in AIDS. J Theor Biol. 1993;160(2):249-264.

118. Biancotto A, Iglehart SJ, Vanpouille C, Condack CE, Lisco A, Ruecker E, et al. HIV-1 induced activation of CD4+ T cells creates new targets for HIV-1 infection in human lymphoid tissue ex vivo. Blood. 2008;111(2):699-704.

119. Cote-Daigneault J, Carrier FM, Toledano K, Wartelle-Bladu C, Willems B. Herpes simplex hepatitis after liver transplantation: case report and literature review. Transpl Infect Dis. 2014;16(1):130-134.

120. Levitsky J, Duddempudi AT, Lakeman FD, Whitley RJ, Luby JP, Lee WM, et al. Detection and diagnosis of herpes simplex virus infection in adults with acute liver failure. Liver Transpl. 2008;14(10):1498-1504.

121. Piret J, Boivin G. Antiviral resistance in herpes simplex virus and varicella-zoster virus infections: diagnosis and management. Curr Opin Infect Dis. 2016;29(6):654-662.

122. Widener RW, Whitley RJ. Herpes simplex virus. Handbook of clinical neurology. 2014;123:251-263.

123. Whitley RJ, Roizman B. Herpes Simplex Viruses. Clinical Virology, Third Edition: American Society of Microbiology; 2009.

124. Piret J, Boivin G. Resistance of Herpes Simplex Viruses to Nucleoside Analogues: Mechanisms, Prevalence, and Management. Antimicrobial Agents and Chemotherapy. 2011;55(2):459-472.

125. Miller WH, Miller RL. Phosphorylation of acyclovir diphosphate by cellular enzymes. Biochem Pharmacol. 1982;31(23):3879-3884.

126. Miller WH, Miller RL. Phosphorylation of acyclovir (acycloguanosine) monophosphate by GMP kinase. J Biol Chem. 1980;255(15):7204-7207.

127. Reardon JE, Spector T. Herpes simplex virus type 1 DNA polymerase. Mechanism of inhibition by acyclovir triphosphate. J Biol Chem. 1989;264(13):7405-7411.

128. Elion GB. Acyclovir: discovery, mechanism of action, and selectivity. J Med Virol. 1993;Suppl 1:2-6.

129. Derse D, Cheng YC, Furman PA, St Clair MH, Elion GB. Inhibition of purified human and herpes simplex virus-induced DNA polymerases by 9-(2-hydroxyethoxymethyl)guanine triphosphate. Effects on primer-template function. J Biol Chem. 1981;256(22):11447-11451.

130. Beutner KR. Valacyclovir: a review of its antiviral activity, pharmacokinetic properties, and clinical efficacy. Antiviral Res. 1995;28(4):281-290.

131. Perry CM, Faulds D. Valaciclovir. A review of its antiviral activity, pharmacokinetic properties and therapeutic efficacy in herpesvirus infections. Drugs. 1996;52(5):754-772.

132. Duan J, Liuzzi M, Paris W, Liard F, Browne A, Dansereau N, et al. Oral bioavailability and in vivo efficacy of the helicase-primase inhibitor BILS 45 BS against acyclovir-resistant herpes simplex virus type 1. Antimicrob Agents Chemother. 2003;47(6):1798-1804.

133. Crute JJ, Grygon CA, Hargrave KD, Simoneau B, Faucher AM, Bolger G, et al. Herpes simplex virus helicase-primase inhibitors are active in animal models of human disease. Nat Med. 2002;8(4):386-391.

134. Xiong X, Smith JL, Chen MS. Effect of incorporation of cidofovir into DNA by human cytomegalovirus DNA polymerase on DNA elongation. Antimicrobial Agents and Chemotherapy. 1997;41(3):594-599.

135. Cono J, Casey CG, Bell DM, Centers for Disease C, Prevention. Smallpox vaccination and adverse reactions. Guidance for clinicians. MMWR Recomm Rep. 2003;52(RR-4):1-28.

136. Oberg B. Antiviral effects of phosphonoformate (PFA, foscarnet sodium). Pharmacol Ther. 1982;19(3):387-415.

137. Razonable RR. Antiviral drugs for viruses other than human immunodeficiency virus. Mayo Clin Proc. 2011;86(10):1009-1026.

138. Gottlieb SL, Giersing BK, Hickling J, Jones R, Deal C, Kaslow DC. Meeting report: Initial World Health Organization consultation on herpes simplex virus (HSV) vaccine preferred product characteristics, March 2017. Vaccine. 2017.

139. Chentoufi AA, Kritzer E, Yu DM, Nesburn AB, Benmohamed L. Towards a rational design of an asymptomatic clinical herpes vaccine: the old, the new, and the unknown. Clin Dev Immunol. 2012;2012:187585.

140. Long D, Skoberne M, Gierahn TM, Larson S, Price JA, Clemens V, et al. Identification of novel virus-specific antigens by CD4(+) and CD8(+) T cells from asymptomatic HSV-2 seropositive and seronegative donors. Virology. 2014;464-465:296-311.

141. Dutton JL, Woo WP, Chandra J, Xu Y, Li B, Finlayson N, et al. An escalating dose study to assess the safety, tolerability and immunogenicity of a Herpes Simplex Virus DNA vaccine, COR-1. Hum Vaccin Immunother. 2016;12(12):3079-3088.

142. Dutton JL, Li B, Woo WP, Marshak JO, Xu Y, Huang ML, et al. A novel DNA vaccine technology conveying protection against a lethal herpes simplex viral challenge in mice. PLoS One. 2013;8(10):e76407.

143. Lan K, Luo MH. Herpesviruses: epidemiology, pathogenesis, and interventions. Virol Sin. 2017;32(5):347-348.

144. Booy FP, Newcomb WW, Trus BL, Brown JC, Baker TS, Steven AC. Liquid-crystalline, phage-like packing of encapsidated DNA in herpes simplex virus. Cell. 1991;64(5):1007-1015.

145. Heming JD, Conway JF, Homa FL. Herpesvirus Capsid Assembly and DNA Packaging. Adv Anat Embryol Cell Biol. 2017;223:119-142.

146. Bauer DW, Huffman JB, Homa FL, Evilevitch A. Herpes virus genome, the pressure is on. J Am Chem Soc. 2013;135(30):11216-11221.

147. McGeoch DJ. On the predictive recognition of signal peptide sequences. Virus Res. 1985;3(3):271-286.

148. Preston CM, McGeoch DJ. Identification and mapping of two polypeptides encoded within the herpes simplex virus type 1 thymidine kinase gene sequences. J Virol. 1981;38(2):593-605.

149. Murchie MJ, McGeoch DJ. DNA sequence analysis of an immediate-early gene region of the herpes simplex virus type 1 genome (map coordinates 0.950 to 0.978). J Gen Virol. 1982;62(Pt 1):1-15.

150. Quinn JP, McGeoch DJ. DNA sequence of the region in the genome of herpes simplex virus type 1 containing the genes for DNA polymerase and the major DNA binding protein. Nucleic Acids Res. 1985;13(22):8143-8163.

151. McGeoch DJ, Davison AJ. DNA sequence of the herpes simplex virus type 1 gene encoding glycoprotein gH, and identification of homologues in the genomes of varicella-zoster virus and Epstein-Barr virus. Nucleic Acids Res. 1986;14(10):4281-4292.

152. McGeoch DJ, Dolan A, Frame MC. DNA sequence of the region in the genome of herpes simplex virus type 1 containing the exonuclease gene and neighbouring genes. Nucleic Acids Res. 1986;14(8):3435-3448.

153. McGeoch DJ, Davison AJ. Alphaherpesviruses possess a gene homologous to the protein kinase gene family of eukaryotes and retroviruses. Nucleic Acids Res. 1986;14(4):1765-1777.

154. Davison AJ, Wilkie NM. Nucleotide sequences of the joint between the L and S segments of herpes simplex virus types 1 and 2. J Gen Virol. 1981;55(Pt 2):315-331.

155. Perry LJ, Rixon FJ, Everett RD, Frame MC, McGeoch DJ. Characterization of the IE110 gene of herpes simplex virus type 1. J Gen Virol. 1986;67(Pt 11):2365-2380.

156. Dalrymple MA, McGeoch DJ, Davison AJ, Preston CM. DNA sequence of the herpes simplex virus type 1 gene whose product is responsible for transcriptional activation of immediate early promoters. Nucleic Acids Res. 1985;13(21):7865-7879.

157. McGeoch DJ, Dalrymple MA, Davison AJ, Dolan A, Frame MC, McNab D, et al. The complete DNA sequence of the long unique region in the genome of herpes simplex virus type 1. J Gen Virol. 1988;69(Pt 7):1531-1574.

158. Wagner EK, Sandri-Goldin RM. Herpes Simplex Viruses: Molecular Biology A2 - Mahy, Brian W.J. In: Regenmortel MHVV, editor. Encyclopedia of Virology (Third Edition). Oxford: Academic Press; 2008. p. 397-405.

159. Kennedy PG, Rovnak J, Badani H, Cohrs RJ. A comparison of herpes simplex virus type 1 and varicella-zoster virus latency and reactivation. J Gen Virol. 2015;96(Pt 7):1581-1602.

160. Honess RW, Roizman B. Regulation of herpesvirus macromolecular synthesis. I. Cascade regulation of the synthesis of three groups of viral proteins. J Virol. 1974;14(1):8-19.

161. Chou J, Roizman B. The herpes simplex virus 1 gene for ICP34.5, which maps in inverted repeats, is conserved in several limited-passage isolates but not in strain 17syn+. J Virol. 1990;64(3):1014-1020.

162. Umene K, Oohashi S, Yoshida M, Fukumaki Y. Diversity of the a sequence of herpes simplex virus type 1 developed during evolution. J Gen Virol. 2008;89(Pt 4):841-852.

163. Locker H, Frenkel N. BamI, KpnI, and SalI restriction enzyme maps of the DNAs of herpes simplex virus strains Justin and F: occurrence of heterogeneities in defined regions of the viral DNA. J Virol. 1979;32(2):429-441.

164. Weller SK, Coen DM. Herpes simplex viruses: mechanisms of DNA replication. Cold Spring Harb Perspect Biol. 2012;4(9):a013011.

165. Delius H, Clements JB. A partial denaturation map of herpes simplex virus type 1 DNA: evidence for inversions of the unique DNA regions. J Gen Virol. 1976;33(1):125-133.

166. Hayward GS, Frenkel N, Roizman B. Anatomy of herpes simplex virus DNA: strain differences and heterogeneity in the locations of restriction endonuclease cleavage sites. Proc Natl Acad Sci U S A. 1975;72(5):1768-1772.

167. Hayward GS, Jacob RJ, Wadsworth SC, Roizman B. Anatomy of herpes simplex virus DNA: evidence for four populations of molecules that differ in the relative orientations of their long and short components. Proc Natl Acad Sci U S A. 1975;72(11):4243-4247.

168. Sheldrick P, Berthelot N. Inverted repetitions in the chromosome of herpes simplex virus. Cold Spring Harb Symp Quant Biol. 1975;39 Pt 2:667-678.

169. Wadsworth S, Jacob RJ, Roizman B. Anatomy of herpes simplex virus DNA. II. Size, composition, and arrangement of inverted terminal repetitions. J Virol. 1975;15(6):1487-1497.

170. Jurak I, Kramer MF, Mellor JC, van Lint AL, Roth FP, Knipe DM, et al. Numerous conserved and divergent microRNAs expressed by herpes simplex viruses 1 and 2. J Virol. 2010;84(9):4659-4672.

171. Weir JP. Regulation of herpes simplex virus gene expression. Gene. 2001;271(2):117-130.

172. Schrag JD, Prasad BV, Rixon FJ, Chiu W. Three-dimensional structure of the HSV1 nucleocapsid. Cell. 1989;56(4):651-660.

173. Brown JC, Newcomb WW. Herpesvirus capsid assembly: insights from structural analysis. Curr Opin Virol. 2011;1(2):142-149.

174. Conway JF, Homa FL. Nucleocapsid structure, assembly and DNA packaging of herpes simplex virus. Alphaheresviruses Caister Academic Press, Norwich, United Kingdom. 2011:175-193.

175. Newcomb WW, Trus BL, Booy FP, Steven AC, Wall JS, Brown JC. Structure of the herpes simplex virus capsid. Molecular composition of the pentons and the triplexes. J Mol Biol. 1993;232(2):499-511.

176. Huet A, Makhov AM, Huffman JB, Vos M, Homa FL, Conway JF. Extensive subunit contacts underpin herpesvirus capsid stability and interior-to-exterior allostery. Nat Struct Mol Biol. 2016;23(6):531-539.

177. Booy FP, Trus BL, Newcomb WW, Brown JC, Conway JF, Steven AC. Finding a needle in a haystack: detection of a small protein (the 12-kDa VP26) in a large complex (the 200-MDa capsid of herpes simplex virus). Proc Natl Acad Sci U S A. 1994;91(12):5652-5656.

178. Newcomb WW, Juhas RM, Thomsen DR, Homa FL, Burch AD, Weller SK, et al. The UL6 gene product forms the portal for entry of DNA into the herpes simplex virus capsid. J Virol. 2001;75(22):10923-10932.

179. Trus BL, Cheng N, Newcomb WW, Homa FL, Brown JC, Steven AC. Structure and polymorphism of the UL6 portal protein of herpes simplex virus type 1. J Virol. 2004;78(22):12668-12671.

180. Newcomb WW, Homa FL, Brown JC. Involvement of the portal at an early step in herpes simplex virus capsid assembly. J Virol. 2005;79(16):10540-10546.

181. Cardone G, Winkler DC, Trus BL, Cheng N, Heuser JE, Newcomb WW, et al. Visualization of the herpes simplex virus portal in situ by cryo-electron tomography. Virology. 2007;361(2):426-434.

182. Ogasawara M, Suzutani T, Yoshida I, Azuma M. Role of the UL25 gene product in packaging DNA into the herpes simplex virus capsid: location of UL25 product in the capsid and demonstration that it binds DNA. J Virol. 2001;75(3):1427-1436.

183. Thurlow JK, Murphy M, Stow ND, Preston VG. Herpes simplex virus type 1 DNA-packaging protein UL17 is required for efficient binding of UL25 to capsids. J Virol. 2006;80(5):2118-2126.

184. Trus BL, Newcomb WW, Cheng N, Cardone G, Marekov L, Homa FL, et al. Allosteric signaling and a nuclear exit strategy: binding of UL25/UL17 heterodimers to DNA-Filled HSV-1 capsids. Mol Cell. 2007;26(4):479-489.

185. Cockrell SK, Huffman JB, Toropova K, Conway JF, Homa FL. Residues of the UL25 protein of herpes simplex virus that are required for its stable interaction with capsids. J Virol. 2011;85(10):4875-4887.

186. Snijder J, Radtke K, Anderson F, Scholtes L, Corradini E, Baines J, et al. Vertex-Specific Proteins pUL17 and pUL25 Mechanically Reinforce Herpes Simplex Virus Capsids. J Virol. 2017;91(12).

187. Toropova K, Huffman JB, Homa FL, Conway JF. The herpes simplex virus 1 UL17 protein is the second constituent of the capsid vertex-specific component required for DNA packaging and retention. J Virol. 2011;85(15):7513-7522.

188. Loret S, Guay G, Lippé R. Comprehensive characterization of extracellular herpes simplex virus type 1 virions. J Virol. 2008;82(17):8605-8618.

189. Stegen C, Yakova Y, Henaff D, Nadjar J, Duron J, Lippé R. Analysis of virion-incorporated host proteins required for herpes simplex virus type 1 infection through a RNA interference screen. PLoS One. 2013;8(1):e53276.

190. Owen DJ, Crump CM, Graham SC. Tegument Assembly and Secondary Envelopment of Alphaherpesviruses. Viruses. 2015;7(9):5084-5114.

191. Newcomb WW, Jones LM, Dee A, Chaudhry F, Brown JC. Role of a reducing environment in disassembly of the herpesvirus tegument. Virology. 2012;431(1-2):71-79.

192. Wolfstein A, Nagel CH, Radtke K, Dohner K, Allan VJ, Sodeik B. The inner tegument promotes herpes simplex virus capsid motility along microtubules in vitro. Traffic. 2006;7(2):227-237.

193. Sandbaumhuter M, Dohner K, Schipke J, Binz A, Pohlmann A, Sodeik B, et al. Cytosolic herpes simplex virus capsids not only require binding inner tegument protein pUL36 but also pUL37 for active transport prior to secondary envelopment. Cell Microbiol. 2013;15(2):248-269.

194. Diefenbach RJ. Conserved tegument protein complexes: Essential components in the assembly of herpesviruses. Virus Res. 2015;210:308-317.

195. Loret S, Lippé R. Biochemical analysis of infected cell polypeptide (ICP)0, ICP4, UL7 and UL23 incorporated into extracellular herpes simplex virus type 1 virions. J Gen Virol. 2012;93(Pt 3):624-634.

196. Henaff D, Remillard-Labrosse G, Loret S, Lippé R. Analysis of the early steps of herpes simplex virus 1 capsid tegumentation. J Virol. 2013;87(9):4895-4906.

197. Guo H, Shen S, Wang L, Deng H. Role of tegument proteins in herpesvirus assembly and egress. Protein Cell. 2010;1(11):987-998.

198. Kelly BJ, Fraefel C, Cunningham AL, Diefenbach RJ. Functional roles of the tegument proteins of herpes simplex virus type 1. Virus Res. 2009;145(2):173-186.

199. Xu X, Che Y, Li Q. HSV-1 tegument protein and the development of its genome editing technology. Virol J. 2016;13:108.

200. Henaff D, Radtke K, Lippé R. Herpesviruses exploit several host compartments for envelopment. Traffic. 2012;13(11):1443-1449.

201. Lanfranca MP, Mostafa HH, Davido DJ. HSV-1 ICP0: An E3 Ubiquitin Ligase That Counteracts Host Intrinsic and Innate Immunity. Cells. 2014;3(2):438-454.

202. Boutell C, Everett RD. Regulation of alphaherpesvirus infections by the ICP0 family of proteins. J Gen Virol. 2013;94(Pt 3):465-481.

203. Parkinson J, Lees-Miller SP, Everett RD. Herpes simplex virus type 1 immediate-early protein vmw110 induces the proteasome-dependent degradation of the catalytic subunit of DNA-dependent protein kinase. J Virol. 1999;73(1):650-657.

204. Melroe GT, DeLuca NA, Knipe DM. Herpes simplex virus 1 has multiple mechanisms for blocking virus-induced interferon production. J Virol. 2004;78(16):8411-8420.

205. Lin R, Noyce RS, Collins SE, Everett RD, Mossman KL. The herpes simplex virus ICP0 RING finger domain inhibits IRF3- and IRF7-mediated activation of interferon-stimulated genes. J Virol. 2004;78(4):1675-1684.

206. Batchelor AH, Wilcox KW, O'Hare P. Binding and repression of the latency-associated promoter of herpes simplex virus by the immediate early 175K protein. J Gen Virol. 1994;75(Pt 4):753-767.

207. van Genderen IL, Brandimarti R, Torrisi MR, Campadelli G, van Meer G. The phospholipid composition of extracellular herpes simplex virions differs from that of host cell nuclei. Virology. 1994;200(2):831-836.

208. Mettenleiter TC. Pathogenesis of neurotropic herpesviruses: role of viral glycoproteins in neuroinvasion and transneuronal spread. Virus Res. 2003;92(2):197-206.

209. Heldwein EE, Krummenacher C. Entry of herpesviruses into mammalian cells. Cell Mol Life Sci. 2008;65(11):1653-1668.

210. Reske A, Pollara G, Krummenacher C, Chain BM, Katz DR. Understanding HSV-1 entry glycoproteins. Rev Med Virol. 2007;17(3):205-215.

211. Farnsworth A, Wisner TW, Webb M, Roller R, Cohen G, Eisenberg R, et al. Herpes simplex virus glycoproteins gB and gH function in fusion between the virion envelope and the outer nuclear membrane. Proc Natl Acad Sci U S A. 2007;104(24):10187-10192.

212. Wisner TW, Wright CC, Kato A, Kawaguchi Y, Mou F, Baines JD, et al. Herpesvirus gB-induced fusion between the virion envelope and outer nuclear membrane during virus egress is regulated by the viral US3 kinase. J Virol. 2009;83(7):3115-3126.

213. Wright CC, Wisner TW, Hannah BP, Eisenberg RJ, Cohen GH, Johnson DC. Fusion between perinuclear virions and the outer nuclear membrane requires the fusogenic activity of herpes simplex virus gB. J Virol. 2009;83(22):11847-11856.

214. Šedý JR, Spear PG, Ware CF. Cross-regulation between herpesviruses and the TNF superfamily members. Nature Reviews Immunology. 2008;8:861.

215. Nagashunmugam T, Lubinski J, Wang L, Goldstein LT, Weeks BS, Sundaresan P, et al. In vivo immune evasion mediated by the herpes simplex virus type 1 immunoglobulin G Fc receptor. J Virol. 1998;72(7):5351-5359.

216. Johnson DC, Feenstra V. Identification of a novel herpes simplex virus type 1-induced glycoprotein which complexes with gE and binds immunoglobulin. J Virol. 1987;61(7):2208-2216.

217. Hutchinson L, Browne H, Wargent V, Davis-Poynter N, Primorac S, Goldsmith K, et al. A novel herpes simplex virus glycoprotein, gL, forms a complex with glycoprotein H (gH) and affects normal folding and surface expression of gH. J Virol. 1992;66(4):2240-2250.

218. Frank I, Friedman HM. A novel function of the herpes simplex virus type 1 Fc receptor: participation in bipolar bridging of antiviral immunoglobulin G. J Virol. 1989;63(11):4479-4488.

219. Thellman NM, Triezenberg SJ. Herpes Simplex Virus Establishment, Maintenance, and Reactivation: In Vitro Modeling of Latency. Pathogens. 2017;6(3).

220. Deshmane SL, Fraser NW. During latency, herpes simplex virus type 1 DNA is associated with nucleosomes in a chromatin structure. J Virol. 1989;63(2):943-947.

221. Knipe DM, Cliffe A. Chromatin control of herpes simplex virus lytic and latent infection. Nat Rev Microbiol. 2008;6(3):211-221.

222. Kukhanova MK, Korovina AN, Kochetkov SN. Human herpes simplex virus: life cycle and development of inhibitors. Biochemistry (Mosc). 2014;79(13):1635-1652.

223. Connolly SA, Jackson JO, Jardetzky TS, Longnecker R. Fusing structure and function: a structural view of the herpesvirus entry machinery. Nat Rev Microbiol. 2011;9(5):369-381.

224. Koyama AH, Uchida T. The mode of entry of herpes simplex virus type 1 into Vero cells. Microbiol Immunol. 1987;31(2):123-130.

225. Cheshenko N, Del Rosario B, Woda C, Marcellino D, Satlin LM, Herold BC. Herpes simplex virus triggers activation of calcium-signaling pathways. J Cell Biol. 2003;163(2):283-293.

226. Nicola AV, Hou J, Major EO, Straus SE. Herpes simplex virus type 1 enters human epidermal keratinocytes, but not neurons, via a pH-dependent endocytic pathway. J Virol. 2005;79(12):7609-7616.

227. Nicola AV, McEvoy AM, Straus SE. Roles for endocytosis and low pH in herpes simplex virus entry into HeLa and Chinese hamster ovary cells. J Virol. 2003;77(9):5324-5332.

228. Nicola AV, Straus SE. Cellular and viral requirements for rapid endocytic entry of herpes simplex virus. J Virol. 2004;78(14):7508-7517.

229. Milne RS, Nicola AV, Whitbeck JC, Eisenberg RJ, Cohen GH. Glycoprotein D receptor-dependent, low-pH-independent endocytic entry of herpes simplex virus type 1. J Virol. 2005;79(11):6655-6663.

230. Akhtar J, Shukla D. Viral entry mechanisms: cellular and viral mediators of herpes simplex virus entry. FEBS J. 2009;276(24):7228-7236.

231. Campadelli-Fiume G, Amasio M, Avitabile E, Cerretani A, Forghieri C, Gianni T, et al. The multipartite system that mediates entry of herpes simplex virus into the cell. Rev Med Virol. 2007;17(5):313-326.

232. Spear PG. Herpes simplex virus: receptors and ligands for cell entry. Cell Microbiol. 2004;6(5):401-410.

233. Campadelli-Fiume G, Menotti L, Avitabile E, Gianni T. Viral and cellular contributions to herpes simplex virus entry into the cell. Curr Opin Virol. 2012;2(1):28-36.

234. Arii J, Uema M, Morimoto T, Sagara H, Akashi H, Ono E, et al. Entry of herpes simplex virus 1 and other alphaherpesviruses via the paired immunoglobulin-like type 2 receptor alpha. J Virol. 2009;83(9):4520-4527.

235. Karger A, Saalmuller A, Tufaro F, Banfield BW, Mettenleiter TC. Cell surface proteoglycans are not essential for infection by pseudorabies virus. J Virol. 1995;69(6):3482-3489.

236. Banfield BW, Leduc Y, Esford L, Schubert K, Tufaro F. Sequential isolation of proteoglycan synthesis mutants by using herpes simplex virus as a selective agent: evidence for a proteoglycan- independent virus entry pathway. J Virol. 1995;69(6):3290-3298.

237. Bender FC, Whitbeck JC, Lou H, Cohen GH, Eisenberg RJ. Herpes simplex virus glycoprotein B binds to cell surfaces independently of heparan sulfate and blocks virus entry. J Virol. 2005;79(18):11588-11597.

238. Satoh T, Arii J, Suenaga T, Wang J, Kogure A, Uehori J, et al. PILRalpha is a herpes simplex virus-1 entry coreceptor that associates with glycoprotein B. Cell. 2008;132(6):935-944.

239. Gianni T, Amasio M, Campadelli-Fiume G. Herpes simplex virus gD forms distinct complexes with fusion executors gB and gH/gL in part through the C-terminal profusion domain. J Biol Chem. 2009;284(26):17370-17382.

240. Avitabile E, Forghieri C, Campadelli-Fiume G. Cross talk among the glycoproteins involved in herpes simplex virus entry and fusion: the interaction between gB and gH/gL does not necessarily require gD. J Virol. 2009;83(20):10752-10760.

241. Atanasiu D, Whitbeck JC, Cairns TM, Reilly B, Cohen GH, Eisenberg RJ. Bimolecular complementation reveals that glycoproteins gB and gH/gL of herpes simplex virus

interact with each other during cell fusion. Proc Natl Acad Sci U S A. 2007;104(47):18718-18723.

242. Lycke E, Hamark B, Johansson M, Krotochwil A, Lycke J, Svennerholm B. Herpes simplex virus infection of the human sensory neuron. An electron microscopy study. Arch Virol. 1988;101(1-2):87-104.

243. Morrison EE, Wang YF, Meredith DM. Phosphorylation of structural components promotes dissociation of the herpes simplex virus type 1 tegument. J Virol. 1998;72(9):7108-7114.

244. Morrison EE, Stevenson AJ, Wang YF, Meredith DM. Differences in the intracellular localization and fate of herpes simplex virus tegument proteins early in the infection of Vero cells. J Gen Virol. 1998;79(Pt 10):2517-2528.

245. Luxton GW, Haverlock S, Coller KE, Antinone SE, Pincetic A, Smith GA. Targeting of herpesvirus capsid transport in axons is coupled to association with specific sets of tegument proteins. Proc Natl Acad Sci U S A. 2005;102(16):5832-5837.

246. Granzow H, Klupp BG, Mettenleiter TC. Entry of pseudorabies virus: an immunogold-labeling study. J Virol. 2005;79(5):3200-3205.

247. Copeland AM, Newcomb WW, Brown JC. Herpes simplex virus replication: roles of viral proteins and nucleoporins in capsid-nucleus attachment. J Virol. 2009;83(4):1660-1668.

248. Luxton GW, Lee JI, Haverlock-Moyns S, Schober JM, Smith GA. The Pseudorabies Virus VP1/2 Tegument Protein Is Required for Intracellular Capsid Transport. J Virol. 2006;80(1):201-209.

249. Radtke K, Kieneke D, Wolfstein A, Michael K, Steffen W, Scholz T, et al. Plus- and minus-end directed microtubule motors bind simultaneously to herpes simplex virus capsids using different inner tegument structures. PLoS Pathog. 2010;6(7):e1000991.

250. Sodeik B, Ebersold MW, Helenius A. Microtubule-mediated transport of incoming herpes simplex virus 1 capsids to the nucleus. J Cell Biol. 1997;136(5):1007-1021.

251. Döhner K, Wolfstein A, Prank U, Echeverri C, Dujardin D, Vallee R, et al. Function of dynein and dynactin in herpes simplex virus capsid transport. Mol Biol Cell. 2002;13(8):2795-2809.

252. Döhner K, Radtke K, Schmidt S, Sodeik B. Eclipse phase of herpes simplex virus type 1 infection: Efficient dynein-mediated capsid transport without the small capsid protein VP26. J Virol. 2006;80(16):8211-8224.

253. Smith GA, Pomeranz L, Gross SP, Enquist LW. Local modulation of plus-end transport targets herpesvirus entry and egress in sensory axons. Proc Natl Acad Sci U S A. 2004;101(45):16034-16039.

254. Diefenbach RJ, Miranda-Saksena M, Douglas MW, Cunningham AL. Transport and egress of herpes simplex virus in neurons. Rev Med Virol. 2008;18(1):35-51.

255. Lyman MG, Enquist LW. Herpesvirus interactions with the host cytoskeleton. J Virol. 2009;83(5):2058-2066.

256. Antinone SE, Smith GA. Retrograde axon transport of herpes simplex virus and pseudorabies virus: a live-cell comparative analysis. J Virol. 2010;84(3):1504-1512.

257. Batterson W, Furlong D, Roizman B. Molecular genetics of herpes simplex virus. VIII. further characterization of a temperature-sensitive mutant defective in release of viral DNA and in other stages of the viral reproductive cycle. J Virol. 1983;45(1):397-407.

258. Knipe DM, Batterson W, Nosal C, Roizman B, Buchan A. Molecular genetics of herpes simplex virus. VI. Characterization of a temperature-sensitive mutant defective in the expression of all early viral gene products. J Virol. 1981;38(2):539-547.

259. Roberts AP, Abaitua F, O'Hare P, McNab D, Rixon FJ, Pasdeloup D. Differing roles of inner tegument proteins pUL36 and pUL37 during entry of herpes simplex virus type 1. J Virol. 2009;83(1):105-116.

260. Abaitua F, Souto RN, Browne H, Daikoku T, O'Hare P. Characterization of the herpes simplex virus (HSV)-1 tegument protein VP1-2 during infection with the HSV temperature-sensitive mutant tsB7. J Gen Virol. 2009;90(Pt 10):2353-2363.

261. Abaitua F, Daikoku T, Crump CM, Bolstad M, O'Hare P. A single mutation responsible for temperature-sensitive entry and assembly defects in the VP1-2 protein of herpes simplex virus. J Virol. 2011;85(5):2024-2036.

262. Pasdeloup D, Blondel D, Isidro AL, Rixon FJ. Herpesvirus capsid association with the nuclear pore complex and viral DNA release involve the nucleoporin CAN/Nup214 and the capsid protein pUL25. J Virol. 2009;83(13):6610-6623.

263. Benetti L, Munger J, Roizman B. The herpes simplex virus 1 US3 protein kinase blocks caspase-dependent double cleavage and activation of the proapoptotic protein BAD. J Virol. 2003;77(11):6567-6573.

264. Benetti L, Roizman B. In transduced cells, the US3 protein kinase of herpes simplex virus 1 precludes activation and induction of apoptosis by transfected procaspase 3. J Virol. 2007;81(19):10242-10248.

265. Benetti L, Roizman B. Herpes simplex virus protein kinase US3 activates and functionally overlaps protein kinase A to block apoptosis. Proc Natl Acad Sci U S A. 2004;101(25):9411-9416.

266. Smiley JR, Elgadi MM, Saffran HA. Herpes simplex virus vhs protein. Methods Enzymol. 2001;342:440-451.

267. Smiley JR. Herpes simplex virus virion host shutoff protein: immune evasion mediated by a viral RNase? J Virol. 2004;78(3):1063-1068.

268. Strom T, Frenkel N. Effects of herpes simplex virus on mRNA stability. J Virol. 1987;61(7):2198-2207.

269. Honess RW, Roizman B. Regulation of herpesvirus macromolecular synthesis: sequential transition of polypeptide synthesis requires functional viral polypeptides. Proc Natl Acad Sci U S A. 1975;72(4):1276-1280.

270. Gruffat H, Marchione R, Manet E. Herpesvirus Late Gene Expression: A Viral-Specific Pre-initiation Complex Is Key. Front Microbiol. 2016;7:869.

271. Muggeridge MI, Fraser NW. Chromosomal organization of the herpes simplex virus genome during acute infection of the mouse central nervous system. J Virol. 1986;59(3):764-767.

272. Pignatti PF, Cassai E. Analysis of herpes simplex virus nucleoprotein complexes extracted from infected cells. J Virol. 1980;36(3):816-828.

273. Oh J, Fraser NW. Temporal association of the herpes simplex virus genome with histone proteins during a lytic infection. J Virol. 2008;82(7):3530-3537.

274. Cliffe AR, Knipe DM. Herpes simplex virus ICP0 promotes both histone removal and acetylation on viral DNA during lytic infection. J Virol. 2008;82(24):12030-12038.

275. Cliffe AR, Garber DA, Knipe DM. Transcription of the herpes simplex virus latency-associated transcript promotes the formation of facultative heterochromatin on lytic promoters. J Virol. 2009;83(16):8182-8190.

276. Gu H, Liang Y, Mandel G, Roizman B. Components of the REST/CoREST/histone deacetylase repressor complex are disrupted, modified, and translocated in HSV-1-infected cells. Proc Natl Acad Sci U S A. 2005;102(21):7571-7576.

277. Gu H, Roizman B. Herpes simplex virus-infected cell protein 0 blocks the silencing of viral DNA by dissociating histone deacetylases from the CoREST-REST complex. Proc Natl Acad Sci U S A. 2007;104(43):17134-17139.

278. Herrera FJ, Triezenberg SJ. VP16-dependent association of chromatin-modifying coactivators and underrepresentation of histones at immediate-early gene promoters during herpes simplex virus infection. J Virol. 2004;78(18):9689-9696.

279. Kent JR, Zeng PY, Atanasiu D, Gardner J, Fraser NW, Berger SL. During lytic infection herpes simplex virus type 1 is associated with histones bearing modifications that correlate with active transcription. J Virol. 2004;78(18):10178-10186.

280. Huang J, Kent JR, Placek B, Whelan KA, Hollow CM, Zeng PY, et al. Trimethylation of histone H3 lysine 4 by Set1 in the lytic infection of human herpes simplex virus 1. J Virol. 2006;80(12):5740-5746.

281. Kutluay SB, Triezenberg SJ. Regulation of histone deposition on the herpes simplex virus type 1 genome during lytic infection. J Virol. 2009;83(11):5835-5845.

282. Lomonte P, Thomas J, Texier P, Caron C, Khochbin S, Epstein AL. Functional interaction between class II histone deacetylases and ICP0 of herpes simplex virus type 1. J Virol. 2004;78(13):6744-6757.

283. Mackem S, Roizman B. Structural features of the herpes simplex virus alpha gene 4, 0, and 27 promoter-regulatory sequences which confer alpha regulation on chimeric thymidine kinase genes. J Virol. 1982;44(3):939-949.

284. Garfinkle B, McAuslan BR. Regulation of herpes simplex virus-induced thymidine kinase. Biochem Biophys Res Commun. 1974;58(3):822-829.

285. Costa RH, Devi BG, Anderson KP, Gaylord BH, Wagner EK. Characterization of a major late herpes simplex virus type 1 mRNA. J Virol. 1981;38(2):483-496.

286. Jones PC, Roizman B. Regulation of herpesvirus macromolecular synthesis. VIII. The transcription program consists of three phases during which both extent of transcription and accumulation of RNA in the cytoplasm are regulated. J Virol. 1979;31(2):299-314.

287. Weller SK. HSV-1 DNA replication. In Alphaherpesviruses: Molecular Virology: Caister Academic Press; 2011. p. 89-112.

288. Olsson M, Tang KW, Persson C, Wilhelmsson LM, Billeter M, Elias P. Stepwise evolution of the herpes simplex virus origin binding protein and origin of replication. J Biol Chem. 2009;284(24):16246-16255.

289. Chattopadhyay S, Weller SK. DNA binding activity of the herpes simplex virus type 1 origin binding protein, UL9, can be modulated by sequences in the N terminus: correlation between transdominance and DNA binding. J Virol. 2006;80(9):4491-4500.

290. Makhov AM, Boehmer PE, Lehman IR, Griffith JD. The herpes simplex virus type 1 origin-binding protein carries out origin specific DNA unwinding and forms stem-loop structures. EMBO J. 1996;15(7):1742-1750.

291. Makhov AM, Lee SS, Lehman IR, Griffith JD. Origin-specific unwinding of herpes simplex virus 1 DNA by the viral UL9 and ICP8 proteins: visualization of a specific preunwinding complex. Proc Natl Acad Sci U S A. 2003;100(3):898-903.

292. Makhov AM, Sen A, Yu X, Simon MN, Griffith JD, Egelman EH. The bipolar filaments formed by herpes simplex virus type 1 SSB/recombination protein (ICP8) suggest a mechanism for DNA annealing. J Mol Biol. 2009;386(2):273-279.

293. Chattopadhyay S, Chen Y, Weller SK. The two helicases of herpes simplex virus type 1 (HSV-1). Front Biosci. 2006;11:2213-2223.

294. Weller SK. Herpes simplex virus reorganizes the cellular DNA repair and protein quality control machinery. PLoS Pathog. 2010;6(11):e1001105.

295. Everett RD, Sourvinos G, Orr A. Recruitment of herpes simplex virus type 1 transcriptional regulatory protein ICP4 into foci juxtaposed to ND10 in live, infected cells. J Virol. 2003;77(6):3680-3689.

296. Garber DA, Beverley SM, Coen DM. Demonstration of circularization of herpes simplex virus DNA following infection using pulsed field gel electrophoresis. Virology. 1993;197(1):459-462.

297. Strang BL, Stow ND. Circularization of the herpes simplex virus type 1 genome upon lytic infection. J Virol. 2005;79(19):12487-12494.

298. Everett RD, Zafiropoulos A. Visualization by live-cell microscopy of disruption of ND10 during herpes simplex virus type 1 infection. J Virol. 2004;78(20):11411-11415.

299. Everett RD, Sourvinos G, Leiper C, Clements JB, Orr A. Formation of nuclear foci of the herpes simplex virus type 1 regulatory protein ICP4 at early times of infection: localization, dynamics, recruitment of ICP27, and evidence for the de novo induction of ND10-like complexes. J Virol. 2004;78(4):1903-1917.

300. Boutell C, Canning M, Orr A, Everett RD. Reciprocal activities between herpes simplex virus type 1 regulatory protein ICP0, a ubiquitin E3 ligase, and ubiquitin-specific protease USP7. J Virol. 2005;79(19):12342-12354.

301. Everett RD, Murray J. ND10 components relocate to sites associated with herpes simplex virus type 1 nucleoprotein complexes during virus infection. J Virol. 2005;79(8):5078-5089.

302. Boutell C, Everett R, Hilliard J, Schaffer P, Orr A, Davido D. HSV-1 ICP0 phosphorylation mutants impair the E3 ubiquitin ligase activity of ICP0 in a cell type manner. J Virol. 2008.

303. Livingston CM, DeLuca NA, Wilkinson DE, Weller SK. Oligomerization of ICP4 and rearrangement of heat shock proteins may be important for herpes simplex virus type 1 prereplicative site formation. J Virol. 2008;82(13):6324-6336.

304. Pires de Mello CP, Bloom DC, Paixao IC. Herpes simplex virus type-1: replication, latency, reactivation and its antiviral targets. Antivir Ther. 2016;21(4):277-286.

305. Boehmer PE, Lehman IR. Herpes simplex virus DNA replication. Annu Rev Biochem. 1997;66:347-384.

306. Aslani A, Olsson M, Elias P. ATP-dependent unwinding of a minimal origin of DNA replication by the origin-binding protein and the single-strand DNA-binding protein ICP8 from herpes simplex virus type I. J Biol Chem. 2002;277(43):41204-41212.

307. Macao B, Olsson M, Elias P. Functional properties of the herpes simplex virus type I origin-binding protein are controlled by precise interactions with the activated form of the origin of DNA replication. J Biol Chem. 2004;279(28):29211-29217.

308. Taylor TJ, Brockman MA, McNamee EE, Knipe DM. Herpes simplex virus. Front Biosci. 2002;7:d752-764.

309. Marsden HS, Cross AM, Francis GJ, Patel AH, MacEachran K, Murphy M, et al. The herpes simplex virus type 1 UL8 protein influences the intracellular localization of the UL52 but not the ICP8 or POL replication proteins in virus-infected cells. J Gen Virol. 1996;77 (Pt 9):2241-2249.

310. Carrington-Lawrence SD, Weller SK. Recruitment of polymerase to herpes simplex virus type 1 replication foci in cells expressing mutant primase (UL52) proteins. J Virol. 2003;77(7):4237-4247.

311. Kennard J, Rixon FJ, McDougall IM, Tatman JD, Preston VG. The 25 amino acid residues at the carboxy terminus of the herpes simplex virus type 1 UL26.5 protein are required for the formation of the capsid shell around the scaffold. J Gen Virol. 1995;76(Pt 7):1611-1621.

312. Henry BE, Newcomb WW, O'Callaghan DJ. Alterations in virus protein synthesis and capsid production in infection with DI particles of herpesvirus. J Gen Virol. 1980;47(2):343-353.

313. Huffman JB, Newcomb WW, Brown JC, Homa FL. Amino acids 143 to 150 of the herpes simplex virus type 1 scaffold protein are required for the formation of portal-containing capsids. J Virol. 2008;82(13):6778-6781.

314. Spencer JV, Newcomb WW, Thomsen DR, Homa FL, Brown JC. Assembly of the herpes simplex virus capsid: preformed triplexes bind to the nascent capsid. J Virol. 1998;72(5):3944-3951.

315. Thomsen DR, Newcomb WW, Brown JC, Homa FL. Assembly of the herpes simplex virus capsid: requirement for the carboxyl-terminal twenty-five amino acids of the proteins encoded by the UL26 and UL26.5 genes. J Virol. 1995;69(6):3690-3703.

316. Newcomb WW, Homa FL, Thomsen DR, Trus BL, Cheng N, Steven A, et al. Assembly of the herpes simplex virus procapsid from purified components and identification of small complexes containing the major capsid and scaffolding proteins. J Virol. 1999;73(5):4239-4250.

317. Homa FL, Brown JC. Capsid assembly and DNA packaging in herpes simplex virus. Rev Med Virol. 1997;7(2):107-122.

318. Newcomb WW, Homa FL, Thomsen DR, Ye Z, Brown JC. Cell-free assembly of the herpes simplex virus capsid. J Virol. 1994;68(9):6059-6063.

319. Newcomb WW, Homa FL, Brown JC. Herpes simplex virus capsid structure: DNA packaging protein UL25 is located on the external surface of the capsid near the vertices. J Virol. 2006;80(13):6286-6294.

320. Trus BL, Booy FP, Newcomb WW, Brown JC, Homa FL, Thomsen DR, et al. The herpes simplex virus procapsid: structure, conformational changes upon maturation, and roles of the triplex proteins VP19c and VP23 in assembly. J Mol Biol. 1996;263(3):447-462.

321. Newcomb WW, Homa FL, Thomsen DR, Booy FP, Trus BL, Steven AC, et al. Assembly of the herpes simplex virus capsid: characterization of intermediates observed during cell-free capsid formation. J Mol Biol. 1996;263(3):432-446.

322. Liu F, Roizman B. Characterization of the protease and other products of amino-terminus- proximal cleavage of the herpes simplex virus 1 UL26 protein. J Virol. 1993;67(3):1300-1309.

323. Rixon FJ, Cross AM, Addison C, Preston VG. The products of herpes simplex virus type 1 gene UL26 which are involved in DNA packaging are strongly associated with empty but not with full capsids. J Gen Virol. 1988;69(Pt 11):2879-2891.

324. Nicholson P, Addison C, Cross AM, Kennard J, Preston VG, Rixon FJ. Localization of the herpes simplex virus type 1 major capsid protein VP5 to the cell nucleus requires the abundant scaffolding protein VP22a. J Gen Virol. 1994;75(Pt 5):1091-1099.

325. Tatman JD, Preston VG, Nicholson P, Elliott RM, Rixon FJ. Assembly of herpes simplex virus type 1 capsids using a panel of recombinant baculoviruses. J Gen Virol. 1994;75(Pt 5):1101-1113.

326. Rixon FJ, Addison C, McGregor A, Macnab SJ, Nicholson P, Preston VG, et al. Multiple interactions control the intracellular localization of the herpes simplex virus type 1 capsid proteins. J Gen Virol. 1996;77(Pt 9):2251-2260.

327. Desai P, Person S. Molecular interactions between the HSV-1 capsid proteins as measured by the yeast two-hybrid system. Virology. 1996;220(2):516-521.

328. Walters JN, Sexton GL, McCaffery JM, Desai P. Mutation of single hydrophobic residue I27, L35, F39, L58, L65, L67, or L71 in the N terminus of VP5 abolishes interaction with the scaffold protein and prevents closure of herpes simplex virus type 1 capsid shells. J Virol. 2003;77(7):4043-4059.

329. Chang JT, Schmid MF, Rixon FJ, Chiu W. Electron cryotomography reveals the portal in the herpesvirus capsid. J Virol. 2007;81(4):2065-2068.

330. Newcomb WW, Thomsen DR, Homa FL, Brown JC. Assembly of the herpes simplex virus capsid: identification of soluble scaffold-portal complexes and their role in formation of portal-containing capsids. J Virol. 2003;77(18):9862-9871.

331. Baines JD. Herpes simplex virus capsid assembly and DNA packaging: a present and future antiviral drug target. Trends Microbiol. 2011;19(12):606-613.

332. Albright BS, Nellissery J, Szczepaniak R, Weller SK. Disulfide Bond Formation in the HSV-1 UL6 Protein is Required for Portal Ring Formation and Genome Encapsidation. J Virol. 2011.

333. Nellissery JK, Szczepaniak R, Lamberti C, Weller SK. A putative leucine zipper within the herpes simplex virus type 1 UL6 protein is required for portal ring formation. J Virol. 2007;81(17):8868-8877.

334. Singer GP, Newcomb WW, Thomsen DR, Homa FL, Brown JC. Identification of a region in the herpes simplex virus scaffolding protein required for interaction with the portal. J Virol. 2005;79(1):132-139.

335. Yang K, Baines JD. Domain within herpes simplex virus 1 scaffold proteins required for interaction with portal protein in infected cells and incorporation of the portal vertex into capsids. J Virol. 2008;82(10):5021-5030.

336. Yang K, Baines JD. Proline and tyrosine residues in scaffold proteins of herpes simplex virus 1 critical to the interaction with portal protein and its incorporation into capsids. J Virol. 2009;83(16):8076-8081.

337. Newcomb WW, Trus BL, Cheng N, Steven AC, Sheaffer AK, Tenney DJ, et al. Isolation of herpes simplex virus procapsids from cells infected with a protease-deficient mutant virus. J Virol. 2000;74(4):1663-1673.

338. Rixon FJ, McNab D. Packaging-competent capsids of a herpes simplex virus temperature-sensitive mutant have properties similar to those of in vitro-assembled procapsids. J Virol. 1999;73(7):5714-5721.

339. Gao M, Matusick-Kumar L, Hurlburt W, DiTusa SF, Newcomb WW, Brown JC, et al. The protease of herpes simplex virus type 1 is essential for functional capsid formation and viral growth. J Virol. 1994;68(6):3702-3712.

340. Robertson BJ, McCann PJ, 3rd, Matusick-Kumar L, Newcomb WW, Brown JC, Colonno RJ, et al. Separate functional domains of the herpes simplex virus type 1 protease: evidence for cleavage inside capsids. J Virol. 1996;70(7):4317-4328.

341. Sheaffer AK, Newcomb WW, Gao M, Yu D, Weller SK, Brown JC, et al. Herpes simplex virus DNA cleavage and packaging proteins associate with the procapsid prior to its maturation. J Virol. 2001;75(2):687-698.

342. Roos WH, Radtke K, Kniesmeijer E, Geertsema H, Sodeik B, Wuite GJ. Scaffold expulsion and genome packaging trigger stabilization of herpes simplex virus capsids. Proc Natl Acad Sci U S A. 2009;106(24):9673-9678.

343. Homa FL, Huffman JB, Toropova K, Lopez HR, Makhov AM, Conway JF, et al. Structure of the pseudorabies virus capsid: comparison with herpes simplex virus type 1 and differential binding of essential minor proteins. J Mol Biol. 2013;425(18):3415-3428.

344. Addison C, Rixon FJ, Preston VG. Herpes simplex virus type 1 UL28 gene product is important for the formation of mature capsids. J Gen Virol. 1990;71(Pt 10):2377-2384.

345. McNab AR, Desai P, Person S, Roof LL, Thomsen DR, Newcomb WW, et al. The product of the herpes simplex virus type 1 UL25 gene is required for encapsidation but not for cleavage of replicated viral DNA. J Virol. 1998;72(2):1060-1070.

346. al-Kobaisi MF, Rixon FJ, McDougall I, Preston VG. The herpes simplex virus UL33 gene product is required for the assembly of full capsids. Virology. 1991;180(1):380-388.

347. Baines JD, Poon AP, Rovnak J, Roizman B. The herpes simplex virus 1 UL15 gene encodes two proteins and is required for cleavage of genomic viral DNA. J Virol. 1994;68(12):8118-8124.

348. Poon AP, Roizman B. Characterization of a temperature-sensitive mutant of the UL15 open reading frame of herpes simplex virus 1. J Virol. 1993;67(8):4497-4503.

349. Salmon B, Cunningham C, Davison AJ, Harris WJ, Baines JD. The herpes simplex virus type 1 U(L)17 gene encodes virion tegument proteins that are required for cleavage and packaging of viral DNA. J Virol. 1998;72(5):3779-3788.

350. Tengelsen LA, Pederson NE, Shaver PR, Wathen MW, Homa FL. Herpes simplex virus type 1 DNA cleavage and encapsidation require the product of the UL28 gene: isolation and characterization of two UL28 deletion mutants. J Virol. 1993;67(6):3470-3480.

351. Cockrell SK, Sanchez ME, Erazo A, Homa FL. Role of the UL25 protein in herpes simplex virus DNA encapsidation. J Virol. 2009;83(1):47-57.

352. Beard PM, Taus NS, Baines JD. DNA cleavage and packaging proteins encoded by genes U(L)28, U(L)15, and U(L)33 of herpes simplex virus type 1 form a complex in infected cells. J Virol. 2002;76(10):4785-4791.

353. Beard PM, Baines JD. The DNA cleavage and packaging protein encoded by the UL33 gene of herpes simplex virus 1 associates with capsids. Virology. 2004;324(2):475-482.

354. Beilstein F, Higgs MR, Stow ND. Mutational analysis of the herpes simplex virus type 1 DNA packaging protein UL33. J Virol. 2009.

355. Higgs MR, Preston VG, Stow ND. The UL15 protein of herpes simplex virus type 1 is necessary for the localization of the UL28 and UL33 proteins to viral DNA replication centres. J Gen Virol. 2008;89(Pt 7):1709-1715.

356. Loret S, El Bilali N, Lippé R. Analysis of herpes simplex virus type I nuclear particles by flow cytometry. Cytometry A. 2012;81(11):950-959.

357. Tandon R, Mocarski ES, Conway JF. The A, B, Cs of herpesvirus capsids. Viruses. 2015;7(3):899-914.

358. Fan WH, Roberts AP, McElwee M, Bhella D, Rixon FJ, Lauder R. The large tegument protein pUL36 is essential for formation of the capsid vertex-specific component at the capsid-tegument interface of herpes simplex virus 1. J Virol. 2015;89(3):1502-1511.

359. Mettenleiter TC, Muller F, Granzow H, Klupp BG. The way out: what we know and do not know about herpesvirus nuclear egress. Cell Microbiol. 2013;15(2):170-178.

360. Dong C, Skalak R, Sung KL. Cytoplasmic rheology of passive neutrophils. Biorheology. 1991;28(6):557-567.

361. Versaevel M, Grevesse T, Gabriele S. Spatial coordination between cell and nuclear shape within micropatterned endothelial cells. Nature communications. 2012;3:671.

362. Guilak F, Tedrow JR, Burgkart R. Viscoelastic properties of the cell nucleus. Biochem Biophys Res Commun. 2000;269(3):781-786.

363. Mettenleiter TC, Minson T, Wild P. Egress of alphaherpesviruses. J Virol. 2006;80(3):1610-1612.

364. Campadelli-Fiume G, Roizman B. The egress of herpesviruses from cells: the unanswered questions. J Virol. 2006;80(13):6716-6717; author replies 6717-6719.

365. Mettenleiter TC, Minson T. Egress of alphaherpesviruses. J Virol. 2006;80(3):1610-1611; author reply 1611-1612.

366. Johnson DC, Spear PG. Monensin inhibits the processing of herpes simplex virus glycoproteins, their transport to the cell surface, and the egress of virions from infected cells. J Virol. 1982;43(3):1102-1112.

367. Granzow H, Klupp BG, Fuchs W, Veits J, Osterrieder N, Mettenleiter TC. Egress of alphaherpesviruses: comparative ultrastructural study. J Virol. 2001;75(8):3675-3684.

368. Reynolds AE, Wills EG, Roller RJ, Ryckman BJ, Baines JD. Ultrastructural localization of the herpes simplex virus type 1 UL31, UL34, and US3 proteins suggests specific roles in primary envelopment and egress of nucleocapsids. J Virol. 2002;76(17):8939-8952.

369. Fuchs W, Klupp BG, Granzow H, Osterrieder N, Mettenleiter TC. The interacting UL31 and UL34 gene products of pseudorabies virus are involved in egress from the host-cell nucleus and represent components of primary enveloped but not mature virions. J Virol. 2002;76(1):364-378.

370. Wild P, Engels M, Senn C, Tobler K, Ziegler U, Schraner EM, et al. Impairment of nuclear pores in bovine herpesvirus 1-infected MDBK cells. J Virol. 2005;79(2):1071-1083.

371. Leuzinger H, Ziegler U, Schraner EM, Fraefel C, Glauser DL, Heid I, et al. Herpes simplex virus 1 envelopment follows two diverse pathways. J Virol. 2005;79(20):13047-13059.

372. Hetzer MW. The nuclear envelope. Cold Spring Harb Perspect Biol. 2010;2(3):a000539.

373. Doucet CM, Hetzer MW. Nuclear pore biogenesis into an intact nuclear envelope. Chromosoma. 2010;119(5):469-477.

374. Pante N, Kann M. Nuclear pore complex is able to transport macromolecules with diameters of about 39 nm. Mol Biol Cell. 2002;13(2):425-434.

375. Wild P, Senn C, Manera CL, Sutter E, Schraner EM, Tobler K, et al. Exploring the nuclear envelope of herpes simplex virus 1-infected cells by high-resolution microscopy. J Virol. 2009;83(1):408-419.

376. Hofemeister H, O'Hare P. Nuclear pore composition and gating in herpes simplex virus-infected cells. J Virol. 2008;82(17):8392-8399.

377. Granzow H, Klupp B, Fuchs W, Veits J, Osterrieder N, Mettenleiter T. Egress of alphaherpesviruses: comparative ultrastructural study. J Virol. 2001;75:3675 - 3684.

378. Mettenleiter TC. Herpesvirus assembly and egress. J Virol. 2002;76(4):1537-1547.

379. Mettenleiter T. Budding events in herpesvirus morphogenesis. Virus Res. 2004;106:167 - 180.

380. Mettenleiter TC, Klupp BG, Granzow H. Herpesvirus assembly: a tale of two membranes. Curr Opin Microbiol. 2006;9(4):423-429.

381. Mettenleiter TC, Klupp BG, Granzow H. Herpesvirus assembly: an update. Virus Res. 2009;143(2):222-234.

382. Passvogel L, Trube P, Schuster F, Klupp BG, Mettenleiter TC. Mapping of sequences in Pseudorabies Virus pUL34 required for formation and function of the nuclear egress complex. J Virol. 2013.

383. Johnson DC, Baines JD. Herpesviruses remodel host membranes for virus egress. Nat Rev Microbiol. 2011;9(5):382-394.

384. Smith GA. Assembly and Egress of an Alphaherpesvirus Clockwork. In: Osterrieder K, editor. Cell Biology of Herpes Viruses. Cham: Springer International Publishing; 2017. p. 171-193.

385. Bailer SM. Venture from the Interior-Herpesvirus pUL31 Escorts Capsids from Nucleoplasmic Replication Compartments to Sites of Primary Envelopment at the Inner Nuclear Membrane. Cells. 2017;6(4).

386. Lee CP, Chen MR. Escape of herpesviruses from the nucleus. Rev Med Virol. 2010;20(4):214-230.

387. Turcotte S, Letellier J, Lippé R. Herpes simplex virus type 1 capsids transit by the trans-Golgi network, where viral glycoproteins accumulate independently of capsid egress. J Virol. 2005;79(14):8847-8860.

388. Rémillard-Labrosse G, Guay G, Lippé R. Reconstitution of herpes simplex virus type 1 nuclear capsid egress in vitro. J Virol. 2006;80(19):9741-9753.

389. Skepper JN, Whiteley A, Browne H, Minson A. Herpes simplex virus nucleocapsids mature to progeny virions by an envelopment --> deenvelopment --> reenvelopment pathway. J Virol. 2001;75(12):5697-5702.

390. Chang YE, Roizman B. The product of the UL31 gene of herpes simplex virus 1 is a nuclear phosphoprotein which partitions with the nuclear matrix. J Virol. 1993;67(11):6348-6356.

391. Roller RJ, Zhou Y, Schnetzer R, Ferguson J, DeSalvo D. Herpes simplex virus type 1 U(L)34 gene product is required for viral envelopment. J Virol. 2000;74(1):117-129.

392. Klupp BG, Granzow H, Keil GM, Mettenleiter TC. The capsid-associated UL25 protein of the alphaherpesvirus pseudorabies virus is nonessential for cleavage and encapsidation of genomic DNA but is required for nuclear egress of capsids. J Virol. 2006;80(13):6235-6246.

393. Leelawong M, Guo D, Smith GA. A physical link between the pseudorabies virus capsid and the nuclear egress complex. J Virol. 2011;85(22):11675-11684.

394. Hellberg T, Paßvogel L, Schulz KS, Klupp BG, Mettenleiter TC. Chapter Three - Nuclear Egress of Herpesviruses: The Prototypic Vesicular Nucleocytoplasmic Transport. In: Kielian M, Maramorosch K, Mettenleiter TC, editors. Advances in Virus Research. 94: Academic Press; 2016. p. 81-140.

395. Yang K, Baines JD. Selection of HSV capsids for envelopment involves interaction between capsid surface components pUL31, pUL17, and pUL25. Proc Natl Acad Sci U S A. 2011;108(34):14276-14281.

396. Yang K, Wills E, Lim HY, Zhou ZH, Baines JD. Association of Herpes Simplex Virus pUL31 with Capsid Vertices and Components of the Capsid Vertex Specific Complex. J Virol. 2014.

397. Fossum E, Friedel CC, Rajagopala SV, Titz B, Baiker A, Schmidt T, et al. Evolutionarily conserved herpesviral protein interaction networks. PLoS Pathog. 2009;5(9):e1000570.

398. Klupp BG, Granzow H, Mettenleiter TC. Effect of the pseudorabies virus US3 protein on nuclear membrane localization of the UL34 protein and virus egress from the nucleus. J Gen Virol. 2001;82(Pt 10):2363-2371.

399. Mou F, Wills E, Baines JD. Phosphorylation of the UL31 protein of herpes simplex virus 1 by the US3 encoded kinase regulates localization of the nuclear envelopment complex and egress of nucleocapsids. J Virol. 2009;83(10):5181-5191.

400. Reynolds AE, Ryckman BJ, Baines JD, Zhou Y, Liang L, Roller RJ. U(L)31 and U(L)34 proteins of herpes simplex virus type 1 form a complex that accumulates at the nuclear rim and is required for envelopment of nucleocapsids. J Virol. 2001;75(18):8803-8817.

401. Wills E, Mou F, Baines JD. The U(L)31 and U(L)34 gene products of herpes simplex virus 1 are required for optimal localization of viral glycoproteins D and M to the inner nuclear membranes of infected cells. J Virol. 2009;83(10):4800-4809.

402. Klupp BG, Granzow H, Mettenleiter TC. Primary envelopment of pseudorabies virus at the nuclear membrane requires the UL34 gene product. J Virol. 2000;74(21):10063-10073.

403. Fuchs W, Klupp BG, Granzow H, Hengartner C, Brack A, Mundt A, et al. Physical interaction between envelope glycoproteins E and M of pseudorabies virus and the major tegument protein UL49. J Virol. 2002;76(16):8208-8217.

404. Roller RJ, Bjerke SL, Haugo AC, Hanson S. Analysis of a charge cluster mutation of herpes simplex virus type 1 UL34 and its extragenic suppressor suggests a novel interaction between pUL34 and pUL31 that is necessary for membrane curvature around capsids. J Virol. 2010;84(8):3921-3934.

405. Dechat T, Pfleghaar K, Sengupta K, Shimi T, Shumaker DK, Solimando L, et al. Nuclear lamins: major factors in the structural organization and function of the nucleus and chromatin. Genes Dev. 2008;22(7):832-853.

406. Mou F, Forest T, Baines JD. US3 of herpes simplex virus type 1 encodes a promiscuous protein kinase that phosphorylates and alters localization of lamin A/C in infected cells. J Virol. 2007;81(12):6459-6470.

407. Cano-Monreal GL, Wylie KM, Cao F, Tavis JE, Morrison LA. Herpes simplex virus 2 UL13 protein kinase disrupts nuclear lamins. Virology. 2009.

408. Milbradt J, Webel R, Auerochs S, Sticht H, Marschall M. Novel mode of phosphorylation-triggered reorganization of the nuclear lamina during nuclear egress of human cytomegalovirus. J Biol Chem. 2010;285(18):13979-13989.

409. Mou F, Wills EG, Park R, Baines JD. Effects of lamin A/C, lamin B1, and viral US3 kinase activity on viral infectivity, virion egress, and the targeting of herpes simplex virus UL34 encoded protein to the inner nuclear membrane. J Virol. 2008;82(16):8094-8104.

410. Kato A, Yamamoto M, Ohno T, Tanaka M, Sata T, Nishiyama Y, et al. Herpes simplex virus 1-encoded protein kinase UL13 phosphorylates viral Us3 protein kinase and

regulates nuclear localization of viral envelopment factors UL34 and UL31. J Virol. 2006;80(3):1476-1486.

411. Gershburg S, Geltz J, Peterson KE, Halford WP, Gershburg E. The UL13 and US3 Protein Kinases of Herpes Simplex Virus 1 Cooperate to Promote the Assembly and Release of Mature, Infectious Virions. PLoS One. 2015;10(6):e0131420.

412. Bjerke SL, Roller RJ. Roles for herpes simplex virus type 1 U(L)34 and U(S)3 proteins in disrupting the nuclear lamina during herpes simplex virus type 1 egress. Virology. 2006;347(2):261-276.

413. Park R, Baines JD. Herpes simplex virus type 1 infection induces activation and recruitment of protein kinase C to the nuclear membrane and increased phosphorylation of lamin B. J Virol. 2006;80(1):494-504.

414. Reynolds AE, Liang L, Baines JD. Conformational changes in the nuclear lamina induced by herpes simplex virus type 1 require genes U(L)31 and U(L)34. J Virol. 2004;78(11):5564-5575.

415. Simpson-Holley M, Colgrove RC, Nalepa G, Harper JW, Knipe DM. Identification and functional evaluation of cellular and viral factors involved in the alteration of nuclear architecture during herpes simplex virus 1 infection. J Virol. 2005;79(20):12840-12851.

416. Bosse JB, Hogue IB, Feric M, Thiberge SY, Sodeik B, Brangwynne CP, et al. Remodeling nuclear architecture allows efficient transport of herpesvirus capsids by diffusion. Proc Natl Acad Sci U S A. 2015;112(42):E5725-5733.

417. Baines JD, Wills E, Jacob RJ, Pennington J, Roizman B. Glycoprotein M of herpes simplex virus 1 is incorporated into virions during budding at the inner nuclear membrane. J Virol. 2007;81(2):800-812.

418. Stannard LM, Himmelhoch S, Wynchank S. Intra-nuclear localization of two envelope proteins, gB and gD, of herpes simplex virus. Arch Virol. 1996;141(3-4):505-524.

419. Naldinho-Souto R, Browne H, Minson T. Herpes simplex virus tegument protein VP16 is a component of primary enveloped virions. J Virol. 2006;80(5):2582-2584.

420. Liu Z, Kato A, Shindo K, Noda T, Sagara H, Kawaoka Y, et al. Herpes simplex virus 1 UL47 interacts with viral nuclear egress factors UL31, UL34, and Us3 and regulates viral nuclear egress. J Virol. 2014;88(9):4657-4667.

421. Kato A, Liu Z, Minowa A, Imai T, Tanaka M, Sugimoto K, et al. Herpes Simplex Virus 1 Protein Kinase Us3 and Major Tegument Protein UL47 Reciprocally Regulate Their Subcellular Localization in Infected Cells. J Virol. 2011;85(18):9599-9613.

422. Padula ME, Sydnor ML, Wilson DW. Isolation and preliminary characterization of herpes simplex virus 1 primary enveloped virions from the perinuclear space. J Virol. 2009;83(10):4757-4765.

423. Read GS, Patterson M. Packaging of the virion host shutoff (Vhs) protein of herpes simplex virus: two forms of the Vhs polypeptide are associated with intranuclear B and C capsids, but only one is associated with enveloped virions. J Virol. 2007;81(3):1148-1161.

424. Baines JD, Hsieh CE, Wills E, Mannella C, Marko M. Electron tomography of nascent herpes simplex virus virions. J Virol. 2007;81(6):2726-2735.

425. Leach N, Bjerke SL, Christensen DK, Bouchard JM, Mou F, Park R, et al. Emerin is hyperphosphorylated and redistributed in herpes simplex virus type 1-infected cells in a manner dependent on both UL34 and US3. J Virol. 2007;81(19):10792-10803.

426. Ryckman BJ, Roller RJ. Herpes simplex virus type 1 primary envelopment: UL34 protein modification and the US3-UL34 catalytic relationship. J Virol. 2004;78(1):399-412.

427. Schumacher D, Tischer BK, Trapp S, Osterrieder N. The protein encoded by the US3 orthologue of Marek's disease virus is required for efficient de-envelopment of

perinuclear virions and involved in actin stress fiber breakdown. J Virol. 2005;79(7):3987-3997.

428. Roller RJ, Baines JD. Herpesvirus Nuclear Egress. In: Osterrieder K, editor. Cell Biology of Herpes Viruses. Cham: Springer International Publishing; 2017. p. 143-169.

429. Weed DJ, Nicola AV. Herpes simplex virus Membrane Fusion. In: Osterrieder K, editor. Cell Biology of Herpes Viruses. Cham: Springer International Publishing; 2017. p. 29-47.

430. Cai WZ, Person S, Warner SC, Zhou JH, DeLuca NA. Linker-insertion nonsense and restriction-site deletion mutations of the gB glycoprotein gene of herpes simplex virus type 1. J Virol. 1987;61(3):714-721.

431. Forrester A, Farrell H, Wilkinson G, Kaye J, Davis-Poynter N, Minson T. Construction and properties of a mutant of herpes simplex virus type 1 with glycoprotein H coding sequences deleted. J Virol. 1992;66(1):341-348.

432. Roop C, Hutchinson L, Johnson DC. A mutant herpes simplex virus type 1 unable to express glycoprotein L cannot enter cells, and its particles lack glycoprotein H. J Virol. 1993;67(4):2285-2297.

433. Hutchinson L, Johnson DC. Herpes simplex virus glycoprotein K promotes egress of virus particles. J Virol. 1995;69(9):5401-5413.

434. Baines JD, Ward PL, Campadelli-Fiume G, Roizman B. The UL20 gene of herpes simplex virus 1 encodes a function necessary for viral egress. J Virol. 1991;65(12):6414-6424.

435. Mossman KL, Sherburne R, Lavery C, Duncan J, Smiley JR. Evidence that herpes simplex virus VP16 is required for viral egress downstream of the initial envelopment event. J Virol. 2000;74(14):6287-6299.

436. Nozawa N, Kawaguchi Y, Tanaka M, Kato A, Kimura H, Nishiyama Y. Herpes simplex virus type 1 UL51 protein is involved in maturation and egress of virus particles. J Virol. 2005;79(11):6947-6956.

437. Hirohata Y, Arii J, Liu Z, Shindo K, Oyama M, Kozuka-Hata H, et al. Herpes Simplex Virus 1 Recruits CD98 Heavy Chain and beta1 Integrin to the Nuclear Membrane for Viral De-Envelopment. J Virol. 2015;89(15):7799-7812.

438. Liu Z, Kato A, Oyama M, Kozuka-Hata H, Arii J, Kawaguchi Y. Role of Host Cell p32 in Herpes Simplex Virus 1 De-Envelopment during Viral Nuclear Egress. J Virol. 2015;89(17):8982-8998.

439. Wang Y, Yang Y, Wu S, Pan S, Zhou C, Ma Y, et al. p32 Is a Novel Target for Viral Protein ICP34.5 of Herpes Simplex Virus Type 1 and Facilitates Viral Nuclear Egress. J Biol Chem. 2014;289(52):35795-35805.

440. Maric M, Shao J, Ryan RJ, Wong CS, Gonzalez-Alegre P, Roller RJ. A functional role for TorsinA in herpes simplex virus 1 nuclear egress. J Virol. 2011;85(19):9667-9679.

441. Sosa BA, Rothballer A, Kutay U, Schwartz TU. LINC complexes form by binding of three KASH peptides to domain interfaces of trimeric SUN proteins. Cell. 2012;149(5):1035-1047.

442. Starr DA, Fridolfsson HN. Interactions between nuclei and the cytoskeleton are mediated by SUN-KASH nuclear-envelope bridges. Annu Rev Cell Dev Biol. 2010;26:421-444.

443. Crisp M, Liu Q, Roux K, Rattner JB, Shanahan C, Burke B, et al. Coupling of the nucleus and cytoplasm: role of the LINC complex. J Cell Biol. 2006;172(1):41-53.

444. Sosa BA, Kutay U, Schwartz TU. Structural insights into LINC complexes. Curr Opin Struct Biol. 2013;23(2):285-291.

445. Cain NE, Starr DA. SUN proteins and nuclear envelope spacing. Nucleus. 2015;6(1):2-7.

446. Rothballer A, Schwartz TU, Kutay U. LINCing complex functions at the nuclear envelope: what the molecular architecture of the LINC complex can reveal about its function. Nucleus. 2013;4(1):29-36.

447. Gundersen GG, Worman HJ. Nuclear positioning. Cell. 2013;152(6):1376-1389.

448. Lombardi ML, Jaalouk DE, Shanahan CM, Burke B, Roux KJ, Lammerding J. The interaction between nesprins and sun proteins at the nuclear envelope is critical for force transmission between the nucleus and cytoskeleton. J Biol Chem. 2011;286(30):26743-26753.

449. Lombardi ML, Lammerding J. Keeping the LINC: the importance of nucleocytoskeletal coupling in intracellular force transmission and cellular function. Biochem Soc Trans. 2011;39(6):1729-1734.

450. Klupp BG, Hellberg T, Granzow H, Franzke K, Dominguez Gonzalez B, Goodchild RE, et al. Integrity of the Linker of Nucleoskeleton and Cytoskeleton Is Required for Efficient Herpesvirus Nuclear Egress. J Virol. 2017;91(19).

451. Chang YE, Van Sant C, Krug PW, Sears AE, Roizman B. The null mutant of the U(L)31 gene of herpes simplex virus 1: construction and phenotype in infected cells. J Virol. 1997;71(11):8307-8315.

452. Liang L, Tanaka M, Kawaguchi Y, Baines JD. Cell lines that support replication of a novel herpes simplex virus 1 UL31 deletion mutant can properly target UL34 protein to the nuclear rim in the absence of UL31. Virology. 2004;329(1):68-76.

453. Maric M, Haugo AC, Dauer W, Johnson D, Roller RJ. Nuclear envelope breakdown induced by herpes simplex virus type 1 involves the activity of viral fusion proteins. Virology. 2014;460-461:128-137.

454. Lee JH, Vittone V, Diefenbach E, Cunningham AL, Diefenbach RJ. Identification of structural protein-protein interactions of herpes simplex virus type 1. Virology. 2008;378(2):347-354.

455. Mettenleiter TC. Intriguing interplay between viral proteins during herpesvirus assembly or: the herpesvirus assembly puzzle. Vet Microbiol. 2006;113(3-4):163-169.

456. Vittone V, Diefenbach E, Triffett D, Douglas MW, Cunningham AL, Diefenbach RJ. Determination of Interactions between Tegument Proteins of Herpes Simplex Virus Type 1. J Virol. 2005;79(15):9566-9571.

457. Schipke J, Pohlmann A, Diestel R, Binz A, Rudolph K, Nagel CH, et al. The C terminus of the large tegument protein pUL36 contains multiple capsid binding sites that function differently during assembly and cell entry of herpes simplex virus. J Virol. 2012;86(7):3682-3700.

458. Bucks MA, O'Regan KJ, Murphy MA, Wills JW, Courtney RJ. Herpes simplex virus type 1 tegument proteins VP1/2 and UL37 are associated with intranuclear capsids. Virology. 2007;361(2):316-324.

459. Donnelly M, Elliott G. Nuclear localization and shuttling of herpes simplex virus tegument protein VP13/14. J Virol. 2001;75(6):2566-2574.

460. Donnelly M, Verhagen J, Elliott G. RNA binding by the herpes simplex virus type 1 nucleocytoplasmic shuttling protein UL47 is mediated by an N-terminal arginine-rich domain that also functions as its nuclear localization signal. J Virol. 2007;81(5):2283-2296.

461. Pomeranz LE, Blaho JA. Modified VP22 localizes to the cell nucleus during synchronized herpes simplex virus type 1 infection. J Virol. 1999;73(8):6769-6781.

462. Newcomb WW, Brown JC. Structure and capsid association of the herpesvirus large tegument protein UL36. J Virol. 2010;84(18):9408-9414.

463. Cardone G, Newcomb WW, Cheng N, Wingfield PT, Trus BL, Brown JC, et al. The UL36 tegument protein of herpes simplex virus 1 has a composite binding site at the capsid vertices. J Virol. 2012;86(8):4058-4064.

464. Coller KE, Lee JI, Ueda A, Smith GA. The capsid and tegument of the alphaherpesviruses are linked by an interaction between the UL25 and VP1/2 proteins. J Virol. 2007;81(21):11790-11797.

465. Mohl BS, Bottcher S, Granzow H, Kuhn J, Klupp BG, Mettenleiter TC. Intracellular localization of the pseudorabies virus large tegument protein pUL36. J Virol. 2009;83(19):9641-9651.

466. Klupp BG, Fuchs W, Granzow H, Nixdorf R, Mettenleiter TC. Pseudorabies virus UL36 tegument protein physically interacts with the UL37 protein. J Virol. 2002;76(6):3065-3071.

467. Fuchs W, Klupp BG, Granzow H, Mettenleiter TC. Essential function of the pseudorabies virus UL36 gene product is independent of its interaction with the UL37 protein. J Virol. 2004;78(21):11879-11889.

468. Bucks MA, Murphy MA, O'Regan KJ, Courtney RJ. Identification of interaction domains within the UL37 tegument protein of herpes simplex virus type 1. Virology. 2011;416(1-2):42-53.

469. McLauchlan J. The abundance of the herpes simplex virus type 1 UL37 tegument protein in virus particles is closely controlled. J Gen Virol. 1997;78:189-194.

470. Michael K, Klupp BG, Mettenleiter TC, Karger A. Composition of Pseudorabies Virus Particles Lacking Tegument Protein US3, UL47, or UL49 or Envelope Glycoprotein E. J Virol. 2006;80(3):1332-1339.

471. Bohannon KP, Jun Y, Gross SP, Smith GA. Differential protein partitioning within the herpesvirus tegument and envelope underlies a complex and variable virion architecture. Proc Natl Acad Sci U S A. 2013;110(17):E1613-1620.

472. Ko DH, Cunningham AL, Diefenbach RJ. The major determinant for addition of tegument protein pUL48 (VP16) to capsids in herpes simplex virus type 1 is the presence of the major tegument protein pUL36 (VP1/2). J Virol. 2010;84(3):1397-1405.

473. Svobodova S, Bell S, Crump CM. Analysis of the interaction between the essential herpes simplex virus 1 tegument proteins VP16 and VP1/2. J Virol. 2012;86(1):473-483.

474. Apcarian A, Cunningham AL, Diefenbach RJ. Identification of binding domains in the herpes simplex virus type 1 small capsid protein pUL35 (VP26). J Gen Virol. 2010;91(Pt 11):2659-2663.

475. Kato K, Daikoku T, Goshima F, Kume H, Yamaki K, Nishiyama Y. Synthesis, subcellular localization and VP16 interaction of the herpes simplex virus type 2 UL46 gene product. Arch Virol. 2000;145(10):2149-2162.

476. Smibert CA, Popova B, Xiao P, Capone JP, Smiley JR. Herpes simplex virus VP16 forms a complex with the virion host shutoff protein vhs. J Virol. 1994;68(4):2339-2346.

477. Elliott G, Mouzakitis G, O'Hare P. VP16 interacts via its activation domain with VP22, a tegument protein of herpes simplex virus, and is relocated to a novel macromolecular assembly in coexpressing cells. J Virol. 1995;69(12):7932-7941.

478. Fuchs W, Granzow H, Klupp BG, Kopp M, Mettenleiter TC. The UL48 tegument protein of pseudorabies virus is critical for intracytoplasmic assembly of infectious virions. J Virol. 2002;76(13):6729-6742.

479. Heilingloh CS, Krawczyk A. Role of L-Particles during Herpes Simplex Virus Infection. Front Microbiol. 2017;8:2565.

480. Lin AE, Greco TM, Dohner K, Sodeik B, Cristea IM. A proteomic perspective of inbuilt viral protein regulation: pUL46 tegument protein is targeted for degradation by ICP0 during herpes simplex virus type 1 infection. Mol Cell Proteomics. 2013;12(11):3237-3252.

481. Scholtes LD, Yang K, Li LX, Baines JD. The capsid protein encoded by U(L)17 of herpes simplex virus 1 interacts with tegument protein VP13/14. J Virol. 2010;84(15):7642-7650.

482. Hambleton S, Gershon MD, Gershon AA. The role of the trans-Golgi network in varicella zoster virus biology. Cell Mol Life Sci. 2004;61(24):3047-3056.

483. Gershon AA, Sherman DL, Zhu Z, Gabel CA, Ambron RT, Gershon MD. Intracellular transport of newly synthesized varicella-zoster virus: final envelopment in the trans-Golgi network. J Virol. 1994;68(10):6372-6390.

484. El Kasmi I, Lippé R. Herpes Simplex Virus 1 gN Partners with gM To Modulate the Viral Fusion Machinery. J Virol. 2015;89(4):2313-2323.

485. Sugimoto K, Uema M, Sagara H, Tanaka M, Sata T, Hashimoto Y, et al. Simultaneous tracking of capsid, tegument, and envelope protein localization in living cells infected with triply fluorescent herpes simplex virus 1. J Virol. 2008;82(11):5198-5211.

486. Loomis JS, Bowzard JB, Courtney RJ, Wills JW. Intracellular trafficking of the UL11 tegument protein of herpes simplex virus type 1. J Virol. 2001;75(24):12209-12219.

487. Kelly BJ, Diefenbach E, Fraefel C, Diefenbach RJ. Identification of host cell proteins which interact with herpes simplex virus type 1 tegument protein pUL37. Biochem Biophys Res Commun. 2012;417(3):961-965.

488. Jambunathan N, Chouljenko D, Desai P, Charles AS, Subramanian R, Chouljenko VN, et al. Herpes Simplex Virus 1 Protein UL37 Interacts with Viral Glycoprotein gK and Membrane Protein UL20 and Functions in Cytoplasmic Virion Envelopment. J Virol. 2014;88(11):5927-5935.

489. Chouljenko DV, Kim IJ, Chouljenko VN, Subramanian R, Walker JD, Kousoulas KG. Functional hierarchy of herpes simplex virus 1 viral glycoproteins in cytoplasmic virion envelopment and egress. J Virol. 2012;86(8):4262-4270.

490. Nozawa N, Daikoku T, Yamauchi Y, Takakuwa H, Goshima F, Yoshikawa T, et al. Identification and characterization of the UL7 gene product of herpes simplex virus type 2. Virus Genes. 2002;24(3):257-266.

491. Nozawa N, Daikoku T, Koshizuka T, Yamauchi Y, Yoshikawa T, Nishiyama Y. Subcellular localization of herpes simplex virus type 1 UL51 protein and role of palmitoylation in Golgi apparatus targeting. J Virol. 2003;77(5):3204-3216.

492. Klupp BG, Granzow H, Klopfleisch R, Fuchs W, Kopp M, Lenk M, et al. Functional analysis of the pseudorabies virus UL51 protein. J Virol. 2005;79(6):3831-3840.

493. Roller RJ, Fetters R. The HSV-1 UL51 Protein Interacts with the UL7 Protein and Plays a Role in Its Recruitment into the Virion. J Virol. 2014.

494. Tanaka M, Sata T, Kawaguchi Y. The product of the Herpes simplex virus 1 UL7 gene interacts with a mitochondrial protein, adenine nucleotide translocator 2. Virol J. 2008;5:125.

495. Fuchs W, Granzow H, Klopfleisch R, Klupp BG, Rosenkranz D, Mettenleiter TC. The UL7 gene of pseudorabies virus encodes a nonessential structural protein which is involved in virion formation and egress. J Virol. 2005;79(17):11291-11299.

496. Loomis JS, Courtney RJ, Wills JW. Binding partners for the UL11 tegument protein of herpes simplex virus type 1. J Virol. 2003;77(21):11417-11424.

497. Yeh PC, Meckes DG, Jr., Wills JW. Analysis of the interaction between the UL11 and UL16 tegument proteins of herpes simplex virus. J Virol. 2008;82(21):10693-10700.

498. Yeh PC, Han J, Chadha P, Meckes DG, Jr., Ward MD, Semmes OJ, et al. Direct and Specific Binding of the UL16 Tegument Protein of Herpes Simplex Virus to the Cytoplasmic Tail of Glycoprotein E. J Virol. 2011;85(18):9425-9436.

499. Han J, Chadha P, Starkey JL, Wills JW. Function of glycoprotein E of herpes simplex virus requires coordinated assembly of three tegument proteins on its cytoplasmic tail. Proc Natl Acad Sci U S A. 2012;109(48):19798-19803.

500. Harper AL, Meckes DG, Jr., Marsh JA, Ward MD, Yeh PC, Baird NL, et al. Interaction domains of the UL16 and UL21 tegument proteins of herpes simplex virus. J Virol. 2010;84(6):2963-2971.

501. Leege T, Fuchs W, Granzow H, Kopp M, Klupp BG, Mettenleiter TC. Effects of simultaneous deletion of pUL11 and glycoprotein M on virion maturation of herpes simplex virus type 1. J Virol. 2009;83(2):896-907.

502. Starkey JL, Han J, Chadha P, Marsh JA, Wills JW. Elucidation of the block to herpes simplex virus egress in the absence of tegument protein UL16 reveals a novel interaction with VP22. J Virol. 2014;88(1):110-119.

503. Baines JD, Roizman B. The UL11 gene of herpes simplex virus 1 encodes a function that facilitates nucleocapsid envelopment and egress from cells. J Virol. 1992;66(8):5168-5174.

504. Fulmer P, Melancon J, Baines J, Kousoulas K. UL20 protein functions precede and are required for the UL11 functions of herpes simplex virus type 1 cytoplasmic virion envelopment. J Virol. 2007;81:3097 - 3108.

505. Kopp M, Granzow H, Fuchs W, Klupp B, Mettenleiter TC. Simultaneous deletion of pseudorabies virus tegument protein UL11 and glycoprotein M severely impairs secondary envelopment. J Virol. 2004;78(6):3024-3034.

506. McMillan TN, Johnson DC. Cytoplasmic domain of herpes simplex virus gE causes accumulation in the trans-Golgi network, a site of virus envelopment and sorting of virions to cell junctions. J Virol. 2001;75(4):1928-1940.

507. Desai PJ. A null mutation in the UL36 gene of herpes simplex virus type 1 results in accumulation of unenveloped DNA-filled capsids in the cytoplasm of infected cells. J Virol. 2000;74(24):11608-11618.

508. Foster TP, Melancon JM, Olivier TL, Kousoulas KG. Herpes simplex virus type 1 glycoprotein K and the UL20 protein are interdependent for intracellular trafficking and trans-Golgi network localization. J Virol. 2004;78(23):13262-13277.

509. Lau SY, Crump CM. HSV-1 gM and the gK/pUL20 complex are important for the localization of gD and gH/L to viral assembly sites. Viruses. 2015;7(3):915-938.

510. Jayachandra S, Baghian A, Kousoulas KG. Herpes simplex virus type 1 glycoprotein K is not essential for infectious virus production in actively replicating cells but is required for efficient envelopment and translocation of infectious virions from the cytoplasm to the extracellular space. J Virol. 1997;71(7):5012-5024.

511. Maringer K, Stylianou J, Elliott G. A network of protein interactions around the herpes simplex virus tegument protein VP22. J Virol. 2012;86(23):12971-12982.

512. Guo Y, Sirkis DW, Schekman R. Protein sorting at the trans-Golgi network. Annu Rev Cell Dev Biol. 2014;30:169-206.

513. Alconada A, Bauer U, Hoflack B. A tyrosine-based motif and a casein kinase II phosphorylation site regulate the intracellular trafficking of the varicella-zoster virus

glycoprotein I, a protein localized in the trans-Golgi network. Embo J. 1996;15(22):6096-6110.

514. Alconada A, Bauer U, Baudoux L, Piette J, Hoflack B. Intracellular transport of the glycoproteins gE and gI of the varicella- zoster virus. gE accelerates the maturation of gI and determines its accumulation in the trans-Golgi network. J Biol Chem. 1998;273(22):13430-13436.

515. Alconada A, Bauer U, Sodeik B, Hoflack B. Intracellular traffic of herpes simplex virus glycoprotein gE: characterization of the sorting signals required for its trans-Golgi network localization. J Virol. 1999;73(1):377-387.

516. Beitia Ortiz de Zarate I, Kaelin K, Rozenberg F. Effects of mutations in the cytoplasmic domain of herpes simplex virus type 1 glycoprotein B on intracellular transport and infectivity. J Virol. 2004;78(3):1540-1551.

517. Beitia Ortiz de Zarate I, Cantero-Aguilar L, Longo M, Berlioz-Torrent C, Rozenberg F. Contribution of endocytic motifs in the cytoplasmic tail of herpes simplex virus type 1 glycoprotein B to virus replication and cell-cell fusion. J Virol. 2007;81(24):13889-13903.

518. Nixdorf R, Klupp BG, Mettenleiter TC. Role of the cytoplasmic tails of pseudorabies virus glycoproteins B, E and M in intracellular localization and virion incorporation. J Gen Virol. 2001;82(Pt 1):215-226.

519. Favoreel HW, Van Minnebruggen G, Nauwynck HJ, Enquist LW, Pensaert MB. A tyrosine-based motif in the cytoplasmic tail of pseudorabies virus glycoprotein B is important for both antibody-induced internalization of viral glycoproteins and efficient cell-to-cell spread. J Virol. 2002;76(13):6845-6851.

520. Van Minnebruggen G, Favoreel HW, Nauwynck HJ. Internalization of pseudorabies virus glycoprotein B is mediated by an interaction between the YQRL motif in its

cytoplasmic domain and the clathrin-associated AP-2 adaptor complex. J Virol. 2004;78(16):8852-8859.

521. Ficinska J, Van Minnebruggen G, Nauwynck HJ, Bienkowska-Szewcz K, Favoreel HW. Pseudorabies Virus Glycoprotein gD Contains a Functional Endocytosis Motif That Acts in Concert with an Endocytosis Motif in gB To Drive Internalization of Antibody-Antigen Complexes from the Surface of Infected Monocytes. J Virol. 2005;79(11):7248-7254.

522. Crump CM, Bruun B, Bell S, Pomeranz LE, Minson T, Browne HM. Alphaherpesvirus glycoprotein M causes the relocalization of plasma membrane proteins. J Gen Virol. 2004;85(Pt 12):3517-3527.

523. Ren Y, Bell S, Zenner HL, Lau SY, Crump CM. Glycoprotein M is important for the efficient incorporation of glycoprotein H-L into herpes simplex virus type 1 particles. J Gen Virol. 2012;93(Pt 2):319-329.

524. Liu SL, Wu QM, Zhang LJ, Wang ZG, Sun EZ, Zhang ZL, et al. Three-dimensional tracking of Rab5- and Rab7-associated infection process of influenza virus. Small. 2014;10(22):4746-4753.

525. Edinger TO, Pohl MO, Stertz S. Entry of influenza A virus: host factors and antiviral targets. J Gen Virol. 2014;95(Pt 2):263-277.

526. Meertens L, Bertaux C, Dragic T. Hepatitis C virus entry requires a critical postinternalization step and delivery to early endosomes via clathrin-coated vesicles. J Virol. 2006;80(23):11571-11578.

527. Sieczkarski SB, Whittaker GR. Differential requirements of Rab5 and Rab7 for endocytosis of influenza and other enveloped viruses. Traffic. 2003;4(5):333-343.

528. Rauma T, Tuukkanen J, Bergelson JM, Denning G, Hautala T. rab5 GTPase regulates adenovirus endocytosis. J Virol. 1999;73(11):9664-9668.

529. Spearman P. Viral interactions with host cell Rab GTPases. Small GTPases. 2018;9(1-2):192-201.

530. Hodge TW, Murray JL. Rab-GTPases: dual roles in vesicular transport and viral replication. Future virology. 2006;1(6):811-822.

531. Baschieri F, Farhan H. Crosstalk of small GTPases at the Golgi apparatus. Small GTPases. 2012;3(2):80-90.

532. Zerial M, Stenmark H. Rab GTPases in vesicular transport. Curr Opin Cell Biol. 1993;5(4):613-620.

533. Chavrier P, Goud B. The role of ARF and Rab GTPases in membrane transport. Curr Opin Cell Biol. 1999;11(4):466-475.

534. Chua CE, Gan BQ, Tang BL. Involvement of members of the Rab family and related small GTPases in autophagosome formation and maturation. Cell Mol Life Sci. 2011;68(20):3349-3358.

535. Hutagalung AH, Novick PJ. Role of Rab GTPases in Membrane Traffic and Cell Physiology. Physiological Reviews. 2011;91(1):119-149.

536. Zenner HL, Yoshimura S, Barr FA, Crump CM. Analysis of Rab GTPase-activating proteins indicates that Rab1a/b and Rab43 are important for herpes simplex virus 1 secondary envelopment. J Virol. 2011;85(16):8012-8021.

537. Hollinshead M, Johns HL, Sayers CL, Gonzalez-Lopez C, Smith GL, Elliott G. Endocytic tubules regulated by Rab GTPases 5 and 11 are used for envelopment of herpes simplex virus. EMBO J. 2012.

538. Kobayashi K, Suemasa F, Sagara H, Nakamura S, Ino Y, Kobayashi K, et al. MiR-199a Inhibits Secondary Envelopment of Herpes Simplex Virus-1 Through the Downregulation of Cdc42-specific GTPase Activating Protein Localized in Golgi Apparatus. Sci Rep. 2017;7(1):6650.

539. Martin-Serrano J, Zang T, Bieniasz PD. Role of ESCRT-I in retroviral budding. J Virol. 2003;77(8):4794-4804.

540. Votteler J, Sundquist WI. Virus budding and the ESCRT pathway. Cell Host Microbe. 2013;14(3):232-241.

541. Mi S, Qin XW, Lin YF, He J, Chen NN, Liu C, et al. Budding of Tiger Frog Virus (an Iridovirus) from HepG2 Cells via Three Ways Recruits the ESCRT Pathway. Sci Rep. 2016;6:26581.

542. Davies BA, Azmi IF, Katzmann DJ. Regulation of Vps4 ATPase activity by ESCRT-III. Biochem Soc Trans. 2009;37(Pt 1):143-145.

543. Russell MR, Shideler T, Nickerson DP, West M, Odorizzi G. Class E compartments form in response to ESCRT dysfunction in yeast due to hyperactivity of the Vps21 Rab GTPase. J Cell Sci. 2012;125(Pt 21):5208-5220.

544. Crump CM, Yates C, Minson T. Herpes simplex virus type 1 cytoplasmic envelopment requires functional Vps4. J Virol. 2007;81(14):7380-7387.

545. Pawliczek T, Crump CM. Herpes simplex virus type 1 production requires a functional ESCRT-III complex but is independent of TSG101 and ALIX expression. J Virol. 2009;83(21):11254-11264.

546. Calistri A, Sette P, Salata C, Cancellotti E, Forghieri C, Comin A, et al. Intracellular trafficking and maturation of herpes simplex virus type 1 gB and virus egress require functional biogenesis of multivesicular bodies. J Virol. 2007;81(20):11468-11478.

547. Kharkwal H, Smith CG, Wilson DW. Blocking ESCRT-mediated envelopment inhibits microtubule-dependent trafficking of alphaherpesviruses in vitro. J Virol. 2014;88(24):14467-14478.

548. Miranda-Saksena M, Boadle RA, Aggarwal A, Tijono B, Rixon FJ, Diefenbach RJ, et al. Herpes simplex virus utilizes the large secretory vesicle pathway for anterograde

transport of tegument and envelope proteins and for viral exocytosis from growth cones of human fetal axons. J Virol. 2009;83(7):3187-3199.

549. Griffiths SJ, Koegl M, Boutell C, Zenner HL, Crump CM, Pica F, et al. A systematic analysis of host factors reveals a Med23-interferon-lambda regulatory axis against herpes simplex virus type 1 replication. PLoS Pathog. 2013;9(8):e1003514.

550. Johns HL, Gonzalez-Lopez C, Sayers CL, Hollinshead M, Elliott G. Rab6 Dependent Post-Golgi Trafficking of HSV1 Envelope Proteins to Sites of Virus Envelopment. Traffic. 2014;15(2):157-178.

551. Bello-Morales R, Crespillo AJ, Fraile-Ramos A, Tabares E, Alcina A, Lopez-Guerrero JA. Role of the small GTPase Rab27a during herpes simplex virus infection of oligodendrocytic cells. BMC Microbiol. 2012;12:265.

552. Rémillard-Labrosse G, Mihai C, Duron J, Guay G, Lippé R. Protein kinase D-dependent trafficking of the large Herpes simplex virus type 1 capsids from the TGN to plasma membrane. Traffic. 2009;10(8):1074-1083.

553. Wilson AC, Mohr I. A cultured affair: HSV latency and reactivation in neurons. Trends Microbiol. 2012;20(12):604-611.

554. Grinde B. Herpesviruses: latency and reactivation - viral strategies and host response. Journal of oral microbiology. 2013;5(2):678-707.

555. Brown JC. Herpes Simplex Virus Latency: The DNA Repair-Centered Pathway. Adv Virol. 2017;2017:7028194.

556. Aranda AM, Epstein AL. [Herpes simplex virus type 1 latency and reactivation: an update]. Medecine sciences : M/S. 2015;31(5):506-514.

557. Bloom DC. Chapter Two - Alphaherpesvirus Latency: A Dynamic State of Transcription and Reactivation. In: Kielian M, Maramorosch K, Mettenleiter TC, editors. Advances in Virus Research. 94: Academic Press; 2016. p. 53-80.

558. Furuta Y, Takasu T, Fukuda S, Inuyama Y, Sato KC, Nagashima K. Latent herpes simplex virus type 1 in human vestibular ganglia. Acta Otolaryngol Suppl. 1993;503:85-89.

559. Warren KG, Brown SM, Wroblewska Z, Gilden D, Koprowski H, Subak-Sharpe J. Isolation of latent herpes simplex virus from the superior cervical and vagus ganglions of human beings. N Engl J Med. 1978;298(19):1068-1069.

560. La Boissiere S, Hughes T, O'Hare P. HCF-dependent nuclear import of VP16. Embo J. 1999;18(2):480-489.

561. Kalamvoki M, Roizman B. The histone acetyltransferase CLOCK is an essential component of the herpes simplex virus 1 transcriptome that includes TFIID, ICP4, ICP27, and ICP22. J Virol. 2011;85(18):9472-9477.

562. Liang Y, Vogel JL, Narayanan A, Peng H, Kristie TM. Inhibition of the histone demethylase LSD1 blocks alpha-herpesvirus lytic replication and reactivation from latency. Nat Med. 2009;15(11):1312-1317.

563. Gerster T, Roeder RG. A herpesvirus trans-activating protein interacts with transcription factor OTF-1 and other cellular proteins. Proc Natl Acad Sci U S A. 1988;85(17):6347-6351.

564. Scherer J, Yaffe ZA, Vershinin M, Enquist LW. Dual-color Herpesvirus Capsids Discriminate Inoculum from Progeny and Reveal Axonal Transport Dynamics. J Virol. 2016.

565. Hafezi W, Lorentzen EU, Eing BR, Muller M, King NJ, Klupp B, et al. Entry of herpes simplex virus type 1 (HSV-1) into the distal axons of trigeminal neurons favors the onset of nonproductive, silent infection. PLoS Pathog. 2012;8(5):e1002679.

566. Kristie TM, Vogel JL, Sears AE. Nuclear localization of the C1 factor (host cell factor) in sensory neurons correlates with reactivation of herpes simplex virus from latency. Proc Natl Acad Sci U S A. 1999;96(4):1229-1233.

567. Lakin ND, Palmer R, Lillycrop KA, Howard MK, Burke LC, Thomas NS, et al. Down regulation of the octamer binding protein Oct-1 during growth arrest and differentiation of a neuronal cell line. Brain Res Mol Brain Res. 1995;28(1):47-54.

568. Kolb G, Kristie TM. Association of the cellular coactivator HCF-1 with the Golgi apparatus in sensory neurons. J Virol. 2008;82(19):9555-9563.

569. Nicoll MP, Proença JT, Efstathiou S. The molecular basis of herpes simplex virus latency. Fems Microbiology Reviews. 2012;36(3):684-705.

570. Bloom DC, Giordani NV, Kwiatkowski DL. Epigenetic regulation of latent HSV-1 gene expression. Biochim Biophys Acta. 2010;1799(3-4):246-256.

571. Preston CM. Repression of viral transcription during herpes simplex virus latency. J Gen Virol. 2000;81(Pt 1):1-19.

572. Thomas DL, Lock M, Zabolotny JM, Mohan BR, Fraser NW. The 2-Kilobase Intron of the Herpes Simplex Virus Type 1 Latency-Associated Transcript Has a Half-Life of Approximately 24 Hours in SY5Y and COS-1 Cells. Journal of Virology. 2002;76(2):532-540.

573. Arthur J, Efstathiou S, Simmons A. Intranuclear foci containing low abundance herpes simplex virus latency-associated transcripts visualized by non-isotopic in situ hybridization. J Gen Virol. 1993;74 (Pt 7):1363-1370.

574. Zwaagstra JC, Ghiasi H, Slanina SM, Nesburn AB, Wheatley SC, Lillycrop K, et al. Activity of herpes simplex virus type 1 latency-associated transcript (LAT) promoter in neuron-derived cells: evidence for neuron specificity and for a large LAT transcript. J Virol. 1990;64(10):5019-5028.

575. Rock DL, Nesburn AB, Ghiasi H, Ong J, Lewis TL, Lokensgard JR, et al. Detection of latency-related viral RNAs in trigeminal ganglia of rabbits latently infected with herpes simplex virus type 1. J Virol. 1987;61(12):3820-3826.

576. Nicoll MP, Hann W, Shivkumar M, Harman LE, Connor V, Coleman HM, et al. The HSV-1 Latency-Associated Transcript Functions to Repress Latent Phase Lytic Gene Expression and Suppress Virus Reactivation from Latently Infected Neurons. PLoS Pathog. 2016;12(4):e1005539.

577. Wang QY, Zhou C, Johnson KE, Colgrove RC, Coen DM, Knipe DM. Herpesviral latency-associated transcript gene promotes assembly of heterochromatin on viral lytic-gene promoters in latent infection. Proc Natl Acad Sci U S A. 2005;102(44):16055-16059.

578. Kubat NJ, Amelio AL, Giordani NV, Bloom DC. The herpes simplex virus type 1 latency-associated transcript (LAT) enhancer/rcr is hyperacetylated during latency independently of LAT transcription. J Virol. 2004;78(22):12508-12518.

579. Kubat NJ, Tran RK, McAnany P, Bloom DC. Specific histone tail modification and not DNA methylation is a determinant of herpes simplex virus type 1 latent gene expression. J Virol. 2004;78(3):1139-1149.

580. Amelio AL, McAnany PK, Bloom DC. A chromatin insulator-like element in the herpes simplex virus type 1 latency-associated transcript region binds CCCTC-binding factor and displays enhancer-blocking and silencing activities. J Virol. 2006;80(5):2358-2368.

581. Cliffe AR, Coen DM, Knipe DM. Kinetics of facultative heterochromatin and polycomb group protein association with the herpes simplex viral genome during establishment of latent infection. MBio. 2013;4(1).

582. Perng GC, Slanina SM, Yukht A, Drolet BS, Keleher W, Jr., Ghiasi H, et al. A herpes simplex virus type 1 latency-associated transcript mutant with increased virulence and reduced spontaneous reactivation. J Virol. 1999;73(2):920-929.

583. Perng GC, Slanina SM, Yukht A, Ghiasi H, Nesburn AB, Wechsler SL. The latency-associated transcript gene enhances establishment of herpes simplex virus type 1 latency in rabbits. J Virol. 2000;74(4):1885-1891.

584. Perng GC, Jones C, Ciacci-Zanella J, Stone M, Henderson G, Yukht A, et al. Virus-induced neuronal apoptosis blocked by the herpes simplex virus latency-associated transcript. Science. 2000;287(5457):1500-1503.

585. Piedade D, Azevedo-Pereira JM. The Role of microRNAs in the Pathogenesis of Herpesvirus Infection. Viruses. 2016;8(6).

586. Du T, Han Z, Zhou G, Roizman B. Patterns of accumulation of miRNAs encoded by herpes simplex virus during productive infection, latency, and on reactivation. Proc Natl Acad Sci U S A. 2015;112(1):E49-55.

587. Zheng SQ, Li YX, Zhang Y, Li X, Tang H. MiR-101 regulates HSV-1 replication by targeting ATP5B. Antiviral Res. 2011;89(3):219-226.

588. Spivack JG, Fraser NW. Expression of herpes simplex virus type 1 latency-associated transcripts in the trigeminal ganglia of mice during acute infection and reactivation of latent infection. J Virol. 1988;62(5):1479-1485.

589. George VG, Hierholzer JC, Ades EW. 1 - Cell culture A2 - Mahy, Brian WJ. In: Kangro HO, editor. Virology Methods Manual. London: Academic Press; 1996. p. 3-23.

590. Killington RA, Stokes A, Hierholzer JC. 4 - Virus purification A2 - Mahy, Brian WJ. In: Kangro HO, editor. Virology Methods Manual. London: Academic Press; 1996. p. 71-89.

591. McCance DJ. 10 - DNA viruses: DNA extraction, purification and characterization A2 - Mahy, Brian WJ. In: Kangro HO, editor. Virology Methods Manual. London: Academic Press; 1996. p. 191-230.

592. Leland DS, Ginocchio CC. Role of cell culture for virus detection in the age of technology. Clin Microbiol Rev. 2007;20(1):49-78.

593. Carter J, Saunders VA. Virology: principles and applications: John Wiley & Sons; 2007.

594. Dimmock NJ, Easton AJ, Leppard KN. Introduction to modern virology: John Wiley & Sons; 2016.

595. Teunis PFM, Lodder WJ, Heisterkamp SH, de Roda Husman AM. Mixed plaques: Statistical evidence how plaque assays may underestimate virus concentrations. Water Research. 2005;39(17):4240-4250.

596. Zhou S, Liu R, Zhao X, Huang C, Wei Y. Viral proteomics: the emerging cutting-edge of virus research. Sci China Life Sci. 2011;54(6):502-512.

597. Oxford KL, Wendler JP, McDermott JE, White Iii RA, Powell JD, Jacobs JM, et al. The landscape of viral proteomics and its potential to impact human health. Expert Rev Proteomics. 2016;13(6):579-591.

598. Pasa-Tolic L, Masselon C, Barry RC, Shen YF, Smith RD. Proteomic analyses using an accurate mass and time tag strategy. BioTechniques. 2004;37(4):621-+.

599. Zhang Y, Wen Z, Washburn MP, Florens L. Improving label-free quantitative proteomics strategies by distributing shared peptides and stabilizing variance. Anal Chem. 2015;87(9):4749-4756.

600. Maxwell KL, Frappier L. Viral proteomics. Microbiol Mol Biol Rev. 2007;71(2):398-411.

601. Johannsen E, Luftig M, Chase MR, Weicksel S, Cahir-McFarland E, Illanes D, et al. Proteins of purified Epstein-Barr virus. Proc Natl Acad Sci U S A. 2004;101(46):16286-16291.

602. Kattenhorn LM, Mills R, Wagner M, Lomsadze A, Makeev V, Borodovsky M, et al. Identification of proteins associated with murine cytomegalovirus virions. J Virol. 2004;78(20):11187-11197.

603. Varnum SM, Streblow DN, Monroe ME, Smith P, Auberry KJ, Pasa-Tolic L, et al. Identification of proteins in human cytomegalovirus (HCMV) particles: the HCMV proteome. J Virol. 2004;78(20):10960-10966.

604. Bechtel JT, Winant RC, Ganem D. Host and viral proteins in the virion of Kaposi's sarcoma-associated herpesvirus. J Virol. 2005;79(8):4952-4964.

605. Zhu FX, Chong JM, Wu L, Yuan Y. Virion proteins of Kaposi's sarcoma-associated herpesvirus. J Virol. 2005;79(2):800-811.

606. Rozen R, Sathish N, Li Y, Yuan Y. Virion-wide protein interactions of Kaposi's sarcoma-associated herpesvirus. J Virol. 2008;82(10):4742-4750.

607. El Kasmi I, Khadivjam B, Lackman M, Duron J, Bonneil E, Thibault P, et al. Extended Synaptotagmin 1 Interacts with Herpes Simplex Virus 1 Glycoprotein M and Negatively Modulates Virus-Induced Membrane Fusion. J Virol. 2018;92(1).

608. Rieseberg M, Kasper C, Reardon KF, Scheper T. Flow cytometry in biotechnology. Appl Microbiol Biotechnol. 2001;56(3-4):350-360.

609. Bergquist PL, Hardiman EM, Ferrari BC, Winsley T. Applications of flow cytometry in environmental microbiology and biotechnology. Extremophiles. 2009;13(3):389-401.

610. Bonar MM, Tilton JC. High sensitivity detection and sorting of infectious human immunodeficiency virus (HIV-1) particles by flow virometry. Virology. 2017;505:80-90.

611. Arakelyan A, Fitzgerald W, King DF, Rogers P, Cheeseman HM, Grivel JC, et al. Flow virometry analysis of envelope glycoprotein conformations on individual HIV virions. Sci Rep. 2017;7(1):948.

612. Tang VA, Renner TM, Varette O, Le Boeuf F, Wang J, Diallo JS, et al. Single-particle characterization of oncolytic vaccinia virus by flow virometry. Vaccine. 2016;34(42):5082-5089.

613. Wang Y, Hammes F, De Roy K, Verstraete W, Boon N. Past, present and future applications of flow cytometry in aquatic microbiology. Trends Biotechnol. 2010;28(8):416-424.

614. Zamora JLR, Aguilar HC. Flow virometry as a tool to study viruses. Methods. 2018;134-135:87-97.

615. Zicari S, Arakelyan A, Fitzgerald W, Zaitseva E, Chernomordik LV, Margolis L, et al. Evaluation of the maturation of individual Dengue virions with flow virometry. Virology. 2016;488:20-27.

616. Vlasak J, Hoang VM, Christanti S, Peluso R, Li F, Culp TD. Use of flow cytometry for characterization of human cytomegalovirus vaccine particles. Vaccine. 2016;34(20):2321-2328.

617. Gaudin R, Barteneva NS. Sorting of small infectious virus particles by flow virometry reveals distinct infectivity profiles. Nature communications. 2015;6:6022.

618. Baines J, Duffy C. Nucleocapsid Assembly and Envelopment of Herpes Simplex Virus. In: Sandri-Goldin RM, editor. Alpha Herpesviruses. Norfolk: Caister Academic Press; 2006. p. 175-204.

619. Clarke RW, Monnier N, Li H, Zhou D, Browne H, Klenerman D. Two-color fluorescence analysis of individual virions determines the distribution of the copy number of proteins in herpes simplex virus particles. Biophys J. 2007;93(4):1329-1337.

620. Leslie J, Rixon FJ, McLauchlan J. Overexpression of the herpes simplex virus type 1 tegument protein VP22 increases its incorporation into virus particles. Virology. 1996;220(1):60-68.

621. Zhang YQ, Lai W, Li H, Li G. Inhibition of herpes simplex virus type 1 by small interfering RNA. Clin Exp Dermatol. 2008;33(1):56-61.

622. Rémillard-Labrosse G, Lippé R. In vitro nuclear egress of herpes simplex virus type 1 capsids. Methods. 2011;55(2):153-159.

623. Antinone SE, Zaichick SV, Smith GA. Resolving the assembly state of herpes simplex virus during axon transport by live-cell imaging. J Virol. 2010;84(24):13019-13030.

624. Liu M, Schmidt EE, Halford WP. ICP0 dismantles microtubule networks in herpes simplex virus-infected cells. PLoS One. 2010;5(6):e10975.

625. Desai P, Person S. Incorporation of the green fluorescent protein into the herpes simplex virus type 1 capsid. J Virol. 1998;72(9):7563-7568.

626. Desai P, Sexton GL, Huang E, Person S. Localization of herpes simplex virus type 1 UL37 in the Golgi complex requires UL36 but not capsid structures. J Virol. 2008;82(22):11354-11361.

627. Willard M. Rapid directional translocations in virus replication. J Virol. 2002;76(10):5220-5232.

628. La Boissiere S, Izeta A, Malcomber S, O'Hare P. Compartmentalization of VP16 in cells infected with recombinant herpes simplex virus expressing VP16-green fluorescent protein fusion proteins. J Virol. 2004;78(15):8002-8014.

629. Elliott G, O'Hare P. Live-cell analysis of a green fluorescent protein-tagged herpes simplex virus infection. J Virol. 1999;73(5):4110-4119.

630. Bhuyan PK, Kariko K, Capodici J, Lubinski J, Hook LM, Friedman HM, et al. Short interfering RNA-mediated inhibition of herpes simplex virus type 1 gene expression

and function during infection of human keratinocytes. J Virol. 2004;78(19):10276-10281.

631. Zhe R, Mei-Ying Z, Kitazato K, Kobayash N, Qin-Chang Z, Pei-Zhuo Z, et al. Effect of siRNA on HSV-1 plaque formation and relative expression levels of UL39 mRNA. Arch Virol. 2008;153(7):1401-1406.

632. Ullal AJ, Pisetsky DS, Reich CF, 3rd. Use of SYTO 13, a fluorescent dye binding nucleic acids, for the detection of microparticles in in vitro systems. Cytometry A. 2010;77(3):294-301.

633. Grunewald K, Desai P, Winkler DC, Heymann JB, Belnap DM, Baumeister W, et al. Three-dimensional structure of herpes simplex virus from cryo-electron tomography. Science. 2003;302(5649):1396-1398.

634. Laine RF, Albecka A, van de Linde S, Rees EJ, Crump CM, Kaminski CF. Structural analysis of herpes simplex virus by optical super-resolution imaging. Nature communications. 2015;6:5980.

635. Fuchs W, Granzow H, Mettenleiter TC. A pseudorabies virus recombinant simultaneously lacking the major tegument proteins encoded by the UL46, UL47, UL48, and UL49 genes is viable in cultured cells. J Virol. 2003;77(23):12891-12900.

636. del Rio T, DeCoste CJ, Enquist LW. Actin is a component of the compensation mechanism in pseudorabies virus virions lacking the major tegument protein VP22. J Virol. 2005;79(13):8614-8619.

637. Nagel CH, Döhner K, Fathollahy M, Strive T, Borst EM, Messerle M, et al. Nuclear egress and envelopment of herpes simplex virus capsids analyzed with dual-color fluorescence HSV1(17+). J Virol. 2008;82(6):3109-3124.

638. Dunsing V, Luckner M, Zuhlke B, Petazzi RA, Herrmann A, Chiantia S. Optimal fluorescent protein tags for quantifying protein oligomerization in living cells. Sci Rep. 2018;8(1):10634.

639. Shaner NC, Steinbach PA, Tsien RY. A guide to choosing fluorescent proteins. Nat Methods. 2005;2(12):905-909.

640. Sae-Ueng U, Li D, Zuo X, Huffman JB, Homa FL, Rau D, et al. Solid-to-fluid DNA transition inside HSV-1 capsid close to the temperature of infection. Nat Chem Biol. 2014;10(10):861-867.

641. Perdue ML, Cohen JC, Randall CC, O'Callaghan DJ. Biochemical studies of the maturation of herpesvirus nucleocapsid species. Virology. 1976;74(1):194-208.

Annexes

Annexe I : Liste des gènes et des protéines du VHS-1

Gène	Potéine	Gène	Potéine
RL1	ICP34.5, facteur de neurovirulence, module la synthése protéique par la liaison à la protéine	**U_L34**	PU_L34 (NEMP), protéine membranaire de type II associée à la membrane nuclaire interne
RL2	ICP0, E3 ubiquitine ligase	**U_L35**	VP26, petite protéine de la caspide, placé au sommet de chaque hexon de la capside
R_S1	ICP4, facteur de transcription viral majeur	**U_L36**	ICP1/2, VP1/2, large protéine du tégument
UL1	Glycoprotéine L (gL), forme un complexe avec gH, impliquée dans l'entrée et la propagation cellule en cellule.	**U_L37**	ICP32, LTPpb, protéine du tégument avec un signal d'export nucléaire, impliquée dans la sortie.
U_L2	Uracil-ADN-glycosylase, UDG	**U_L38**	VP19C, sous unité du triplexe de la capside.
U_L3	pU_L3, phosphoprotéine nucléaire	**U_L39**	ICP6, sous unité de la ribonucléase réductase.
U_L4	pU_L4, protéine nucléaire, colocalise avec U_L3 et ICP22.	**U_L40**	Sous unité de la ribonucléase réductase.
U_L5	ADN hélicase (HP1), sous-unité du complexe primase-hélicase	**U_L41**	Vhs, virion host shut off, impliquée dans la dégradation de l'ARN messager.
U_L6	PORT, associée à la capside, sous-unité du complex portal.	**U_L42**	Sous-unité catalytique de l'ADN polymérase
U_L7	EEP, associée à la capside intracellulaire	**U_L43**	NEMP, protéine associée à la membrane
U_L8	Sous-unité du complexe primase-hélicase.	**U_L44**	Glycoprotéine C (gC); initiation de la fixation.
U_L9	OriBP, protéine de liaison à l'origine de réplication.	**U_L45**	pU_L45 protéine membranaire de type II.
U_L10	gM, glycoprotéine, régulateur de fusion, rôle dans l'enveloppement secondaire.	**U_L46**	VP11/12, intéragit avec UL48 (VP16).

U_L11	CETP, Protéine du virion myristolée, impliquée dans la sortie.	**U_L47**	VP13/14, protéine du tégument qui déclenche l'expression des gènes IE (immédiats-précoces).
U_L12	NUC, Exonucléase alkaline, intervient dans l'empaquetage de l'ADN viral.	**U_L48**	VP16, ICP25, α-TIF, protéine du tégument, stimule l'expression des gènes IE (immédiats-précoces).
U_L12.5	pU_L12.5, Activité exonucléase	**U_L49**	VP22, protéine du tégument, rôle dans le trafic intercellulaire.
U_L13	Protéine kinase sérine/thréonine	**U_L49.5**	gN, U_L49A glycoprotéine, forme un complexe avec gM en stimulant la fusion membranaire.
U_L14	Sous-unité du complexe de la terminase	**U_L50**	dUTPase,désoxyuridine triphosphatase
U_L15	TER1, activité ADN-terminase	**U_L51**	CEF1, protéine du virion palmitoylée, associée au Golgi.
U_L16	CETPpb, protéine du tégument, impliquée dans l'empaquetage de l'ADN viral.	**U_L52**	Sous-unité du complexe primase-hélicase
U_L17	Protéine d'empaquetage de l'ADN.	**U_L53**	Glycoprotéine K (gK), impliquée dans la sortie du virus, plusieurs mutations syncytiales
U_L18	VP23, sous-unité du triplex de la capside, forme un complexe avec VP19c.	**U_L54**	ICP27 (MRE), régulation post-transcriptionnelle de l'expresison génes.
U_L19	VP5, ICP5, protéine majeure de la capside	**U_L55**	pU_L55, protéine nucléaire, protéine de liaison à la matrice nucléaire
U_L20	pU_L20, impliquée dans la sortie.	**U_L56**	pU_L56, protéine membranaire de type II, associée au Golgi et aux endosomes primaires.
U_L21	CEF2, protéine du tégument associée aux microtubules	**U_S1**	ICP22, stimule l'expression des gènes tardifs.
U_L22	Glycoprotéine H (gH) forme un complexe avec gL, impliquée dans l'entrée et la propagation cellule en cellule.	**U_S2**	pU_S2, protéine du virion, interagit avec cytokératine.
U_L23	Thymidine kinase, TK	**U_S3**	Protéine kinase sérine/thréonine

U_L24	pU_L24, protéine du virion, impliquée dans les modifications nucléaires durant l'infection et dans la sortie nucléaire de la caspide.	**U_S4**	Glycoprotéine G (gG), protéine de l'enveloppe impliquée dans l'entrée et la sortie.
U_L25	Protéine d'empaquetage de l'ADN	**U_S5**	Glycoprotéine J (gJ), protéine de l'enveloppe impliquée dams la protection de l'apoptose médiée par Fas.
U_L26	Protéine d'échafaudage VP21 et VP24 (protéase)	**U_S6**	Glycoprotéine D (gD), rôle dans l'entrée , se lie au HVEM.
U_L26.5	VP22a, protéine d'échafaudage clivée après l'emcapsidation de l'ADN.	**U_S7**	Glycoprotéine (gI), forme un complexe avec gE, propogation cellule à cellule.
U_L27	Glycoprotéine B (gB), forme un dimére et essentielle pour l'entrée.	**U_S8**	Glycoprotéine E (gE), forme un complexe avec gI, propoagation cellule à cellule.
U_L28	ICP18.5, sous unité du complexe de la terminase	**U_S8.5**	pU_S8.5
U_L29	ICP8, protéine de laison à l'ADN simple brin.	**U_S9**	pU_S9, protéine membranaire de type II
U_L30	Sous-unité catalytique de l'ADN polymérase	**U_S10**	pU_S10 Protéine du tégument associée à la capside.
U_L31	pUL31, interagit avec UL34, protéine de liaison à la matrice nucléaire	**U_S11**	Protéine du tégument, de liaison à l'ARN
U_L32	Protéine de l'empaquetage de l'ADN	**U_S12**	ICP47, TAPpb, protéine de liaison à TAP, impliquée dans la régulation négative de (CMH-I)
U_L33	Sous-unité du complexe de la terminase		

Annexe II : Contribution dans l'article "Analysis of herpes simplex virus type I nuclear particles by flow cytometry"

La contribution de Nabil El Bilali dans ce travail a été par la réalisation des expériences de la détection de l'ADN viral intranucléaire (ADN encapsidé) par qPCR tel que décrit dans la section « Materials and Methods », sous-section « Efficient Detection of Intranuclear DNA », et l'écriture de la partie Matériels et Méthodes pour cette sous-section. Il a également effectué l'analyse de toutes les expériences de cytométrie en flux pour le papier par le logiciel « FlowJo » ainsi que le montage des figures 1 à 4 par le logiciel « Illustrator ».

Les données et les résultats présentés dans cet article ont tous été générés durant les études de doctorat du candidat Nabil El Bilali.

ORIGINAL ARTICLE

Cytometry PART A
Journal of the International Society for Advancement of Cytometry

MIFlowCyt

Analysis of Herpes Simplex Virus Type I Nuclear Particles by Flow Cytometry

Sandra Loret, Nabil El Bilali, Roger Lippé*

Department of Pathology and Cell Biology, University of Montreal, Montreal, Quebec, Canada H3C 3J7

Received 20 April 2012; Revision Received 4 June 2012; Accepted 28 June 2012

Additional Supporting Information may be found in the online version of this article.

Grant sponsor: Canadian Institutes of Health Research; Grant number: MOP82921.

*Correspondence to: Roger Lippé, Department of Pathology and Cell Biology, University of Montreal, PO Box 6128, Succursale Centre-Ville, Montreal, Quebec, Canada H3C 3J7.

Email: roger.lippe@umontreal.ca

Published online 28 August 2012 in Wiley Online Library (wileyonlinelibrary.com)

DOI: 10.1002/cyto.a.22107

Abstract

Flow cytometry has been instrumental to characterize cell populations and examine their inner molecules and processes. In most instances, whole cells are analyzed, and hence, particle size is not an issue. Viruses are 2–3 orders of magnitude smaller than cells so flow cytometry has typically been used to study viral markers within whole infected cells. However, the ability to separate and purify viral particles representing different maturation stages within a viral life cycle would be a useful tool to analyze them in details and characterize the host proteins they associate with. Herpes simplex virus Type 1 is a 250 nm enveloped DNA virus that replicates in the nucleus where it assembles new viral particles called capsids. These capsids eventually travel to the cell surface and are modified along the way, producing several intermediate particles. In the nucleus, three types of stable nonenveloped 125 nm nuclear capsids exist that differ in protein composition and genome content. This includes so-called nuclear C-capsids that are the precursors of mature extracellular virions. We report that we can apply flow cytometry to sort these nuclear C-capsid intermediates by labeling the viral genome with Syto 13, a fluorescent marker that binds to nucleic acids. This is the first time flow cytometry has been used not only to detect but also to purify an intracellular viral maturation intermediate. This opens new research avenues in virology to study capsid assembly, maturation and egress, analyze mutant phenotypes, and define host factors associated with specific viral intermediates. © 2012 International Society for Advancement of Cytometry

Key terms

HSV; herpes; viral particle; nuclear capsids; virions; flow cytometry; Syto 13; C-capsid; fluorescence-activated cell sorting; FACS; small particles

CELLS and their constituent molecules and processes have been studied by various techniques over the years, including biochemical and genetic approaches, diverse microscopy techniques [electron microscopy (EM), epifluorescence, confocal] and more recently by system biology tools such as DNA and RNA arrays, two-hybrid screens, and multiple "omics" approaches. One of the first widely available larger scale analysis tools has been flow cytometry and its derivative, flow cytometric sorting, both widely used since the early 1970s (1). Amazingly, refinements of these techniques now allow several markers to be followed in parallel, hence allowing complex processes to be finely monitored and new research avenues to be explored (2). One limitation of flow cytometry has been the size of objects under study. Typical experiments examine whole cells, which are up to tens of microns in diameters and are thus well above the recommended lower detection threshold of a half micron for most instruments. However, viruses are much smaller entities ranging in the tens (e.g., Adeno-associated virus, 20 nm icosahedral) to hundreds of nanometers (e.g., Poxvirus, 250 × 300-nm brick shape). Consequently, viral research using flow cytometry has often relied on viral markers within whole infected cells.

Thus far, a number of studies demonstrated the feasibility to use flow cytometry to analyze sub-micron particles (3–7). Bacteria, which are below the detection limit

ISAC
International Society for Advancement of Cytometry

of common flow cytometry instruments, have indeed been detected with success when labeled with fluorescent dyes (8). Furthermore, early work by Shapiro and coworkers (9) indicated it might be possible to study by this technique the small T_2 bacteriophage, a tubular virus of roughly 100 nm in diameter (10), and Reovirus, which has a 600–800 nm icosahedral capsid (11). More recently, the laboratories of Brussaard and Steen (12–15) extended these findings to several other viruses including herpes simplex virus Type 1 (HSV-1) and the related cytomegalovirus stained with SYBR green. However, this powerful technique has yet to be used to separate different viral particle populations. This would provide new means to learn about virus assembly, viral intermediates, and their interactions with host proteins.

HSV-1 is a human pathogen causing mild to severe conditions ranging from cold sores to blindness, encephalitis, and serious new born complications as well as being an aggravating factor for AIDS (16–18). It has a 152 kb double-stranded DNA genome within a 125 nm icosahedral capsid shell, itself wrapped by a complex layer of proteins termed the tegument and an external host-derived envelope, for a final size of roughly 250–300 nm (19). Following entry of the virus at the cell surface, the viral genome is ultimately delivered to the nucleus, where it replicates and leads to the assembly of new capsids. Four distinct nonenveloped capsid species are present in the nucleus. The first one is procapsids that are rarely detected because they are thermodynamically unstable (20). These procapsids are believed to give rise to three stable nuclear capsid populations. A-capsids appear to be capsids that fail to properly incorporate the viral genome (21). Similarly, B-capsids also lack viral DNA but, unlike A-capsids, are thought to never initiate the genome packaging step. They can be distinguished from the former capsids on the basis of their distinctive protein contents. In contrast to these two abortive particles, C-capsids incorporate the viral genome and ultimately form mature enveloped virions. According to common belief, only mature nuclear C-capsids travel across the two nuclear membranes by an envelopment/de-envelopment mechanism and are ultimately re-enveloped elsewhere in the cell, likely at the trans Golgi network (TGN) (22–25). These viral particles subsequently leave the TGN toward the cell surface by a constitutive pathway implicating the host protein kinase D and myosin Va (26–28). This maturation process from the nucleus to the cell surface is the subject of intense scrutiny as it is poorly understood, in part because of the several viral intermediates along the way. It would thus be most useful to individually isolate these intermediates to better characterize them.

This study probes the possibility to sort intracellular viral intermediates by focusing on HSV-1 viral nuclear C-capsids. We now report that we can detect these 125 nm particles by flow cytometry and sort them according to their DNA content by labeling them with the capsid permeable and nucleophilic Syto 13 fluorescent stain. PCR and EM were consistent with the isolation of C-capsids with minimal contamination from A- and B-capsids. These findings now enable a detailed analysis of this important viral intermediate. Moreover, this approach should be applicable to other HSV-1 intermediates and even to other viruses to study different maturation stages in an effort to sort our way through their viral life cycles.

Materials and Methods

Cells and Viruses

Human HeLa S3 cells (ATCC # CCL-2.2) adapted to suspension culture were grown at 37°C in JMEM (Joklik's modified Eagle's medium; Sigma-Aldrich) supplemented with 5% fetal bovine serum, 0.1 mM nonessential amino acids, 100 U/mL penicillin, and 100 μg/mL streptomycin. HSV-1 F strain and the recombinant K26GFP KOS strain, which expresses green fluorescence protein (GFP) tagged VP26 capsid protein (29), were originally provided from Beate Sodeik (Hannover Medical School, Germany) and Prashant Desai (The Johns Hopkins University, USA), respectively. Both viruses were amplified on BHK and tittered on Vero cells as previously described (22).

Isolation of Total Nuclear Capsids

HeLa S3 cells were infected with wild type HSV-1 or K26GFP for 8 h at a multiplicity of infection of 5. The nuclei were then harvested by mechanical disruption of the cells and density centrifugation in the presence of a protease inhibition cocktail (8.25 μM de chymostatin, 1.05 μM leupeptin, 0.38 μM aprotinin, 0.73 μM pepstatin A; Sigma-Aldrich) as described before (30). These nuclei were subsequently topped up with 1% d'IGEPAL CA-630 (Sigma-Aldrich) and incubated for 30 min at 4°C. They were then treated with 500 U/mL DNase I (Roche) and 25 μg/mL of RNAse A for 10 min at 37°C to remove nonencapsidated nucleic acids. To isolate the nuclear viral capsids, the nuclear lysates were briefly sonicated and large debris removed by low speed centrifugation (5 min/4°C at 300*g*). The supernatant, containing the nuclear capsids, was filtered through a 0.45 μm filter and spun 1 h through a 35% (w/w) sucrose cushion at 100,000*g* at 4°C. The total capsid pellet was finally resuspended in 100 μL of MNT (30 mM MES, 100 mM NaCl, 20 mM Tris-HCl pH 7.4). The capsids were either frozen or analyzed immediately (see below).

Fluorescent Labeling of Viral Particles

Four microliters of a diluted fraction of DNAse/RNAse treated nuclear capsids were incubated for 30 min at 4°C with 1–5 μM Syto 11–14, 16, 21, 24, or 25 (Invitrogen). Alternatively, 5 μg/mL of Hoechst 33342 was used to label the capsid bound DNA. These labeled capsids were finally examined by fluorescence microscopy and by flow cytometry.

Efficient Detection of Intranuclear DNA

To determine the ability of Syto 13 to specifically label encapsidated viral genomes, 200 μL of wild type or K26GFP nuclear lysates (see above) were (A) treated for 10 min at 55°C with 1 mg/mL of proteinase K (recombinant, PCR grade, Roche) to disassemble the protein-based capsids and free their genome content and thus obtain the total DNA present in the nuclei; (B) first treated for 10 min at 37°C with 500 U/mL of DNAse I (Roche) to digest both cellular and nonencapsidated viral DNA then with proteinase K to only keep the capsid

bound viral DNA; or (C) first treated with proteinase K subsequently inactivated for 10 min at 95°C (to avoid the degradation of the DNAse I) and finally incubated with DNAse I in the presence of 10 mM $CaCl_2$ to protect the DNAse I from any residual proteinase K activity (31). In this last scenario, no DNA should remain because both encapsidated and nonencapsidated DNA should be digested. In all cases, the samples were processed as per manufacturer's instructions to isolate the non digested DNA with a GenElute Mammalian Genomic DNA Miniprep Kit (Sigma-Aldrich), which contains RNAse I. These samples were ultimately analyzed by quantitative PCR using GFP specific primers to detect the K26GFP viral genome (forward: 5′ACGTAAACGGCCACAAGTTC3′; reverse: 5′AAG TCGTGCTGCTTCATGTG3′) or GAPDH specific primers to detect cellular DNA (forward: 5′AGGGCCCTGACAACTCT TTT3′; reverse: 5′AGGGGTCTACATGGCAACTG3′). This was performed with a LightCycler 480 (Roche) using the PerfeCTa SYBR Green SuperMix (Quanta BIOSCIENCES). The data were finally analyzed using LightCycler® 480 software version 1.5 and expressed in relative genome copy. Two independent experiments, each done in duplicates, were pooled.

Fluorescence Microscopy

Fluorescently labeled capsids were examined on an Axiophot microscope (Zeiss) equipped with a Retiga 1300 camera (Q imaging) or, for confocal microscopy, on a DM IRBE inverted microscope (Leica) coupled to a SP1 spectrometer and argon (488 nm), argon-krypton (568 nm), and helium-neon (647 nm) lasers. Epifluorescent images were analyzed with Northern Eclipse (Empix imaging) and Photoshop CS5 (Adobe), whereas confocal images were processed with the LCS Lite software and Photoshop CS5.

Flow Cytometry

Polystyrene beads from Estapor (100 and 800 nm) or Polysciences (200 nm) were diluted 1:1,000 in MNT and analyzed on a FACSAria IIu sorter (BD Biosciences) equipped with a 100 μm nozzle and 405, 488, and 633 nm lasers. The original concentrations of the samples were 6.36×10^{13} (100 nm), 5.68×10^{12} (200 nm), and 2.34×10^{11} (800 nm) beads/mL. A 100 μm nozzle, rather than a smaller one, was used to reduce the pressure and hence maximize the excitation time and signal strength. The fluorescently labeled viral capsid preparations were diluted 1:500 and analyzed on the above instrument. In that case, the concentration of the stocks is unknown and varied from preparation to preparation. For GFP and Syto labeled capsids, 502 nm longpass and 530/30 bandpass filters were used. Analysis and sorting were performed at low pressure (23 psi) and flow rate between 1 and 3 for a maximum of 3,000 events/sec to minimize coincidental events. In all cases, a minimal threshold of 200 for the SSC channel was use to remove some of the background signal. The data were initially acquired with the FACSDiva software (BD Biosciences) and then processed with FlowJo (TreeStar). After sorting, the diluted capsids were concentrated at 100,000*g* at 4°C for 1 h on a 35% sucrose cushion (w/w). The capsid pellet was then resuspended in MNT and frozen at −80°C.

The instrument was cleaned between every sample with BD FACS Clean (with 10% bleach) and back flushed with sheath. However, only one large sample was normally analyzed per day. When multiple samples were analyzed, we started with unlabeled capsids and finished with labeled ones. Each solution, including the control MNT buffer and sheath, was 0.22 μm filtered. At the end of the day, the instrument was cleaned with 1% Virkon (Antec International).

Electron Microscopy

The samples were processed for negative staining as previously described (32). Briefly, 5 μL of the sorted capsids were deposited on a copper grid previously coated with Formvar and carbon (Canemco & Marivac). Excess liquid was removed with a filter paper and the samples contrasted with 2% uranyl acetate (Canemco & Marivac). Following a quick wash in water, the grids were air dried and examined on a Philips 300 transmission electron microscope. Quantification of the capsids found in the samples was done from randomly selected fields from at least three independent experiments.

PCR

To independently evaluate the presence of viral DNA in the flow cytometry sorted samples (Fig. 5), they were analyzed by standard PCR using HSV-1 UL20 specific primers and limited cycling as before (29) (sense primer: 5′atgaccatgcggg atgaccttc3′; antisense primer: 5′ttagaacgcgacgggtgcattc3′). The amplified fragments were separated on a 1.5% agarose gel and revealed with ethidium bromide. For these experiments, the positive control consisted of viral DNA extracted from infected cells, whereas the negative control was DNA extracted from noninfected cells.

Results

Detection of Small Particles by Flow Cytometry

To evaluate if flow cytometry may be a practical approach to sort viral capsids, we first tested commercially available microspheres of different sizes. This was particularly important given the 0.5 μm detection limit stated by the instrument manufacturer, a limit four times above the size of HSV-1 nuclear particles, which are 125 nm in diameter. We, therefore, analyzed by flow cytometry 100 nm, 200 nm, and 800 nm beads at a low flow rate for optimal detection. Figure 1 shows that the 800 nm beads (i.e., above the instrument threshold) were readily detected by both side and forward scattering. The smaller 100 and 200 nm beads differed substantially from the larger beads but not one from another. These smaller beads were also indistinguishable in the FSC channel from the buffer control, where 0.22 μm filtered MNT was passed over the instrument. However, one could clearly distinguish them in the SSC channel, which revealed both individual and aggregated beads. Together, this showed that particles as small as 100 nm could indeed be detected but not sorted from 200 nm particles based on their size. Interestingly, this implied that the 125 nm HSV-1 nuclear capsids should be detected by flow cytometry, not based of their size but rather the ability of such small particles to reflect light as measured by side scattering.

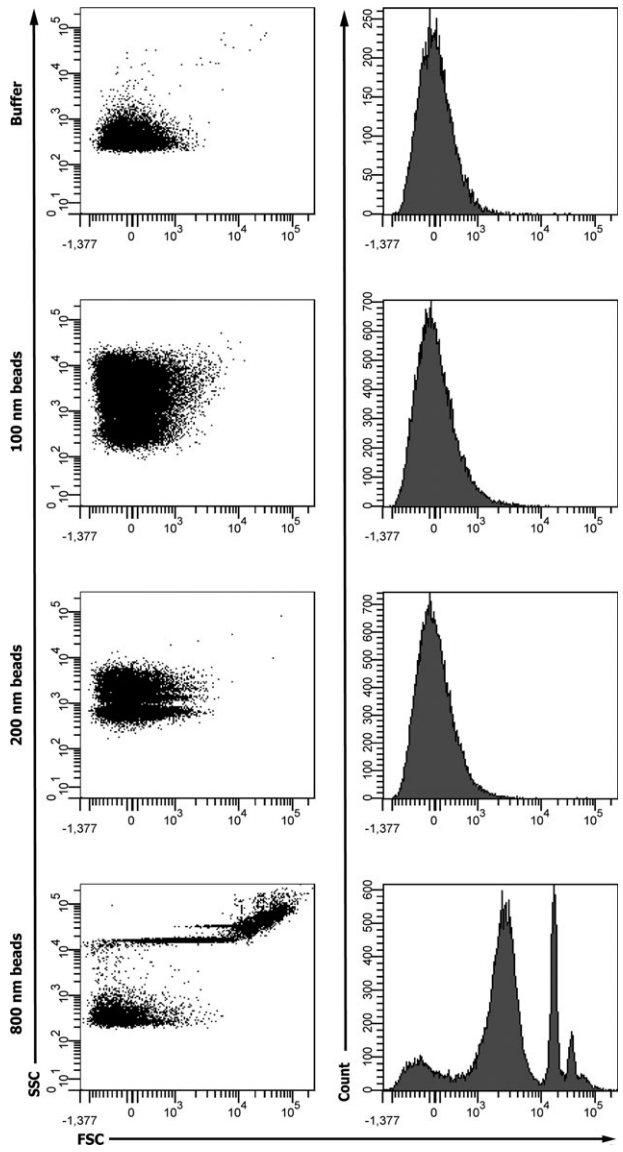

Figure 1. Flow cytometric sorting of fluorescent beads. Commercially available 100, 200, or 800 nm fluorescent beads were diluted 1:1,000 in MNT to reduce the number of events/sec and analyzed on a BD FACSAria sorter. The left panels denote the forward (FSC) and side (SSC) scattering, whereas the right panels show their forward scattering distribution. The smaller peaks for the 800 nm beads were attributed to bead aggregates. ''Buffer'' refers to the MNT used to dilute the beads. A minimal threshold of 200 for the SSC channel was applied to remove some of the background signal. No gates were applied so the dot plots represent 100% of the samples.

Detection of GFP Tagged HSV-1 Capsids

As for many other viruses, several components of the HSV-1 virions have been tagged with fluorescent moieties. Hence, genetically modified HSV-1 strains encode a labeled component of the capsid, the tegument or a glycoprotein present in the viral envelope. One such strain named K26GFP tags the essential HSV-1 VP26 viral capsid protein and is, thus, a useful marker to follow intracellular viral capsids at different stages of infection (22,29). To directly assess the ability of the flow cytometer to detect HSV-1 capsids, we took advantage of this recombinant strain. Cells were infected with K26GFP or control nonfluorescent wild type virus and the nuclei harvested 8 h later. As detailed in "Materials and Methods" section, capsids were then isolated from these nuclei. As expected from the above results, both types of capsids were detectable by light scattering (Fig. 2, left panels). Excitingly, the K26GFP capsids gave a significant fluorescence signal, whereas the untagged wild type capsids had none (Fig. 2, middle and right panels). We, therefore, concluded that GFP tagged HSV-1 capsids can indeed be detected by flow cytometry by light scattering and fluorescence.

Detection of Mature Nuclear C-Capsids by Labeling Their DNA Content

The ability to detect HSV-1 capsids enabled us to evaluate if it is possible to enrich the preparation in nuclear C-capsids, the precursor of mature virions. Because A- and B-capsids are devoid of viral genome and C-capsids are loaded with a complete viral genome, we tested various fluorescent DNA dyes to label the latter capsids. Initial staining of nuclear capsids with Hoechst or Dapi revealed spotty signals that partially overlapped with K26GFP by immunofluorescence but failed to give a signal by flow cytometry, presumably because the intensity of the dyes was too weak (data not show). Given that Syto 13, a RNA and DNA binding fluorescent stain, was recently used to successfully detect 0.1–1.0 μm microparticles (3), we probed a commercial sampler kit consisting of eight different Syto reagents (Invitrogen). Each of these membrane permeable cyanine derived stains has unique properties in terms of nucleic acid affinity and fluorescence energy with distinct but similar excitation/emission spectra. Collectively, they bind nucleic acids by multiple means, including intercalation, direct interaction with the nucleic acid backbone and reportedly by binding to the DNA groove (33). Most importantly, as free molecules they produce low background signals that are significantly enhanced once they bind to nucleic acid (quantum yield greater than 0.4). Enriched nuclear capsid preparations were, thus, individually labeled with each of the dyes as per manufacturer's instructions and first examined by immunofluorescence. While most gave no apparent specific signal over the background (i.e., Syto 12, 14, 16, 21, 24, 25), two proved promising and exhibited significant signals (Syto 11 and 13; data not shown). Moreover, this indicated that these two reagents could associate with viral DNA present in assembled capsids.

To evaluate if we specifically target viral capsids with the Syto dyes, we first treated whole nuclear lysates with DNAse I to digest both cellular and nonencapsidated viral DNA and then released the viral genome from the capsids with proteinase K. Under these conditions, only viral DNA within the capsids is expected (34). We then evaluated by qPCR the presence of viral and cellular DNA in the samples following the purification of total genomic and viral DNA with a commercial kit containing RNAse A (see "Materials and Methods" section). As control, we solely digested the samples with proteinase K to get the total amount of cellular or viral DNA present in the

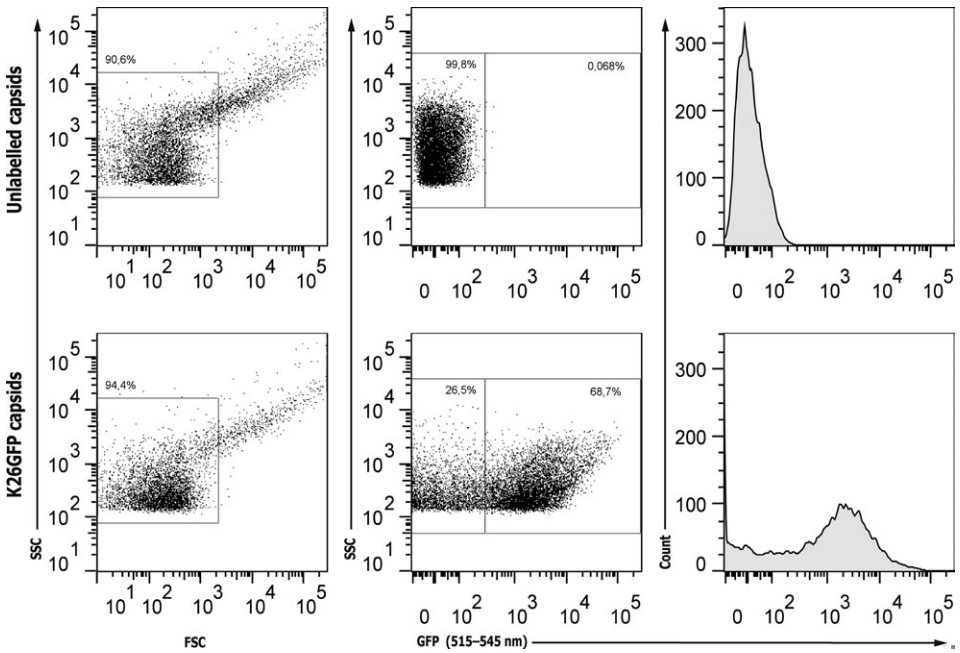

Figure 2. Detection of GFP tagged capsids by flow cytometry. DNAse/RNAse treated nuclear capsids were prepared from wild type (i.e., nonfluorescent) infected cells or from cells infected with the K26GFP strain (i.e., fluorescent capsids). They were then diluted 500-fold in MNT to reduce the number of events/sec and examined by flow cytometry. A minimal threshold of 200 for the SSC channel was once again used to remove some of the background signal. The left panels show the dot plots of the scattering (SSC vs. FSC) that were used to define gates (see boxes). These gates contained the bulk of the capsids (>90%) and excluded the larger capsid aggregates. The samples were excited with a 488 nm laser coupled to an emission filter allowing the 515-545 nm wavelengths to go through. The middle and right panels show the fluorescence profiles of the gated material (dot plots and histograms, respectively).

nuclear lysates. We additionally inverted the DNAse I/proteinase K steps by first treating the nuclear lysates with proteinase K then DNAse I to remove all DNA from the sample. As expected, strong cellular and viral signals were present when the nuclear lysates were treated with proteinase K only and no signal was found when first treated with proteinase K then DNAse I (Supporting Information Fig. 1). In contrast, when the samples were first digested with DNAse I then treated with proteinase K, 1–2% of the total viral DNA was detected within the capsids, whereas no cellular DNA was detected. This indicated that these conditions were appropriate to specifically label the encapsidated DNA, that only a small proportion of the viral DNA was encapsidated, and that no cellular DNA was detectable within the capsids. We concluded it was thus possible to label the encapsidated viral DNA with nucleic acid reagents under these conditions.

Because gating on the capsids was possible, we examined by flow cytometry the fluorescence levels of nuclear capsids labeled with either Syto 11 or 13. We, thus, isolated viral capsids from DNAse I/RNAse A infected nuclei and then stained the capsids. Naturally, proteinase K was absent in these experiments to preserve the integrity of the capsids. As controls, we included unstained wild type or K26GFP capsids along with wild type capsids stained with Syto 24, which labeled the capsids less efficient than Syto 11 or 13. As expected, the level of fluorescence for unlabeled wild type capsids was minimal [mean fluorescence intensity (MFI) of 13; Fig. 3]. The data confirmed a stronger signal for the tagged K26GFP capsids (MFI of 2,878), in agreement with our immunofluorescence observations. Interestingly, Syto 11- and Syto 13-stained capsids gave an even stronger fluorescent signal (MFI of 25,700 and 53,600, respectively). Syto 24-labeled capsids had an intermediate signal that was oddly bimodal (MFI of 11,400). Altogether, this meant that it is possible to stain the encapsidated viral genome in intact HSV-1 nuclear C- capsids and detect them by both light scattering and fluorescence. Given the best signal obtained with the Syto 13 dye, all remaining experiments were performed with this dye.

Sorting of Nuclear Capsids

Given the ability of flow cytometry to physically detect the viral particles and the possibility to specifically fluorescently stain the viral genome within intact capsids, we proceeded to sort by flow cytometry the HSV-1 nuclear capsids. Wild type nuclear capsids were isolated from infected cells as before and incubated with Syto 13 to label the encapsidated viral DNA. They were then sorted according to their fluorescence profiles, gating on the capsids by both side scattering and strength of Syto 13 emission. Interestingly, a reproducibly continuous fluorescence signal ranging from low to high was observed (Fig. 4). Moreover, a change of slope was always observed past the mid point in the fluorescence channel. We then arbitrarily defined three regions of interest, with fraction 1 having no fluorescence signal (no DNA content), fraction 2 with an intermediate signal and fraction 3 with the highest signal (high DNA content), with the change of slope as the

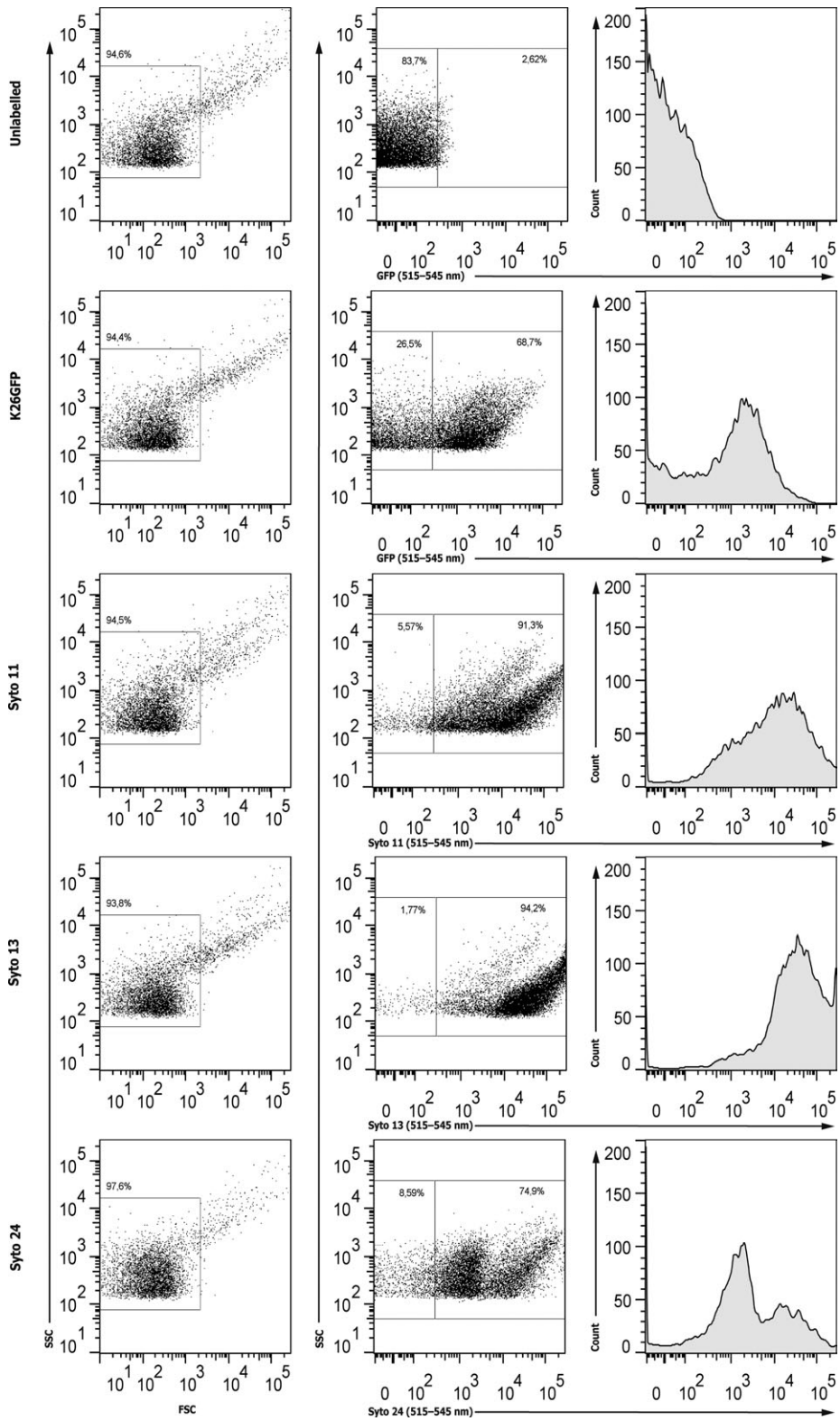

Figure 3. Testing of Syto fluorescent nucleic acid stains. DNAse and RNAse treated nuclear capsids were isolated as before from wild type infected cells and stained with Syto 11, 13, or 24. As control, unstained wild type or K26GFP nuclear capsids were used. All capsids were diluted 500-fold and analyzed by flow cytometry. The samples were excited with a 488 nm laser coupled to an emission filter allowing the 515-545 nm wavelengths to go through. The left panels show the light scattering of the samples (SSC vs. FSC). Once again, a minimal threshold of 200 for the SSC channel was applied as before to remove some of the background signal. The boxes represent the gates (greater than 90% of the samples) used for analysis in the middle and right panels. These panels show the fluorescence profiles of the gated samples (dot plots and histograms, respectively). The signals for Syto 13 stained capsids (MFI of 53,600) was significantly above that for Syto 11 (MFI of 25,700), Syto24 (MFI of 11,400), or K26GFP (MFI of 2,878).

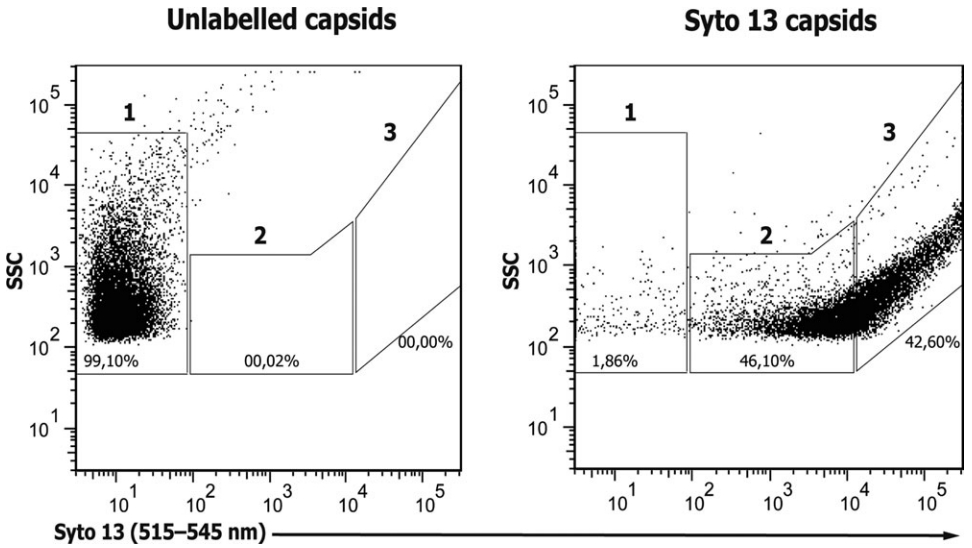

Figure 4. Sorting of Syto 13 labeled capsids. DNAse and RNAse treated nuclear capsids were stained with Syto 13, diluted 500-fold and sorted by flow cytometry. As control, unstained nuclear capsids were used. Three gates were arbitrarily defined in the SSC/fluorescent channels. Fraction 1 was based on the control capsids, which were not fluorescent. The remainder of the signal was divided up into two fractions (2 and 3) with the change of slope in the SSC channel as the boundary between the two fractions. The mean fluorescence intensities were −532 (fraction 1), 9,970 (fraction 2), and 70,719 (fraction 3) in the experiments depicted here. The samples were excited with a 488 nm laser coupled to an emission filter allowing the 515-545 nm wavelengths to go through. A minimal threshold of 200 for the SSC channel was used to remove some of the background signal.

boundary between fractions 2 and 3 (see Fig. 4). Fraction 1 was reproducibly detected and represented a small portion of all viral particles (1.86% in the experiment shown; 4.6% ± 0.9 on average from 9 independent flow cytometry analyses). Similarly, fractions 2 and 3 were also always detected and on average contained 57.1% ± 4.5 and 36.1% ± 5.9 of total capsids, respectively. The three fractions exhibited increased levels of fluorescence (fraction 1: MFI of −532; fraction 2: 9,970 and fraction 3: 70,719 in the experiment depicted in Fig. 4). In contrast, unlabeled wild type capsids were exclusively found in the first fraction (97.8% ± 0.8 of all capsids; average of 4 independent experiments) with an average fluorescence of 3 in the experiment shown in Figure 4. Thus, it seemed possible to distinguish different capsid populations in these nuclear preparations.

Characterization of the Viral Fractions Sorted by Flow Cytometry

To insure that the particles previously sorted were indeed of viral origin and examine how the three fractions correlate with A-, B-, and C-capsids, we performed a PCR amplification using HSV-1 specific primers, taking advantage of the fact that A- and B-capsids differ from C-capsids in their genome content. Note that the sorted capsids were pretreated with DNAse I as described in "Materials and Methods" section, so the PCR reaction only monitored encapsidated viral DNA. Although sorting was a slow process due to the low pressure and flow rate required to avoid coincidental events, we retrieved in the order of 1–10 μg of total proteins for A- and B-capsids for roughly 24 h of sorting. This was significantly higher for C-capsids, for which we obtained up to 30 μg. These differences in yields were not surprising because A-, B-, and C-capsids are not in equal abundance in the nucleus and even vary among cell types. We, therefore, normalized the PCR by total protein content, as determined by the commercial Bradford assay (Bio-Rad). As expected, a control HSV-1 total cell lysate was positive by PCR, whereas a cell lysate prepared from noninfected cells was negative (Fig. 5). The data further indicated that fraction 1 (no fluorescence by flow cytometry), did not contain any detectable viral genome, con-

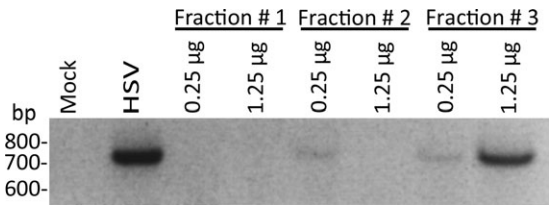

Figure 5. PCR of flow cytometry sorted capsids. DNA I treated and flow cytometry sorted nuclear capsids were concentrated by high speed centrifugation and analyzed by standard PCR using primers specific for the HSV-1 UL20 gene. DNA purified from either mock or HSV-1 infected cell lysates was included as negative and positive controls respectively. Either 0.25 or 1.25 μg of total protein of each fraction was used for the PCR reactions. Following amplification, the samples were resolved by electrophoresis on an agarose gel stained with ethidium bromide. For clarity, the image of the stained gel was inverted to better show the signals. Note the positive signal for fractions 2 and 3. The size of the fragment is indicated to the left of the figure. The absence of signal for the 1.25 μg of fraction 2 is likely caused by the large volume of sample needed for the PCR reaction which may be inhibitory. In this particular experiment, 1.25 μg of protein corresponded to 5 μL, 31.5 μL, and 12.5 μL for fractions 1, 2, and 3, respectively. The PCR reaction is done in 50 μL, so fraction 2 constitutes more than 60% of the total volume.

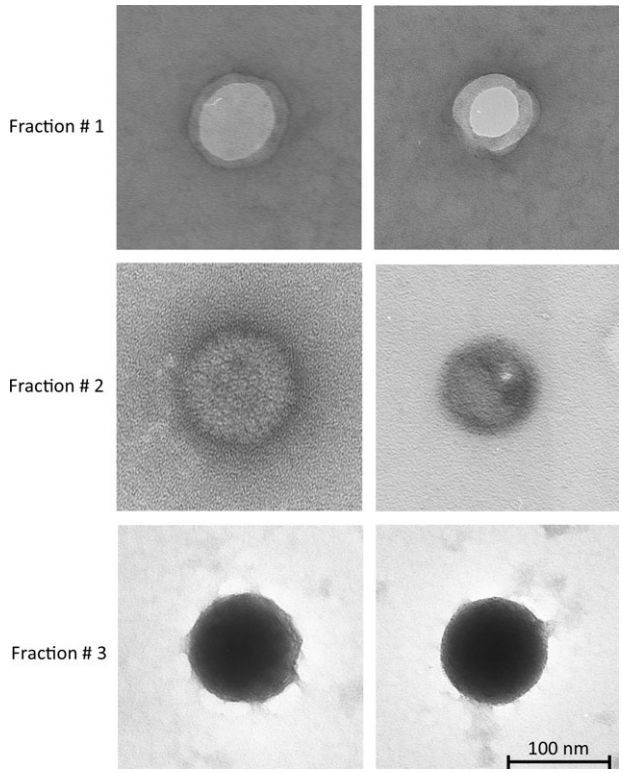

Figure 6. EM of flow cytometry sorted capsids. HSV-1 viral capsids were harvested from nuclei as above and flow cytometry sorted into three different fractions based on their DNA content (none, low, and high). Following their concentration by high speed centrifugation and resuspension in MNT, the capsids were examined by negative staining. Typical capsids are shown for each of the three fractions. Fraction 1 (top panels) contained mostly empty A-capsids, whereas fractions 2 (medium panels) and 3 (lower panels) were enriched for B- and C-capsids, respectively.

sistent with DNA free capsids. At the other end of the spectrum, particles from fraction 3, which were strongly stained by Syto 13, were clearly positive by PCR, thus confirming that it contained viral DNA as would be expected from C-capsids. Interestingly, fraction 2 contained a faint but detectable level of HSV-1 DNA in line with the weak Syto 13 staining pattern seen by flow cytometric sorting.

Thus far, the results were most consistent with the enrichment of C-viral particles in the third fraction and the presence of DNA free capsids in fractions 1 and 2. To insure this was the case, we next examined the sorted fractions by EM negative staining. This technique is widely used to formally identify viral particles and distinguish different HSV-1 viral intermediates. C-capsids have a dark center by this technique, whereas DNA free A- and B-capsids are whitish and grayish, respectively. We, thus, contrasted the samples with uranyl acetate and visually inspected them (Fig. 6). Although somewhat dilute, even after concentration of the samples by high speed centrifugation, capsids were indeed detected in each of the fractions. Although some heterogeneity was present, capsids in fraction 1 nearly always contained capsids with a whitish empty core reminiscent of A-capsids (21), whereas fraction 3 mostly contained strongly stained electron dense capsid cores typical of C-capsids (30). Finally, fraction 2 was the most heterogeneous with capsids with cores of intermediate densities between A- and C- capsids similar to B-capsids reported elsewhere (21,35).

Quantification of the capsids by EM mirrored the flow cytometry results. Hence, the distribution of nuclear capsids before flow cytometric sorting was 13.7% $\pm$ 5.7 (A-capsids), 58.0% $\pm$ 2.6 (B-capsids), and 28.0% $\pm$ 7.0 (C-capsids) as determined by negative staining (n = 387). Meanwhile, as mentioned above, 4.6% $\pm$ 0.9 of the capsids were sorted to fraction 1, whereas 57.1% $\pm$ 4.5 and 36.1% $\pm$ 5.9 were in fractions 2 and 3, respectively. Unfortunately, it was not possible to evaluate the purity of fractions 1 and 2 by EM due to their low capsid content. However, EM quantification revealed that fraction 3 was composed of 90.7% $\pm$ 5.7 of C-capsids and only minor amounts of contaminating A- and B-capsids (6.3% $\pm$ 6.8 and 3% $\pm$ 3.5, respectively; n = 167), representing ~3-fold enrichment of the C-capsids by flow cytometry. Taken together, the data hint that fractions 1 and 2 could tentatively be A- and B-capsids, respectively, and that fraction 3 was most likely C-capsids. Thus, flow cytometric sorting constitutes a valid and novel method in the current toolbox to purify HSV-1 nuclear C-capsids, which are the precursors of mature extracellular virions.

Discussion

Viruses are small entities that are below the recommended size fractionation limit of common flow cytometry instruments. This study reveals that while particles in the 100–200 nm range cannot be resolved one from another, they are nonetheless detectable (Fig. 1). A slow flow rate is likely an important factor to prevent coincidental events and favor single detection of such small particles. Furthermore, incorporation of a fluorescent tag in the capsid or staining of the viral genome with a fluorescent reagent is also sufficient to detect them. Why some dyes worked better than others is unclear at the moment. It is likely an issue of specific binding sites, affinity, and emission energy. It may also be that some dyes better traverse the protein shell of the capsids. Interestingly, labeling of the HSV-1 DNA with the permeable nuclei acid Syto 13 stain proved more efficient to detect these particles than tagging one of the capsid proteins with GFP (Figs. 2 and 3). This is somewhat surprising given the high copy number of VP26 in the capsids, which is estimated at 952 copies (36). However, it is not known how many copies of Syto 13 bind to the very large HSV-1 genome and what the relative fluorescence intensity of this stain is compared with GFP. Importantly, this signal was not due to contaminating cellular nucleic acids or free viral DNA because the capsids were pretreated with RNAse A and DNAse I to remove all the nonencapsidated nuclei acids. Altogether, this means that it is possible to detect viral capsids by both light scattering and fluorescence and that labeling of the viral genome with Syto 13 is even better than when the minor capsid component VP26 is GFP tagged.

Light scattering and fluorescence signals provided a mean to sort the nuclear HSV-1 viral capsids. Although populations

Table 1. HSV-1 capsid types analyzed

	STABILITY AT 4°C	DNA CONTENT	CAPSID SHAPE	FINAL OUTCOME	COMMENT
Properties					
Nuclear capsids					
Procapsids	Unstable	None	Round	A, B and C capsids	Not Analyzed
A-capsids	Stable	None	Icosahedral	Abortive	
B-capsids	Stable	None	Icosahedral	Abortive	
C-capsids	Stable	Viral genome	Icosahedral	Mature virus	
	DETECTION BY FLOW CYTOMETRY				
	SIDE SCATTERING	FLUORESCENCE	PCR	EM	INTERPRETATION
This study					
Fraction					
1	YES	No fluorescence	No Signal	Light core	Possible A-capsids[a]
2	YES	Low fluorescence[b]	Low signal[b]	Variable	Possible B-capsids[a]
3	YES	High fluorescence	Strong signal	Dense dark core	C-capsids

The four nuclear capsid types found in HSV-1 infected cells are listed along with their known stability at 4°C and DNA content in the top portion of table. The bottom half of the table shows the results of this study.

Procapsids were not analyzed in this study since the samples were isolated at 4°C.

[a] Biochemical analysis required (see text).

[b] Likely due to some contamination by C-capsids.

were initially arbitrarily defined (Fig. 4), an analysis of these fractions by PCR (Fig. 5) and EM (Fig. 6) strongly suggested that fraction 3 is enriched in C-nuclear capsids, whereas fractions 1 and 2 were suggestive of A- and B- nuclear capsids, respectively. Hence, fraction 1 was devoid of any detectable viral DNA and had an empty core by negative staining, which is reminiscent of nuclear A-capsids as shown by others (21). Fraction 2 was somewhat problematic to define, because it was minimally positive for the viral genome and had an intermediate core density by negative staining. Although their appearance by EM hinted at nuclear B-capsids, the low DNA signals observed by flow cytometry and PCR were not consistent with that conclusion given these capsids are normally considered DNA free (21,35). The most likely explanation is that some contaminating C-capsids were present in this fraction and accounted for the weak DNA signal. Technically, one alternative explanation would be if we detected a partial incorporation of DNA in B-capsids or if they contained DNA in a form that binds less efficiently the Syto dye. However, these possibilities require further validation before they can be considered. To formally define fractions 1 and 2, a detailed biochemical characterization will be needed. However, this may be complicated by cross contamination because it is not be possible to distinguish by Western blotting between reduced but biologically relevant levels of particular proteins in one capsid type versus a limited detection due to low contamination by other capsid types. This is exemplified by sucrose sedimentation studies of HSV-1 nuclear capsids that show the enrichment of viral scaffold proteins in B-capsids but also trace amounts of these molecules in other fractions (e.g., (37–40)).

In contrast to first two fractions, the data strongly suggest that fraction 3 is C-capsids because PCR specifically detected the viral genome in those particles, that this viral genome is normally DNAse I resistant but DNAse I sensitive when pretreated with proteinase K (i.e., that genome is present within a protein shell), and the particles are of the right size. At times, one can also see the angular form of the icosahedral capsids on some images. Finally, these particles also exhibited a classical dense core by negative staining typical of C-capsids (30). EM analysis of this fraction revealed it was significantly enriched for that capsid type (90.7% $\pm$ 5.7 were indeed C-capsids) with less than 10% contamination by A- or B-capsids. This is slightly better than the reported 25% contamination by the classical 20–50% sucrose gradient purification (40). While neither approach yields perfectly pure samples, flow cytometric sorting thus constitutes a novel purification step that does not supplant classical sedimentation protocols but rather complements them when strongly enriched nuclear capsids are desired.

One particularly puzzling observation was the reproducible change of slope between fractions 2 and 3 in the SSC channel (Fig. 4). At this point, we do not know what is causing such change. Given that side scattering is influenced by surface granularity as opposition to particle size, it might be that C-capsids differ in that respect from the other two capsid populations but at this point it is difficult to ascertain the nature of this difference. Such slope change could theoretically be imparted by different DNA conformations, as mentioned above. Additional work is needed to clarify this point.

Flow cytometric analysis and sorting of cells has been instrumental to study various important cellular processes such as B and T cell biology, hematopoiesis, and stem cell differentiation to name a few. However, host-pathogen interactions involving viruses has often been limited to follow viral markers in infected cells due to the small size of these pathogens. This study shows that one can use flow cytometry not only to detect but also to sort nuclear HSV-1 intermediates (Table 1), despite an inappropriate size resolution at that

range. This hints that the sorting limit of flow cytometry instruments is in essence lower than the half micron stated by the manufacturers when viral particles are coupled to a DNA labeling dye or a GFP tagged virion component. This opens up exciting new avenues to study the life cycle of viruses and their interaction with their hosts. For instance, it should now be possible to incorporate flow cytometric sorting as a purification step in combination with classical sedimentation techniques to enrich specific viral intermediates and further analyze them in isolation from other viral intermediates. This may be particularly useful to study capsid maturation and egress, the complex coating of the capsids with the tegument, analyze mutants or define the interactions of specific viral intermediates with host proteins such as motor proteins, kinases, cytoskeletal components, or cellular proteins that might be incorporated in the viral particles. Moreover, this opens new research avenues to study different maturation stages of other viruses.

Acknowledgments

The authors thank Danièle Gagné of the IRIC's flow cytometry platform for her excellent technical skills, expertise, and advice. They also thank Kerstin Radtke, Danièle Gagné, and Daniel Henaff for critical reading of the manuscript.

Literature Cited

1. Davies D. Cell sorting by flow cytometry. In: Macey MG, editor. Flow Cytometry: Principles and Applications. Totowa, NJ: Humana Press; 2007. pp 257–276.
2. Tarnok A. Cytometry—The full circle. Cytometry A 2012;81A:3–4.
3. Ullal AJ, Pisetsky DS, Reich CF III. Use of SYTO 13, a fluorescent dye binding nucleic acids, for the detection of microparticles in in vitro systems. Cytometry A 2010;77A:294–301.
4. Hoen EN, van der Vlist EJ, Aalberts M, Mertens HC, Bosch BJ, Bartelink W, Mastrobattista E, van Gaal EV, Stoorvogel W, Arkesteijn GJ, Wauben MH. Quantitative and qualitative flow cytometric analysis of nanosized cell-derived membrane vesicles. Nanomedicine 2012;8:712–720.
5. van Gaal EV, Spierenburg G, Hennink WE, Crommelin DJ, Mastrobattista E. Flow cytometry for rapid size determination and sorting of nucleic acid containing nanoparticles in biological fluids. J Controlled Release 2010;141:328–338.
6. Fuller RR, Sweedler JV. Characterizing submicron vesicles with wavelength-resolved fluorescence in flow cytometry. Cytometry 1996;25:144–155.
7. Vorauer-Uhl K, Wagner A, Borth N, Katinger H. Determination of liposome size distribution by flow cytometry. Cytometry 2000;39:166–171.
8. Tracy BP, Gaida SM, Papoutsakis ET. Flow cytometry for bacteria: Enabling metabolic engineering, synthetic biology and the elucidation of complex phenotypes. Curr Opin Biotechnol 2010;21:85–99.
9. Hercher M, Mueller W, Shapiro HM. Detection and discrimination of individual viruses by flow cytometry. J Histochem Cytochem 1979;27:350–352.
10. DeBlois RW, Wesley RK. Sizes and concentrations of several type C oncornaviruses and bacteriophage T2 by the resistive-pulse technique. J Virol 1977;23:227–233.
11. Loh PC, Hohl HR, Soergel M. Fine structure of reovirus type 2. J Bacteriol 1965;89:1140–1144.
12. Brussaard CP, Marie D, Bratbak G. Flow cytometric detection of viruses. J Virol Methods 2000;85:175–182.
13. Brussaard CP. Optimization of procedures for counting viruses by flow cytometry. Appl Environ Microbiol 2004;70:1506–1513.
14. Steen HB. Flow cytometers for characterization of microorganisms. Curr Protoc Cytom 2001; Chapter 1: Unit 1.11.
15. Steen HB. Flow cytometer for measurement of the light scattering of viral and other submicroscopic particles. Cytometry A 2004;57A:94–99.
16. Brady RC, Bernstein DI. Treatment of herpes simplex virus infections. Antiviral Res 2004;61:73–81.
17. Palu G, Benetti L, Calistri A. Molecular basis of the interactions between herpes simplex viruses and HIV-1. Herpes 2001;8:50–55.
18. Van de Perre P, Segondy M, Foulongne V, Ouedraogo A, Konate I, Huraux JM, Mayaud P, Nagot N. Herpes simplex virus and HIV-1: Deciphering viral synergy. Lancet Infect Dis 2008;8:490–497.
19. Roizman B, Sears AE. Herpes simplex viruses and their replication. In: Fields BN, editor. Fields Virology, 3rd ed. Vol. 2. Philadelphia: Lippincott-Raven Publishers; 1996. pp 2231–2295.
20. Rixon FJ, McNab D. Packaging-competent capsids of a herpes simplex virus temperature-sensitive mutant have properties similar to those of in vitro-assembled procapsids. J Virol 1999;73:5714–5721.
21. Conway JF, Homa F. Nucleocapsid structure, assembly and DNA packaging of herpes simplex virus. In: Weller SK, editor. Alphaherpesviruses: Molecular Virology. Norfolk, UK: Caister Academic Press; 2011. pp 175–193.
22. Turcotte S, Letellier J, Lippe R. Herpes simplex virus type 1 capsids transit by the trans-Golgi network, where viral glycoproteins accumulate independently of capsid egress. J Virol 2005;79:8847–8860.
23. Mettenleiter TC, Klupp BG, Granzow H. Herpesvirus assembly: An update. Virus Res 2009;143:222–234.
24. Johnson DC, Baines JD. Herpesviruses remodel host membranes for virus egress. Nat Rev Microbiol 2011;9:382–394.
25. Henaff D, Radtke K, Lippé R. Herpesviruses exploit several host compartments for envelopment. Traffic 2012; In press.
26. Remillard-Labrosse G, Mihai C, Duron J, Guay G, Lippe R. Protein kinase D-dependent trafficking of the large herpes simplex virus type 1 capsids from the TGN to plasma membrane. Traffic 2009;10:1074–1083.
27. Remillard-Labrosse G, Lippe R. Meeting of conventional and unconventional pathways at the TGN. Commun Integr Biol 2009;2:434–436.
28. Roberts KL, Baines JD. Myosin Va enhances secretion of herpes simplex virus 1 virions and cell surface expression of viral glycoproteins. J Virol 2010;84:9889–9896.
29. Desai P, Person S. Incorporation of the green fluorescent protein into the herpes simplex virus type 1 capsid. J Virol 1998;72:7563–7568.
30. Remillard-Labrosse G, Guay G, Lippe R. Reconstitution of herpes simplex virus type 1 nuclear capsid egress in vitro. J Virol 2006;80:9741–9753.
31. Tullis RH, Rubin H. Calcium protects DNase I from proteinase K: A new method for the removal of contaminating RNase from DNase I. Anal Biochem 1980;107:260–264.
32. Loret S, Guay G, Lippe R. Comprehensive characterization of extracellular herpes simplex virus type 1 virions. J Virol 2008;82:8605–8618.
33. Tarnok A. SYTO dyes and histoproteins—Myriad of applications. Cytometry A 2008;73A:477–479.
34. Church GA, Dasgupta A, Wilson DW. Herpes simplex virus DNA packaging without measurable DNA synthesis. J Virol 1998;72:2745–2751.
35. Newcomb WW, Thomsen DR, Homa FL, Brown JC. Assembly of the herpes simplex virus capsid: Identification of soluble scaffold-portal complexes and their role in formation of portal-containing capsids. J Virol 2003;77:9862–9871.
36. Baines J, Duffy C. Nucleocapsid assembly and envelopment of herpes simplex virus. In: Sandri-Goldin RM, editor. Alpha Herpesviruses. Norfolk: Caister Academic Press; 2006. pp 175–204.
37. Gibson W, Roizman B. Proteins specified by herpes simplex virus. 8. Characterization and composition of multiple capsid forms of subtypes 1 and 2. J Virol 1972;10:1044–1052.
38. Desai P, Watkins SC, Person S. The size and symmetry of B capsids of herpes simplex virus type 1 are determined by the gene products of the UL26 open reading frame. J Virol 1994;68:5365–5374.
39. Sheaffer AK, Newcomb WW, Brown JC, Gao M, Weller SK, Tenney DJ. Evidence for controlled incorporation of herpes simplex virus type 1 UL26 protease into capsids. J Virol 2000;74:6838–6848.
40. Roos WH, Radtke K, Kniesmeijer E, Geertsema H, Sodeik B, Wuite GJ. Scaffold expulsion and genome packaging trigger stabilization of herpes simplex virus capsids. Proc Natl Acad Sci USA 2009;106:9673–9678.

Annexe III : Contribution dans l'article "The ATP-Dependent RNA Helicase DDX3X Modulates Herpes Simplex Virus 1 Gene Expression"

La contribution de Nabil El Bilali dans ce travail a été par la conception, la réalisation et l'analyse des expériences de RT-qPCR pour les figures 11 à 13.

Les données et les résultats présentés dans cet article ont tous été générés durant les études de doctorat du candidat Nabil El Bilali.

AMERICAN SOCIETY FOR MICROBIOLOGY | Journal of Virology®

VIRUS-CELL INTERACTIONS

The ATP-Dependent RNA Helicase DDX3X Modulates Herpes Simplex Virus 1 Gene Expression

Bita Khadivjam,[a] Camille Stegen,[a] Marc-Aurèle Hogue-Racine,[a] Nabil El Bilali,[a] Katinka Döhner,[b] Beate Sodeik,[b] Roger Lippé[a]

Department of Pathology and Cell biology, University of Montreal, Montreal, Quebec, Canada[a]; Institute of Virology, Hannover Medical School, Hannover, Germany[b]

ABSTRACT The human protein DDX3X is a DEAD box ATP-dependent RNA helicase that regulates transcription, mRNA maturation, and mRNA export and translation. DDX3X concomitantly modulates the replication of several RNA viruses and promotes innate immunity. We previously showed that herpes simplex virus 1 (HSV-1), a human DNA virus, incorporates DDX3X into its mature particles and that DDX3X is required for optimal HSV-1 infectivity. Here, we show that viral gene expression, replication, and propagation depend on optimal DDX3X protein levels. Surprisingly, DDX3X from incoming viral particles was not required for the early stages of the HSV-1 infection, but, rather, the protein controlled the assembly of new viral particles. This was independent of the previously reported ability of DDX3X to stimulate interferon type I production. Instead, both the lack and overexpression of DDX3X disturbed viral gene transcription and thus subsequent genome replication. This suggests that in addition to its effect on RNA viruses, DDX3X impacts DNA viruses such as HSV-1 by an interferon-independent pathway.

IMPORTANCE Viruses interact with a variety of cellular proteins to complete their life cycle. Among them is DDX3X, an RNA helicase that participates in most aspects of RNA biology, including transcription, splicing, nuclear export, and translation. Several RNA viruses and a limited number of DNA viruses are known to manipulate DDX3X for their own benefit. In contrast, DDX3X is also known to promote interferon production to limit viral propagation. Here, we show that DDX3X, which we previously identified in mature HSV-1 virions, stimulates HSV-1 gene expression and, consequently, virion assembly by a process that is independent of its ability to promote the interferon pathway.

KEYWORDS DDX3X, helicase, herpes, host-pathogen interaction, DNA virus, RNA virus, interferon, herpes simplex virus, host-pathogen interactions, transcriptional regulation, translational control

The human DDX3 protein is a member of a large family of DEAD box ATP-dependent RNA helicases. In humans, it is encoded by the X (DDX3X) and Y (DDX3Y) chromosomes, albeit the latter is restricted to testes (1). It participates in different stages of cellular gene expression, such as transcription, mRNA maturation, and mRNA export and translation (2). Given these crucial roles in RNA biology, several RNA viruses interact with DDX3X, often with important consequences for viral replication. This includes hepatitis C virus (HCV), norovirus, West Nile virus, and Japanese encephalitis virus (3–7). This is also the case for HIV and hepatitis B virus (HBV), a peculiar DNA virus that relies on an RNA template and reversed transcription to replicate its genome (8, 9). Furthermore, DDX3X also contributes to innate immunity against these viruses. For instance, DDX3X stimulates interferon (IFN) type I production by binding IKKε (IκB kinase epsilon) and TBK1 (tank-binding kinase 1), leading to IRF3 phosphorylation and activation (10,

Received 15 December 2016 **Accepted** 25 January 2017

Accepted manuscript posted online 1 February 2017

Citation Khadivjam B, Stegen C, Hogue-Racine M-A, El Bilali N, Döhner K, Sodeik B, Lippé R. 2017. The ATP-dependent RNA helicase DDX3X modulates herpes simplex virus 1 gene expression. J Virol 91:e02411-16. https://doi.org/10.1128/JVI.02411-16.

Editor Rozanne M. Sandri-Goldin, University of California, Irvine

Address correspondence to Roger Lippé, roger.lippe@umontreal.ca.

11). These findings position DDX3X as a critical player for the replication and immunity against RNA-based viruses. However, its role is not restricted to these viruses since it also impacts innate immunity against DNA viruses. For instance, the HBV viral polymerase binds IKKε and blocks its ability to interact with DDX3X, thereby hampering interferon production to the benefit of the virus (12). Similarly, the vaccinia virus (VACV) K7 protein binds and sequesters DDX3X and prevents its interaction with the above kinases, once again blocking interferon activation in favor of viral propagation (13). DDX3X is therefore an important mediator of host-pathogen interactions that acts via multiple and likely parallel routes on many RNA and at least two distinct DNA viruses.

Herpes simplex virus 1 (HSV-1) is a ubiquitous human pathogen that is dormant in 80 to 90% of the population but causes clinical symptoms in roughly a third of humans. It is primarily associated with cold sores but is also responsible for severe infections in both immunocompetent and immunodeficient individuals (14). Replication of herpesviruses occurs in the cell nucleus, where the virus takes over the host gene expression machinery during an active infection. Three classes of HSV-1 genes, namely, the immediate early (IE), early (E), and late (L) genes, are expressed in a sequential manner by the cellular RNA polymerase II and a collection of transcriptional and translational cellular factors (15). This expression cascade is stimulated by ICP0, ICP4, and VP16, three tegument components present in mature viral particles that promptly act as transactivators following viral entry in the cell (16–20). As for other viruses, HSV-1 gene expression is clearly dependent on both viral and host proteins.

Past studies from our laboratory revealed that HSV-1 incorporates DDX3X into its mature particles (16). Most interestingly, depleting either the viral or the cellular pool of DDX3X significantly impairs HSV-1 infectivity (21). As the exact function of DDX3X in the HSV-1 replication cycle is not clear, we examined more closely the nature of this host-pathogen interaction. The present data from multiple assays show that DDX3X impacts the propagation of HSV-1. They also reveal that the portion of DDX3X present in the incoming virions is not required for the early stages of HSV-1 entry. In contrast, depletion of DDX3X from the cell impacted viral particle assembly and intracellular and extracellular viral yields. Interestingly, either reducing or overexpressing the cellular pool of DDX3X downregulated HSV-1 gene expression. This dependency on DDX3X protein levels was corroborated in rescue experiments using cells that were depleted by a small interfering RNA (siRNA) targeting DDX3X (siDDX3X) and that concomitantly expressed an siRNA-resistant DDX3X construct. At the mechanistic level, DDX3X modulated the transcription of immediate early, early, and late viral genes, including the aforementioned viral transactivating proteins ICP0, ICP4, and VP16. This appeared independent of the ability of DDX3X to promote IFN-β production. We conclude that DDX3X modulates HSV-1 yields by a novel mechanism implicating viral gene transcription, irrespective of the interferon pathway.

RESULTS

DDX3X is required for optimal viral yields. We previously reported by proteomics that HSV-1 incorporates the host protein DDX3X in mature virions (16) and that both the cellular and virion-incorporated pools of DDX3X influence viral yields (21). To independently validate the role of the cellular DDX3X in viral replication, we resorted to the BHK21-derived tsET24 cell line, which harbors a temperature-sensitive (ts) DDX3X inactive at 39.5°C but functional at 34°C (22). Infection of the tsET24 and parental BHK21 cell lines with wild-type HSV-1 showed that viral yields were strongly reduced at the nonpermissive temperature in the tsET24 cell line but not affected in the parental cell line (Fig. 1). This confirmed that DDX3X is indeed a modulator of the HSV-1 life cycle. It also ruled out that nonspecific off-target effects were responsible for our past findings (21).

HSV-1 yields are sensitive to DDX3X levels. Given that viral yields were lowered upon depletion of the host protein DDX3X, we probed whether overexpression of the protein would have the opposite effect on HSV-1. An initial examination by immunofluorescence microscopy indicated that overexpression did not influence the subcellu-

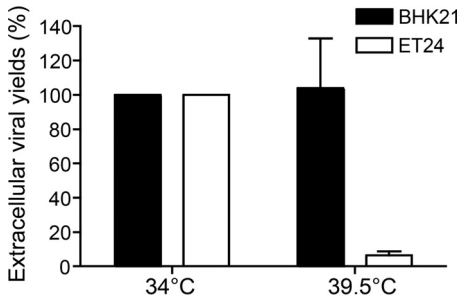

FIG 1 DDX3X is necessary for HSV-1 replication. The DDX3X thermosensitive tsET24 and parental BHK21 cell lines were incubated for 24 h prior to infection at the permissive (34°C) or nonpermissive (39.5°C) temperature and infected with HSV-1 K26GFP (MOI of 5) for an additional 24 h at that same temperature. Afterwards, supernatants were collected and titrated on Vero cells. Titers were normalized to the mean value obtained with samples infected at 34°C (arbitrarily set to 100%). Data represent the averages of two independent experiments, each titrated in duplicates. The error bars represent the standard deviations of the means.

lar localization of DDX3X and that the level of exogenous DDX3X, based on quantitation with the DDX3X antibody, was similar to that of its endogenous counterpart (Fig. 2A). Thus, cells were first transfected with wild-type DDX3X and then infected, and extracellular virus production was measured by plaque assay. Unexpectedly, an excess of DDX3X also reduced viral infectivity (Fig. 2B). This suggested that optimal viral replication required a carefully controlled level of DDX3X.

To better define the relationship between DDX3X and the infection, we opted to rescue DDX3X in siRNA-depleted cells. To this end, we first determined which of the four siRNAs targeting DDX3X worked best (Fig. 3A) and generated a translationally silent DDX3X mutation resistant to this specific siRNA. We then treated cells with this unique siRNA to reduce endogenous DDX3X levels and rescued them with the above-described siRNA-resistant DDX3X construct. Cells were subsequently infected with HSV-1 K26GFP, a recombinant virus expressing a green fluorescent protein (GFP)-tagged VP26 minor capsid component (23), and the presence of DDX3X and the virus was monitored by fluorescence microscopy. Note that the exogenous DDX3X was expressed at levels similar to those of its endogenous counterpart and double the total DDX3X in the absence of siRNA (Fig. 3B and C, compare GS-DDX3X and transfection agent only). The results also revealed that, as expected, silencing DDX3X significantly reduced DDX3X. Interestingly, overexpression of DDX3X nearly abolished HSV-1 production (Fig. 3B and C). Rescuing the depleted cells with exogenous DDX3X restored the infection up to 63% compared to the level in untransfected cells (Fig. 3B and C, bottom). The virus was clearly sensitive to the DDX3X protein levels.

The virus functionally interacts with endogenous DDX3X. To understand the role of DDX3X in the viral life cycle, we next examined whether the virus influenced DDX3X levels. To this end, we probed DDX3X expression by Western blotting in three cell lines commonly used to study HSV-1, namely, HeLa, 143B, and Vero cells. HSV-1 infection had no impact on DDX3X protein levels in HeLa and Vero cells but reduced them by half in 143B cells (Fig. 4). We also examined whether the virus altered the subcellular localization of DDX3X. As shown in Fig. 5 (left panels), the endogenous DDX3X was primarily localized in cytoplasmic granules in uninfected cells. Attempts to identify these granules with a variety of markers unfortunately failed to unambiguously identify them. In agreement with previous studies, some DDX3X could also be detected in the nucleus (Fig. 5, insets), consistent with its shuttling across the nuclear envelopes (24, 25). Upon infection, DDX3X levels were once again unaffected in HeLa and Vero cells but reduced in 143B cells, as reported above. However, DDX3X was somewhat aggregated in all three cell lines (Fig. 5A, compare left and right panels). Furthermore, the GFP-tagged viral particles often, but not always, colocalized with DDX3X in the cytoplasm (Fig. 5B), in agreement with the incorporation of this cellular protein in mature virions (21). A time course revealed that DDX3X started to aggregate between 3 and 6 h postinfection

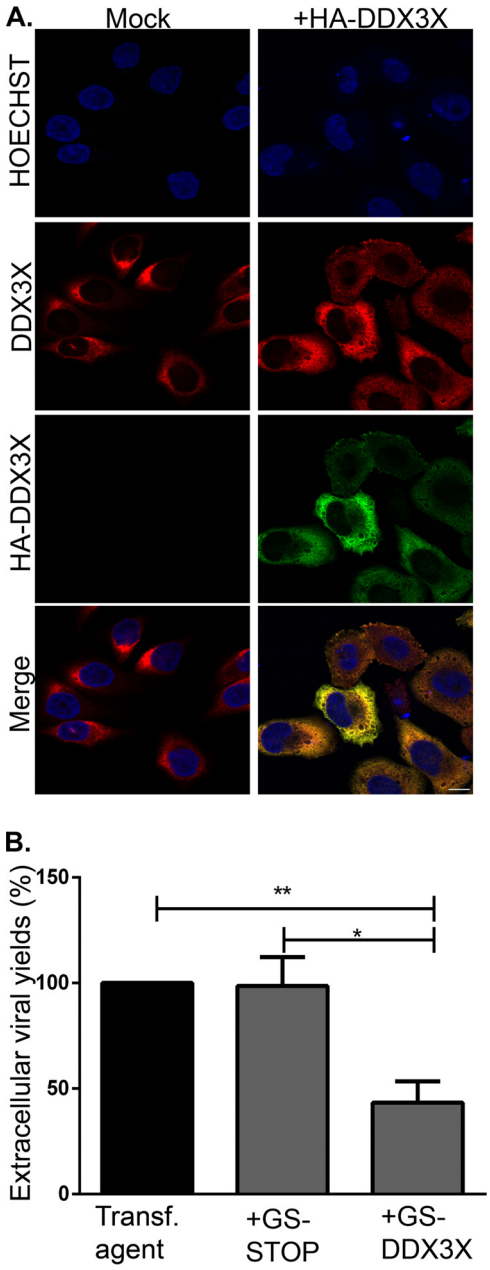

FIG 2 (A) Overexpressed DDX3X colocalizes with endogenous DDX3X. HeLa cells grown on coverslips were mock treated or transfected with pSG-N-4xHA-TEV-N-term DDX3X for 24 h. Cells were fixed and reacted with antibodies against total DDX3X (red) or HA-specific antibodies to detect exogenous DDX3X (green). Nuclei were labeled with Hoechst (blue). Samples were analyzed by confocal laser scanning microscopy. Scale bar, 10 μm. These results are representative of three individual experiments. (B) Effect of DDX3X overexpression on HSV-1 infectivity. HeLa cells grown in six-well plates were either mock treated or transfected with plasmids that express only the tag (GS-STOP) or the exogenous DDX3X fused to the tag (GS-DDX3X) for 24 h and then infected with wild-type HSV-1 at an MOI of 5 for 18 h. Supernatants, containing extracellular viruses, were then collected and titrated on Vero cells. Data represents the pool of five individual experiments. Bilateral Student's *t* tests (with standard deviations shown) were performed to detect significant hits compared to results with the transfection agent-only control. (*, $P < 0.05$; **, $P < 0.01$).

(hpi) and that this intensified with time (Fig. 6). As noted above, DDX3X also partially colocalized with the ICP4 viral marker within the nucleus. Albeit the virus can alter the localization of DDX3X and although viral proteins partially colocalize with it, we cannot at this point formally infer that viral particles themselves functionally interact with DDX3X. However, given that the cellular protein is incorporated in mature virions, this

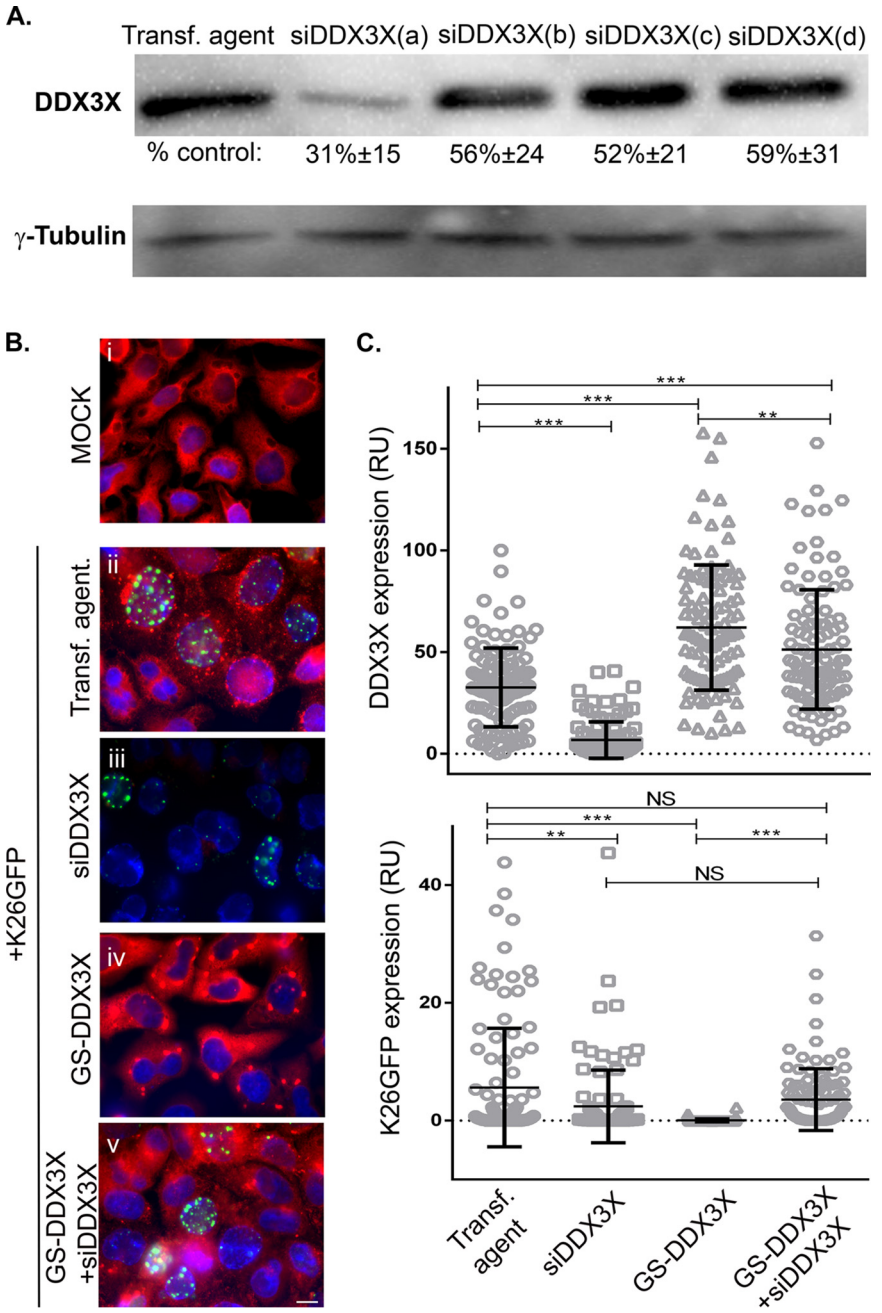

FIG 3 (A) RNA interference efficiency. HeLa cells seeded in 24 wells were individually transfected for 48 h with each of the different siRNAs against DDX3X (a, b, c, and d) that are present in the SMARTpool. Cell lysates were collected, and Western blotting was done as described previously. Values represent the amounts with respect to the untransfected control. The data are representative of two individual experiments. Normal levels of DDX3X best support HSV-1 propagation. (B) HeLa cells grown on coverslips were sequentially mock transfected or treated with siDDX3Xa in the presence or absence of a plasmid coding for the siRNA-resistant DDX3X mutant (pGS-TAP-tagged DDX3X, here called GS-DDX3X) for 48 h. All but the mock-infected samples were subsequently infected at an MOI of 5 with HSV-1 K26GFP (green signal) for 18 h. The cells were finally fixed and reacted with primary antibodies against DDX3X and appropriate secondary antibodies, a method which detects both endogenous and exogenous DDX3X (red signal), while nuclei were labeled with Hoechst (blue signal). Samples were analyzed by fluorescence microscopy. (C) Fluorescence intensities (relative units [RU]) were quantified for 100 cells using ImageJ. Scale bar, 10 μm. The data are representative of three independent experiments. Bars indicate the means and error bars indicate standard deviations of the mean (bilateral Student *t* tests; **, $P < 0.01$ and ***, $P < 0.001$; NS, not significant).

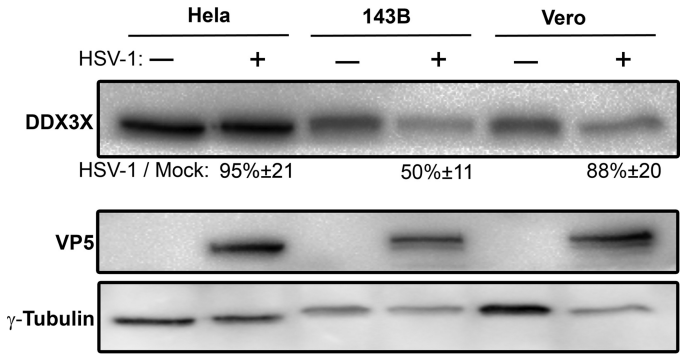

FIG 4 Impact of HSV-1 on endogenous DDX3X cellular levels. HeLa, Vero, and 143B cells were seeded in 10-cm plates 24 h prior to infection. Cells were then either mock treated (−) or infected (+) with wild-type HSV-1 at an MOI of 5 for 18 h. Total cell lysates were then collected, and DDX3X cellular levels were probed by Western blotting. γ-Tubulin was used as a loading control. Numbers below the blots indicate the average levels of DDX3X, normalized for γ-tubulin, from five independent experiments.

seems plausible, and it would be interesting to find whether this occurs in the nucleus, cytoplasm, or elsewhere.

DDX3X downregulation alters novel viral particle assembly. A number of scenarios may justify the presence of a host protein in mature virions. One explanation might be that it is needed immediately after cell entry to initiate an infection. A second scenario would be that the protein boosts viral replication postentry. A third one is that DDX3X virion incorporation may be a bystander effect of a previously occurring interaction taking place during viral particle assembly or transport toward the cell periphery. Note that these options are not mutually exclusive. To address the first of these scenarios, we directly probed whether the virion-associated pool of DDX3X is required for viral entry. To this end, we used a viral strain that encodes luciferase under a constitutive cytomegalovirus (CMV) immediate early promoter (26). We concomitantly infected cells with this virus, a wild-type virus (i.e., without the luciferase cassette), or no virus at all (mock infection). To specifically probe the role of DDX3X during entry, we additionally infected the cells with the luciferase-coding virus depleted of DDX3X or, as a control, depleted of VP16, a transactivating viral protein incorporated in virions and known to jump-start viral gene expression (21). To synchronize the infection, viral adsorption was performed at 4°C for 1 h, and the cells were subsequently transferred to 37°C for an additional hour. Other control cells were maintained at 4°C throughout the experiment to prevent viral entry. Entry of the virus into the cells was then monitored via luciferase expression. Viruses devoid of the luciferase gene, mock-infected cells, or the luciferase-encoding virus incubated at 4°C all gave signals at the background level (Fig. 7). In contrast, incubation of the untreated luciferase-positive virus at 37°C gave a strong signal, which was normalized to 100%. Infection by VP16- or DDX3X-depleted luciferase-positive virions resulted in similar signals, indicating that their presence in the mature virus was not essential for this early phase of the infection. This also suggested that the CMV immediate early promoter driving the luciferase is insensitive to VP16, as expected. Together, these observations suggested that DDX3X acted downstream of viral entry.

Thus far, our findings pointed to a requirement for DDX3X in the HSV-1 life cycle at some time after viral entry. To define whether this phenomenon is due to a block in viral egress from the intracellular to the extracellular environment or to a reduction in the assembly of viral particles, we next examined intracellular viral yields. The results indicated that DDX3X depletion from cells significantly reduced the amount of intracellular viral particles, as did the knockdown of the transactivator and structural VP16 protein (Fig. 8). Consistently, less GFP signal was observed by immunofluorescence following an HSV-1 K26 GFP viral infection after DDX3X or VP16 depletion (Fig. 9). Thus, DDX3X was required for the efficient assembly of nascent viral particles. To ascertain

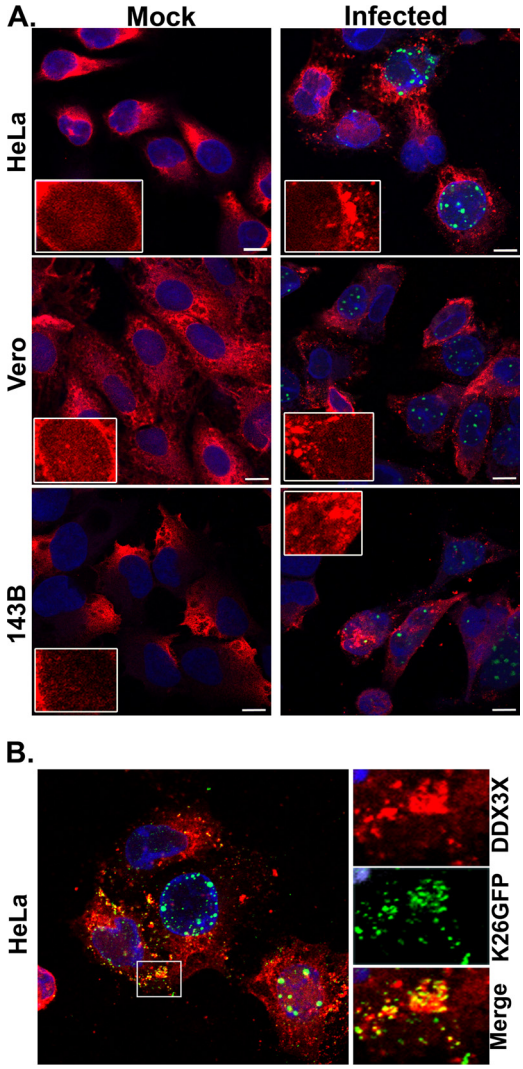

FIG 5 Endogenous DDX3X subcellular localization. (A) HeLa, Vero, and 143B cells were seeded on coverslips 24 h prior to infection. Cells were then either mock infected or inoculated with HSV-1 K26GFP (green) at an MOI of 5 for 18 h. Cells were then fixed, permeabilized, and immunostained with an antibody specific for DDX3X (red), and the nuclei were stained with Hoechst (blue). Cells were finally analyzed by confocal laser scanning microscopy. (B) Close-up view in the cytoplasm of infected HeLa cells. Scale bar, 10 μm. Results are representative of three independent experiments.

whether this truly translated into fewer viral particles, we performed an electron microscopy analysis under depleted or DDX3X overexpression conditions. As shown in Fig. 10A and quantified in panel B, both scenarios significantly reduced the total number of viral particles associated with the cells, as did the control siVP16 depletion.

DDX3X modulates viral gene expression. Given the reduced production of viral particles upon DDX3X depletion and given that DDX3X is a known modulator of host gene transcription and translation, we wondered if DDX3X could also regulate viral gene expression. To address this, we probed representative candidates of the three viral kinetics classes, namely, ICP0 and ICP4 (immediate early proteins), ICP8 and pUL23 (early proteins), and VP16 and pUL31 (late proteins) under normal, reduced (siDDX3X), or enhanced (DDX3X overexpression) conditions. We infected cells for 9 h since it is an intermediate time point when both early and late viral proteins are detectable. Both DDX3X conditions negatively affected the expression of all classes of viral proteins, including once again VP16 (Fig. 11A). Note that these Western blots were not performed with film but, rather, with a ChemiDoc digital instrument, which gives very

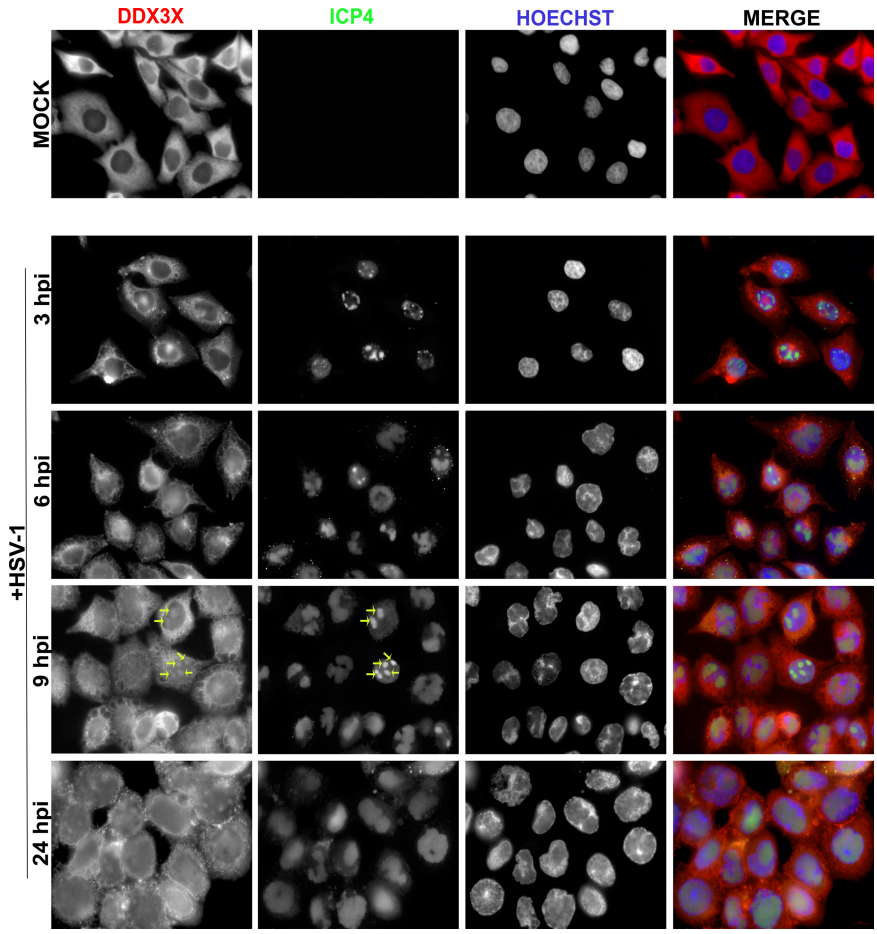

FIG 6 Time course of DDX3X aggregation. HeLa cells grown on coverslips were infected with wild-type HSV-1 at MOI of 5 for 3, 6, 9, and 24 hpi. Cells were fixed at the indicated time points and reacted with antibodies against endogenous DDX3X (red) or ICP4 (green; to delineate infected cells), while nuclei were labeled with Hoechst (blue). Samples were analyzed by fluorescence microscopy. Scale bar, 10 μm. These results are representative of two individual experiments. Arrows indicate the colocalization of DDX3X with ICP4.

good linear detection signals (Fig. 11B). Quantification of several independent experiments, which were normalized against a γ-tubulin loading control, confirmed these findings (Fig. 11C). To evaluate if the reduced protein levels were the consequence of reduced transcription, the samples were further analyzed by quantitative reverse transcription-PCR (qRT-PCR). The data showed that most of the viral gene transcripts were negatively impacted by both reduced and overabundant DDX3X (Fig. 12), albeit the changes were slightly less than those in the corresponding protein levels (Table 1).

DDX3X's effect on the virus is independent of IFN-β production. Given the role of DDX3X in innate immunity (see introduction), we probed by qRT-PCR the impact of DDX3X modulation on interferon type I production using IFN-β as a gauge. As reported elsewhere (10), depleting endogenous DDX3X had no effect on the already low level of IFN-β mRNA in uninfected cells, while DDX3X overexpression strongly stimulated its expression (Fig. 13). Meanwhile, IFN-β production was slightly increased by the virus compared to the level in mock-treated cells, but this was not statistically significant, which is perhaps consistent with the ability of the virus to counteract this innate response. Not surprisingly in this context, depleting or overproducing DDX3X in infected cells did not have any major impact on IFN-β levels (Fig. 13). Thus, as previously documented by other investigators, DDX3X positively promoted IFN-β levels in uninfected cells but had a limited effect in HSV-1-infected cells. Therefore, the well-known ability of DDX3X to modulate the interferon type I pathway did not appear

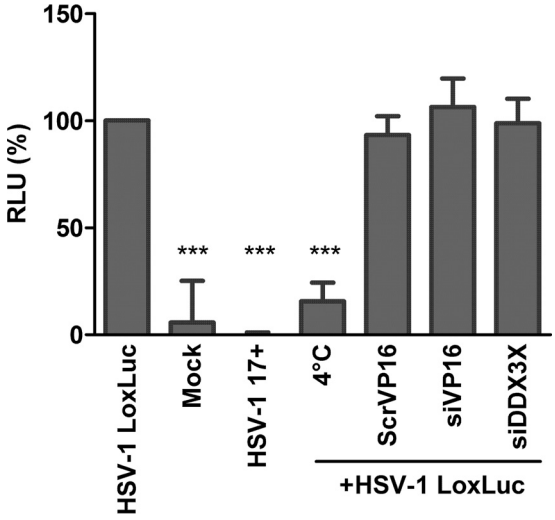

FIG 7 Virion-associated DDX3X has no effect on HSV-1 entry. 143B cells preseeded in 24-well plates were mock infected or infected at an MOI of 30 for 1 h at 4°C with various HSV-1 viruses, as indicated below each bar. These included wild-type HSV-1 (luciferase-negative) and untreated and DDX3X- or VP16-depleted HSV-1(17^{+})Lox-Luc viruses. To enable viral entry, the cells were then incubated at 37°C for another hour and subsequently lysed at room temperature for 30 min in the presence of luciferin and energy. As a control, one sample was left at 4°C throughout the experiment to prevent viral entry. Samples were then transferred to 96-well plates and analyzed with a luminometer. Values represent the mean relative light units (RLU) from two independent experiments, and error bars indicate the standard deviations of the means. Asterisks indicate the results of bilateral Student's *t* tests (***, $P < 0.001$). ScrVP16, scrambled siRNA targeting VP16.

to play a critical role here since both DDX3X knockdown and overexpression reduced viral gene transcription. This suggested that DDX3X may act on viral propagation by an interferon-independent pathway.

To independently evaluate if DDX3X significantly impacted HSV-1 propagation via innate immunity, we measured viral genome copies by quantitative PCR (qPCR) under normal, depleted, or overexpressed DDX3X conditions. The data illustrated that viral genome replication was strongly inhibited under conditions of both depletion and overexpression (Fig. 14), in agreement with the scenario whereby DDX3X acted on the

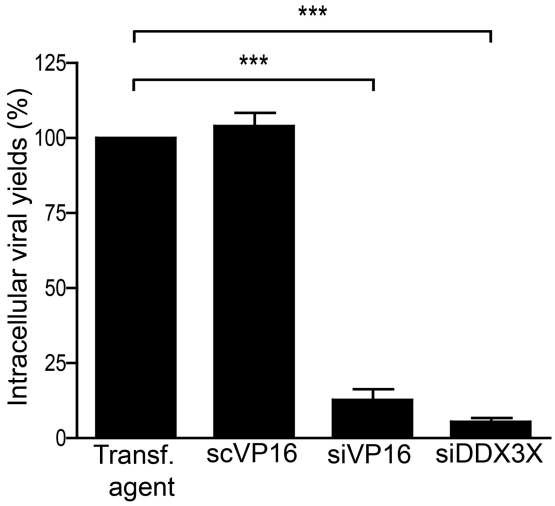

FIG 8 Impact of DDX3X knockdown on intracellular virions. 143B cells were transfected with siRNA pools targeting DDX3X or VP16 and infected with K26GFP at an MOI of 5. Cells were collected and lysed, and viruses were titrated on Vero cells. The error bars show the standard deviations of the means of two independent experiments. Bilateral Student's *t* tests were performed to detect significant hits compared to results with the transfection agent-only control (***, $P < 0.001$).

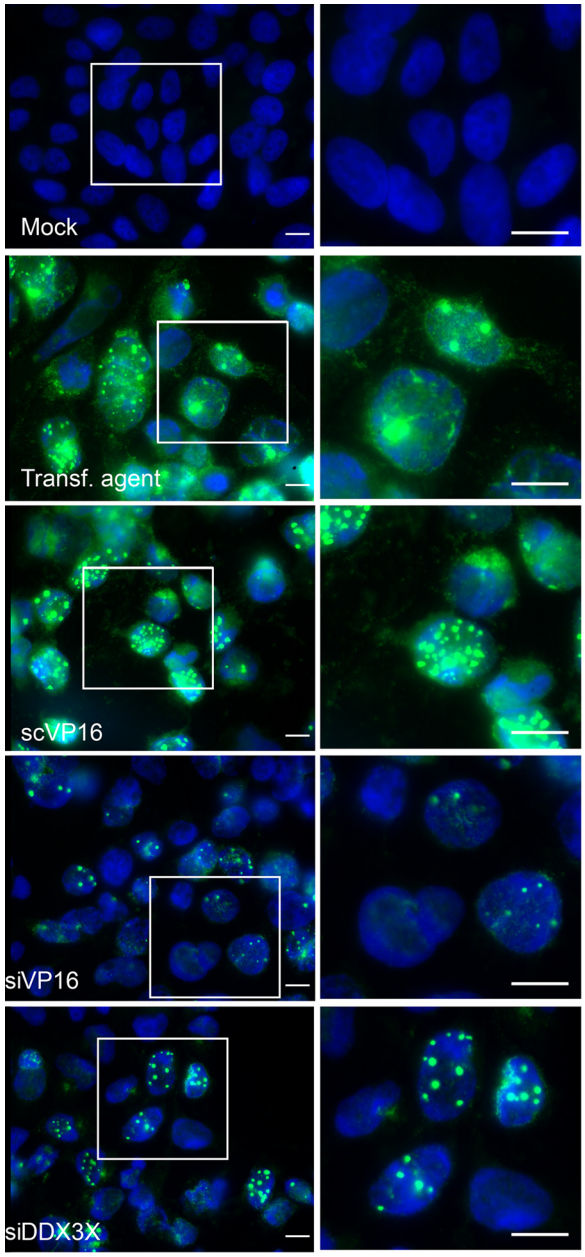

FIG 9 Inhibition of DDX3X-reduced viral particle assembly. 143B cells were mock infected, mock transfected, or treated with a nontargeting siRNA or with pooled siRNAs against DDX3X or VP16 as indicated. All but the mock-infected samples were incubated with HSV-1 K26GFP (green signal) at an MOI of 5 for 18 h. The cells were fixed, and the nuclei were stained with Hoechst 33342 (blue). Right panels are enlargements of the boxed sections present in the left panels. Scale bar, 10 μm.

virus independently of its ability to modulate IFN-β production. To confirm this hypothesis, we resorted to a well-characterized DDX3X point mutant (K230A) that abolishes its ATPase—and consequently helicase—activities without perturbing its ability to modulate the interferon pathway (8, 10, 13). Our rationale was that if DDX3X primarily acted via the interferon type I pathway, the mutant should behave like wild-type DDX3X and block viral propagation, but if the ATPase activity is the main driver, the mutant would not have any impact and would allow the virus to replicate normally. The data showed that the K230A mutant was normally expressed and completely inactive (Fig. 15B). This indicated that DDX3X acted on the virus via its ATPase/helicase activities independently of the interferon pathway.

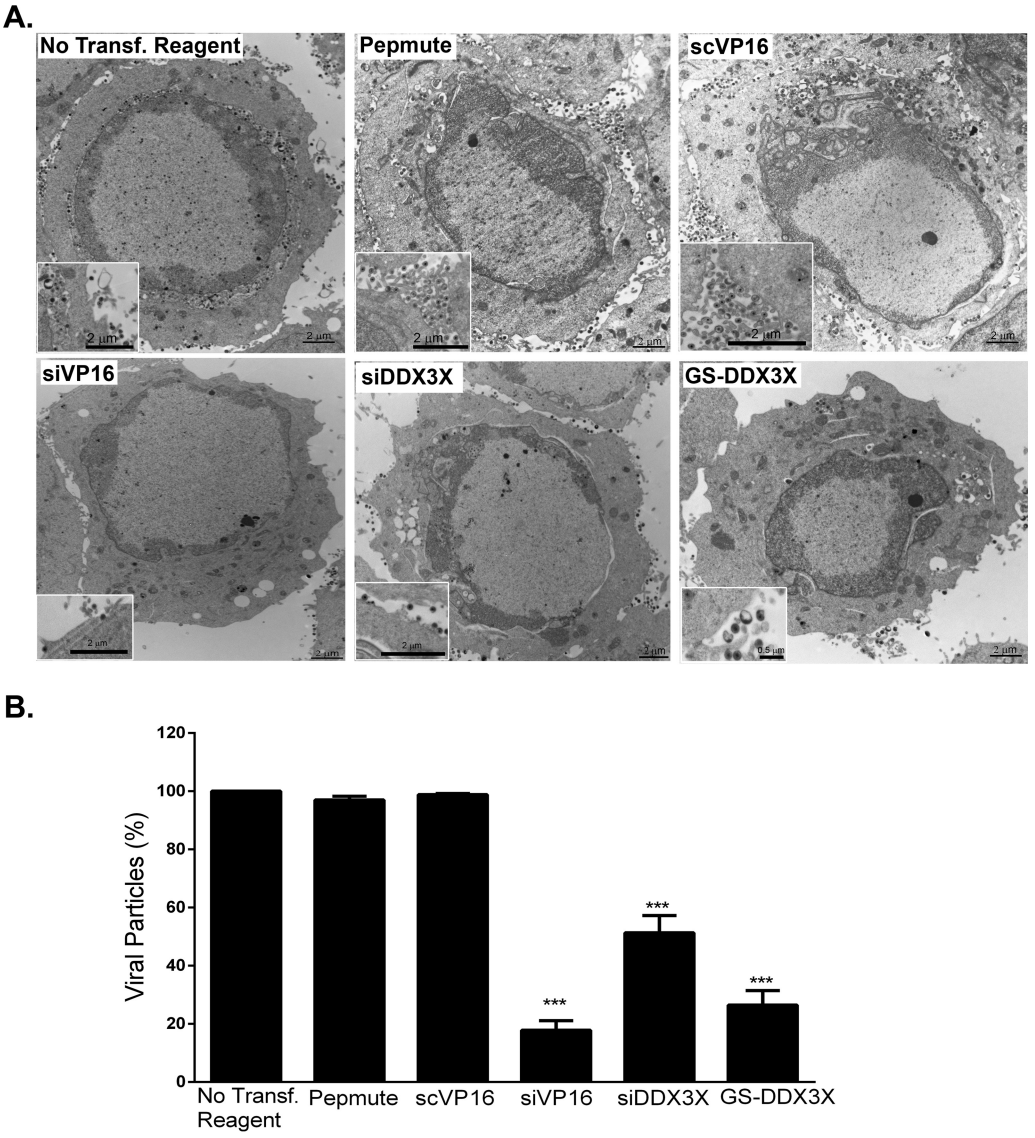

FIG 10 DDX3X plays a role in viral assembly. HeLa cells were either transfected with siDDX3X, siVP16, GS-DDX3X or just treated with a nontargeting siRNA (scVP16) or transfection reagent (Pepmute). All but the mock-infected samples were infected with HSV-1 strain 17^{+} at an MOI of 5 for 18 h. The cells were fixed and processed for Epon embedding (see Materials and Methods) to be observed by electron microscopy. (A) Representative cells for each condition. Enlargements (boxed higher-magnification images) were added to help visualize the mature virions more clearly. (B) The data represent the quantification of total cell-associated viral particles, both intracellular and those bound to the extracellular surface of the cells, for 12 individual cells of each condition from two independent experiments. Error bars indicate the standard deviations of the means Asterisks show the results of bilateral Student's *t* tests (***, $P < 0.001$). Scale bars are as indicated on each figure.

DISCUSSION

The DDX3X RNA helicase modulates HSV-1 propagation. The present data, along with our past findings (21), indicate that depletion of DDX3X either in cells or in HSV-1 mature viral particles led to a significant reduction of infectious HSV-1 particles. Two independent data sets confirmed that this was specific and not the result of off-target effects associated with RNA interference. First, viral yields were significantly rescued by an siRNA-resistant DDX3X construct (Fig. 3). Second, orthogonal validation of the results with the tsET24 cell line, where DDX3X is nonfunctional at the restrictive temperature, further proved that the phenotypes were directly linked to DDX3X (Fig. 1). We conclude that DDX3X is required for optimal HSV-1 propagation.

Despite the contribution of DDX3X to viral yields, overexpression of DDX3X unexpectedly also reduced virus production (Fig. 2 and 3). This was corroborated by the fact

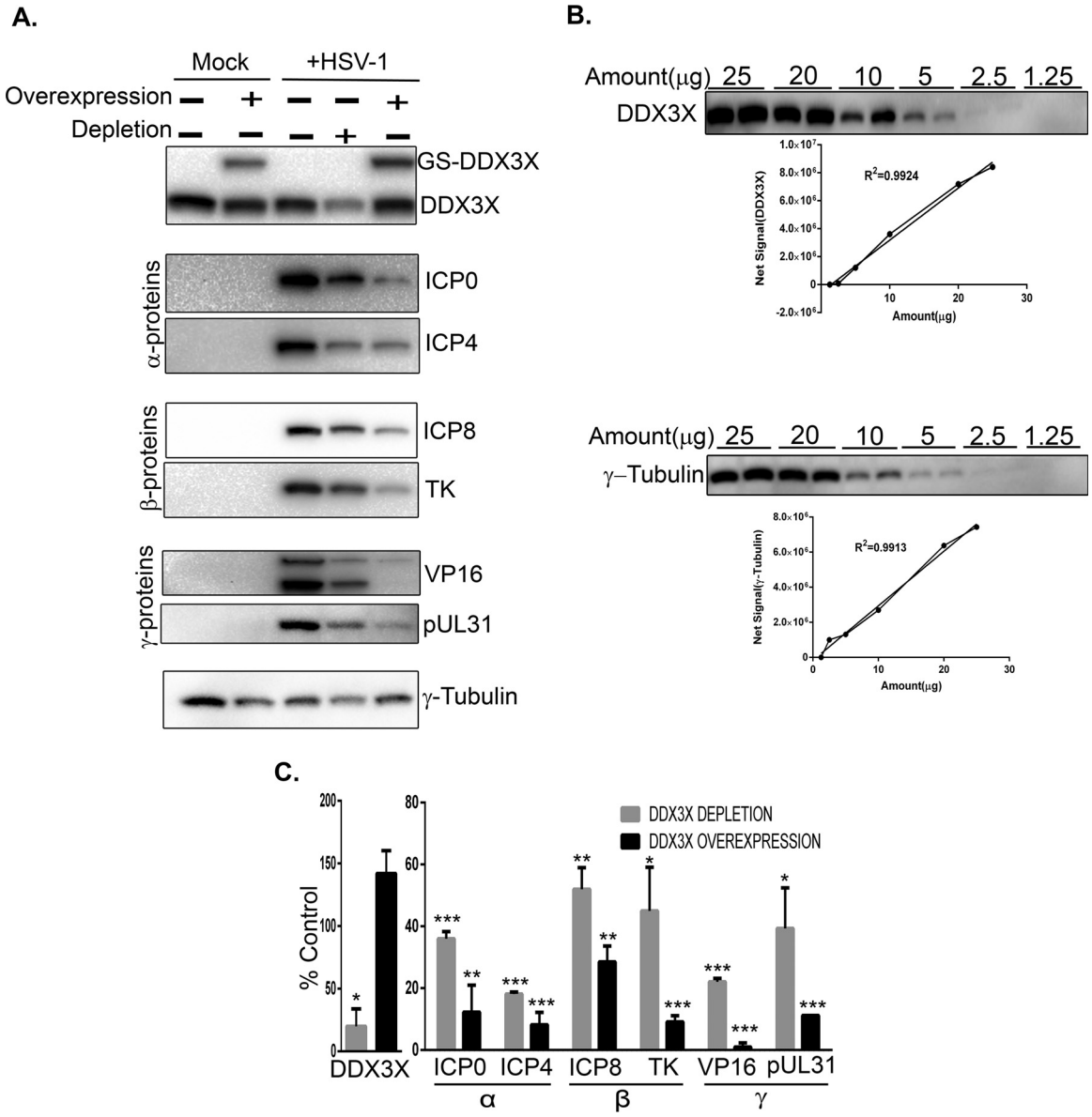

FIG 11 Effect of depletion or overexpression of DDX3X on HSV-1 gene expression. (A) HeLa cells seeded in six-well plates were transfected for 48 h with pooled siRNA against DDX3X and/or a plasmid coding for siRNA-resistant DDX3X. Cells were subsequently infected at an MOI of 5 with wild-type HSV-1 and harvested at 9 hpi and lysed. Twenty micrograms of the lysates was directly loaded onto SDS-PAGE gels and analyzed by Western blotting. γ-Tubulin was used as the loading control. (B) HeLa cells were seeded in a 10-cm petri dish for 24 h; cell lysates were then collected using three freeze-thaw cycles. Different amounts of cell lysate were loaded on an SDS-PAGE gel in duplicates to exclude potential loading errors. Western blotting was done using DDX3X or γ-tubulin antibodies. Linearity of the results was assayed by measuring the signal intensity of each point (mean of the duplicates). R^2 values were measured using GraphPad Prism, version 6. (C) Protein expression was evaluated, normalized to the level of γ-tubulin, and compared to the values obtained for infected but nontransfected cells. The reported values represent the average of two experiments. The error bars indicate standard deviations of the means. Bilateral Student's *t* tests were performed (*, $P < 0.05$; **, $P < 0.01$, ***, $P < 0.001$). Note that throughout this study, Western blots were quantified on a ChemiDoc MP system with a 4 orders of magnitude dynamic range, not film which has a poor linearity. In panels A and C, proteins are classified as immediate early (α), early (β), and late (γ).

that we detected HSV-1 K26GFP expression in only 0.9% of the cells overexpressing DDX3X (Fig. 3). This inhibition notably required the ATPase and helicase activities of DDX3X (Fig. 15). Though initially counterintuitive, this apparent contradiction has also been reported for hepatitis B and C viruses (9, 27). We presume that reduced or overabundant DDX3X levels exert their effects by distinct mechanisms and postulate that DDX3X stimulates viral production when it is present in rate-limiting or normal amounts. In contrast, overabundant functional DDX3X may compete with one of its

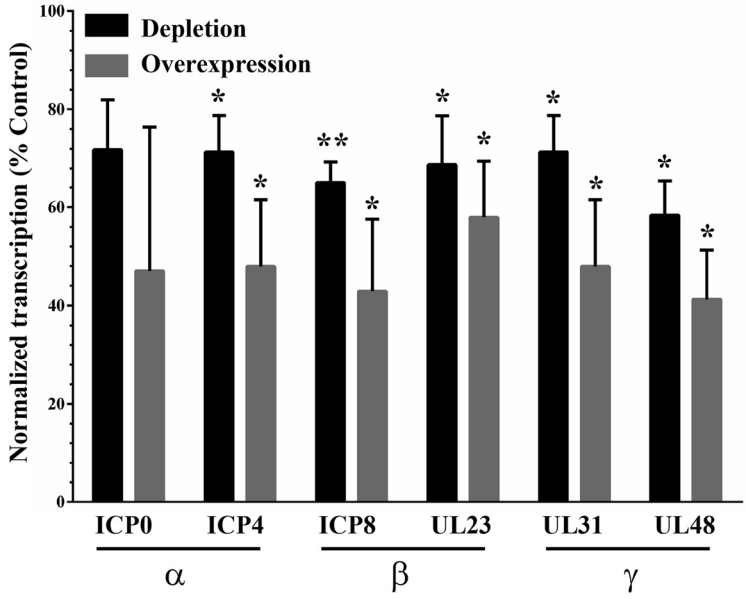

FIG 12 Impact of DDX3X on viral gene transcription. HeLa cells were seeded in six-well plates and transfected for 48 h either with siDDX3Xa or an siRNA-resistant DDX3X plasmid. Following 8 h of infection with wild-type virus at an MOI of 5, total RNA was collected and reverse transcribed into cDNAs. Expression levels of immediate early (α), early (β), or late (γ) viral genes were analyzed by qRT-PCR. Values represent the averages of two experiments. All the values were normalized to the level of GAPDH. Bilateral Student's *t* tests were performed to detect significant hits compared to results with the transfection agent-only control, arbitrarily set at 100% (*, $P < 0.05$; **, $P < 0.01$).

molecular partners and repress the endogenous DDX3X machinery. This seemed in line with our inability to generate cell lines stably overexpressing DDX3X (data not shown). In this context, it is worth noting that HSV-1 did not alter the DDX3X protein levels in HeLa and Vero cells (Fig. 4 and 5). Why the virus reduced DDX3X protein levels to a significant extent in 143B cells remains to be elucidated. Nonetheless, our working hypothesis is supported by our rescue experiments whereby transfection of siDDX3X-resistant exogenous DDX3X in siDDX3X-treated cells partially rescued both normal levels of DDX3X and viral output (Fig. 3). Hence, DDX3X is an important host partner for HSV-1.

DDX3X acts on HSV-1 gene expression. Distinct nonexclusive scenarios could explain the presence of DDX3X in mature HSV-1 particles. First, the virion-associated DDX3X may be required to initiate an efficient infection. However, this was mandatory as viral entry was unperturbed by the depletion of DDX3X within the viral particles prior to the entry assay (Fig. 7). It remains possible, though, that the cellular pool of DDX3X takes over this task. Second, DDX3X incorporation in virions could be due to an interaction of the host protein and structural components of the virus and merely

TABLE 1 Effect of DDX3X depletion or overexpression on HSV-1 gene expression

		Value under the indicated DDX3X condition (%)[a]			
		Depletion		Overexpression	
Gene	Protein	mRNA level	Protein level	mRNA level	Protein level
RL2	ICP0	72 ± 10	36 ± 2*	47 ± 29	12 ± 9
RS1	ICP4	71 ± 7	18 ± 0.6†	48 ± 14	8 ± 4*
UL29	ICP8	65 ± 4	52 ± 6	43 ± 15	28 ± 5
UL23	TK	69 ± 10	44 ± 14	58 ± 12	9 ± 2*
UL31	pUL31	71 ± 7	39 ± 13	48 ± 14	11 ± 0.04
UL48	VP16	58 ± 7	22 ± 1*	41 ± 10	1 ± 1*

[a]Significant differences between mRNA and protein levels (means ± standard deviations) for each condition in two independent experiments based on bilateral Student's *t* tests are indicated. *, $P < 0.05$; †, $P < 0.001$.

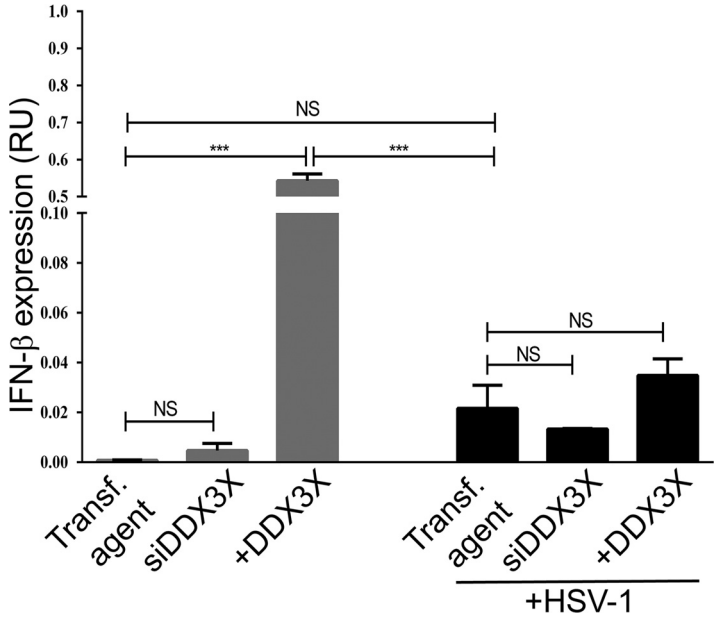

FIG 13 IFN transcription levels. HeLa cells grown in six-well plates were transfected for 48 h with siDDX3Xa and/or an siRNA-resistant DDX3X plasmid. Cells were either mock treated or subsequently infected with wild-type virus for 8 h at an MOI of 5. Total RNA was collected, and IFN-β mRNA was measured by qRT-PCR normalized to GAPDH levels. Data represent the average of two independent experiments. Bilateral Student's *t* tests were performed to detect significant hits compared to results with the transfection agent-only control (NS, not significant; ***, $P < 0.001$). RU, relative units.

reflect a past role(s) or simply a sticky protein. Although we cannot formally rule this out, it is clear that DDX3X plays an active role in the assembly of novel viral particles by regulating the transcription of viral genes (Fig. 11). Given the stronger impact of DDX3X on viral protein levels than on transcription (Table 1), it is conceivable that DDX3X also acts on other steps of viral gene expression, namely, mRNA transport, stability, or translation or even viral protein stability. On the other hand, the more pronounced effect of DDX3X on protein levels may simply be the consequence of the relative abundance of viral transcripts, albeit this is hard to correlate (28). We conclude that DDX3X clearly modulates HSV-1 gene transcription with potential impacts on other steps of gene expression. The presence of DDX3X in various mature extracellular herpesviruses, including HSV-1, pseudorabies virus (PRV), and human CMV (HCMV) (29), suggests that the present findings may apply to several viruses. One major outstanding question is why these viruses incorporate DDX3X in their viral particles.

Mechanism of DDX3X action. Whether DDX3X acts directly on various viral genes or indirectly via a few select molecules is unclear. Thus far, DDX3X was shown to bind to the IFN-β and the tumor suppressor p21 promoters, thus suggesting a direct role as a transcription cofactor (10, 30). However, precise binding motifs have yet to be identified.

An intriguing scenario is the stimulatory role that DDX3X plays in innate immunity upon TBK1 and IKKε binding and IRF3 activation (10, 13, 31). As expected, modulating DDX3X levels did alter interferon production in uninfected cells but had minimal impacts in infected cells (Fig. 12), presumably because of the well-documented ability of the virus to circumvent this pathway (32). Since either increasing or decreasing DDX3X levels reduced viral yields (Fig. 1 to 3 and 8 to 10), gene expression (Fig. 11 and 12 and Table 1), and genome copy numbers (Fig. 14), this suggested that DDX3X acted on HSV-1 independently of the interferon pathway. This model is supported by the observation that a helicase-deficient DDX3X mutant, which is still able to stimulate interferon production (10, 13), was completely dead in our hands and failed to limit HSV-1 propagation (Fig. 15). So, we conclude that DDX3X most likely modulates HSV-1 gene expression in an interferon-independent manner.

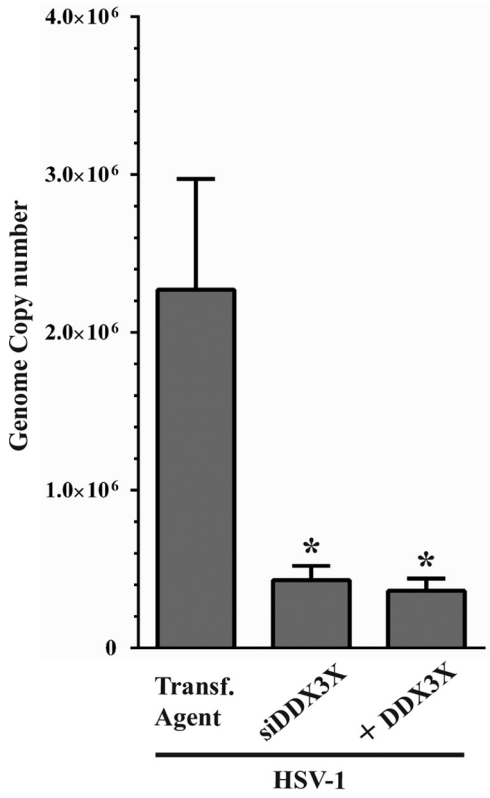

FIG 14 Viral genome copies upon siDDX3X depletion or overexpression. HeLa cells seeded in six-well plates were transfected for 48 h with siDDX3Xa and/or an siRNA-resistant DDX3X plasmid. Cells were then infected with wild-type virus for 8 h at an MOI of 5. Total DNA was then collected, and viral genome copy numbers were measured by qPCR. Data represent the average of two experiments. Bilateral Student's *t* tests were performed to detect significant hits compared to results with the transfection agent-only control (*, $P < 0.05$).

DDX3X is a key player for both RNA and DNA viruses. DDX3X is a multifunctional cellular protein that interacts with viruses at several levels. Much of the current literature focuses on RNA viruses, given that DDX3X has RNA helicase activity. Not surprisingly, DDX3X was found to promote genome replication of many RNA viruses (33). However, DDX3X binds TBK1/IKKε, which stimulate both IRF3 activation and interferon type I production, thereby promoting an antiviral state (10, 11). This implies that DDX3X has dual functions that can either facilitate or hamper viruses. Interestingly, the latter property is not limited to RNA viruses but also operates on vaccinia virus and hepatitis B virus, two DNA viruses (12, 13). Accordingly, DDX3X influences viral outcomes both via innate immunity and RNA viral gene duplication. The present study further suggests that DDX3X also acts on DNA viruses by a third mechanism, namely, by modulating viral gene expression.

MATERIALS AND METHODS

Cells, viruses, and plasmids. HeLa (ATCC CCL-2), Vero (ATCC CCL-81), 143B thymidine kinase-negative (TK⁻) (ATCC CRL-8303), tsET24, and BHK21 cells were grown in Dulbecco's modified Eagle's medium (DMEM) supplemented with 2 mM L-glutamine and either 10% fetal bovine serum (FBS) or 5% bovine growth serum (BGS). 143B cells were also supplemented with 15 μg/ml 5-bromo-2 deoxyuridine (BrdU; Sigma) except prior to transfection and infection. The tsET24 thermosensitive and parental BHK21 cell lines (a kind gift from Takeshi Sekiguchi, Kyushu University [22]) were passaged at the permissive temperature of 34°C.

HSV-1 K26GFP (strain KOS; provided by Prashant Desai, Johns Hopkins University [23]) is a fluorescent virus tagging the minor VP26 capsid component. Wild-type HSV-1 strain F was obtained from the American Type Culture Collection (ATCC VR-735). The HSV-1(17⁺)Lox-Luc viral strain is derived from strain 17⁺ and encodes a luciferase gene under the constitutive immediate early CMV promoter positioned between the UL55 and UL56 HSV-1 genes (26). All viruses were propagated on BHK cells and titrated on Vero cells as previously described (34).

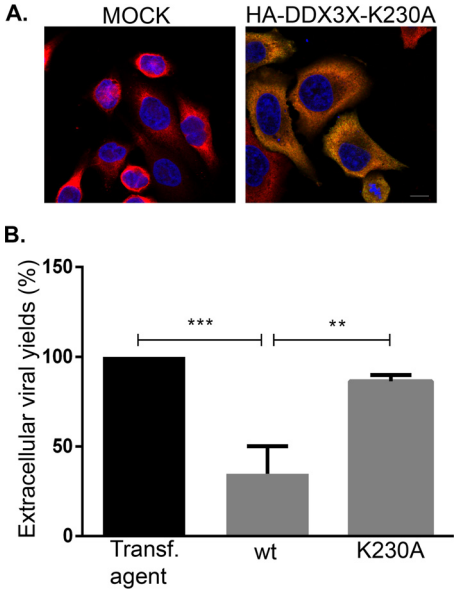

FIG 15 (A) The K230A DDX3X mutant is expressed at levels similar to those of the wild type. HeLa cells grown on coverslips were mock treated or transfected with pSG-N-4xHA-TEV-N-term K230A for 24 h. Cells were fixed and labeled with antibodies against total DDX3X (red) or with HA-specific antibodies to detect mutant DDX3X (green). Nuclei were labeled with Hoechst (blue). Samples were analyzed using confocal laser scanning microscopy. Images are representative of three individual experiments. Scale bar, 10 μm. (B) Overexpression of an ATPase/helicase-inactive but interferon-competent DDX3X mutant has no impact on viral propagation. HeLa cells grown in six-well plates were either mock treated or transfected for 24 h with exogenous wild-type (wt) DDX3X or the ATPase/helicase-deficient but interferon-competent K230A mutant. They were then infected with wild-type HSV-1 for 18 h at an MOI of 5. Extracellular viruses in the supernatant were then collected and titrated on Vero cells. Data represents the pool of five individual experiments. Statistical significance was assessed based on bilateral Student's *t* tests (**, $P < 0.01$; ***, $P < 0.001$).

The pGS-TAP-tagged DDX3X (DDX3X fused to protein G and streptavidin binding peptide with a tandem affinity purification [TAP] tag), pSG-N-4xHA-TEV-N-term DDX3X (hemagglutinin [HA]-tagged DDX3X; TEV is tobacco etch virus) and pSG-N-4xHA-TEV-N-term K230A (defective mutant) eukaryotic expression plasmids were a kind gift from G. Superti-Furga (Research Center for Molecular Medicine) (10). An siRNA-resistant plasmid was derived from pGS-TAP-tagged DDX3X using a QuikChange II XL site-directed mutagenesis kit (Agilent Technologies) and forward primer 5′-GGAAAGAGGAAAGATTGATTAG ACTTTTG**T**AA**G**TA**TC**TGGT**CC**T**G**GATGAAGCTGATCGGATGTTGGATATGGG-3′ and reverse primer 5′-CCCC ATATCCAACATCCGATCAGCTTCATC**C**A**GG**ACCA**GA**TA**CTA**CAAAAGTCTAATCCAATCTTTCCTCTTTCC-3′, as per the manufacturer's instructions (bold sequences indicate the silent point mutations). We also generated a plasmid that expresses only the GS tag by changing the first methionine in the DDX3X sequence to a stop codon. In addition, three other amino acids at the beginning of the DDX3X sequence were also changed to stop codons to make sure that protein was not expressed, using the following primers: forward primer, 5′-CTG GTC CAG CCC GAG CGC **ATT** TTA CAC **TCA** CAC **TTA** ACT **CTA** GGA GCC TGC TTT TTT GTA CAA AC-3′; reverse primer, 5′-GTT TGT ACA AAA AAG CAG GCT CC **TAG** AGT **TAA** GTG **TGA** GTG **TAA** AAT GCG CTC GGG CTG GAC CAG-3′ (mutations are in boldface). This plasmid served as a negative control in our experiments and is referred to as GS-STOP in the manuscript.

Antibodies. Primary antibodies were as follows: the anti-human DDX3 rabbit R648 polyclonal serum (immunofluorescence, 1:200; Western blot, 1:2,000) was a kind gift from A. Patel (University of Glasgow Centre for Virus Research) (35). Viral antibodies were generously provided by several laboratories and used at the indicated dilutions for Western blotting: VP16 (1:1,000; Helena Browne), TK (1:2,500; James R. Smiley), and pUL31 (1:1,000; Joel D. Baines). All other antibodies were purchased from commercial vendors, including anti-VP5 (1:5,000; Cedarlane), γ-tubulin (1:5,000; Sigma-Aldrich), and ICP4 (immunofluorescence, 1:500; Western blot, 1:5,000), ICP8 (1:1,000), and ICP0 (1:1,000) were all purchased from Abcam. All secondary antibodies were purchased from Molecular Probes.

Fluorescence microscopy. HeLa, Vero, or 143B cells were seeded overnight on coverslips in 24-well plates at a concentration of 1.5×10^4 cells/well. Cells were mock treated or infected with HSV-1 K26GFP at a multiplicity of infection (MOI) of 5. After a 1-h adsorption at 37°C, cells were washed twice in phosphate-buffered saline (PBS), fresh medium was added, and the cells were incubated for another 18 h prior to fixation and permeabilization with 3% paraformaldehyde and 0.1% Triton X-100. The cells were then incubated with a rabbit anti-DDX3X antibody for 1 h and further incubated for 45 min with a goat anti-rabbit antibody coupled to Alexa Fluor 568 (Molecular Probes). The samples were finally stained with Hoechst 33342 (Sigma-Aldrich) and examined on an Axiophot epifluorescence or LSM700 confocal

microscope (Zeiss). Fluorescence intensities were calculated by ImageJ by subtracting the background signal then dividing this net signal by the cell area.

Western blotting. HeLa, Vero, or 143B cells were mock treated or infected with wild-type HSV-1 at an MOI of 5 and collected 18 h later by scraping them in lysis buffer (10 mM Tris, pH 7.4, 150 mM NaCl, 2 mM $MgCl_2$, 5 mM dithiothreitol [DTT], 1 mM EDTA, 1% Igepal, and a cocktail of protease inhibitors). After centrifugation for 5 min at 4°C and 500 × *g*, cell pellets were resuspended in lysis buffer and incubated on ice for 1 h. Then they were passed through 27-gauge 1/2-in. needles three times and treated with DNase for 30 min at 37°C (500 U/ml; Roche). Cell debris was removed by spinning at 2,500 × *g* for 10 min, and cell lysates were collected. Samples (typically 20 μg) were loaded on 8% acrylamide SDS-PAGE gels in protein sample buffer (50 mM Tris-HCl, pH 6.8, 2% SDS, 0.1% bromophenol blue, 10% glycerol, and 2% β-mercaptoethanol). Proteins were then transferred to polyvinylidene difluoride (PVDF) membranes, which were then incubated for 1 h in blocking buffer (5% nonfat dry milk, 13.7 mM NaCl, 0.27 mM KCl, 0.2 mM KH_2PO_4, 1 mM Na_2HPO_4, and 0.1% Tween 20). The membranes were ultimately reacted with antibodies as indicated in each figure legend. When indicated (Fig. 3A, 4, and 11), protein expression levels were quantified with a ChemiDoc MP System (Bio-Rad), which has a dynamic range of 4 orders of magnitude, and Image lab, version 5.0, software (Bio-Rad).

Thermosensitive DDX3X. Thermosensitive tsET24 and parental BHK21 cells were plated in six-well plates and incubated at the permissive temperature of 34°C or the nonpermissive temperature of 39.5°C for 24 h. The cells were then mock treated or infected with HSV-1 K26GFP at an MOI of 5 at 34°C or 39.5°C. Cells and supernatants were collected at 24 h postinfection (hpi), and HSV-1 production was titrated on Vero cells by plaque assays.

DDX3X Overexpression. HeLa cells were seeded on coverslips in 24-well plates at a concentration of 2.0×10^4 cells/well. The next day, cells were transfected for 24 h with 0.5 μg/well of pGS-TAP-tagged DDX3X using LipoD293 reagent (SignaGen). Cells were subsequently infected for a further 18 h with wild-type HSV-1 K26GFP at an MOI of 5. The samples were finally fixed and permeabilized as described above and observed on an Axiophot epifluorescence microscope (Zeiss). To measure the impact of DDX3X overexpression on viral yields, HeLa cells were seeded at a concentration of 5.5×10^5 cells/well in six-well plates and transfected with pSG-N-4xHA-TEV-N-term DDX3X or pSG-N-4xHA-TEV-N-term K230A for 24 h with 4 μg/well of DDX3X constructs. Cells were then infected for a further 18 h with wild-type HSV-1 at an MOI of 5. Supernatants containing extracellular viruses were collected and titrated on Vero cells.

RNA interference. siRNAs against human DDX3X were either used as a SMARTpool of four siRNAs (Dharmacon) or individually tested as indicated in the respective figure legends. These siRNA were the following: siDDX3Xa, GCAAATACTTGGTGTTAGA; siDDX3Xb, ACATTGAGCTTACTCGTTA; siDDX3Xc, CTAT ATTCCTCCTCATTTA; and siDDX3Xd, GGTATTAGCACCAACGAGA. siRNAs (25-nm) were transfected into 143B or HeLa cells using either Pepmute (Signagen) or Lipofectamine 2000 (Thermo Fisher) for 48 h.

Generation of depleted virions. To produce depleted virions, 1×10^6 143B cells were seeded in 10-cm dishes for 24 h. These cells were then either transfected or mock treated for 48 h with 25 nM siRNA against DDX3X, VP16, or scVP16 (scrambled siRNA targeting VP16) (21) using Lipofectamine 2000 (Invitrogen). Cells were then infected for another 24 h with HSV-1(17^+)Lox-Luc or wild-type virus at an MOI of 5. In order to separate intracellular and extracellular virions, the tissue culture medium was first removed, and cells were scraped, centrifuged at 250 × *g* for 5 min at 4°C, and resuspended in MNT (30 mM morpholinoethanesulfonic acid, 100 mM NaCl, and 20 mM Tris, pH 7.4). Meanwhile, the extracellular medium was concentrated at 40,000 × *g* for 40 min at 4°C, and viral pellets were resuspended in the MNT buffer. All viruses were then titrated on Vero cells.

DDX3X rescue. HeLa cells were seeded on coverslips at a concentration of 2.0×10^4 cells/well. Cells were transfected for 24 h with 25 nM siRNA against DDX3X (siDDX3Xa) or with transfection agent only as control. Cells were then transfected a second time with an siRNA-resistant DDX3X construct using LipoD293 reagent for a further 24 h. They were finally infected with HSV-1 K26GFP at an MOI of 5 for 18 h. The cells were then fixed and permeabilized as described above and examined with an Axiophot epifluorescence microscope. Quantification of fluorescence signals was done with ImageJ (version 1.48), and values were normalized per cell areas.

Entry assay. 143B cells were seeded in 24-well plates 24 h before infection at a concentration of 1×10^5 cells/well. Cells were inoculated with wild-type HSV-1, untreated HSV-1(17^+)Lox-Luc, depleted viruses (see above), or, as a control, no virus at all under conditions that enable the virus to bind the cells but not penetrate them (MOI of 30; 4°C for 1 h). Samples were then shifted to 37°C for another 1 h and lysed for 30 min at room temperature with 100 μl/well of lysis buffer from a firefly luciferase assay kit (Biotium). Samples were then transferred to 96-well plates and analyzed by a LUMIstar Galaxy luminometer (BMG Labtech). Luminescence was quantified using LUMIstar Galaxy software, version 4.30-0.

qRT-PCR. Following DDX3X depletion or overexpression (see above), HeLa cells were infected with wild-type HSV-1 for 8 h. Total RNA was extracted using an SV Total RNA Isolation System (Promega). The RNA was then reverse transcribed with a high-capacity cDNA reverse transcription kit (Applied Biosystems) according to the manufacturer's instructions. The cDNA was then analyzed by quantitative PCR using a LightCycler 480 (Roche). Viral (ICP0, ICP4, UL23, ICP8, VP16, and UL31) or cellular (DDX3X and IFN-β) genes were quantified using the standard curve method and normalized to an endogenous control (glyceraldehyde-3-phosphate dehydrogenase [GAPDH]). All PCRs were performed using SYBR Green (Molecular Probes), and primers are as indicated in Table 2.

Viral genome copies. DDX3X was either depleted or overexpressed in HeLa cells as detailed above. Cells were then infected with wild-type HSV-1 for 8 h. Total DNA was purified from each condition using GenElute Mammalian Genomic DNA Miniprep kits (Sigma) as per the manufacturer's instructions. For the

TABLE 2 PCR primers

Gene	Protein	Forward primer (5′ → 3′)	Reverse primer (5′ → 3′)
RL2	ICP0	CTGTCGCCTTACGTGAACAA	CATCCAGAGGCTGTTCCACT
RS1	ICP4	CGACACGGATCCACGACCC	GATCCCCCTCCCGCGCTTCGTCCG
UL23	TK	GTAATGACAAGCGCCCAGAT	ATGCTGCCCATAAGGTATCG
UL29	ICP8	ACATTACGTTCACGGCCTTC	GGCCATCGACACGATAGACT
UL48	VP16	GGACGAGCTCCACTTAGACG	AGGGCATCGGTAAACATCTG
UL31	pUL31	GTGAAGACCACTCCCGTCTC	ATCGTGTTGATCTGCTGCAC
UL55	gB	TTTGTGTACATGTCCCCGTTTTAC	AGAAGCCGTCGACCTGCTT
DDX3X	DDX3X	TGCTGGCCTAGACCTGAACT	TTGATCCACTTCCACGATCA
GAPDH	GAPDH	GAGTCAACGGATTTGGTCGT	TTGATTTTGGAGGGATCTCG
IFN-β	IFN-β	AAACTCATGAGCAGTCTGCA	AGGAGATCTTCAGTTTCGGAGG

qPCR analysis, gB-specific primers (Table 2) were used with the above SYBR Green assay using GAPDH as the internal control.

Electron microscopy. HeLa cells seeded in 10-cm dishes were either depleted of DDX3X or VP16 with an siRNA or transfected to overexpress DDX3X. Forty-eight hours later, the cells were infected with HSV-1 strain 17^+ for 18 h. Samples were subsequently fixed (2.5% glutaraldehyde, 2% paraformaldehyde, 0.1 M cacodylate buffer, pH 7.2). Fixed cells were washed twice in 0.1 M cacodylate buffer, pH 7.2, and spun at 3,300 $\times$ *g*. The cells were resuspended in postfixation buffer (1% osmium tetroxide, 0.1 M cacodylate buffer) for 1 h at 4°C. Next, samples were gradually dehydrated using ethanol at 30%, 50%, 70%, 95%, and 100%. Cells were permeabilized with propylene oxide and then embedded in Epon [Epon 812; dodecenyl succinic anhydride (DDSA), nadic methyl anhydride (NMA) plus tri(dimethyl amino methyl) phenol (DMP-30)]. Embedded samples were cut with a Leica (MZ6) Ultracut UCT ultramicrotome (80- to 90-nm thickness). A Phillips 300 transmission electron microscope was used to analyze the sections.

Statistical analysis. Virus titers, protein abundance, and fluorescence were normalized to the values obtained for the controls as mentioned in each figure legend and analyzed with bilateral Student's *t* tests using GraphPad Prism, version 5 (GraphPad Software).

ACKNOWLEDGMENTS

We are indebted to Arvind Patel, Helena Browne, James R. Smiley, Joel D. Baines, Giulio Superti-Furga, Takeshi Sekiguchi, and Prashant Desai for antibodies, viruses, plasmids, and cell lines. We also thank Diana Matheoud for her kind guidance to determine interferon levels and for her critical readings of the manuscript.

This study was funded by the Canadian Institutes of Health Research to R.L. (grant MOP258030). B.S. has been funded by the Deutsche Forschungsgemeinschaft (German Research Council; Program Project Grant SFB900, TP C2; Excellence Cluster EXC 62/1, Rebirth—From Regenerative Biology to Reconstructive Therapy).

The funders had no role in study design, data collection and interpretation, or the decision to submit the work for publication.

We declare that we have no conflicts of interest.

REFERENCES

1. Ditton HJ, Zimmer J, Kamp C, Rajpert-De Meyts E, Vogt PH. 2004. The AZFa gene DBY (DDX3Y) is widely transcribed but the protein is limited to the male germ cells by translation control. Hum Mol Genet 13:2333–2341. https://doi.org/10.1093/hmg/ddh240.
2. Sharma D, Jankowsky E. 2014. The Ded1/DDX3 subfamily of DEAD-box RNA helicases. Crit Rev Biochem Mol Biol 49:343–360. https://doi.org/10.3109/10409238.2014.931339.
3. Ariumi Y, Kuroki M, Abe K, Dansako H, Ikeda M, Wakita T, Kato N. 2007. DDX3 DEAD-box RNA helicase is required for hepatitis C virus RNA replication. J Virol 81:13922–13926. https://doi.org/10.1128/JVI.01517-07.
4. Randall G, Panis M, Cooper JD, Tellinghuisen TL, Sukhodolets KE, Pfeffer S, Landthaler M, Landgraf P, Kan S, Lindenbach BD, Chien M, Weir DB, Russo JJ, Ju J, Brownstein MJ, Sheridan R, Sander C, Zavolan M, Tuschl T, Rice CM. 2007. Cellular cofactors affecting hepatitis C virus infection and replication. Proc Natl Acad Sci U S A 104:12884–12889. https://doi.org/10.1073/pnas.0704894104.
5. Ko C, Lee S, Windisch MP, Ryu WS. 2014. DDX3 DEAD-box RNA helicase is a host factor that restricts hepatitis B virus replication at the transcriptional level. J Virol 88:13689–13698. https://doi.org/10.1128/JVI.02035-14.
6. Vashist S, Urena L, Chaudhry Y, Goodfellow I. 2012. Identification of RNA-protein interaction networks involved in the norovirus life cycle. J Virol 86:11977–11990. https://doi.org/10.1128/JVI.00432-12.
7. Chahar HS, Chen S, Manjunath N. 2013. P-body components LSM1, GW182, DDX3, DDX6 and XRN1 are recruited to WNV replication sites and positively regulate viral replication. Virology 436:1–7. https://doi.org/10.1016/j.virol.2012.09.041.
8. Yedavalli VS, Neuveut C, Chi YH, Kleiman L, Jeang KT. 2004. Requirement of DDX3 DEAD box RNA helicase for HIV-1 Rev-RRE export function. Cell 119:381–392. https://doi.org/10.1016/j.cell.2004.09.029.
9. Wang H, Kim S, Ryu WS. 2009. DDX3 DEAD-Box RNA helicase inhibits hepatitis B virus reverse transcription by incorporation into nucleocapsids. J Virol 83:5815–5824. https://doi.org/10.1128/JVI.00011-09.
10. Soulat D, Burckstummer T, Westermayer S, Goncalves A, Bauch A, Stefanovic A, Hantschel O, Bennett KL, Decker T, Superti-Furga G. 2008. The DEAD-box helicase DDX3X is a critical component of the TANK-binding kinase 1-dependent innate immune response. EMBO J 27:2135–2146. https://doi.org/10.1038/emboj.2008.126.
11. Gu L, Fullam A, Brennan R, Schroder M. 2013. Human DEAD box helicase 3 couples IκB kinase epsilon to interferon regulatory factor 3 activation. Mol Cell Biol 33:2004–2015. https://doi.org/10.1128/MCB.01603-12.

12. Wang H, Ryu WS. 2010. Hepatitis B virus polymerase blocks pattern recognition receptor signaling via interaction with DDX3: implications for immune evasion. PLoS Pathog 6:e1000986. https://doi.org/10.1371/journal.ppat.1000986.
13. Schroder M, Baran M, Bowie AG. 2008. Viral targeting of DEAD box protein 3 reveals its role in TBK1/IKKepsilon-mediated IRF activation. EMBO J 27:2147–2157. https://doi.org/10.1038/emboj.2008.143.
14. Pellett PE, Roizman B. 2007. The family Herpesviridae: a brief introduction, p 2479–2500. *In* Knipe DM, Howley PM, Griffin DE, Lamb RA, Martin MA, Roizman B, Straus SE (ed), Fields virology, 5th ed. Lippincott Williams & Wilkins, Philadelphia, PA.
15. Weir JP. 2001. Regulation of herpes simplex virus gene expression. Gene 271:117–130. https://doi.org/10.1016/S0378-1119(01)00512-1.
16. Loret S, Guay G, Lippé R. 2008. Comprehensive characterization of extracellular herpes simplex virus type 1 virions. J Virol 82:8605–8618. https://doi.org/10.1128/JVI.00904-08.
17. Loret S, Lippé R. 2012. Biochemical analysis of infected cell polypeptide (ICP)0, ICP4, UL7 and UL23 incorporated into extracellular herpes simplex virus type 1 virions. J Gen Virol 93:624–634. https://doi.org/10.1099/vir.0.039776-0.
18. Everett RD. 2000. ICP0, a regulator of herpes simplex virus during lytic and latent infection. Bioessays 22:761–770. https://doi.org/10.1002/1521-1878(200008)22:8<761::AID-BIES10>3.0.CO;2-A.
19. Watson RJ, Clements JB. 1980. A herpes simplex virus type 1 function continuously required for early and late virus RNA synthesis. Nature 285:329–330. https://doi.org/10.1038/285329a0.
20. Yang WC, Devi-Rao GV, Ghazal P, Wagner EK, Triezenberg SJ. 2002. General and specific alterations in programming of global viral gene expression during infection by VP16 activation-deficient mutants of herpes simplex virus type 1. J Virol 76:12758–12774. https://doi.org/10.1128/JVI.76.24.12758-12774.2002.
21. Stegen C, Yakova Y, Henaff D, Nadjar J, Duron J, Lippé R. 2013. Analysis of virion-incorporated host proteins required for herpes simplex virus type 1 infection through a RNA interference screen. PLoS One 8:e53276. https://doi.org/10.1371/journal.pone.0053276.
22. Sekiguchi T, Iida H, Fukumura J, Nishimoto T. 2004. Human DDX3Y, the Y-encoded isoform of RNA helicase DDX3, rescues a hamster temperature-sensitive ET24 mutant cell line with a DDX3X mutation. Exp Cell Res 300:213–222. https://doi.org/10.1016/j.yexcr.2004.07.005.
23. Desai P, Person S. 1998. Incorporation of the green fluorescent protein into the herpes simplex virus type 1 capsid. J Virol 72:7563–7568.
24. Soto-Rifo R, Ohlmann T. 2013. The role of the DEAD-box RNA helicase DDX3 in mRNA metabolism. Wiley Interdiscip Rev RNA 4:369–385. https://doi.org/10.1002/wrna.1165.
25. Pene V, Li Q, Sodroski C, Hsu CS, Liang TJ. 2015. Dynamic interaction of stress granules, DDX3X, and IKK-α mediates multiple functions in hepatitis C virus infection. J Virol 89:5462–5477. https://doi.org/10.1128/JVI.03197-14.
26. Nagel CH, Pohlmann A, Sodeik B. 2014. Construction and characterization of bacterial artificial chromosomes (BACs) containing herpes simplex virus full-length genomes. Methods Mol Biol 1144:43–62. https://doi.org/10.1007/978-1-4939-0428-0_4.
27. Shih JW, Tsai TY, Chao CH, Wu Lee YH. 2008. Candidate tumor suppressor DDX3 RNA helicase specifically represses cap-dependent translation by acting as an eIF4E inhibitory protein. Oncogene 27:700–714. https://doi.org/10.1038/sj.onc.1210687.
28. Wren JD, Conway T. 2006. Meta-analysis of published transcriptional and translational fold changes reveals a preference for low-fold inductions. OMICS 10:15–27. https://doi.org/10.1089/omi.2006.10.15.
29. Lippé R. 2012. Deciphering novel host-herpesvirus interactions by virion proteomics. Front Microbiol 3:181. https://doi.org/10.3389/fmicb.2012.00181.
30. Chao CH, Chen CM, Cheng PL, Shih JW, Tsou AP, Lee YH. 2006. DDX3, a DEAD box RNA helicase with tumor growth-suppressive property and transcriptional regulation activity of the $p21^{waf1/cip1}$ promoter, is a candidate tumor suppressor. Cancer Res 66:6579–6588. https://doi.org/10.1158/0008-5472.CAN-05-2415.
31. Pomerantz JL, Baltimore D. 1999. NF-kappaB activation by a signaling complex containing TRAF2, TANK and TBK1, a novel IKK-related kinase. EMBO J 18:6694–6704. https://doi.org/10.1093/emboj/18.23.6694.
32. Paladino P, Mossman KL. 2009. Mechanisms employed by herpes simplex virus 1 to inhibit the interferon response. J Interferon Cytokine Res 29:599–607. https://doi.org/10.1089/jir.2009.0074.
33. Schroder M. 2011. Viruses and the human DEAD-box helicase DDX3: inhibition or exploitation? Biochem Soc Trans 39:679–683. https://doi.org/10.1042/BST0390679.
34. Turcotte S, Letellier J, Lippé R. 2005. Herpes simplex virus type 1 capsids transit by the trans-Golgi network, where viral glycoproteins accumulate independently of capsid egress. J Virol 79:8847–8860. https://doi.org/10.1128/JVI.79.14.8847-8860.2005.
35. Angus AG, Dalrymple D, Boulant S, McGivern DR, Clayton RF, Scott MJ, Adair R, Graham S, Owsianka AM, Targett-Adams P, Li K, Wakita T, McLauchlan J, Lemon SM, Patel AH. 2010. Requirement of cellular DDX3 for hepatitis C virus replication is unrelated to its interaction with the viral core protein. J Gen Virol 91:122–132. https://doi.org/10.1099/vir.0.015909-0.